Dissertation

submitted to the

Combined Faculty of Natural Sciences and Mathematics

of the Ruperto Carola University Heidelberg, Germany

for the degree of

Doctor of Natural Sciences

(Dr. rer. nat)

Presented by

Bianca Janine Kuhn

M.Sc. Biology

born in Schwäbisch Gmünd, Germany

Oral examination on the 14th of December 2021

The LATS1 and LATS2 tumor suppressor kinases: a comprehensive multilayered MS-based analysis of their functional roles in breast cancer

Referees:

Apl. Prof. Dr. Matthias Mayer

Prof. Dr. Jeroen Krijgsveld

I. Abstract

The Large Tumor Suppressor 1 and 2 (LATS1 and LATS2) were originally identified as core effectors of the Hippo signaling pathway, directly regulating the oncogenes YAP and TAZ. However, intense research in recent years has implicated the two kinases LATS1 and LATS2 in a number of functions outside this pathway, such as cell cycle regulation, maintenance of genome stability, or the control of cell proliferation, differentiation, and apoptosis. In addition, the expression levels of LATS1 and LATS2 are downregulated in many cancers, indicative of their role as tumor suppressors, as reflected in their naming. Since both paralogues are involved in the same biological processes, they have long been considered functionally redundant. However, there is emerging evidence that unique features of LATS1 and LATS2 could account for potential differences in protein function. Yet, little is known about the mechanism through which LATS1 and LATS2 operate, and in particular their direct kinase targets. In the present study, different knockdown and overexpression cell systems derived from female breast tissue were established, allowing for individual manipulations of LATS1 or LATS2 protein levels. As a read-out for LATS1- or LATS2-induced cell signaling, in-depth multi-layered MS-based proteomics, including global proteome, translatome, and phosphoproteome analysis, was applied.

The data generated from a luminal B breast cancer cell line supports the hypothesis of a novel cell cycle arrest in late anaphase, induced by LATS1 and LATS2 overexpression. Furthermore, data from a non-tumorigenic cell line supports the hypothesis that LATS1 and LATS2 can act as promotors of the cell cycle besides their known roles as tumor suppressors. Additionally, the present study allows for novel insights into (i) the role of LATS1 and LATS2 in cell cycle regulation, underlined by interaction networks between LATS1/2 and the APC/C complex, or the Aurora kinases, (ii) their cross-talk with other tumor suppressors such as RUNX3 and p53, (iii) their interplay with signaling pathways such as the cell polarity pathway (PCP), or the SLIT/ROBO signaling, and (vi) potential candidates for LATS1- and LATS2-substrates.

Together, this study provides rich datasets of LATS1/2-mediated effects on cell signaling, as well as potentially novel LATS1/2 kinase substrates which will support the understanding and in-depth characterization of these tumor suppressors, and facilitate the identification of cancer vulnerabilities.

II. Zusammenfassung

Large Tumor Suppressor 1 und 2 (LATS1 und LATS2) wurden ursprünglich als zentrale Effektoren des Hippo-Signalwegs identifiziert, welche direkt die Onkogene YAP und TAZ regulieren. Die intensive Forschung der letzten Jahre hat jedoch gezeigt, dass die beiden Kinasen LATS1 und LATS2 eine Reihe von Funktionen außerhalb dieses Signalwegs ausüben, wie z. B. die Regulierung des Zellzyklus, die Aufrechterhaltung der Genomstabilität oder die Kontrolle von Zellproliferation, Differenzierung und Apoptose. Darüber hinaus ist die Expression von LATS1 und LATS2 bei vielen Krebsarten herabreguliert, was auf ihre Rolle als Tumorsuppressoren hindeutet, worauf schon ihre Namensgebung hinweist. Da beide Paraloge an denselben biologischen Prozessen beteiligt sind, wurden sie lange Zeit als funktionell redundant angesehen. Es gibt jedoch zunehmend Hinweise darauf, dass einzigartige Merkmale von LATS1 und LATS2 für mögliche Unterschiede in der Proteinfunktion verantwortlich sein könnten. Dennoch ist wenig über die Mechanismen bekannt, durch die LATS1 und LATS2 agieren, und insbesondere über ihre direkten Kinase-Substrate. In der vorliegenden Studie wurden verschiedene Knockdown- und Überexpressions-Zellsysteme aus weiblichem Brustgewebe etabliert, die eine individuelle Manipulation der LATS1- oder LATS2-Proteinspiegel ermöglichen. Als Auslese für die LATS1- oder LATS2-induzierten Zellsignalkaskaden wurden umfassende, mehrschichtige MS-basierte Proteomanalysen durchgeführt, welche globale Proteom-, Translatom- und Phosphoproteomanalyse umfassen.

Die aus einer luminalen B-Brustkrebszelllinie gewonnenen Daten unterstützen die Hypothese eines neuartigen Zellzyklusarrests in der späten Anaphase, der durch eine Überexpression von LATS1 und LATS2 ausgelöst wird. Darüber hinaus stützen die Daten einer nicht-tumorigenen Zelllinie die Hypothese, dass LATS1 und LATS2 neben ihrer bekannten Rolle als Tumorsuppressoren auch als Promotoren des Zellzyklus wirken können. Des Weiteren ermöglicht die vorliegende Studie neue Einblicke in (i) die Rolle von LATS1 und LATS2 bei der Regulierung des Zellzyklus, was durch Interaktionsnetzwerke zwischen LATS1/2 und dem APC/C-Komplex oder den Aurora-Kinasen unterstrichen wird, (ii) ihr Cross-Talk mit anderen Tumorsuppressoren wie RUNX3 und p53, (iii) ihr Zusammenspiel mit Signalwegen wie dem Zellpolaritätssignalweg (PCP) oder dem

SLIT/ROBO-Signalweg und (vi) potenzielle Kandidaten für LATS1- und LATS2-Kinase-Substrate.

Diese Studie liefert reichhaltige Datensätze über LATS1/2-vermittelte Effekte auf die Zellsignalkaskaden sowie potenziell neue LATS1/2-Kinase-Substrate, die das Verständnis und die eingehende Charakterisierung dieser Tumorsuppressoren unterstützen und die Identifizierung von Krebsschwachstellen erleichtern werden.

III. Table of content

IV. List of Abbreviations

ACN	Acetonitrile
AGC	Automatic gain control
AmBic	Ammonium bicarbonate
BCA	Bicinchoninic acid assay
CAA	2-Chloroacetamide
CDK	Cyclin-dependent kinase
CDS	Coding Sequence
CID	Collision induced dissociation
DDA	Data-dependent acquisition
DKFZ	Deutsches Krebsforschungszentrum (Heidelberg, Germany)
DMEM	Dulbecco's modified Eagle's medium
DOX	Doxycycline
DTT	Dithiothreitol
EDTA	Ethylenediaminetetraacetic acid
ESI	Electrospray ionization
EtOH	Ethanol
FA	Formic acid
FACS	Fluorescence-activated cell sorting
FBS	Fetal bovine serum
FDR	False discovery rate
FWHM	Full width at half maximum
GFP	Green Fluorescent Protein
GO	Gene ontology
GOI	Gene of interest
GSEA	Gene set enrichment analysis
HCD	Higher-energy collision dissociation
hpH-RPLC	high pH reversed-phase liquid chromatography
IAA	Iodoacetamide
IMAC	Immobilized metal affinity chromatography
LB	Lysogeny broth
LC	Liquid Chromatography
LC-MS	Liquid chromatography coupled to mass spectrometry
LFQ	Label-free quantification
Limma	linear models for microarray data
MBR	Match between runs
MeOH	Methanol
min	Minutes
MS	Mass spectrometry
MS/MS	Tandem mass spectrometry
MS^1	First or full scan of precursor Ions in tandem mass spectrometry
MS^2	Second scan of fragment ions in tandem mass spectrometry

MS^3	Third scan of fragment ions after a second dissociation step
m/z	mass over charge
PBS	Phosphate-buffered saline
PCR	Polymerase chain reaction
PTM	Post-translational modification
QE HF	Q-Exactive High Field Mass Spectrometer
qPCR	quantitative polymerase chain reaction
rpm	Revolutions per minute
RT	Room temperature
RT-PCR	Reverse transcription-quantitative polymerase chain reaction
s	Seconds
SD	Standard deviation
SDC	Sodium deoxycholate
SDS	Sodium dodecylsulfate
SILAC	Stable isotope labeling by amino acids in cell culture
SPS	Synchronous precursor selection
TCEP	Tris(2-carboxyethyl)phosphine
TEAB	Triethylammonium bicarbonate
TFA	Trifluoroacetic acid
TMT	Tandem mass-tag
t-SNE	t-distributed stochastic neighbor embedding
UMAP	Uniform manifold approximation and projection
(U) HPLC	(Ultra) high-performance liquid chromatography
V	Volt
WIZ	Weizmann Institute of Science (Rehovot, Israel)
x g	Times gravitational foce

1. INTRODUCTION

1.1. The tumor suppressor kinases LATS1 and LATS2

1.1.1. LATS1 and LATS2 as core effectors of the Hippo signaling pathway

In 1995 two research groups identified a novel tumor suppressor in *Drosophila melanogaster*, independently from each other. Using a genetic mosaic screen, one of the groups described a mutant with a dramatic overproliferation phenotype and various developmental defects, which they named *lats* (large tumor suppressor) (Xu *et al*, 1995). Furthermore, in this study, they found that *lats* shares extensive sequence similarity with the cell cycle serine/threonine kinases *Dbf20* and *Dbf2* in *Saccharomyces cerevisiae*. Eventually, the discovery of the homologs in yeast provided the ultimate hint for *lats* itself being a serine/threonine kinase. At the same time, examining somatic cell mutants, the other group observed both, an excessive overproliferation phenotype and atypical hypertrophy of epithelial cells in adult flies (Justice *et al*, 1995). Inspired by this phenotype, the gene was named *warts*. Over the next decade, *lats/warts* (hereafter referred to as *warts* (*wts*)) became an established core component of the Hippo signaling pathway (Pan, 2010).

The Hippo pathway can be divided into the upstream regulatory kinase module, including the Ste20- like protein kinase Hippo (Hpo) and Warts (Wts), controlling the activity of the downstream transcriptional co-activator Yorkie (Yki) (**Figure 1**) (Wu *et al*, 2003; Udan *et al*, 2003; Harvey *et al*, 2003; Jia *et al*, 2003; Pantalacci *et al*, 2003; Huang *et al*, 2005). Each kinase is accompanied by a scaffold adaptor protein ensuring their full activity. For example, Hippo builds a signaling module with the WW domain-containing protein Salvador (Sav) and Warts forms a complex with the adaptor protein Mob-as-tumor-suppressor (Mats) (Tapon *et al*, 2002; Lai *et al*, 2005). Once activated a phosphorylation cascade starts with the active Hpo-Sav complex which phosphorylates and thereby activates Wts-Mats (Wu *et al*, 2003; Wei *et al*, 2007). Activate Wts in turn mediates the phosphorylation of its prime target Yki (Huang *et al*, 2005). Importantly, the latter phosphorylation leads to Yki binding to 14-3-3 adaptor proteins, enforcing cytoplasmatic retention and thereby inhibition of gene transcription (Dong *et al*, 2007; Oh & Irvine, 2008; Ren *et al*, 2010). On the contrary, when Yki is not inhibited, it translocates into the nucleus

where it binds and co-activates transcription factors such as Scalloped (Sd) (Goulev *et al*, 2008; Wu *et al*, 2008). This induces the expression of genes involved in cell growth, cell proliferation, and cell survival (Tapon *et al*, 2002; Harvey *et al*, 2003; Jia *et al*, 2003; Udan *et al*, 2003; Wu *et al*, 2003; Huang *et al*, 2005; Goulev *et al*, 2008; Wu *et al*, 2008). Together, these studies defined the kinase complex Hpo-Sav and Wts-Mats as tumor suppressors which control the activity of the growth-promoting oncogene Yki.

Although the phosphorylation-mediated cascade of the major components of the Hippo pathway is well understood, the molecular mechanisms that activate the pathway upstream are not. Intensive research in recent years has shown that a variety of intrinsic and extrinsic signals influence Hippo pathway activity, including cell-cell contact, stiffness of the extracellular matrix, stress signals, and cell polarity (Bae & Luo, 2018). Well-known examples are the membrane-associated proteins Kibra, Merlin, and Expanded, which form spatially separated complexes with other Hippo regulators at the cell cortex or at intercellular junctions to integrate upstream signals for activation of the central Hippo cascade (Su *et al*, 2017). However, the exact molecular mechanisms are not yet fully understood. A complicating factor is also that these signals can affect the Hippo signaling pathway at different levels, i.e. not all activators act on Hpo itself but instead can also act on downstream targets, such as Wts. Thus, it is still largely unclear how these molecular signals are integrated and what the upstream mediators are, illustrating that there is still much to be elucidated to understand the regulation of the Hippo signaling pathway.

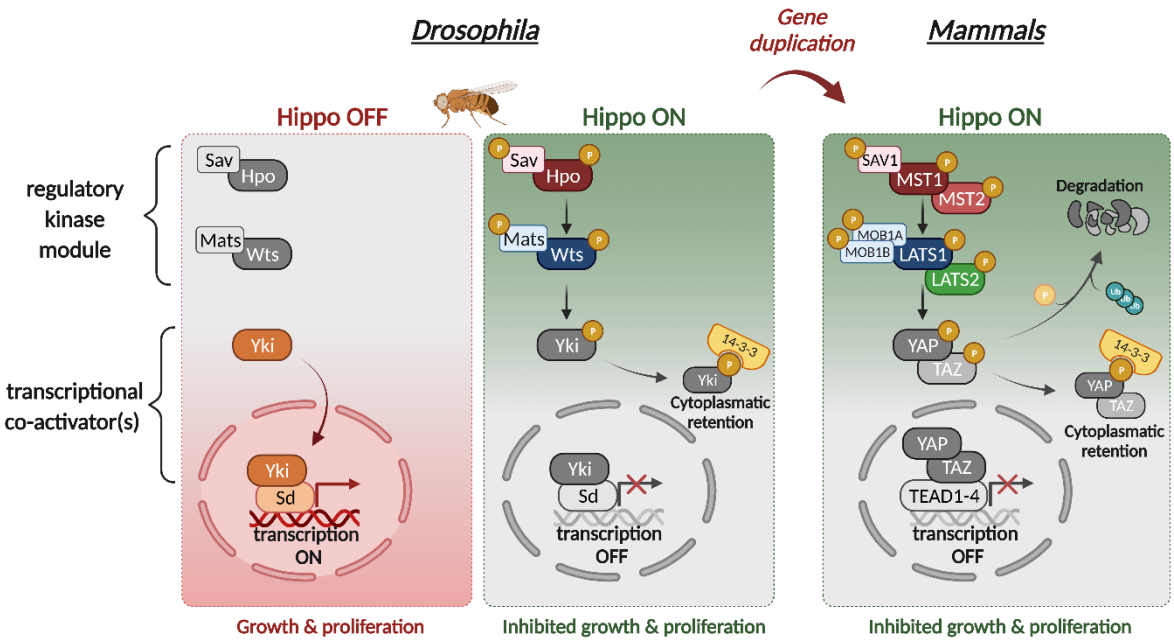

Figure 1: The Hippo signaling pathway in *Drosophila melanogaster* and mammals. The left and middle panels show the Hippo signaling pathway in *Drosophila melanogaster* in an inactive (OFF) and active state (ON), respectively. The right panel shows the Hippo pathway in mammals in the active state. Proteins are shown either in colors or in grey, indicating the active or inactive state of the particular component, respectively. In the Hippo-OFF state, the kinase module is inactive, resulting in active Yorkie (Yki) that translocate into the nucleus facilitating target gene expression by binding to transcription factors such as Scalloped (Sd). In the Hippo-ON state, the core kinases MST1 and MST2 (ortholog: Hpo) phosphorylate and thereby activate LATS1 and LATS2 (ortholog: Wts) that in turn phosphorylate YAP and TAZ (ortholog: Yki). Each kinase is accompanied by a scaffold adaptor protein ensuring their full activity: MST1/2 build a signaling module with SAV1 and LATS1/2 form a complex with the adaptor proteins MOB1A/B. LATS1/2-induced phosphorylation prevents YAP/TAZ binding to transcription factors such as TEAD1-4 (ortholog: Sd). Distinct phosphorylation sites negatively regulate YAP/TAZ activity either by nuclear exclusion or proteasomal degradation. The latter phosphorylation site is recognized by CK1, which in turn adds an additional phosphorylation that is recognized by SCFβ-TRCP E3 ubiquitin ligase (not shown in this Figure). Subsequently, SCFβ-TRCP E3 ubiquitination leads to YAP/TAZ degradation (Dong *et al*, 2007; Zhao *et al*, 2007, 2010; Liu *et al*, 2010). Further abbreviations: SAV1, Protein salvador homolog 1; MST1/2 - also known as STK4/3, Mammalian STE20-like protein kinase 1/2, serine/threonine-protein kinase 4/3; MOB1A/B, MOB kinase activator 1A/B; LATS1/2, Large tumor suppressor 1/2; YAP - short for YAP1, Yes-associated protein 1; TAZ, transcriptional coactivator with PDZ-binding motif - also known as WWTR1, WW domain-containing transcription regulator protein 1; TEAD1-4, Transcriptional enhancer factor TEF-1 -4; P, phosphorylation site; Ub, ubiquitin modification. Figure was created with BioRender.com.

The emerging roles in the control of organ size and growth, proliferation, and apoptosis stimulated intense research of the Hippo signaling pathway in the past decades. It became evident that the Hippo pathway core components are evolutionary highly conserved from flies to mammals (Halder *et al*, 2011; Chen *et al*, 2020). Moreover, during evolution, the *hpo, wts, and yki* loci underwent duplications leading to the emergence of two paralogs for each gene in mammals, which likely gave way for an expansion of their repertoire of molecular activities (**Figure 1**). Thus, in mammals, the core kinases MST1 and MST2 (mammalian STE20-like protein kinase 1 and -2, Hpo orthologs), and LATS1 and LATS2 (large tumor suppressor 1 and -2; Wts orthologs) control the activity of the two downstream oncogenic transcriptional co-activators YAP and TAZ (Yes-associated protein, also known as YAP1, and transcriptional co-activator with PDZ-binding motif, also known as WWRT1; Yki orthologs) (Yabuta *et al*, 2000; Hori *et al*, 2000; Halder *et al*, 2011). Interestingly, ectopic expression of human *LATS1* rescues mutant *lats* mosaic flies (Tao W. 1999), illustrating the high conservation and the strength of the *Drosophila* model for studying LATS functions.

In mammals, upon Hippo pathway activation, the core kinases MST1 and MST2 phosphorylate and thereby activate LATS1 and LATS2 that in turn phosphorylate and thereby inhibit YAP and TAZ - in analogy with *Drosophila* (**Figure 1**). LATS1/2-mediated

phosphorylation negatively regulates YAP/TAZ activity by two critical phosphorylation sites resulting in either nuclear exclusion (YAP^{S127}, TAZ^{S89}) or in proteasomal degradation (YAP^{S381}, TAZ^{S311}). The latter phosphorylation sites are recognized by CK1, which in turn adds an additional phosphorylation. Subsequently, SCFβ-TRCP E3 recognizes both phosphorylation sites which leads to ubiquitination and thus YAP/TAZ degradation (Dong *et al*, 2007; Zhao *et al*, 2007, 2010; Liu *et al*, 2010).

In a wide range of cancers, the repression of the oncogenes YAP and TAZ is lost, resulting in hyperactivation and tumor formation by aberrant cell proliferation, resistance to cell death, reprogramming of non-stem tumor cells to cancer stem cells, induction of chemoresistance, and metastasis (Harvey *et al*, 2013; Zanconato *et al*, 2016). Surprisingly, the aberrant YAP/TAZ activation cannot be explained by somatic mutations in the core effectors of the Hippo pathway, since these are relatively rare in human tumors (Barron & Kagey, 2014; He *et al*, 2021). Yet, gene amplification and epigenetic modulations have been found to be one cause for YAP/TAZ hyperactivation in many cancers (Harvey *et al*, 2013; He *et al*, 2021). However, neither under physiological conditions nor in the context of cancer, the Hippo pathway has been fully understood. Thus, it is essential to not only focus on the oncogenes YAP/TAZ but also gain full insights into the tumor suppressor kinases that directly control essential functions such as organ growth, cell proliferation, and apoptosis by keeping the oncogenes in check.

1.1.2. LATS1 and LATS2: shared and distinct functional roles beyond the Hippo pathway

In recent years, more attention was brought towards the Hippo-independent roles of LATS1 and LATS2 (Visser & Yang, 2010a; Hergovich, 2013; Furth & Aylon, 2017). Interestingly, the two paralogues have been shown to be involved in essential mechanisms such as **cell cycle regulation**, the **maintenance of genome stability**, **control of cell proliferation,** and **cell death,** as well as **cell differentiation** (Section 1.1.2.3). Intriguingly, in contrast to their role as tumor suppressors, there have been a few studies, implying LATS1 and LATS2 in **growth-promoting roles** (Section 1.1.2.4).

Classically, since both paralogues are involved in the same biological processes, LATS1 and LATS2 have long been considered functionally redundant proteins, often referred to as “LATS1/2” or ”LATS”. Indeed, LATS1 and LATS2 share 85% amino acid sequence identity in

their kinase domain (Yabuta *et al*, 2000; Hori *et al*, 2000). Moreover, they display the highest degree of homology to each other within the AGC family of serine/threonine kinases (Visser 2010). Therefore, the paralogues have long been considered redundant. However, by comparing the overall amino acid sequence, they only share 51% sequence similarity which casts doubt on their total redundancy (Hori *et al*, 2000). Indeed, there is emerging evidence that both LATS1 and LATS2 can act independently from each other (Visser & Yang, 2010a; Hergovich, 2013; Furth & Aylon, 2017). This is underlined in many aspects such as their **distinct individual roles in mouse embryogenesis** (Section 1.1.2.1), their **differential gene expression levels** in various tissue and cancer cell lines, their **differences in subcellular localization**, ultimately resulting in their **distinct preferences of binding partners** (Section 1.1.2.2).

These shared and distinct functions of LATS1 and LATS2 beyond the Hippo pathway will be outlined briefly in the following section.

1.1.2.1. LATS1 and LATS2: distinct roles in mouse embryogenesis

Gene knockout studies in mice are a powerful tool to assess the functional role of a gene and to test the hypothesis of whether two genes are functionally redundant. Interestingly, deletion of *Lats2* is embryonic lethal within the first 12.5 days of embryogenesis (McPherson *et al*, 2004; Yabuta *et al*, 2007), whereas, in contrast, loss of *Lats1* is not (St John *et al*, 1999). More specifically, lethality in mice lacking *Lats2* was caused by aberrant proliferation, deregulation of mitosis, and thereby loss of genomic integrity (McPherson *et al*, 2004; Yabuta *et al*, 2007). *Lats1* knock-out mice are viable but suffer from strong impairments, such as infertility, growth retardation, and lack in the development of mammary glands. Additionally, they develop soft-tissue sarcomas and ovarian stromal cell tumors and show increased sensitivity to carcinogens (St John *et al*, 1999).

Taken together, these studies illustrate that, while both LATS1 and LATS2 are essential for embryonic development, their functions are partly distinct.

1.1.2.2. *LATS1 and LATS2: gene expression levels, localization, binding partners*

The ability of proteins to function within a cell is determined by their expression levels and their subcellular localization allowing for specific protein-protein interactions. Comparing publicly available data from the human protein atlas (https://www.proteinatlas.org/), it

becomes evident that LATS1 and LATS2 exhibit differential RNA and protein expression levels in various healthy and cancer tissues. This is exemplified by LATS1 showing high levels in e.g. endocrine tissue, liver and gallbladder, female tissue, and muscle tissue, whereas LATS2 has high protein expression levels in the brain and male tissue. Moreover, comparing RNA expression levels from different cancer entities, LATS1 and LATS2 show differential expression, although general expression is usually low.

Besides to global expression levels of a protein, the localization within the cell helps to elucidate its function. Classically, in the context of the canonical Hippo pathway, both LATS1 and LATS2 have been described to be activated while being tethered to the plasma membrane, and they subsequently phosphorylate YAP/TAZ in the cytoplasm (Yin *et al*, 2013; Hirate *et al*, 2013; Yang *et al*, 2004; Li *et al*, 2003).

In their role as tumor suppressors beyond the Hippo signaling, however, both shared and differential localization patterns have been observed for LATS1 and LATS2, determined by their individual functional requirements. The regulation of mitosis requires both LATS1 and LATS2 to localize at the mitotic apparatus and centrosomes (Nishiyama *et al*, 1999; McPherson *et al*, 2004). Moreover, both are able to localize in the nucleus (Furth & Aylon, 2017). In particular, it has been described that dependent on the cell lineage, LATS1/2 localize either in the nucleus or in the cytoplasm of mammary epithelial cells, regulating breast cell fate (Britschgi *et al*, 2017). Besides, most of the other nuclear functions have been described for LATS2 only. For example upon induced mitotic or oncogenic stress, only LATS2 (but not LATS1) translocates from centrosomes to the nucleus, resulting in maintaining chromosomal integrity via a Lats2–Mdm2–p53 axis (Aylon *et al*, 2006). Moreover, it has been shown that LATS2 counteracts oncogenic Wnt-signaling by inhibiting the interaction between BCL9 and β-catenin, thereby restricting β-catenin-induced transcription (Li *et al*, 2013). These studies show that dependent on different cellular stimuli LATS1 and LATS2 have different localizations, strongly supporting the notion of being involved in different cellular processes.

Along these lines, the localization patterns of a protein are determined by its protein-interaction partners. By summarizing two MS-based studies of the Hippo pathway interactome, Furth and Aylon compiled an overview of the LATS1 and LATS2 protein binding partners (Couzens *et al*, 2013; Wang *et al*, 2014; Furth & Aylon, 2017). As expected, proteins associated with Hippo signaling, tight and gap junctions were enriched among the 104

shared protein binding partners. The latter can be explained by the upstream regulation of LATS1 and LATS2. Interestingly, however, approximately 400 binding partners were exclusively found as binding partners of either one of the two paralogues. From these ~400 binding partners only 15 were unique LATS1 binding partners, involved in estrogen signaling. Whereas LATS2 comprised an interactome of 383 unique binding partners, involved in processes related to cell cycle and metabolism and p53.

Collectively, these studies are valuable sources for characterizing LATS1 and LATS2 functions within and beyond Hippo signaling and indicate unique regulation and activity of the paralogues.

1.1.2.3. LATS1 and LATS2: in cell cycle regulation, genome stability and induction of apoptosis

In 1855, Rudolf Virchow proposed one of the key dogmas in cell biology "omnis cellula e cellula" – every cell must derive from a pre-existing cell. Over 160 years of research later, we know that cell division is accomplished in a tightly controlled process. In eukaryotes, the cell cycle can be divided into four phases: gap or growth phase 1 (G_1), synthesis phase (S), gap or growth phase 2 (G_2), and mitose phase (M). In S phase, DNA synthesis takes place, which is surrounded by G_1 and G_2 phases. In G_1 phase, cells integrate growth signals, thereby obtaining mass by duplication of cell content. In G_2 phase, after DNA synthesis, the duplicated DNA needs to be organized and prepared for chromosome segregation. These three phases are summarized as the interphase, preparing the cell for the equal division of cell material in mitosis, together with the physical division in cytokinesis, to form two daughter cells (Barnum & O'Connell, 2014).

In 1902, Theodor Boveri predicted that errors in mitosis are at the origin of cancer. Therefore, to ensure the integrity of the genome, cell cycle checkpoints can halt cell cycle progression, ensuring that earlier processes are completed without any error (Hartwell & Weinert, 1989; Kastan & Bartek, 2004). At the G_1/S checkpoint, the DNA is checked for any damage such as double-strand breaks, before proceeding with the initiation of replication in S phase (Niida & Nakanishi, 2006). At the G_2/M checkpoint, the completion of DNA replication is checked before proceeding with chromosome alignment in early mitosis. Finally, the mitotic spindle checkpoint ensures proper chromosome alignment and integrity of the spindle apparatus (Gorbsky, 2001). In case of defects, the checkpoint is activated,

leading to a transient cell cycle arrest, until the defect is repaired. However, prolonged activation of the spindle checkpoint can lead to mitotic exit, i.e. cell division without chromosome segregation, resulting in a single surviving tetraploid cell. However, these tetraploid cells are prevented from entering into the next S-phase and enter senescence instead, thereby closing the circle at the G_1/S checkpoint (Margolis *et al*, 2003).

Over 1000 proteins are involved in the cell cycle, orchestrating its progression (Fischer & Müller, 2017). Among them, the cyclin-dependent kinases (CDKs) are the central machines driving cell cycle progression. However, the activity of the CDKs is determined by the conjugation with a corresponding cyclin, activation by cyclin activating kinases (CAK), or inhibition by cyclin-dependent kinase inhibitor proteins (CKI), or inhibitory phosphorylation events (Barnum & O'Connell, 2014).

LATS1 and LATS2 have been described to be involved in the cell cycle by regulating checkpoints and interacting with key players such as Aurora A (AurA) and Aurora B (AurB) or the anaphase-promoting complex/cyclosome (APC/C) (**Figure 2**).

In the **G_1/S checkpoint**, both LATS1 and LATS2 have been implicated in the inhibition of cyclin E/CDK2, induced by different stress triggers (Matsuoka 2007, Pefani D 2014, Li Y 2003) (**Figure 2**). Yet, LATS2 was found to exclusively contribute to G_1/S cell cycle control through its interaction with the tumor-suppressive DREAM complex and p53. The DREAM (dimerization partner (DP), RB-like, E2F and MuvB) complex is a large transcription complex that has been found to promote senescence by repressing genes required for cell cycle progression (Litovchick *et al*, 2011). Interestingly, LATS2 phosphorylates and thereby activates DYRK1A, which in turn phosphorylates LIN52, a component of MuvB. This phosphorylation event ultimately triggers the assembly of the DREAM complex. Thus, by binding either to E2F- or CHR- promotor elements, the DREAM complex represses proteins of G_1/S or G_2/M phase, respectively (Sadasivam & DeCaprio, 2013; Fischer & Müller, 2017). Moreover, it has been shown that there is a positive feedback loop between LATS2 and p53 leading to p53- dependent G_1/S checkpoint activation (Aylon *et al*, 2006, 2009, 2010). In particular, upon oncogenic, metabolic, and developmental stress, LATS2 ensures the stabilization of p53 by inhibition of the p53-inhibitor MDM2 (E3 ubiquitin-protein ligase Mdm2). In turn, p53 enhances *LATS2* gene transcription (Kostic & Shaw, 2000; Aylon *et al*, 2006, 2010).

In the **G_2/M checkpoint**, both kinases have been shown to negatively regulate the Cyclin A/B-Cdc2 complex, yet in mechanistically distinct ways (**Figure 2**). (Please note that Cdc2 is in later studies referred to as CDK1). In two studies it could be shown that overexpression of LATS1 blocks G_2/M transition by inhibiting the kinase activity of the Cyclin A/B-Cdc2 complex. One study in HeLa suggested LATS1 binding to Cdc2 and thereby blocking its ability to bind Cyclin A/B (Tao *et al*, 1999; Yang *et al*, 2001). Moreover, they could show that LATS1 overexpression leads to Caspase-3-activity, ultimately resulting in the induction of apoptosis. Another study in MCF7 cells showed that LATS1 overexpression causes a drop in cyclin A and cyclin B protein levels, and moreover, preventing tumor formation in nude mice (Xia *et al*, 2002). Here, apoptosis was induced by the upregulation of BAX protein levels. Consistently, both studies could show that LATS1 overexpression causes G_2/M arrest ultimately resulting in the control of tumorigenesis by inducing apoptosis.

As mentioned before, LATS2 overexpression also causes a G_2/M arrest by inhibiting Cyclin B-Cdc2 activity, yet, by a distinct mechanism. It has been shown that overexpression of LATS2 in HeLa cells caused an increase in Cdc25C phosphorylation, an activating kinase of Cdc2, enhancing its inhibition and thereby preventing its ability to activate Cyclin B-Cdc2 (Kamikubo *et al*, 2003). Of note, also LATS2 has been implicated in the induction of apoptosis, however, instead of upregulating anti-apoptotic signals, LATS2 was shown to downregulate the pro-apoptotic regulators Bcl-2 and Bcl-x(L) instead (Ke *et al*, 2004).

Intriguingly, in the **M phase**, the paralogues have been found to be involved in cell cycle progression rather than arrest (**Figure 2**). Both by interaction with AurA and AurB, as well as with the APC/C complex. Interestingly, for the LATS1 and LATS2 interaction with AurA and AurB distinct roles have been proposed.

The Aurora kinase family, consisting of the three homologs AurA, AurB, and Aurora C (AurC), fulfills pivotal roles in the onset of mitosis, the spindle assembly, and cytokinesis (Nigg, 2001; Salaun *et al*, 2008; Willems *et al*, 2018). By interaction with or phosphorylation of other cell cycle proteins, they determine the progression through the cell cycle to avoid genomic instability and aneuploidy. In particular, AurA ensures G_2/M transition by promotion of centrosome maturation and mitotic spindle assembly in early mitosis. On the other hand, AurB and AurC, as members of the so-called “chromosome passenger complex”

(CPC) ensure proper chromosome binding to kinetochores and chromosome segregation in middle to late mitosis (Willems *et al*, 2018).

Interestingly, it has been shown that LATS1 and LATS2 are crucial players in this process, proposed as the AurA-LATS1/2-AurB (ALB)-axis (Yabuta *et al*, 2011) (**Figure 2**). Accordingly, it has been shown that AurA phosphorylates LATS2, thereby causing LATS2 to translocate to the central spindle. Here LATS2 is accompanied by LATS1 which in turn phosphorylates AurB, ensuring correct chromosome segregation (Yabuta *et al*, 2011).

Another key player navigating cells through the cell cycle is the anaphase-promoting complex/cyclosome (APC/C). In budding yeast, it has been described that Dfb2, the homolog to human LATS1, activates APC/C^{Cdh1} as part of the Mitotic Exit Network (MEN). In particular, Dfb2 phosphorylates and thereby activates the phosphatase Cdc14, which in turn removes inhibitory phosphorylation from Cdh1 (Zachariae *et al*, 1998; Mohl *et al*, 2009; Zhou *et al*, 2016). In line with this, it was shown that LATS1 and MOB1A are components of the mammalian MEN (Bothos *et al*, 2005). However, in contrast to budding yeast, the modulation of APC/C activity by LATS1 and LATS2 slightly differs in mammals, i.e. that LATS1 and LATS2 positively modulate the activity of APC/C^{Cdh1} by directly phosphorylating the APC/C subunit APC6 (Masuda *et al*, 2015). Interestingly, in another study it has been shown that active APC/C^{Cdh1} targets LATS1 and LATS2 for degradation in G_1 phase. Subsequently, the downregulation of LATS1 and LATS2 allows YAP/TAZ to peak in G_1 and thereby promote cell cycle progression (**Figure 2**). As a result, APC/C^{Cdh1} triggers an intrinsic oscillation of LATS1/2 and YAP/TAZ during cell cycle progression (Kim *et al*, 2019). However, whether and how the activation of APC/C by LATS1/2 and the degradation of LATS1/2 by the APC/C complex are interconnected, remains to be answered.

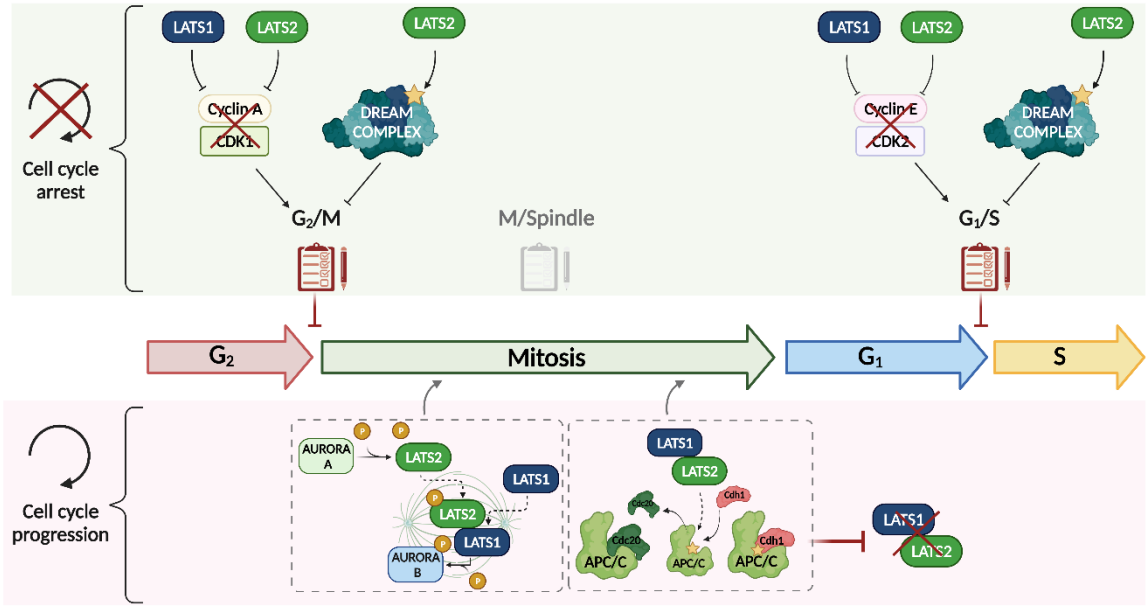

Figure 2: LATS1 and LATS2 in the cell cycle. Upper panel (green background color): role of LATS1 and LATS2 in cell cycle control, potentially inducing cell cycle arrest by blocking G_1/S and G_2/M transition. Bottom panel (red background color): role of LATS1 and LATS2 in cell cycle progression by interaction with Aurora A (AurA) and Aurora B (AurB) in the AurA-LATS1/2-AurB (ALB)-axis, and by promoting anaphase-promoting complex/cyclosome APC/C^{Cdh1}. Further details are explained in this section. Figure was created with BioRender.com.

Together these studies illustrated the pivotal role of LATS1 and LATS2 in both the control of the cell cycle, leading to cell cycle arrest or the induction of apoptosis as well as the promotion of the cell cycle leading to cell cycle progression. These dual roles appear to be orchestrated between LATS1/2 and key cell cycle regulators, such as cyclin-kinase complexes, the Aurora kinase, or the APC/C complex, as well as pro- and anti-apoptotic effectors. Interestingly, however, LATS1 and LATS2 also have non-redundant functions, further increasing the complexity of their functional roles. Also, the direct phosphorylation targets of LATS1/2 have remained unknown and require future investigations.

1.1.2.4. *LATS1 and LATS2: Tumor promoting function*

Originally, LATS1 and LATS2 have been known as tumor suppressors. This notion is strengthened by the fact that in most cancers LATS1/2 expression levels are decreased (Sharif & Hergovich, 2018) (described in more detail in Section 1.1.3). However, in some cases, such as nasopharyngeal carcinoma or acute myeloid leukemia (AML), the expression levels of LATS2 are elevated, and therefore might support tumor growth (Zhang *et al*, 2010; Gholami *et al*, 2014). Accordingly, there are studies demonstrating LATS1/2 promoting cell

cycle growth or epithelial-mesenchymal transition (EMT) in a cell context-dependent manner. In particular, LATS2 has been found to suppress DNA-damage-induced apoptosis by phosphorylation and thereby inactivating the kinase c-Abl (Reuven *et al*, 2013). Intriguingly, in this context YAP is in conjugation with p73, thereby functioning as a tumor suppressor. This p73-YAP complex is activated by the phosphorylation of c-Abl (Levy *et al*, 2008; Agami *et al*, 1999). Thus, by LATS2-induced inhibition of c-Abl, p73-YAP is not activated, thereby resulting in the inhibition of apoptosis (Reuven *et al*, 2013). In another study, the tumor-suppressive function of YAP was shown in lung squamous cell carcinoma. Consequently, in this study LATS1/2-induced inhibition of YAP promoted tumor growth (Huang *et al*, 2017a). Together, these studies illustrate that when YAP functions as a tumor suppressor, LATS1/2 activity can lead to tumor promotion. Therefore, whether LATS1/2 functions in a pro- or anti-apoptotic manner is dependent on YAP binding to pro- or anti-apoptotic transcription factors, such as p73.

Besides, however, it could be shown that LATS1 and LATS2 can function as a tumor promoters, independently of YAP or the Hippo pathway. In particular, LATS2 was described to induce EMT, in mouse and zebrafish embryos by positively modulating the activity of Snail1 (Zhang *et al*, 2012). Moreover, LATS1/2 have been shown to suppress cancer immunity in murine syngeneic tumor models of three different cancer types (melanoma, head and neck squamous cell carcinoma, and breast cancer). In particular, it could be shown that loss of LATS1/2 resulted in the activation of innate and adaptive immune signaling, ultimately reducing tumor growth and enhancing vaccine efficacy (Moroishi *et al*, 2016). Furthermore, in another study, deletion of LATS1/2 in mouse cancer cell lines enhanced anchorage-independent growth in most cell lines. This function of LATS1/2 in cell growth appears to be cell-type as well as attachment-dependent (Pan *et al*, 2019).

Collectively, these studies illustrate that the classical roles for LATS1/2 as tumor suppressors and for YAP/TAZ as oncogenes, might not be universal. Therefore, it is important to determine the function of LATS1/2 and YAP/TAZ in the respective cellular context before choosing a potential cancer therapy. Moreover, the fact that LATS1/2 can act independently of YAP or the Hippo pathway adds further complexity to the role of LATS1/2 as a regulatory kinase.

1.1.3. LATS1 and LATS2 in cancer

In order to survive, tumor cells have to keep tumor suppressors in check. This can be realized on different regulatory levels and with a different mechanism such as loss-of-function mutations of the tumor suppressor, or, gain-of-function mutations in an oncogene. Also, tumor cells utilize epigenetic silencing of tumor suppressors by various mechanisms.

Interestingly, somatic mutations in LATS1/2 or in upstream regulators are rare (Harvey 2013). Exceptions are two positive upstream regulators of LATS1/2 in the Hippo pathway, *NF2* (also known as *Merlin)* and *RASSF1A* which have been shown to be deregulated in many cancers (Harvey *et al*, 2013; Grawenda & O'Neill, 2015; Barron & Kagey, 2014).

According to the Catalogue of Somatic Mutation in Cancer (COSMIC) database (Forbes *et al*, 2011), only 1.9% or 2.3% of more than 53,000 unique human cancer samples harbor mutations in *LATS1* or *LATS2*, respectively. It could be shown that some of these mutations impair the kinase activity of LATS1/2 and thereby the ability to inhibit the oncogenes YAP/TAZ (Yu & Guan, 2013). However, for most of the mutations, further investigations are required to distinguish between passenger or driver mutations, as well as define their impairment on cell signaling. Overall, however, somatic mutations seem not to be the dominant mechanism to impair LATS1/2 activity in cancers. Instead, in numerous human cancers, the expression levels of LATS1 and LATS2 are decreased (summarized by Sharif & Hergovich, 2018), indicating their important role as tumor suppressor kinases. In some of these cancers, the underlying mechanism of decreased expression levels is epigenetic silencing of the promotor by hypermethylation or by binding of long non-coding RNAs (lncRNAs). In particular, hypermethylation was observed for either LATS1 or LATS2 alone, or for both together, in various cancers (summarized by Furth & Aylon, 2017). Promotor silencing by lncRNAs, however, has only been described primarily for LATS2, i.e. in gastric, non-small-cell lung cancer, acute myeloid leukemia (AML) (Wan *et al*, 2016; Shi *et al*, 2018; Li *et al*, 2016; Huang *et al*, 2017b; Feng *et al*, 2020). Of note, besides promotor silencing, promotor activation of LATS2 by lncRNAs has recently been described (Sun *et al*, 2020). In that study, gastric cancer progression was inhibited by the lncRNA LATS2-AS1-001 which was shown to activate LATS2 and thereby inhibit YAP. Although the PIK3CD-AS1 was described to promote the expression of LATS1, in this case, this promotion happened

indirectly by competitive binding of the inhibiting miR-566 rather than by direct binding to the LATS1 promoter region (Song *et al*, 2019). Therefore, the direct regulation of gene expression by lncRNAs seems to be more pronounced for LATS2. Accordingly, numerous micro RNAs (miRNA) have been shown to bind LATS1/2 transcripts, and some of these negatively modulate mRNA stability in the context of cancer (summarized by Furth & Aylon, 2017). However, further investigations will be required to elucidate the functional roles of these miRNAs on LATS1/2.

Collectively, these studies show the high relevance of LATS1/2 in numerous cancers, reflected by the differential mechanism on multiple layers which downregulate both jointly or individually the expression of LATS1 and/or LATS2.

1.1.3.1. *Specific functional roles of LATS1 and LATS2 in breast cancer subtypes*

Among different cancer types, LATS1 and LATS2 show a strong prevalence of deregulation in breast cancer. This is exemplified by diverse mechanisms of downregulation, such as loss of heterozygosity (Fujii *et al*, 1996; Theile *et al*, 1996; Noviello *et al*, 1996; Lee *et al*, 1988), as well as promoter hypermethylation (Takahashi *et al*, 2005) or upregulation of miRNA targeting LATS1 or LATS2 (Hua *et al*, 2016; Xu *et al*, 2019). In line with this, a comparison of relative expression levels of LATS1/2 with matched healthy tissue from The Cancer Genome Atlas (TCGA) breast invasive carcinoma dataset revealed significant downregulation of both kinases in breast cancer (Furth *et al*, 2018). Together, this shows the importance of LATS1/2 in breast cancer.

However, it should be kept in mind that besides arising from the same entity, i.e. the mammary glands, the mutational signatures shaping the characteristics of these tumors are extremely diverse. Therefore, to understand the role of LATS1 and LATS2 in breast cancer, it is advisable to distinguish between the different molecular subtypes. These molecular subtypes of breast cancer are defined by the presence of three hormone receptors, which are estrogen receptor (ER), progesterone receptor (PR), and the receptor tyrosine-protein kinase erbB-2 (ERBB2, also known as HER2). Thereof, classically four breast cancer subtypes are defined, (i) luminal A (ER^+, $PR^{+/-}$, $HER2^-$), (ii) luminal B (ER^+, $PR^{+/-}$, $HER2^{+(/-)}$), (iii) HER2-positive (ER^-, PR^-, $HER2^+$), and (iv) triple-negative, also referred to as basal-like (ER^-, PR^-, $HER2^-$) (Goldhirsch *et al*, 2011). Thus, the first orientation for treatment

options, such as hormone therapy, is given by the molecular subtype. However, the immense diversity of breast cancer subtypes, and thereby the treatment options, goes beyond the status of the hormone receptors. Therefore, defining subtype-specific mutational signatures is indispensable.

Interestingly, by comparing LATS1 and LATS2 expression levels in breast cancer subtypes, it could be shown that significant downregulation of LATS1 was observed in basal-like breast cancer, whereas LATS2 was shown to be most significantly downregulated in the luminal B subtype (Furth *et al*, 2018). Along these lines, in this study they could show that in MMTV-PyMT mice (mouse mammary tumor virus-polyoma middle tumor-antigen, which is a mouse model of breast cancer), mammary-specific deletion of *Lats2* enhances the luminal B tumorigenesis and metabolic rewiring of the tumor cells. *Lats1* deletion, on the other hand, reprogrammed luminal B tumors towards basal-like characteristics. Accordingly, low LATS1 levels correlated with hormone therapy resistance. Collectively, this study indicates that each of the kinases plays different tumor-suppressive roles in basal-like and luminal B breast cancer backgrounds.

Based on the pivotal role of LATS1 and LATS2 in breast cancer, and moreover, their unique roles in different breast cancer subtypes, the luminal B breast cancer cell line ZR75.1, and the luminal A breast cancer cell line MCF7 were chosen for this study. In addition, the cell line MCF10A was studied, serving as a model for the non-tumorigenic genetic background. Together these cell systems allowed for insights into LATS1 and LATS2 functional activities in physiological as well as tumorigenic breast tissue backgrounds.

1.2. Quantitative mass spectrometry-based proteomics in signaling pathway analysis

The word “Protein” is derived from the Greek word “Proteios” that can be translated as “the first rank” or “of utmost importance” (Zimmerman & Snow, 2012; Cristea *et al*, 2004). It was used the first time in 1838 by the Swedish physician and chemist Jöns Jakob Berzelius, suggesting it as a term to the Dutch chemist Gerardus Johannes Mulder who first described proteins chemically (Hartley, 1951). The word emphasizes the importance of these biomolecules in living systems as they serve pivotal functions in essentially all biological processes. Often referred to as the “workhorses” of a cell, proteins provide structure and stability, catalyze metabolic reactions, ensure communication with the environment by receiving, processing, and transmitting information inside and outside the cell.

The entirety of all proteins expressed by a cell or organism at any given time is called the proteome, coined by the Australian scientist Marc Wilkins in 1994 (Wilkins *et al*, 1996). It is a blend of the word protein and genome alluding that the genome encodes for all the proteins that can be expressed by a cell. In the genome, the complete set of genetic information is stored in the form of deoxyribonucleic acid (DNA). As the initial product, the DNA is selectively transcribed into ribonucleic acid (RNA), which in its entirety is referred to as transcriptome. Ultimately, as a final product, the RNA transcript is translated into proteins, as the endpoint of the genetic information flow (Crick, 1958). While the genomic information is static, the proteome is highly dynamic, illustrated by the classical example of the transformation of the caterpillar, into a chrysalis and finally into a butterfly. All three developmental stages have the same genome, however, they differ in their proteome, resulting in these discrete phenotypes. These different phenotypes can be explained by various regulatory mechanisms and events, increasing the complexity throughout the genetic information flow from DNA over RNA to proteins. For instance by the accessibility of genomic regions, defining the genes that can be transcribed, by the splicing of mRNA transcripts that gives rise to different proteoforms, or by the stability of mRNA transcripts that can be influenced by post-transcriptional modifications (Janssen *et al*, 2018; Wilkinson *et al*, 2020; Zhao *et al*, 2016). Finally, the addition of biochemical moieties to specific residues of proteins, adds another layer of information and complexity. These so-called

post-translational modifications (PTMs) serve as molecular switches that can direct the localization, stability, and function of a protein (Dunphy *et al*, 2021).

The large-scale study of proteins and their PTMs, referred to as Proteomics, requires a technique to systematically identify and quantify proteins and their modifications. The discovery and development of protein ionization methods by John Fenn (for which he was honored with the Nobel Prize in 2002), together with the sequencing and decoding of the human genome by the International Human Genome Sequencing Consortium, paved the way for a new era in the field of molecular biology – mass spectrometry (MS)-based proteomics (Yamashita & Fenn, 1984; Lander *et al*, 2001; Craig Venter *et al*, 2001).

Major advances in the field over the last decades enabled insights into the composition, structure, and function of proteins (Choudhary & Mann, 2010; Liu *et al*, 2016). Moreover, MS-based proteomics allows us not only to learn about the composition of the proteome in a given system but also about temporal and spatial changes (Yang *et al*, 2015). Investigating proteomic responses to specific signaling network perturbations, providing valuable insights into cell signaling in health and disease, are driving advances in network-based diagnosis and precision medicine (Duarte & Spencer, 2016). This makes MS-based proteomics an indispensable technology, bridging the blind spot between genotypes and phenotypes by identifying and quantifying thousands of proteins and their modifications in an accurate and unbiased manner (Steen & Mann, 2004; Choudhary & Mann, 2010).

1.2.1. Basics of mass spectrometry-based proteomics

1.2.1.1. A classical "bottom-up" approach

"Top-down", "middle-down" and "bottom-up" are the three main approaches employed for the identification and characterization of proteins and their PTMs by MS-based proteomics (Moradian *et al*, 2014). In this order, the strategies start from intact, over partially digested, to fully digested proteins - each approach having advantages and disadvantages and serving different purposes.

In this study, we used a classical bottom-up approach, also referred to as "shotgun proteomics", which is the most widely used technique in MS-based proteomics and will be briefly explained in the following section.

A classical bottom-up approach usually starts with the extraction of proteins from cultured cells or tissue by protein lysis (**Figure 3**). Extracted proteins are enzymatically digested into peptides (with an average length of 14 amino acids (Burkhart *et al*, 2012)), by proteases such as trypsin, which is most commonly used because of its high proteolytic activity and cleavage specificity. Trypsin specifically cuts carboxyl-terminal after unmodified lysines and arginines, providing doubly charged peptides (Olsen *et al*, 2004). To decrease the sample complexity and thereby increase sample depth, optional fractionation techniques can be applied on the protein or peptide level. In this study, high pH reversed-phase liquid chromatography (hpH-RPLC) was used as an “off-line” (i.e. not directly connected to a mass spectrometer) fractionation step to separate peptides by hydrophobicity at high pH - a separation technique orthogonal to low pH reversed-phase liquid chromatography (lpH-RPLC) (Baghdady & Schug, 2019). Subsequently, the samples are injected onto a microscale capillary of a high-performance liquid chromatography (HPLC) instrument which is “on-line” coupled to an MS instrument. By using a low pH solvent gradient (lpH-RPLC) the peptides are separated in a second dimension. Over the course of the gradient, peptides elute according to their physico-chemical properties at specific retention times from the HPLC column and are converted from liquid- into gas-phase ions by electrospray ionization (ESI) (Steen & Mann, 2004). Once inside the mass spectrometer, the ionized peptide molecules are guided and manipulated by electric fields. In a first scan (MS^1) the masses of the intact peptide ions (precursors) are measured providing specific information about mass over charge (m/z) for each peptide, as well as signal intensities which can be used as abundance estimates. Subsequently, selected precursor ions (usually the top10 most abundant) are fragmented by collision with an inert gas such as nitrogen. Upon collision, peptides break at their weakest bonds which are the amide bonds between amino acids. Depending on where the charge of the ion is retained, sets of fragment ions are generated, most prominently b-ions (extending from N-terminus) and y-ions (extending from C-terminus). These "product-ions" are analyzed in a second MS scan (MS^2). The generated MS^2 spectra are then used for the identification of the amino acid sequence of the peptides (Steen & Mann, 2004). Therefore search engines like SEQUEST (Eng *et al*, 1994) or MASCOT (Perkins *et al*, 1999) are used to compare experimentally acquired spectra against theoretical fragment spectra, determined by *in silico* digestion and fragmentation of a protein database. As a result, a probability-based ranking of matching peptide sequences

is created, which is based on the similarity of experimental and theoretical spectra (Liu 2007). To process the gathered MS^1 and MS^2 data there are many different softwares available, including the most widely used freely available software MaxQuant (Tsiamis *et al*, 2019; Cox & Mann, 2008). These software are employed to (i) find the MS^1 peaks of interest in the spectra ("feature finding"), (ii) match the MS^2 spectra to peptide sequences of databases using specific search engines, (iii) infer proteins based on identified peptides, and (iv) provide the peptide and protein quantification. Thereof a list of proteins and their relative abundance can be compiled - the starting point for subsequent downstream bioinformatic analysis and data interpretation (Sinha & Mann, 2020).

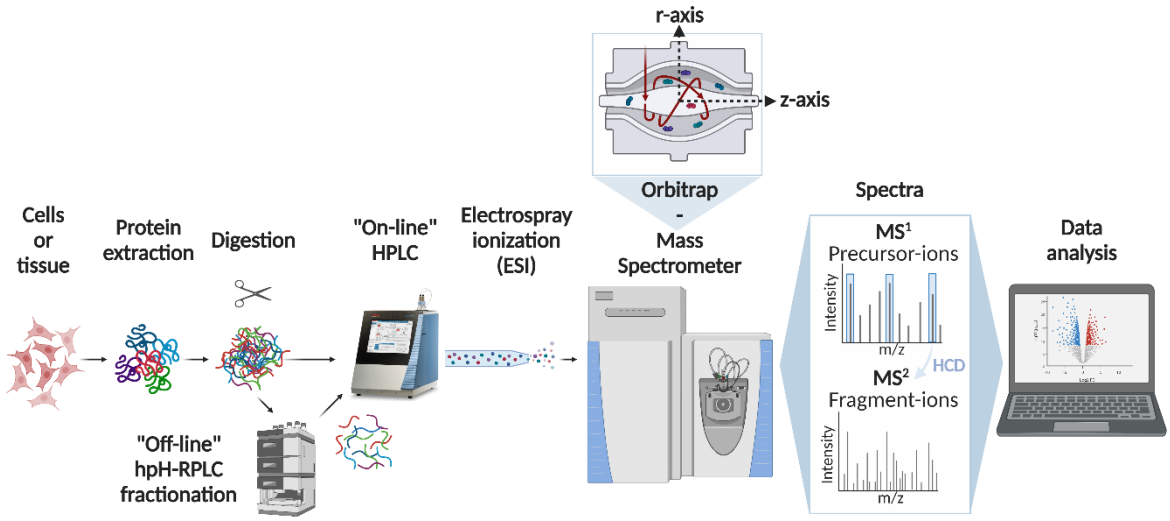

Figure 3: A classical bottom-up MS-based proteomics workflow. Starting from cell culture or tissue, proteins are extracted and enzymatically digested into peptides. Optional: the complexity of peptides can be reduced by "off-line" (i.e. not directly connected to a mass spectrometer) fractionation using high-pH reversed-phase liquid chromatography (hpH-RPLC). Peptides are then injected onto a microscale capillary of a high-performance liquid chromatography (HPLC) instrument which is "on-line" coupled to a mass spectrometer. Peptides eluting from the HPLC column are ionized and converted from liquid- into gas-phase ions by electrospray ionization (ESI) and are thereby transferred into the mass spectrometer (here: Q Exactive HF Hybrid Quadrupole-Orbitrap). Intact peptide ions, so-called precursor ions, are measured in the MS^1 scans, providing specific information about their mass over charge (m/z) and as well as signal intensities which can be used as abundance estimates. For MS^2 scans, selected precursor ions are fragmented into so-called product-ions, by collision with an inert gas, providing information on the peptide sequence. Gathered MS^1 and MS^2 scans are processed by specific software resulting in protein identifications and abundance estimations. Figure was created with BioRender.com.

1.2.1.2. Mass spectrometry instrumentation

Nowadays a plethora of mass spectrometers from different vendors are available on the market, all sharing three general components: an ion source, mass analyzer(s), and detector (s) (Aebersold & Mann, 2003). In an LC-tandem mass spectrometry (LC-MS/MS)

system used for proteomics, these components need to fulfill certain requirements, i.e. (i) ionization of the analyte molecules and their transition from liquid to gas phase, (ii) filtering of the ions based on their m/z, and (iii) selection and fragmentation of ions of interest for sequence analysis (MS^2). Covering a broad range of different requirements, a variety of mass analyzers with different underlying physical principles are used in MS instruments. As a measure to compare the performance of these instruments, usually four parameters are considered: mass accuracy, mass precision, resolution, and dynamic range. The mass accuracy is described as the deviation of the experimentally measured mass to the true mass. The mass precision describes the repeatability of measurements, i.e. the variation of detected masses between several measurements (Cox & Mann, 2009). The resolution is a measure of the ability to separate two neighboring mass spectral peaks (Marshall *et al*, 2013). And finally, the dynamic range is defined by the ratio between the weakest and strongest signal within a spectrum, reflecting the instrument's capability to distinguish between low and high signal intensities.

Several mass analyzers with various underlying physical principles are commonly used. These include time-of-flight (TOF) mass analyzers, quadrupole mass analyzers, linear ion traps, and orbitrap, all designed to separate ions based on their mass to charge ratio. Out of these, the newest and most advanced addition of high-resolution mass analyzers is the orbitrap. Based on the Kingdon trap (Kingdon, 1923), further development by Alexander Makarov resulted in the first orbital ion trap analyzer, which was presented at the American Society for Mass Spectrometry in 1999 (Makarov, 2000). As the name implies, in an orbitrap ions are trapped while oscillating around a central spindle electrode. The frequency of oscillation along the z-axis is proportional to the square root of the m/z of trapped ions (**Figure 3**). Finally, by applying Fourier transformation, axial oscillations of all ions can be converted into a mass spectrum displaying signal intensities over observed m/z. Since the oscillation frequency can be determined with high precision, it allows for high accuracy of the m/z values (Walther & Mann, 2010). Together with unprecedented precision and resolution, the orbitrap mass spectrometers represent an important breakthrough for modern analytical MS-based proteomics (Makarov, 2000). In 2005, the first commercially available Orbitrap mass spectrometer was launched - the LTQ Orbitrap, a hybrid instrument combining a linear ion trap with an orbitrap (Scigelova & Makarov, 2006; Olsen *et al*, 2005). Continuous technological improvements ever since allow for a possible maximum

resolution of 1,000,000 Full Width at Half Maximum (FWHM) at m/z 200 and a sub-1 parts per million (ppm) mass accuracy, implemented in the Orbitrap IQ-X Tribrid mass spectrometer, the newest instrument from Thermo Fisher Scientific, the exclusive vendor of orbitrap mass spectrometers.

In this study, two orbitrap instruments were used, namely the Q Exactive HF Hybrid Quadrupole-Orbitrap Mass Spectrometer (QE-HF) and the Orbitrap Fusion Tribrid Mass Spectrometer (Fusion). Both instruments combine quadrupoles and orbitraps (hybrid), whereas the Fusion comprises an additional linear ion trap (tribrid), allowing for parallelization of MS and MS^n analyses (Michalski *et al*, 2011; Senko *et al*, 2013).

1.2.2. Quantitative proteomics

In addition to the qualitative identification of proteins, MS-based proteomics also allows for the quantification of proteins. Depending on the information provided, absolute and relative quantification can be distinguished. While absolute quantification provides information about the exact concentration or amount of a protein within a sample, relative quantification aims to quantify the difference in abundance between samples (Rozanova *et al*, 2021).

For absolute quantification, a known amount of reference peptides (usually isotopically labeled synthetic peptides) is spiked into the sample (Brönstrup, 2004). By comparison of the peptide signals to that of the spike-in standard peptides, the absolute amount of proteins can be determined.

For relative quantification, several strategies are available, out of which the most prominent are label-free quantification (LFQ), isobaric labeling such as tandem mass tags (TMT) (chemical labeling), and stable isotope labeling by amino acids in cell culture (SILAC) (metabolic labeling) – all of which were used in this study. Each strategy has its advantages and drawbacks and is usually chosen depending on specific experimental requirements, as laid out in the following:

Besides being cost-efficient and easy in handling, the biggest advantage of **label-free quantification** is the unlimited number of samples that can be analyzed, thereby presenting an ideal high-throughput method, well-suited for large-scale proteomics (Lindemann *et al*, 2017; Moulder *et al*, 2016). However, individual preparation and measurement of each

sample can have negative effects on reproducibility and drastically increase instrument time. In contrast, label-based approaches, allow for early combining and multiplexing of samples, increasing the precision of relative quantification and decreasing required instrument time. Here the principle of "the earlier the labeling and mixing, the smaller the technical variance, thus the higher the precision" applies.

Hence, **chemical labeling** comprises a higher precision compared to the label-free approaches, as samples can be already combined on the peptide (or protein) level. Commonly used chemical labeling reagents are dimethyl labeling, isotope-coded affinity tag (ICAT), isobaric tags for relative and absolute quantification (iTRAQ), or TMT. Similar to metabolic labeling, dimethyl labeling, and ICAT labels are introducing a small mass difference into peptides originating from two or more samples, which, upon mixing of the samples, can be distinguished and quantified in the MS^1 scan (Hsu *et al*, 2003; Gygi *et al*, 1999). On the contrary, in TMT and iTRAQ approaches, the introduced labels are isobaric (same m/z in MS^1) but upon fragmentation result in distinct reporter ions (different m/z) on the MS^2 or MS^3 level enabling highly accurate quantification (Ross *et al*, 2004; Thompson *et al*, 2003). The label reagents consist of an amine-reactive group, to conjugate the label to the peptide, a mass balancer, comprising a peptide bond for fragmentation induced breakage, and a reporter group (**Figure 4A**). Heavy carbon, nitrogen, and oxygen isotopes (^{13}C, ^{15}N, and ^{18}O) are distributed within the reporter group as well as the mass balancer that together add up to the same (isobaric) mass for each label (**Figure 4B**). Upon sample mixing, the signal intensities of differentially labeled peptides are summed up due to the isobaric nature of the tags. This increases signal intensities of low abundant proteins in the MS^1 scan. The fragmentation of these precursors is induced by applying higher-energy collision dissociation (HCD) or electron transfer dissociation (ETD), causing the peptide bond between the mass reporter and mass balancer to break. This gives rise to two populations of ions that are acquired in the MS^2 (or MS^3) scan(s), the reporter ions and the peptide fragment ions, allowing for relative quantification and peptide identification, respectively (**Figure 4C** and **4D**).

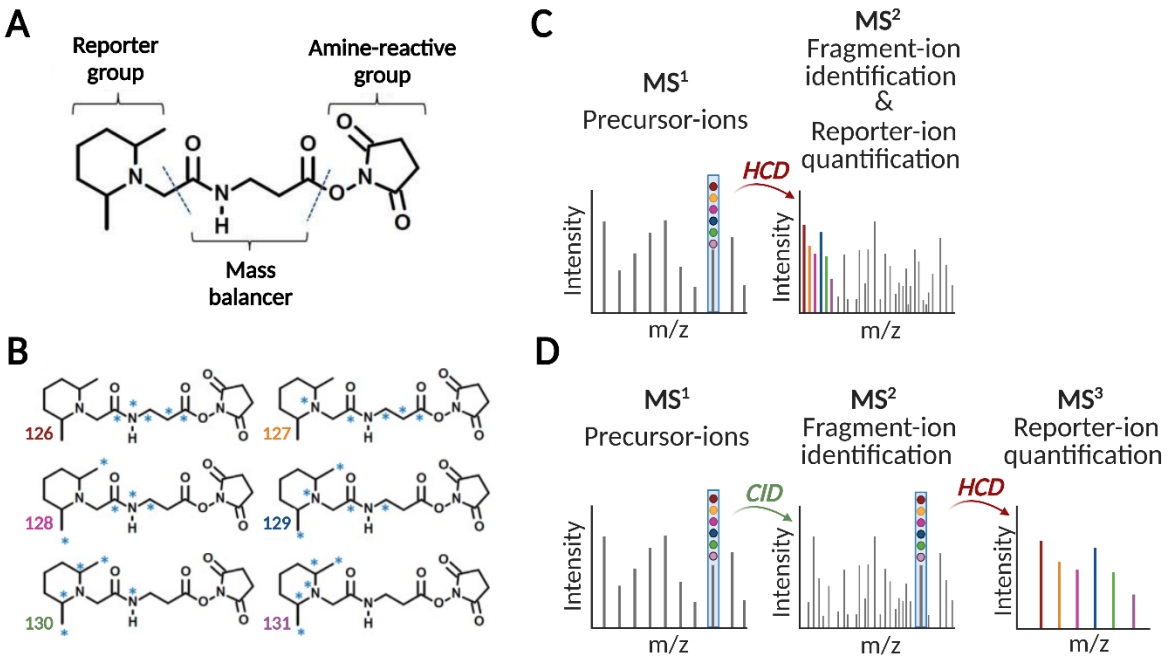

Figure 4: Chemical labeling with TMT isobaric mass tag reagents. (**A**) Chemical structure and functional elements of a tandem mass tag (TMT) label reagent consisting of an amine-reactive group, conjugating the label to the peptide, a mass balancer, comprising a peptide bond for fragmentation induced breakage (via higher-energy collision dissociation (HCD)), and a reporter group. Figure adapted from Rauniyar & Yates, 2014. (**B**) Example of a TMT6plex label illustrating distinct isotope positions (blue asterisks). Figure adapted from Rauniyar & Yates, 2014. (**C**) Schematic illustration of TMT-based relative quantification in MS^2 mode. In the MS^1 scan isobarically labeled precursor ions are selected and subjected to fragmentation via HCD. In the MS^2 scan, resulting fragment-ions are used for peptide identification and reporter-ions are used for relative quantification. (**D**) Schematic illustration of TMT-based relative quantification in MS^3 mode. In the MS^1 scan isobarically labeled precursor ions are selected and subjected to fragmentation via collision-induced dissociation (CID). In the MS^2 scan, resulting fragment-ions are used for peptide identification. A second fragmentation step using HCD gives rise to reporter-ions used for relative quantification in a MS^3 scan. Figure (C) and (D) were created with BioRender.com.

Together, these chemical labeling approaches comprise a high multiplexing capability thereby reducing instrument time. Moreover, chemical labels are applicable to virtually any sample, ranging from primary cells, biological fluids, tissue, or animal samples due to *in vitro* labeling. Another advantage is that by adding several samples into one, the signal intensity of rather low abundant peptides in MS^1 (and MS^2) scans can be enhanced, resulting in increasing sample depth. However, co-fragmentation of co-eluting peptides can lead to the overestimation of the actual protein abundance, resulting in inaccurate quantification. Yet, optimizing strategies using additional fragmentation (MS^3), as it was used in this study, has helped to overcome this challenge (**Figure 4D**) (Ting *et al*, 2011). Moreover, since sample mixing is performed at the protein/peptide level, the technical

variance is smaller compared to label-free approaches. However, this technical variance can be minimized even further.

This is accomplished in a **metabolic labeling** approach (e.g. SILAC) in which the labels are introduced *in vivo* during protein synthesis, hence at the earliest time point of an experiment allowing for accurate and precise quantification (Ong *et al*, 2002; Bantscheff *et al*, 2007). In a typical SILAC experiment, two or three populations of cells are grown in special SILAC media, either containing amino acid(s) with natural isotopes ("light" medium) or stable isotope-labeled amino acid(s) ("medium" or "heavy" medium). The labeling of all proteins *in vivo* allows for mixing of the cell populations as early as the cell level, preventing any variability between the samples during sample preparation. Typically ^{13}C or ^{15}N-labeled arginine or lysine are used since they ensure at least one labeled amino acid in each tryptic peptide. The heavy labeled peptides introduce a confined mass shift compared to their light counterparts allowing for quantification of the samples in the MS^1 scan.

1.2.2.1. Advanced SILAC-based approaches

Over the last two decades, the SILAC approach was expanded to different model organisms, such as *Arabidopsis thaliana* (Gruhler *et al*, 2005), *Mus musculus* (Krüger *et al*, 2008), *Drosophila melanogaster* (Sury *et al*, 2010), *Bacillus subtilis* (Soufi *et al*, 2010), *Caenorhabditis elegans* (Fredens *et al*, 2011) and *Saccharomyces cerevisiae* (Oeljeklaus *et al*, 2014). However, besides the ability of labeling organisms and the high accuracy in quantification, classical SILAC approaches typically have a low multiplexing capability and constrain sample types that are not amenable to metabolic labeling. These limitations were partially overcome by the further development of SILAC-based approaches such as Super-SILAC or spike-in-SILAC. Here a mixture of SILAC-labeled cells can be used for multiplexing or the quantification of samples that can not be labeled metabolically, such as tissue samples (Geiger *et al*, 2010; Shenoy & Geiger, 2014). Another variation of the SILAC approach is pulsed-SILAC in which the metabolic labeling of proteins for only a short period of time, allows for insights into *de novo* protein production and protein turnover rates (Milner 2006, Lam 2007, Schwannhausser 2009). The term "pulse" refers to a swap of the SILAC medium that is executed at the same time with a particular cell treatment that supposedly has an effect on the turnover rate of proteins. Therefore two cell populations are initially grown for example in light (L) SILAC growth-medium. Together with the

treatment, the growth-medium is swapped to either medium (M) (e.g. non-treated control cells) or heavy (H) (e.g. treated cells) SILAC growth-medium for a certain period of time. Thereby, from the starting time of the treatment, all newly synthesized proteins in the treatment sample will have incorporated the H labeled amino acids whereas the ones in the control sample will have incorporated the M labeled amino acids. After combining the samples, the ratio of H/M will facilitate the determination of the turnover rate of newly synthesized proteins under treatment conditions compared to the control. However, in a generally highly complex (SILAC) proteome sample, the detection of small changes in the synthesis of proteins with a slow turnover rate reflects a major challenge of the pulsed-SILAC approach. Moreover, the vast amount of cell signaling processes, i.e. mainintaing cell homeoastasis that are happening at any time within a living cell gives rise to a constant "background signaling". This hampers the distinction of a triggered effect of a certain treatment from the background.

The combination of **pulsed-SILAC and click-chemistry**, used in this study, helped to overcome these challenges (Eichelbaum *et al*, 2012; Eichelbaum & Krijgsveld, 2014). The click-chemistry approach makes use of azidohomoalanine (AHA), an azide-bearing analog of methionine (Dieterich *et al*, 2006). During the pulse, the incorporation of AHA into newly synthesized proteins allows for the enrichment of these proteins by click-chemistry, covalently coupling the azide-containing proteins to an alkyne-activated resin. Combining these two metabolic pulse labeling methods allow for selective enrichment (click-chemistry) and quantification (SILAC) of newly synthesized proteins upon a certain treatment, referred to as **translatome analysis** (workflow illustrated in **Figure 13A**). This method was originally published for quantification of secreted proteins in the presence of serum, in which the presence of high-abundant serum proteins usually limits the detection of low abundant proteins (Eichelbaum *et al*, 2012; Eichelbaum & Krijgsveld, 2014). Together, in addition to protein turnover rates, the pulsed-SILAC and click-chemistry approach allows for the detection of even small changes in protein levels or the detection of low abundant proteins in the presence of a complex background, increasing the overall sensitivity of the proteome analysis.

1.2.2.2. Quantitative Phosphoproteomics

The functional plasticity of a protein is determined by site-specific covalent modifications, the PTMs, influencing their stability, localization, interaction partners, and activity (Dunphy *et al*, 2021). It has been predicted that there are more than 400 types of PTMs, which can be simple modifications such as phosphorylation, acetylation, or complex conjugations such as ubiquitination or glycosylation (Khoury *et al*, 2011; Doerr, 2015). One of the most commonly studied PTM is phosphorylation which is of particular interest for its key role in signal transduction and its deregulation in cancer (Hanahan & Weinberg, 2000). The human genome encodes over 20,000 proteins, out of which over 70% are phosphorylated by at least one out of approximately 518 protein kinases (Manning *et al*, 2002). Due to advances in MS-based technology, almost 300,000 non-redundant phosphorylation sites have been identified and made available in databases such as PhosphoSitePlus (PSP) (Hornbeck *et al*, 2015). Yet, only approximately 18% of these phosphorylation sites can be assigned as substrates to corresponding kinases at present time. This illustrates the necessity for in-depth analysis of dynamic phosphorylation-mediated signaling networks, allowing for a better understanding of signal transduction in health and disease.

Due to their relatively low abundance, phosphopeptides need to be enriched to facilitate their detection by MS. In vertebrates, the estimated abundance of phosphorylated tyrosine (pTyr) is only around ~0.05%, while phosphorylated threonine (pThr) makes up ~10%, and phosphorylated serine (pSer) ~90%, which is why additional anti-pTyr antibody-based immunoaffinity approaches are often used (Hunter, 1998). For global enrichment of pSer, pThr, and pTyr containing peptides, most strategies take advantage of the affinity of phosphate groups to metals, immobilized on carrier resins or beads. Among others, this includes immobilized metal ion affinity chromatography (IMAC) using Fe^{3+}, Ga^{3+}, and Zr^{4+}, or metal oxide affinity chromatography such as titanium dioxide (TiO_2) - sometimes even used in a hybrid of both (Ti-IMAC) (Andersson & Porath, 1986; Posewitz & Tempst, 1999; Zhou *et al*, 2006a; Ficarro *et al*, 2002; Larsen *et al*, 2005; Lai *et al*, 2012). It is being debated in the field whether these methods purify complementary parts of the phosphoproteome, in such that for example Ti-IMAC is preferred over TiO_2 as it is thought to purify basophilic peptides better, whereas Fe-IMAC is supposed to enrich multiply phosphorylated peptides better (Zhou *et al*, 2006a; Thingholm *et al*, 2008; Ruprecht *et al*, 2015). The method used

in this study is an optimized protocol for global phosphoproteome enrichment by **Fe^{3+}-IMAC column chromatography** (Ruprecht *et al*, 2015, 2017; Potel *et al*, 2018). In this method a commercially available Fe-IMAC column is charged with Fe^{3+}, allowing for the enrichment of phosphopeptides over a ~15 min gradient. The method is commonly acknowledged for its robustness and reproducibility, due to low variability in binding capacity and elution efficiency of phosphopeptides to the Fe^{3+}-IMAC column.

In recent years, MS-based phosphoproteomics evolved into a sophisticated discipline, constantly improving (i) the specificity of enrichment strategies, (ii) the sensitivity of detection by mass spectrometers, (iii) the accuracy of localization of phosphorylation sites, (iv) the depth and throughput of the approaches, and (v) the downstream bioinformatic data analysis (Paulo & Schweppe, 2021). Ultimately, this will enable a deeper analysis of signaling pathways by adding another level of information to the classical proteomics approaches and thereby enable the characterization of kinases and their direct targets, which will be key in finding novel drug targets and biomarkers.

1.3. Objectives

The objective of this project is to gain new insights into protein regulation mediated by the two tumor suppressor kinases LATS1 and LATS2, using advanced mass spectrometry-based proteomics approaches in the context of breast (cancer) tissue. For this, LATS1 and LATS2 knock-out and overexpression cell systems will be subject to global proteome, translatome, and phosphoproteome analysis. Together this will help uncover distinct and shared functions of LATS1 and LATS2, and serve as a profound source for their in-depth characterization.

2. MATERIALS

In the following chapter all used materials are listed in alphabetically ordered groups. For products purchased from a company, the catalog number is provided.

2.1. Cells

Table 1: Human cell lines

CELL LINE	COMPANY *CATALOG #*	DESCRIPTION	PROVIDED BY
HEK293T (*H. sapiens*)	ATCC (Wesel, DE) *CRL-3216™*	Embryonic kidney cells	Prof. Claudia Scholl, DKFZ, Heidelberg, DE; originally from Prof. William Hahn, Broad Institute, Cambridge, MA, USA
MCF7 (*H. sapiens*)	ATCC (Wesel, DE) *HTB-22™*	Breast, mammary gland cells	ATCC (Manassas, VA, USA)
MCF10A (*H. sapiens*)	ATCC (Wesel, DE) *CRL-10317™*	Immortalized breast epithelial cells	Prof. Claudia Scholl, DKFZ, Heidelberg, DE
ZR75.1 (*H. sapiens*)	ATCC (Wesel, DE) *CRL-1500™*	Breast, duct, mammary gland cells	Prof. Moshe Oren, WIZ, Rehovot, IL

Table 2: Bacterial cells

STRAIN	COMPANY	CATALOG #
One Shot™ Stbl3™ Chemically Competent (*E. coli)*	Thermo Fisher Scientific (Braunschweig, DE)	C7373-03
Subcloning Efficiency™ DH5α Competent Cells (E. coli)	Thermo Fisher Scientific (Braunschweig, DE)	18265017

2.2. Cell culture media

Table 3: Composition of media for MCF7 cells.

NAME	(i) label-free growth media	(ii) full-SILAC growth media	(iii) pulsed-SILAC growth media	(iv) pulsed-SILAC starvation media	(v) pulsed-SILAC depletion media	(vi) pulsed-SILAC pulse media
MEDIUM	DMEM + phenol red - L-glutamine - sodium pyruvate	DMEM for SILAC + phenol red - L-glutamine - L-lysine - L-arginine	DMEM for SILAC + phenol red - L-glutamine - L-lysine - L-arginine	DMEM for SILAC + phenol red - L-glutamine - L-lysine - L-arginine	DMEM for SILAC (Powder) - phenol red - L-glutamine - sodium bicarbonate - L-leucine - L-lysine - L-arginine - L-methionine	DMEM for SILAC (Powder) - phenol red - L-glutamine - sodium bicarbonate - L-leucine - L-lysine - L-arginine - L-methionine
ADDITIVES	10% (v/v) FBS 1x (v/v) GlutaMax 100 I.U./mL PenStrep 1x (v/v) sodium pyruvate	10% (v/v) dialyzed FBS 1x (v/v) GlutaMax 100 I.U./mL PenStrep 50 mg/mL L-proline 146 mg/mL L-lysine LIGHT: L-lysine, or MEDIUM: D_4-L-lysine, or HEAVY: $^{13}C_6$,$^{15}N_2$-L-lysine 84 mg/mL L-arginine LIGHT: L-arginine, or MEDIUM: $^{13}C_6$-L-arginine, or HEAVY: $^{13}C_6$,$^{15}N_4$-L-arginine	10% (v/v) dialyzed FBS 1x (v/v) GlutaMax 100 I.U./mL PenStrep 50 mg/mL L-proline 146 mg/mL L-lysine MEDIUM: D_4-L-lysine, or 84 mg/mL L-arginine MEDIUM: $^{13}C_6$-L-arginine	4% (v/v) dialyzed FBS 1x (v/v) GlutaMax 100 I.U./mL PenStrep 50 mg/mL L-proline 146 mg/mL L-lysine MEDIUM: D_4-L-lysine, or 84 mg/mL L-arginine MEDIUM: $^{13}C_6$-L-arginine	4% (v/v) dialyzed FBS 1x (v/v) GlutaMax 100 I.U./mL PenStrep 3.7 mg/mL sodium bicorbonate 105 mg/mL L-leucine 50 mg/mL L-proline	4% (v/v) dialyzed FBS 1x (v/v) GlutaMax 100 I.U./mL PenStrep 3.7 mg/mL sodium bicorbonate 105 mg/mL L-leucine 50 mg/mL L-proline 146 mg/mL L-lysine LIGHT: L-lysine, or HEAVY: $^{13}C_6$,$^{15}N_2$-L-lysine 84 mg/mL L-arginine LIGHT: L-arginine, or HEAVY: $^{13}C_6$,$^{15}N_4$-L-arginine 0.1 mM L-azidohomoalanine
EXPERIMENT	GLOBAL PROTEOME (TRANSIENT OVEREXPRESSION)	PHOSPHOPROTEOME ANALYSIS	TRANSLATOME AND SECRETOME ANALYSIS			

Table 4: Composition of media for MCF10A cells.

NAME	(ii) full-SILAC growth media	(iii) pulsed-SILAC growth media	(iv) pulsed-SILAC starvation media	(v) pulsed-SILAC depletion media	(vi) pulsed-SILAC pulse media
MEDIUM	DMEM F12 for SILAC + phenol red - L-glutamine - L-lysine - L-arginine	DMEM F12 for SILAC + phenol red - L-glutamine - L-lysine - L-arginine	DMEM F12 for SILAC + phenol red - L-glutamine - L-lysine - L-arginine	DMEM F12 for SILAC (powder) - phenol red - sodium bicarbonate - L-glutamine - L-leucine - L-lysine - L-arginine - L-methionine	DMEM F12 for SILAC (powder) - phenol red - sodium bicarbonate - L-glutamine - L-leucine - L-lysine - L-arginine - L-methionine
ADDITIVES	5% (v/v) dialyzed horse serum 1x (v/v) GlutaMax 100 I.U./mL PenStrep 0.5 mg/mL hydrocortisone 10 µg/mL insulin 100 ng/mL cholera toxin 20 ng/mL EGF 50 mg/mL L-proline 91.25 mg/mL L-lysine LIGHT: L-lysine, or MEDIUM: D_4-L-lysine, or HEAVY: $^{13}C_6$,$^{15}N_2$-L-lysine 147.5 mg/mL L-arginine LIGHT: L-arginine, or MEDIUM: $^{13}C_6$-L-arginine, or HEAVY: $^{13}C_6$,$^{15}N_4$-L-arginine	5% (v/v) dialyzed horse serum 1x (v/v) GlutaMax 100 I.U./mL PenStrep 0.5 mg/mL hydrocortisone 10 µg/mL insulin 100 ng/mL cholera toxin 20 ng/mL EGF 50 mg/mL L-proline 91.25 mg/mL L-lysine MEDIUM: D_4-L-lysine 147.5 mg/mL L-arginine MEDIUM: $^{13}C_6$-L-arginine	2% (v/v)dialyzed horse serum 1x (v/v) GlutaMax 100 I.U./mL PenStrep 0.5 mg/mL hydrocortisone 10 µg/mL insulin 100 ng/mL cholera toxine - 50 mg/mL L-proline 91.25 mg/mL L-lysine MEDIUM: D_4-L-lysine 147.5 mg/mL L-arginine MEDIUM: $^{13}C_6$-L-arginine	2% (v/v) dialyzed horse serum 1x (v/v) GlutaMax 100 I.U./mL PenStrep 0.5 mg/mL hydrocortisone 10 µg/mL insulin 100 ng/mL cholera toxine - 2.438 mg/mL sodium bicorbonate 59.05 mg/mL L-leucine 50 mg/mL L-proline	2% (v/v) dialyzed horse serum 1x (v/v) GlutaMax 100 I.U./mL PenStrep 0.5 mg/mL hydrocortisone 10 µg/mL insulin 100 ng/mL cholera toxine 20 ng/mL EGF 50 mg/mL L-proline 91.25 mg/mL L-lysine LIGHT: L-lysine, or HEAVY: $^{13}C_6$,$^{15}N_2$-L-lysine 147.5 mg/mL L-arginine LIGHT: L-arginine, or HEAVY: $^{13}C_6$,$^{15}N_4$-L-arginine 0.1 mM L-azidohomoalanine
EXPERIMENT	PHOSPHOPROTEOME ANALYSIS	TRANSLATOME AND SECRETOME ANALYSIS			

Table 5: Composition of media for ZR75.1 cells.

NAME	(i) label-free growth media	(ii) full-SILAC growth media	(iii) pulsed-SILAC growth media	(iv) pulsed-SILAC starvation media	(v) pulsed-SILAC depletion media	(vi) pulsed-SILAC pulse media
MEDIUM	RPMI 1640 + phenol red - L-glutamine - HEPES	RPMI 1640 for SILAC + phenol red - L-glutamine - L-lysine - L-arginine	RPMI 1640 for SILAC + phenol red - L-glutamine - L-lysine - L-arginine	RPMI 1640 for SILAC + phenol red - L-glutamine - L-lysine - L-arginine	RPMI 1640 for SILAC (powder) - phenol red - sodium bicarbonate - L-glutamine - L-leucine - L-lysine - L-arginine - L-methionine	RPMI 1640 for SILAC (powder) - phenol red - sodium bicarbonate - L-glutamine - L-leucine - L-lysine - L-arginine - L-methionine
ADDITIVES	10% (v/v) FBS 1x (v/v) GlutaMax 1x (v/v) HEPES	10% (v/v) dialyzed FBS 1x (v/v) GlutaMax 100 I.U./mL PenStrep 50 mg/mL L-proline <u>40 mg/mL L-lysine</u> LIGHT: L-lysine, or MEDIUM: D_4-L-lysine, or HEAVY: $^{13}C_6$,$^{15}N_2$-L-lysine <u>200 mg/mL L-arginine</u> LIGHT: L-arginine, or MEDIUM: $^{13}C_6$-L-arginine, or HEAVY: $^{13}C_6$,$^{15}N_4$-L-arginine	10% (v/v) dialyzed FBS 1x (v/v) GlutaMax 100 I.U./mL PenStrep 50 mg/mL L-proline <u>40 mg/mL L-lysine</u> MEDIUM: D_4-L-lysine <u>200 mg/mL L-arginine</u> MEDIUM: $^{13}C_6$-L-arginine	4% (v/v) dialyzed FBS 1x (v/v) GlutaMax 100 I.U./mL PenStrep 50 mg/mL L-proline <u>40 mg/mL L-lysine</u> MEDIUM: D_4-L-lysine <u>200 mg/mL L-arginine</u> MEDIUM: $^{13}C_6$-L-arginine	4% (v/v) dialyzed FBS 1x (v/v) GlutaMax 100 I.U./mL PenStrep 1.5 mg/mL sodium bicorbonate 50 mg/mL L-leucine 50 mg/mL L-proline	4% (v/v) dialyzed FBS 1x (v/v) GlutaMax 100 I.U./mL PenStrep 1.5 mg/mL sodium bicorbonate 50 mg/mL L-leucine 50 mg/mL L-proline <u>40 mg/mL L-lysine</u> LIGHT: L-lysine, or HEAVY: $^{13}C_6$,$^{15}N_2$-L-lysine <u>200 mg/mL L-arginine</u> LIGHT: L-arginine, or HEAVY: $^{13}C_6$,$^{15}N_4$-L-arginine 0.1 mM L-azidohomoalanine
EXPERIMENT	GLOBAL PROTEOME (siRNA-MEDIATED KNOCKDOWN & TRANSIENT OVEREXPRESSION)	PHOSPHOPROTEOME ANALYSIS	TRANSLATOME AND SECRETOME ANALYSIS			

2.3. Primers

Table 6: GATEWAY cloning: AttB-PCR Primers

PRIMER NAME	'5 TO 3' SEQUENCE	APPLICATION
LATS1_AttB1_fw	GGGGACAAGTTTGTACAAAAAAGCAGGCTTC ACCATGAAGAGGAGTGAAAAGCCAG	GATEWAY cloning: AttB amplicon LATS1
LATS1_AttB2_rev	GGGGACCACTTTGTACAAGAAAGCTGGGTTT TAAACATATACTAGATCGCGATTTTTAATCTC	GATEWAY cloning: AttB amplicon LATS1
LATS2_AttB1_fw	GGGGACAAGTTTGTACAAAAAAGCAGGCTTC ACCATGAGGCCAAAGACTTTTCCTG	GATEWAY cloning: AttB amplicon LATS2
LATS2_AttB2_rev	GGGGACCACTTTGTACAAGAAAGCTGGGTTC TACACGTACACAGGCTGG	GATEWAY cloning: AttB amplicon LATS2

Table 7: Sanger sequencing primer for plasmid validation

PRIMER NAME	'5 TO 3' SEQUENCE	APPLICATION
CMV_fw	GTCGTAACAACTCCGCCCC	Validation of pEGFP, pENTR, pTRIPZ with LATS1 or LATS2 CDS
EGFP_fw	GGTGAACTTCAAGATCCGCCAC	Validation of pEGFP, pENTR, pTRIPZ with LATS1 or LATS2 CDS
IRES_fw*	TAGGCGTGTACGGTGGG	Validation of pEGFP, pENTR, pTRIPZ with LATS1 or LATS2 CDS
IRES_rev*	TATAGACAAACGCACACCG	Validation of pEGFP, pENTR, pTRIPZ with LATS1 or LATS2 CDS
LATS1_seq1_fw	AGACTTGCAAGCTGCTGGAT	Validation of pEGFP, pENTR, pTRIPZ with LATS1 CDS
LATS1_seq3_fw	GCCCTTCTGCTTTACAAACAGGG	Validation of pEGFP, pENTR, pTRIPZ with LATS1 CDS
LATS1_seq5_fw	CATCAGCAGCGTCTACATCGT	Validation of pEGFP, pENTR, pTRIPZ with LATS1 CDS
LATS1_seq6_fw	GACTGACTTTGGCCTCTGCAC	Validation of pEGFP, pENTR, pTRIPZ with LATS1 CDS
LATS1_seq7_fw	CTTTGCCGAGGACCCGAAGA	Validation of pEGFP, pENTR, pTRIPZ with LATS1 CDS
LATS2_seq1_fw	GGCTACCTGGACCCGAGG	Validation of pEGFP, pENTR, pTRIPZ with LATS2 CDS
LATS2_seq3_fw	GGTGAAGAGCGTGCGTGTG	Validation of pEGFP, pENTR, pTRIPZ with LATS2 CDS
LATS2_seq5_fw	ATGGACTACATCCCTGGTGGG	Validation of pEGFP, pENTR, pTRIPZ with LATS2 CDS
LATS2_seq6_fw	CTGTGACTGGTGGAGTGTTGG	Validation of pEGFP, pENTR, pTRIPZ with LATS2 CDS

*Primer taken from Standard-Primers provided by Microsynth Seqlab (Göttingen)

Table 8: Real-time/ qPCR primer

PRIMER NAME	'5 TO 3' SEQUENCE	APPLICATION
HPRT1_RT_fw	TGACACTGGCAAAACAATGCA	Housekeeping gene for qPCR
HPRT1_RT_rev	GGTCCTTTTCACCAGCAAGCT	Housekeeping gene for qPCR
LATS1_RT_fw	TCATCAGCAGCGTCTACATCG	Accessing relative mRNA expression of LATS1 via qPCR
LATS1_RT_rev	TCCAACCCGCATCATTTCAT	Accessing relative mRNA expression of LATS1 via qPCR
LATS2_RT_fw	GCAGATTGTGCGGGTCATTA	Accessing relative mRNA expression of LATS2 via qPCR
LATS2_RT_rev	GGCATGAGCCCCTTTCCT	Accessing relative mRNA expression of LATS2 via qPCR

2.4. Plasmids

Table 9: Plasmids

PLASMID BACKBONE	CDS	FUNCTION	USED FOR	PROVIDED BY
pEGFP	LATS1; LATS2	Expression plasmid	Transient overexpression of EGFP-tagged GOI	Prof. Moshe Oren, WIZ, Rehovot, IL
pENTR	LATS1; LATS2	Entry vector	GATEWAY cloning: LR reaction	Self-synthesized construct
pDONR™221	LATS1; LATS2	Donor vector	GATEWAY cloning: BP reaction	Prof. Claudia Scholl, DKFZ, Heidelberg, DE; (Thermo Fisher Scientific, Invitrogen™)
pMD2.G	VSV-G	Envelop plasmid	Lentiviral production	Prof. Claudia Scholl, DKFZ, Heidelberg, DE; (Addgene: (Plasmid #12259)
psPAX2	HIV-1 pol	Packaging plasmid	Lentiviral production	Prof. Claudia Scholl, DKFZ, Heidelberg, DE; (Addgene: Plasmid #12260)
pTRIPZ-GW	LATS1; LATS2, tGFP	Expression plasmid	TET-induced overexpression of GOI	Self-synthesized construct

*Plasmid maps and DNA sequences of gene(s) of interest (GOI) can be found in Chapter 6.

2.5. Chemicals/ Enzymes/Reagents and Kits

Table 10: Chemicals, enzymes, and reagents

CHEMICALS/ENZYMES/REAGENTS	COMPANY	CATALOG #
2-Chloroacetamide (CAA)	Merck, Sigma-Aldrich (Darmstadt, DE)	22790
4–15% Mini-PROTEAN TGX™ Precast Protein Gels, 10-well	Bio-Rad Laboratories GmbH (Feldkirchen, DE)	4561084
4x Laemmli Buffer	Bio-Rad Laboratories GmbH (Feldkirchen, DE)	1610747
20% (w/v) SDS Solution	Bio-Rad Laboratories GmbH (Feldkirchen, DE)	1610418
Acetic acid glacial ULC/MS - CC/SFC	Biosolve Chemicals (Dieuze, FR)	001074131BS
Acetonitrile (ACN)	Biosolve Chemicals (Dieuze, FR)	0001204101BS
Agarose	Merck, Sigma-Aldrich (Darmstadt, DE)	A9539
Ammonium formate	Merck, Sigma-Aldrich (Darmstadt, DE)	70221-25G
Ammonium bicarbonate	Merck, Sigma-Aldrich (Darmstadt, DE)	09830
Ammonium hydroxide solution	Fluka Analytical (Munich, DE)	44273-100ML-F
Bovine Serium Albumin (BSA)	Fisher Scientific (Schwerte, DE)	BP9702
Citric acid anhydrous AR	Biosolve Chemicals (Dieuze, FR)	030205
cOmplete, EDTA-free Protease Inhibitor Cocktail	Merck, Roche™ (Darmstadt, DE)	COEDTAF-RO
DharmaFECT 1 Transfection Reagent	Horizon Discovery, Dharmacon (Cambridge, UK)	T-2001-03
Dimethylsulfoxid (DMSO)	Merck, Sigma-Aldrich (Darmstadt, DE)	D8418
Dithiothreitol (DTT)	Biomol GmbH (Hamburg, DE)	04010.25
DNA Gel Loading Dye (6X)	Thermo Fisher Scientific, Fisher Scientific™ (Braunschweig, DE)	R0611

DMEM with high glucose and no glutamine	Thermo Fisher Scientific, Gibco™ (Braunschweig, DE)	11960085
Doxycycline hyclate (DOX)	Merck, Sigma-Aldrich (Darmstadt, DE)	D9891
Ethanol (EtOH), absolute, suitable for HPLC, ≥99.8% (v/v)	Merck (Darmstadt, DE)	34852
Ethanol (EtOH) absolute	VWR International GmbH (Darmstadt, DE)	20821.310
Ethylenediaminetetraacetic acid (EDTA)	Merck, Sigma-Aldrich (Darmstadt, DE)	E9884
Fetal Bovine Serum (FBS)	Thermo Fisher Scientific, Gibco™ (Braunschweig, DE)	10270106
Formic acid (FA)	Biosolve Chemicals (Dieuze, FR)	0006914143BS
Gateway™ pDONR™221 Vector	Thermo Fisher Scientific, Invitrogen™ (Braunschweig, DE)	12536017
Gene Ruler 1kb DNA Ladder	Thermo Fisher Scientific, Fisher Scientific™ (Braunschweig, DE)	SM1331
GlutaMAX supplement	Thermo Fisher Scientific, Gibco™ (Braunschweig, DE)	35050061
Hydrochloric acid (37%)	Merck (Darmstadt, DE)	K51884217943
Hydroxylamine (50%) for TMT experiments	Fisher Scientific (Schwerte, DE)	90115
Iodoacetamide (IAA)	Bio-Rad Laboratories GmbH (Feldkirchen, DE)	1632109
Iron(III) chloride ($FeCl_3$)	Merck, Sigma-Aldrich (Darmstadt, DE)	157740
LC/MS-grade water	Biosolve Chemicals (Dieuze, FR)	00232141B1BS
Methanol (MeOH)	Biosolve Chemicals (Dieuze, FR)	0013684101BS
NP-40 Surfact-Amps™ Detergent Solution	Thermo Fisher Scientific, Fisher Scientific™ (Braunschweig, DE)	85124
Nuclease-Free Water	Thermo Scientific, Invitrogen™ (Schwerte, DE)	10526945
Opti-MEM™ I Reduced Serum Medium	Thermo Fisher Scientific, Gibco™ (Braunschweig, DE)	11058021
ON-TARGETplus Human LATS1 siRNA	Horizon Discovery, Dharmacon (Cambridge, UK)	L-004632-00-0005
ON-TARGETplus Human LATS2 siRNA	Horizon Discovery, Dharmacon (Cambridge, UK)	L-003865-00-0005
ON-TARGETplus Non-targeting Control Pool	Horizon Discovery, Dharmacon (Cambridge, UK)	D-001810-10-05
PenStrep (Penicillin-Streptomycin)	Thermo Fisher Scientific, Gibco™ (Braunschweig, DE)	15140122
PBS pH7.4 (10x) Phosphate buffered saline	Thermo Fisher Scientific, Gibco™ (Braunschweig, DE)	70011036
PhosSTOP™	Merck, Roche™ (Darmstadt, DE)	PHOSS-RO
Pierce HeLa standard	Thermo Scientific, Pierce™ (Schwerte, DE)	88328
Pierce LTQ Velos ESI Positive Ion Calibration Solution	Thermo Scientific, Pierce™ (Schwerte, DE)	88323
Polybrene / Hexadimethrinbromid	Merck, Sigma-Aldrich (Darmstadt, DE)	H9268
PowerUp™ SYBR™ Green Master Mix	Thermo Fisher Scientific, Applied Biosystems™ (Braunschweig, DE)	A25776
Precision Plus Protein Dual Color Standard	Bio-Rad Laboratories GmbH (Feldkirchen, DE)	61-0374
Phusion® High-Fidelity DNA Polymerase	New England BioLabs (Frankfurt am Main, DE)	M0530
RapiGest SF Surfactant	Waters Corporation (Milford, USA)	186001861

Running Buffer: 10x Tris/ Glycine/ SDS	Bio-Rad Laboratories GmbH (Feldkirchen, DE)	1610732
Sequencing grade modified trypsin	Promega (Madison, WI, USA)	V5111
S.O.C. Medium	Thermo Fisher Scientific, Invitrogen™ (Braunschweig, DE)	15544034
Sodium Chloride	Merck, Sigma-Aldrich (Darmstadt, DE)	S1679
Sodium deoxycholate	Merck, Sigma-Aldrich (Darmstadt, DE)	D6750
SYBR™ Safe DNA Gel Stain	Thermo Fisher Scientific, Invitrogen™ (Braunschweig, DE)	S33102
Triethylammonium bicarbonate (TEAB) (1M)	Thermo Scientific (Schwerte, DE)	90114
Trifluoroacetic acid ULC/MS - CC/SFC	Biosolve Chemicals (Dieuze, FR)	202341
Trans-Blot® Turbo™ Mini PVDF	Bio-Rad Laboratories GmbH (Feldkirchen, DE)	1704156
Trizma®-Base	Merck, Sigma-Aldrich (Darmstadt, DE)	93352
Trypsin/Lys-C Mix, Mass Spec Grade	Promega (Madison, WI, USA)	V5071
TWEEN® 20	Merck, Sigma-Aldrich (Darmstadt, DE)	P9416

Table 11: Kits

KITS	COMPANY	CATALOG #
Clarity™ Western ECL Substrate	Bio-Rad Laboratories GmbH (Feldkirchen, DE)	1705060
Click-iT™ Protein Enrichment Kit	Thermo Fisher Scientific, Invitrogen™ (Braunschweig, DE)	C10416
Gateway™ BP Clonase™ II Enzyme mix	Thermo Fisher Scientific, Invitrogen™ (Braunschweig, DE)	11789020
Gateway™ LR Clonase™ II Enzyme mix	Thermo Fisher Scientific, Invitrogen™ (Braunschweig, DE)	11791020
High-Capacity cDNA Reverse Transcription Kit	Thermo Fisher Scientific, Applied Biosystems (Braunschweig, DE)	4368814
Lipofectamine™ 3000 Transfection Reagent	Thermo Fisher Scientific, Applied Biosystems™ (Braunschweig, DE)	L3000015
Mycoplasma PCR detection Kit	Applied Biological Materials Inc. (Richmond, CA)	G238
NucleoBond Xtra Midi kit for transfection-grade plasmid DNA	Macherey-Nagel (Düren, DE)	740410
NucleoSpin RNA, Mini kit for RNA purification	Macherey-Nagel (Düren, DE)	740955
Pierce BCA Protein assay	Thermo Scientific, Pierce™ (Schwerte, DE)	23225
Pierce Quantitative Colorimetric Peptide assay	Thermo Scientific, Pierce™ (Schwerte, DE)	23275
QIAquick Gel Extraction Kit	QIAGEN GmbH (Hilden, DE)	28704
QIAquick PCR Purification Kit	QIAGEN GmbH (Hilden, DE)	28104
QIAprep Spin Miniprep Kit	QIAGEN GmbH (Hilden, DE)	27104

2.6. Antibodies

Table 12: Primary Antibodies

TARGET [CLONE]	COMPANY	CATALOG #
LATS1 [C66B5]	Cell Signaling Technology (Beverely, MA, USA)	3477S
α-Tubulin antibody [GT114]	GeneTex (Irvine, CA, USA)	GTX628802-100

Table 13: Secondary Antibodies

TARGET	COMPANY	CATALOG #
goat anti-rabbit IgG-HRP	Santa Cruz (Dellas, TX, USA)	sc-2004
goat anti-mouse IgG-HRP	Santa Cruz (Dellas, TX, USA)	Sc-2005

2.7. Consumable Material

Table 14: Consumable material

CONSUMABLE MATERIAL	COMPANY	CATALOG #
10 µL tips	Neptune Scientific (San Diego, USA)	BT10XL
20 µL tips	Neptune Scientific (San Diego, USA)	BT20
50 µL Microliter Syringe Model 705 RN	Hamilton (Gräfelfing, DE)	80530
200 µL tips	Neptune Scientific (San Diego, USA)	BT200
1250 XL µL tips	Neptune Scientific (San Diego, USA)	BT1250
6-Well Plate, Round, Nunc™	Thermo Scientific™ (Schwerte, DE)	140685
96-well SuperPlates, skirted	Thermo Scientific™ (Schwerte, DE)	AB-2800
Acclaim™ PepMap C18, 5 µm, 100 Å, 100 µm x 2 cm	Thermo Scientific™ (Schwerte, DE)	164564-CMD
Acclaim™ PepMap RSLC C18, 2 µm, 100 Å, 75 µm x 50 cm	Thermo Scientific™ (Schwerte, DE)	11342103
Amicon® Ultra-15 Centrifugal Filter Unit	Merck, Millipore ™ (Darmstadt, DE)	UFC900396
Biobanking and Cell Culture Cryogenic Tubes, 1.8mL Nunc™	Thermo Scientific™ (Schwerte, DE)	368632
Cell lifter	Merck, Corning™ (Darmstadt, DE)	3008
Cell strainer 70 µm, sterile	Merck, Corning™ (Darmstadt, DE)	CLS431751
EasYFlask™ Cell Culture Flasks, 75cm², Nunc™	Thermo Scientific™ (Schwerte, DE)	10364131
Gemini 3 µm C18 110 Å, LC Column 100 x 1 mm	Phenomenex (Aschaffenburg, DE)	SN: H15-233964
LightCycler® 480 Multiwell Plate 96, white	Roche (Mannheim, DE)	04729692001
Microplate 96-well (e.g., BCA)	Greiner Bio-one GmbH (Frickenhausen, DE)	655101
Microplate 96-well conical bottom, Nunc™	Thermo Scientific™ (Schwerte, DE)	249946
Millex-GS Syringe Filter Unit, 0.22 µm	Merck, Millipore™ (Darmstadt, DE)	SLGS033SB
Millex-HV Filter, 0,45 µm	Merck, Millipore™ (Darmstadt, DE)	SLHV033RS
Mini-Protean TGX Gels (10-well comb)	Bio-Rad Laboratories GmbH (Feldkirchen, DE)	456-1084

Mini-Protean TGX Gels (15-well comb)	Bio-Rad Laboratories GmbH (Feldkirchen, DE)	456-1086
Mr. Frosty™ Freezing Container	Thermo Scientific™ (Schwerte, DE)	5100-0001
nanoEase MZ Peptide BEH C18 130 Å, 1.7 µm, 75 µm x 250 mm	Waters Corporation (Milford, USA)	186008795
Oasis Prime HLB µElution Plate	Waters Corporation (Milford, USA)	186008052
PCR Foil Seal	4titude Ltd. (Berlin, DE)	4ti-0550
PCR-8 stripes	Ratiolab GmbH (Dreieich, DE)	8610040
PicoTip Emitter	New Objective, Inc. (Woburn, USA)	FS360-20-10-D-20
ProPac™ IMAC-10 HPLC Columns	Thermo Scientific™ (Schwerte, DE)	063276
Round-Bottom Polypropylene Test Tubes With Cap	Thermo Scientific, Falcon™ (Schwerte, DE)	352059
Sep-Pak C18 1 cc Vac Cartridge, 50 mg Sorbent	Waters Corporation (Milford, USA)	186000308
Spin-X 0.45 µm filter	Corning Incorporated (Salt Lake City, USA)	17418000
Tissue culture dish 100 x 20 mm	Sarstedt (Nümbrecht, DE)	83.3902
Tissue culture dish 100 x 20 mm	Sarstedt (Nümbrecht, DE)	83.3903
Zone-Free™ Sealing Films	Merck (Darmstadt, DE)	Z721646-50EA

2.8. Instrumentation/Equipment

Table 15: Instrumentation and equipment

INSTRUMENTATION/EQUIPMENT	COMPANY	CATALOG #
-80°C Freezer	Eppendorf - New Brunswick (Edison, USA)	U725-G Innova
1100 Series HPLC system	Agilent Technologies (Santa Clara, USA)	NA
Aspiration System	Integra Bioscience GmbH	Integra Vacusafe
Automated Cell Counter	Bio-Rad Laboratories GmbH (Feldkirchen, DE)	TC20
Bioruptor Pico	Diagenode SA (Seraing, Belgium)	SN:P-152703
Branson Digital Sonifier	Branson Ultrasonic Corporation (USA)	NA
Cell Culture Centrifuge	Thermo Scientific™ (Schwerte, DE)	Heraeus MegaFuge 40
Cell Culture Laminar Flow Hood	Thermo Scientific™ (Schwerte, DE)	MaxiSafe 2020
Centrifuge	Eppendorf (Hamburg, DE)	Centrifuge 5424
Centrifuge 5424 Rotor	Eppendorf (Hamburg, DE)	F-45-32-5-PCR
Centrifuge 5424 Rotor	Eppendorf (Hamburg, DE)	FA-45-24-11 (Eppi's)
Centrifuge 5430R Rotor	Eppendorf (Hamburg, DE)	FA-45-48-11 (Eppi's)
Centrifuge 5430R Rotor	Eppendorf (Hamburg, DE)	A-2-MTP (Plates)
ChemiDoc™ Touch Imaging System	Bio-Rad Laboratories GmbH (Feldkirchen, DE)	1708370
CO_2 Incubator	Thermo Scientific™ (Schwerte, DE)	HeraCell Vios 160i
Cooling Centrifuge	Eppendorf (Hamburg, DE)	Centrifuge 5430R
Easy NanoLC 1200	Thermo Fisher Scientific (Braunschweig, DE)	LC-030145, LC-030146
Extraction Manifold, 20-position	Waters Corporation (Milford, USA)	WAT200608
Extraction Plate Manifold for Oasis 96-Well Plates	Waters Corporation (Milford, USA)	186001831

Heraeus MegaFuge 40 Rotor	Thermo Scientific™ (Schwerte, DE)	75003180
High pH HPLC System (Infinity 1260)	Agilent Technologies (Santa Clara, USA)	G1311B
Ice machine	Ziegra Eismaschinen GmbH (Isernhagen, DE)	SN:151759
Incubator	Thermo Scientific™ (Schwerte, DE)	HeraTherm
LightCycler® 480 System	Roche (Mannheim, DE)	05 015 278 001
Mastercylcer	Eppendorf (Hamburg, DE)	Epgradient S
Microscale	Sartorius Lab Instruments (Göttingen, DE)	MSA125P-000-DA
Minicentrifuge	neoLab (Heidelberg, DE)	3-1810
MiniChiller (Picoruptor)	Diagenode SA / Huber (Seraing, BE)	NA
Mini-PROTEAN® Tetra Vertical Electrophoresis	Bio-Rad Laboratories GmbH (Feldkirchen, DE)	1658004
MonoSleeve Column Heater	Analytical Sales & Services, Inc. (Flanders, USA)	MonoSLEEVE
Multi-image Light Cabinet	Alpha Innotech Corporation (San Leandrio, USA)	NA
NanoDrop™ One spectrophotometer	Thermo Scientific™ (Schwerte, DE)	ND-ONE-W
NanoQuant Plate Reader	Tecan (Männedorf, CH)	Infinite M200pro
Orbital shaking station	Agilent Technologies (Santa Clara, USA)	Variomag Teleshake
Orbitrap Fusion™ Tribrid™ Mass Spectrometer	Thermo Fisher Scientific (Braunschweig, DE)	FSN10395
PCR cycler with lid heating (CHB-T2-D ThermoQ)	Hangzhou BIOER Technologies (Binjiang, CN)	CHB-T2-D ThermoQ
Polymax 2040 Platform shaker	Heidolph Instruments GmbH & Co. KG (Schwabach, DE)	Polymax 2040
Primovert Microscope	Carl Zeiss Microscopy GmbH (Oberkochen, DE)	N/A
Probe Sonicator horn	Branson Ultrasonic Corporation (USA)	102C, SN: OBU15091229G
Q-Exactive HF Orbitrap mass spectrometer	Thermo Fisher Scientific (Braunschweig, DE)	QE-SN05174L
SpeedVac Concentrator	Thermo Scientific (Schwerte, DE)	Savant SPD111V
Stemi 305 Microscope	Carl Zeiss Microscopy GmbH (Oberkochen, DE)	SN: 3943000950
ThermoMixer C	Eppendorf (Hamburg, DE)	5382000015
Trans-Blot® Turbo™ Transfer System	Bio-Rad Laboratories GmbH (Feldkirchen, DE)	1704150
UltiMate 3000 HPLC and UHPLC Systems	Thermo Fisher Scientific (Braunschweig, DE)	IQLAAAGABHFAPBMBFB
Ultrapure Water System	Thermo Scientific™ (Schwerte, DE)	SN:41801405
Ultrasonic Cleaner	VWR International GmbH (Darmstadt, DE)	USC-T
Universal Vacuum System	Thermo Scientific™ (Schwerte, DE)	UVS400A
Vortex	Scientific Industries (Bohemia, USA)	Vortex-Genie 2
Water bath	Thermo Scientific™ (Schwerte, DE)	SWB25

2.9. Softwares and Databases

Table 16: Softwares and databases

SOFTWARE	URL
Affinity Designer (version 1.9.2)	https://affinity.serif.com/de/designer/
BioRender	
A plasmid Editor (ApE) 2.0.45	https://jorgensen.biology.utah.edu/wayned/ape/
Image-lab Software	https://www.bio-rad.com/de-de/product/image-lab-software/
KSEA	https://github.com/casecpb/KSEA/
limma moderated t-statistics (R package version 3.36.3)	https://support.bioconductor.org/p/6124/
MaxQuant (different versions)	https://www.maxquant.org/
Primer 3.0	https://primer3.ut.ee/
PTM-SEA/ssGSEA2.0	https://github.com/broadinstitute/ssGSEA2.0
R (version 4.0.4)	https://www.r-project.org/
Rstudio (version 1.1.453)	http://www.rstudio.com/
R package fgsea (version 1.6.0)	Sergushichev, A. A. An algorithm for fast pre-ranked gene set enrichment analysis using cumulative statistic calculation. *bioRxiv*; doi:10.1101/060012
REACTOME pathway database Gene sets using ReactomePA R package (version 1.24.0)	Yu, G. & He, Q. Y. ReactomePA: An R/Bioconductor package for reactome pathway analysis and visualization. *Mol. Biosyst.* 12, 477–479 (2016).
SnapGene	https://www.snapgene.com/
t-SNE analyses were performed using R package tsne (version 0.1-3)	van der Maaten, Laurens, Hinton E., G. Visualizing Data using t-SNE. *J. Mach. Learn. Res.* 164, 10 (2008).

3. METHODS

3.1. Cell culture

All cell culture work was performed in a biosafety level 1 (S1) tissue culture, except lentiviral production (Section 3.5.5.4) that required biosafety level 2 (S2). To ensure aseptic conditions, all cell handling was performed in a laminar flow hood (Thermo Scientific), using only sterile consumables, media, and other chemicals. All cells were cultured in cell dishes, flasks, or plates in an incubator at 37°C in a humidified atmosphere of 5% CO_2.

Before culturing, all cells were authenticated via single nucleotide polymorphism (SNP)-profiling by using the service of Multiplexion GmbH (Heidelberg) and frequently tested for mycoplasma contamination by using Mycoplasma PCR Detection Kit (Applied Biological Material) according to the manufacturer's protocol.

For passaging, cells were washed with phosphate-buffered saline (PBS) (Thermo Fisher Scientific, Gibco), detached from the surface using 0.25% (w/v) Trypsin-EDTA (Thermo Fisher Scientific, Gibco), and either counted using TC20 automated cell counter (Bio-Rad) or transferred in an appropriate volume to a new dish or flask.

For cell harvesting, detached cells were transferred into a 15 mL tube, centrifuged for 3 min at 350 x g. The cell pellet was washed with PBS and was either immediately processed or flash-frozen in liquid nitrogen and stored at -80°C until further usage.

3.1.1. Cell lines

The luminal A human breast carcinoma cell line MCF7 (ATCC- HTB-22™) was used for transient transfection (Section 3.4) with either green fluorescent protein (GFP)-tagged LATS1- or GFP-tagged LATS2-overexpressing plasmids (**Supplementary Figure 1** and **Supplementary Figure 2**). Furthemore, the MCF7 cells were used for the establishment of the inducible stable cell lines that express turbo GFP, LATS1 or LATS2 (**Supplementary Figure 7**, **Supplementary Figure 9**, and **Supplementary Figure 10,** respectively). The aforementioned cell lines were created by taking advantage of the GATEWAY cloning technology (Section 3.5.5).

The luminal B human breast carcinoma cell line ZR75.1 (ATCC CRL-1500™) was kindly provided by Prof. Moshe Oren, Department of Molecular Cell Biology, Weizmann Institute

of Science (WIZ), Rehovot, IL. The cell line was transiently transfected (Section 3.4) with either GFP-tagged LATS1- or GFP-tagged LATS2-overexpressing plasmids (**Supplementary Figure 1** and **Supplementary Figure 2**). Furthemore, the ZR75.1 cells were used for the establishment of the inducible stable cell lines that express turbo GFP, LATS1 or LATS2 (**Supplementary Figure 7**, **Supplementary Figure 9**, and **Supplementary Figure 10,** respectively). The aforementioned cell lines were created by taking advantage of the GATEWAY cloning technology (Section 3.5.5).

The immortalized non-tumorigenic human mammary epithelial cell line MCF10A (ATCC CRL-10317^{TM}) was kindly provided by Prof. Claudia Scholl, Division of Applied Functional Genomics, German Cancer Research Center (DKFZ), Heidelberg, DE. MCF10A cells were used for the establishment of the inducible stable cell lines that express turbo GFP, LATS1 or LATS2 (**Supplementary Figure 7**, **Supplementary Figure 9**, and **Supplementary Figure 10,** respectively). The aforementioned cell lines were created by taking advantage of the GATEWAY cloning technology (Section 3.5.5).

The human embryonic kidney cell line HEK293T (ATCC CRL-3216™) was kindly provided by Prof. Claudia Scholl (DKFZ), who originally received the cells from Prof. William Hahn, Broad Institute, Cambridge, MA, USA. The HEK293T cells were used for lentiviral production (Section 3.5.5.4).

3.1.2. Cell culture media

Depending on the experimental design, the following media types were used: (i) (label-free) growth media, (ii) full-SILAC growth media, (iii) pulsed-SILAC growth media, (iv) pulsed-SILAC starvation media, (v) pulsed-SILAC depletion media, and pulsed-SILAC pulse media. The compositions of the media for the respective cell lines MCF7, MCF10A, and ZR75.1 are summarized in **Table 3-5**, respectively.

3.1.3. SILAC labeling

For relative quantification of protein abundance, cells were labeled metabolically using stable isotope labeling by amino acids in cell culture (SILAC). When cell populations are mixed they are distiguinshed by MS and then quantified by their relative MS^1 signal. With

this strategy up to three cell populations can be combined. Therefore, cells were grown in SILAC media, composed of either non-labeled (light), medium-labeled (medium), or heavy-labeled (heavy) stable isotopic forms of the amino acids lysine and arginine. To ensure full incorporation of SILAC amino acids, cells were grown for at least six doublings in specialized SILAC growth media (ii) (**Table 3-5**). Labeling efficiency was assessed by MS, upon calculation of the amount of "heavy"- or "medium"-labeled compared to "light" lysine and arginine containing peptides. A minimum of 96% incorporated isotopic amino acids were considered as fully labeled.

3.1.4. Cryopreservation of cell lines

For conservation of cell lines, cells were harvested (Section 4.1.) when they reached 70-80 % confluency in a T75 flask (Thermo Fisher Scientific). Cell pellets from one T75 flask were resuspended in 2 mL freezing media (90% growth media (i) + 10 % (v/v) DMSO (Merck, Sigma-Aldrich), and each 1 mL was transferred into cryogenic tubes (Thermo Fisher Scientific). Gradual freezing was achieved by putting cryogenic tubes into Mr. Frosty™ Freezing Container (Thermo Fisher Scientific) in a -80°C freezer.

For thawing, cells in cryogenic tubes were quickly thawed in a 37°C water bath and transferred into 10 mL prewarmed growth medium. The cell suspension was centrifuged at 300-400 x g for 5 min and the supernatant was discarded. Cells were resuspended in 12 mL fresh growth media and transferred to a T75 flask for cultivation.

3.2. General molecular biology methods

3.2.1. SDS-Page and immunoblotting

Cells were harvested as described (Section 3.1). For immunoblotting of phosphorylated proteins, cells were washed with ice-cold PBS, scraped from the dish with a cell lifter (Merck, Corning) in 1-2 mL PBS on ice and transferred into a tube, followed by 2 min centrifugation at 500 x g at 4 °C. Three times the cell pellet volume of RIPA lysis buffer (**Table 17**) was added, supplemented with 1x (v/v) of cOmplete EDTA-free Protease Inhibitor Cocktail (Merck, Roche cocktail (100x stock: 1 tablet dissolved in 500 µl PBS). For the phospho-samples with additional 1x (v/v) phosphatase inhibitor cocktail PhosSTOP

(Merck, Roche) (10x stock: 1 tablet dissolved in 1 mL PBS) and incubated for 20 min on ice. Complete cell lysis and shearing of chromatin were performed in a Bioruptor Pico (Diagenode) with 15-20 cycles of 30''/30'' (ON/OFF) at 4°C. Samples were centrifuged at 15000 x g for 30 min at 4 °C and protein concentration was determined by bicinchoninic acid assay (BCA) assay following the manufacturer's protocol (Thermo Fisher, Pierce).

Table 17: RIPA lysis buffer

REAGENTS
150 mM NaCl
1% (v/v) NP-40
0.5% (w/v) Sodium deoxycholate (SDC)
0.1% (w/v) Sodium dodecyl sulfate (SDS)
50 mM Tris, pH 8.0

For gel electrophoresis, the Mini-PROTEAN® Tetra Cell System (Bio-Rad) was assembled, equipped with 4–15% precast gradient protein gels (Bio-Rad) and 1x (v/v) Tris/Glycine/SDS running buffer. 30 – 50 µg of protein were mixed in a 1:4 ratio (v/v) with 4x (v/v) Laemmli Sample Buffer (Bio-Rad) reduced and denatured for 5 min at 95 °C. After cooling down to RT, samples were spun down in a centrifuge for 1 min at maximum speed and loaded onto 4–15% precast gels. For protein size estimation 5 µL of Precision Plus protein marker (Bio-Rad) was loaded. The gel was run for 40 - 60 min at 100 Volt (V).

For protein transfer, the Trans-Blot® Turbo™ Transfer System (Bio-Rad) was used, together with Trans-Blot Turbo Mini 0.2 µm PVDF membranes using the pre-installed standard transfer method at up to 25 V and Ampère for 30 min.

After protein transfer, the membrane was rinsed with distilled water and incubated for 1 h in blocking solution (5% (w/v) milk or 3% (w/v) (Bovine Serum Albumin) BSA for phosphorylated-proteins, in PBST (0.1% (v/v) Tween)), with constant rocking at room temperature (RT). The membrane was cut into slices according to the expected protein sizes of the proteins of interest. Subsequently, membrane slices were incubated with the primary antibody (**Table 12**), diluted to the working concentration in blocking solution, and incubated overnight at 4 °C, with constant rocking. The next day, the membrane was washed with PBST three times for 10 min each, with constant rocking. Subsequently, the membrane was incubated for 2 h with the appropriate secondary antibody (**Table 13)**

diluted to the working concentration in blocking solution. Again, the membrane was washed with PBST three times for 10 min each, with constant rocking.

For chemiluminescence detection, ECL substrate A and B (Bio-Rad) were mixed in a 1:1 ratio (v/v) and placed on the membrane followed by one minute incubation at RT. The detection reagent was removed and the membrane was wrapped in plastic folie and imaged using the ChemiDoc Imaging System (Bio-Rad). The images were obtained using the Image-lab software (Bio-Rad) (**Table 16**).

3.2.2. Quantitative Polymerase Chain Reaction (qPCR)

Cells were harvested (Section 3.1), and RNA was isolated from cell pellets using NucleoSpin RNA Mini kit for RNA purification (Macherey-Nagel) according to the manufacturer's instructions. RNA was eluted from the columns with 30 µL nuclease-free water (Thermo Scientific, Invitrogen). Purity and concentration were determined using a NanoDrop spectrophotometer (Thermo Scientific). In particular, RNA concentration was assessed by measuring the UV-absorbance at 260 nm and sample purity was assesedby monitoring the ratios of absorbance at 260 nm to 280 nm (A260/A280; aiming ~ 1.8) and 260 nm to 230 nm (A260/A230; aiming ~2.1-2.3). RNA was either stored at -80 °C or directly transcribed into cDNA. Therefore, 2 µg RNA were reverse transcribed into cDNA via PCR using the High-Capacity cDNA Reverse Transcription Kit (Thermo Fisher Scientific) (**Table 18**).

Table 18: Reaction mix and thermocycler settings for cDNA reverse transcription

REAGENT	VOLUME/ 20 µL REACTION
10x RT buffer	2 µL
25x dNTP mix	0.8 µL
10x random primers	2 µL
Reverse transcriptase	1 µL
RNA sample	2 µg
Nuclease-free water	to 20 µL

TEMP	TIME	CYCLE
25 °C	10 min	
37 °C	120 min	1x
85 °C	5 min	
4 °C	∞	

For quantitative PCR, the generated cDNA and gene-specific primers (**Table 8**), designed with the publically available Primer 3.0 platform (**Table 16**), were used to quantify the relative mRNA abundance of the GOI. Accounting for the fluctuation of total cDNA

concentration, the stably expressed gene Hypoxanthine-guanine phosphoribosyl-transferase (HPRT-1) was used for normalization. For relative quantification, PowerUp™ SYBR™ Green Master Mix (Thermo Fisher Scientific) (**Table 19**) was used and the reaction was measured on a LightCycler® 480 System (Roche).

Table 19: Reaction Mix for qPCR

REAGENT	VOLUME/ 20 µL REACTION
PowerUp™ SYBR™ Green Master Mix	10 µL
Forward primer [10 µM]	0.5 µL
Reverse primer [10 µM]	0.5 µL
DNA sample [e.g. 40 ng/µL]	1 µL
Nuclease-free water	8 µL

To ensure signal specificity for every GOI, a melting curve step was acquired in the range of 65°C to 95°C and for all primer pairs, a water control was added. Also, the primer efficiency was tested by a standard curve, set up by serial dilutions of cDNA ranging from 100 ng/µL to 0.01 ng/µL.
For data analysis of mRNA expression, the ΔΔCq method was applied (Livak & Schmittgen, 2001).

3.3. siRNA-mediated transient knock-down of target genes

3.3.1. siRNA transfection

siRNA-mediated transient knock-down of LATS1, LATS2, and non-targeting control was performed by Noa Furth (WIZ) using Dharmafect I (Horizon Discovery, Dharmacon) transfection reagent and SMARTpool ON-TARGETplus siRNAs (Horizon Discovery, Dharmacon). ZR75.1 cells were seeded , 48 h before transfection in growth media at 1.5 x 10^6 cells per 10 cm dish. Each experiment was conducted in three biological replicates. On the day of the transfection, the medium was changed to growth media lacking antibiotics and reduced to 4 mL per 10 cm dish. A final concentration of 20 nM of SMARTpool ON-TARGETplus siRNAs targeting LATS1, LATS2 and non-targeting control was added according

to the manufacturer's protocol. Cells were incubated for 6 h before the medium was changed to normal growth media. In total after 48 h of transfection, cells were harvested and flash-frozen as described (Section 3.1). Cell pellets were sent on dry ice from the WIZ to the DKFZ and further processed by MS as described in the following Section.

3.3.2. Sample preparation for MS-based LFQ

Flash-frozen cell pellets were kept on ice and resuspended in 210 µL 0.1% (w/v) RapiGest-Surfactant (Waters) in 50 mM ammonium bicarbonate (Ambic) (Merck, Sigma-Aldrich). Full cell lysis and chromatin shearing was accomplished by using a Bioruptor Pico set to 15-20 cycles of 30''/30'' (ON/OFF) at 4°C. Protein concentration was determined by BCA assay following the manufacturer's instructions. Proteins were prepared for tryptic digestion by reduction of disulfide bonds with 5 mM DTT for 30 min at 60 °C and subsequent alkylation with 15 mM CAA for 30 min at RT. Proteolytic digestion was performed with sequencing grade modified trypsin (Promega) in a 1:50 (w/w) protease-to-protein ratio, overnight at 37 °C, shaking at 700 rpm. The next day, digestion was stopped and RapiGest-SF was broken down by adding 0.5- 1% (v/v) trifluoroacetic acid (TFA) (Biosolve), thereby lowering the pH to <2 and incubating at 37 °C for 30 min. The sample was centrifugated at 20,000 x g for 10 min, the supernatant was transferred into a new tube and dried in a vacuum centrifuge.

3.3.3. High pH-reverse phase liquid chromatography fractionation

For sample fractionation prior to LC-MS analysis, high pH- reverse-phase liquid chromatography fractionation (hpH-RPLC) was performed using a 1260 Infinity HPLC system (Agilent) with a Gemini C18 column (3 µm, 110 Å, 100 × 1.0 mm; Phenomenex). Briefly, dried samples were dissolved in 1% (v/v) formic acid (FA) (Bioslove). Subsequently, ammonium formate (pH 10) (Merck, Sigma-Aldrich) was added to final concentration of 20 mM and the sample was fractionated with a linear 60 min gradient. For the mobile phase, solvent A (20 mM ammonium formate) and solvent B (100% acetonitrile (ACN) (Biosolve)) were used in the following gradient: 0% B over 2 min, 0–65% B over 58 min, 65-85% over 2 min, 85% B over 5 min and, holding at 0% B for 8min. 1-minute fractions were collected within the first 60 minutes, resulting in total 60 fractions fthat were concatenated in twelve fractions. Subsequently, fractions were dried down in a vacuum centrifuge. Dried samples

were resuspended in 0.1% (v/v) FA and cleaned prior to LC-MS analysis using Oasis PriME HLB µElution Plate (Waters) as described in the following section.

3.3.4. Desalting and cleaning of peptides with Oasis PriME HLB µElution plate

For desalting and cleaning samples, Oasis PriME HLB µElution Plate was installed on a vacuum extraction plate manifold for oasis 96-well plates (Waters) and after each step, the liquid was passed through the columns by applying vacuum. The Oasis plate was activated, by consecutively adding 200 µL ACN, 200 µL elution buffer (60% (v/v) methanol (MeOH) (Biosolve), 1% (v/v) FA) and two times 200 µL washing buffer (1% (v/v) FA) respectively. The acidified samples (pH <2) were added, followed by consecutive washing steps with 750 µL, 250 µL, 100 µL of washing buffer. For the elution of the sample, 50 µL elution buffer and 50 µL 100% MeOH was added respectively, incubated for 2 min, before applying the vacuum and the samples were collected in a 96-well plate (Thermo Fisher Scientific). Finally, eluates were dried down in a vacuum centrifuge and stored in a -20 °C freezer until MS analysis.

3.3.5. LC-MS data acquisition with 2 hour Top20 method

Each fractionated sample was analyzed using LC-MS on an Orbitrap Q-Exactive High Field (QE HF) mass spectrometer (Thermo Fisher Scientific) coupled to an Easy-nLC 1200 (Thermo Fisher Scientific) ultrahigh-pressure liquid chromatography (UHPLC)system. Peptides were loaded onto an Acclaim PepMap^{TM} 100 C18 Nano-Trap (100 µm x 2cm, nanoViper, C18, 5 µm 100Å pores) (Thermo Scientific) and separated over either a 50 cm Acclaim PepMap^{TM} RSLC analytical column (75 µm × 50 cm, nanoViper, C18, 2 µM, 100Å) (Thermo Scientific) or a 50 cm nanoEase MZ Peptide BEH column (75 µm x 250 mm, nanoViper, C18, 1.7 µm 130 Å pores) (Waters). For the mobile phase, Solvent A (0.1% (v/v) formic acid) and Solvent B (0.1% (v/v) formic acid and 80% (v/v) ACN) were used in the following gradient: 3–8% B over 4 min, 8–10% B over 2 min, 10-32% over 68 min, 32–50% B over 12 min and 50-100% B in 1 min, holding at 100% B for 7 min. The gradient returned to 3% B in 1 min and was held there for 10 min to to equilibrate the analytical column. The flow rate throughout the runs was 300 nL/ min. Samples prepared as described previously were injected into the mass spectrometer by electrospray ionization (ESI) using a 10 µm Picotip coated fused silica emitter (New Objective) and a nanospray-Flex ion source (Thermo Fisher Scientific).

The QE HF mass spectrometer was operated in data-dependent mode (DDA) using a 2 hour top 20 method. Here, full MS spectra were acquired in the orbitrap with a mass range of 350-1500 m/z and a resolution of 60000 full width half maximum (FWHM). The automated gain control (AGC) target was set to $3x10^6$ with a maximum injection time of 32 ms. Precursor ions were filtered according to charge state (required 2-7 z), and monoisotopic peak assignment. Previously interrogated precursors were excluded using a dynamic exclusion window of 15 s ± 10 ppm tolerance. The 20 most intense precursors were selected for a second MS analysis (MS^2). For MS^2 scans AGC target was set to $1x10^5$, a maximum injection time of 50 ms and a resolution of 15000 FWHM. The isolation window was set to m/z 2.0, with a fixed first mass of m/z 110, and normalized collision energy of 26%. The intensity threshold was set to 2×10^4.

3.3.6. Processing of LFQ raw MS-data

The raw mass spectra files were analyzed with the MaxQuant software (version 1.5.1.2) (Cox & Mann, 2008) using the integrated search engine Andromeda (Cox *et al*, 2011). The protein sequence database UniProtKB/Swiss-Prot *Homo sapiens* obtained (13.09.2017) together with the contaminants.fasta which is enabled by default in the MaxQuant software, were used for the peptide searches. Search settings were set as follows: digestion reagent was set to trypsin/P, allowing up for two missed cleavages. Carbamidomethylation of cysteine was set as a fixed modification, oxidation of methionine and acetylation of the peptide N-term were set as variable modifications. The type of quantification was set to LFQ with a minimum ratio count of 2. The MaxQuant software algorithm “Match between runs” (MBR) was enabled with a matching time window of 0.7 min and an alignment time window of 20 min. Precursor and product ion tolerances were set at 4.5 ppm and 20 ppm, respectively. The false discovery rate (FDR) filter for peptides and protein hits was set to 1%, calculated by using a reverse decoy database. For identification, a minimum of 1 unique peptide was set. The remaining settings of MaxQuant were left in their default options. Data interpretation of MaxQuant output files was performed as described in Section 3.8.

3.4. Transient overexpression of target genes

3.4.1. Lipofection

Transient transfection was performed via lipofection in which a cation-lipid-based transfection reagent forms DNA-enclosing liposomes in the aqueous medium. These liposomes fuse with the cell membrane of the host cell to allow for DNA entry into the cytoplasm and eventually to the nucleus. Lipofectamine 3000 (Thermo Fisher Scientific, Invitrogen) was used according to the manufacturer's protocol to transfect the cell lines MCF7 and ZR75.1 with the plasmids GFP-LATS1 and GFP-LATS2 (for vector maps see **Supplementary Figure 7**, **Supplementary Figure 9**, and **Supplementary Figure 10**). The entire experimental setup is illustrated in **Figure 11.** Therefore, cells were seeded in specific cell numbers (**Table 20**) into each two T75 flasks per condition, aiming for 40% confluency on the day of transfection. Each experiment was conducted in three biological replicates. Lipofectamine mix and DNA mix (**Table 21**) were prepared in two separate tubes. Lipofectamine mix was vortexed 2-3 s before DNA mix was added in a 1:1 ratio (v/v) and incubated for 10-15 min at RT to enable the formation of DNA containing liposomes. The DNA liposomes were added to the cells and the flasks were shaken in 8-figure movement for equal distribution. Cells were incubated at 37°C for 24 h, harvested, and subjected to fluorescence-activated cell sorting (FACS) as described in the following section.

Table 20: Seeding cell number for transient transfection

CELL LINE	SEEDING CELL DENSITY [T75 FLASK]
MCF7	2 x 10^5 cells/ 1 day before
ZR75.1	3.5 x 10^5 cells/ 2 days before

Table 21: Lipofectamine and DNA mix

LIPOFECTAMINE MIX (PER T75 FLASK)	VOLUME
Opti-MEM™ Medium	934 µL
Lipofectamine™ 3000 Reagent	28.6 µL

DNA MIX (PER T75 FLASK)	VOLUME
Opti-MEM™ Medium	934 µL
DNA (1 µg/µL)	9.1 µL
P3000™ Reagent (2 µL/µg DNA)	18.2 µL

3.4.2. Fluorescence-activated cell sorting (FACS)

FACS was performed to sort ZR75.1 and MCF7 cells, transiently overexpressing GFP-LATS1 or GFP-tagged-LATS2, in order to obtain pure populations of GFP-positive and GFP-negative cells. Accordingly, after 24 h of transient overexpression cells were harvested with trypsin as described (Section 3.1). After PBS washes, cell pellets were carefully resuspended in FACS Buffer (2 µM EDTA (Merck, Sigma-Aldrich), 3% (v/v) fetal bovine serum (FBS) in PBS) and counted using a TC20 automated cell counter, aiming for a cell concentration of 5-10 x10^6 cells/ mL. To ensure single-cell suspension, cells were carefully passed through a 70 µm nylon mesh cell strainer (Merck, Corning) and stored on ice until FACS. With the assistance of the DKFZ core facility for flow cytometry, the sorting was performed on a FACS Aria II instrument (BD Biosciences). Therfore, a total of 12x 10^6 cells for each condition, chilled at 4 °C, were sorted with a nozzle size of 100 µm and a pressure of 20 psi into 15 mL tubes containing 2 mL of pre-cooled FACS buffer. GFP fluorescence exciting laser wavelength (Exλ_{max}) was set to 480 nm and emission was monitored at a wavelength (Emλ_{max}) to 530/25 nm. After FACS, cells were immediately centrifuged at 300 x g for 5 min at 4°C and washed two times with ice-cold PBS. Subsequently, cell pellets were flash-frozen and stored at -80°C, before they were further processed for TMT-based LC-MS/MS analysis as described in the following sections.

3.4.3. Cell lysis and digestion prior TMT peptide labeling

Flash-frozen cell pellets from FACS were resuspended in in 0.1% (w/v) RapiGest-SF in 100 mM triethylammonium bicarbonate (TEAB) pH 8 (Thermo Scientific). The samples were further processed, i.e. sonicated, reduced, alkylated, digested, and dried down as described in Section 3.3.2.

3.4.4. TMT peptide labeling

For isobaric labeling of peptides, 10-plex TMT reagents were used according to the manufacturer's instructions (Thermo Fisher Scientific). Dried down peptides (Section 3.4.3) were dissolved in 100 mM TEAB (pH 8), and peptide concentration was determined using a quantitative colorimetric peptide assay (Thermo Fisher, Pierce) according to the manufacturer's protocol. TMT10-plex reagents (0.8 mg) were dissolved in 41 µL of LC-MS

grade ACN and incubated at RT for 10 min. Then 10 µg of each sample was combined with 4.1 µL of the corresponding TMT reagent and incubated for 2h at RT. The reaction was quenched by adding 8 µl of 5% (v/v) hydroxylamine (Thermo Scientific) and incubating for 15 min at RT. A small fraction of each sample was desalted using Oasis PriME HLB µElution plate as described in Section 3.3.4 and labeling efficiency was checked by MS. Fully labeled peptides (label efficiency > 96%) were combined in equal amounts and dried down in a vacuum centrifuge.

3.4.5. LC-MS TMT-data acquisition of with 2 hour MS^3 method

Sample fractionation prior to LC-MS analysis was performed as described in Section 3.3.3. Fractions were analyzed by an Easy-nLC 1200 nano-UPLC conjugated to an Orbitrap Fusion™ Tribrid™ (Thermo Fisher Scientific) mass spectrometer with the same setup and gradient as described in Section 3.3.5.

The Fusion mass spectrometer was operated in DDA mode using the vendor-supplied default settings for synchronous precursor selection (SPS) MS^3 fragmentation (McAlister *et al*, 2014). For each cycle, one full MS spectrum was acquired in the orbitrap with a mass range of 380-1500 m/z and a resolution of 120000 FWHM at 200 m/z. The AGC was set to $2x10^5$ with a maximum injection time of 50 ms. Precursor ions were filtered according to charge state (required 2-7 z), and monoisotopic peak assignment. Previously interrogated precursors were excluded using a dynamic exclusion window of 40 s ± 10 ppm tolerance. The most intense precursors with a threshold of $5x10^3$ were selected for MS^2 analysis in the ion trap with collision-induced dissociation (CID), fragmenting in the Top Speed mode, with an isolation width of 0.5 Da. The “Ion Trap Scan Rate” was set to Turbo, with an AGC target of $1x10^4$, and a maximum injection time of 50 ms. The ten most intense precursors were selected for MS^3 with a precursor selection range of 400-1200 m/z, excluding 18 Da below and 5 Da above the precursor ion. The selected ions were transferred into the higher-energy collision dissociation (HCD) cell using the SPS waveform with an isolation width of 2.0 Da and AGC target of $1x\ 10^5$. The HCD collision energy for fragmentation was set to 65% and the scans were acquired in the orbitrap at a resolution of 60 000 at 200 m/z. The scan range was set to 120-500 m/z and the maximum injection time was 120 ms.

3.4.6. Processing of TMT raw MS-data

The raw mass spectra files were analyzed with the MaxQuant software (version 1.5.1.2) (Cox & Mann, 2008) using the integrated search engine Andromeda (Cox *et al*, 2011). The protein sequence database UniProtKB/Swiss-Prot *Homo sapiens* obtained (13.09.2017) together with the contaminants.fasta which is enabled by default in the MaxQuant software, were used for the peptide searches. Search settings were set as follows: digestion reagent was set to trypsin/P, allowing up for two missed cleavages. Carbamidomethylation of cysteine was set as a fixed modification, oxidation of methionine and acetylation of the peptide N-term were set as variable modifications. The type of quantification was set to 'reporter ion MS3' and correction factors for individual 10-plex TMT-kit batch were specified for each channel. Precursor and product ion tolerances were set at 4.5 ppm and 20 ppm, respectively. Label minimum ratio count was set to 2. The FDR filter for peptides and protein hits was set to 1%, calculated by using the reverse decoy database. The remaining settings of MaxQuant were set as default. Data interpretation of MaxQuant output files was performed as described in Section 3.8.

3.5. Establishment of TET-inducible overexpression cell systems

3.5.1. Bacterial (re-)transformation and selection of plasmids

To amplify plasmids required for transient transfection (Section 3.4.1.) and Gateway cloning (Section 3.5.5) subcloning efficiency DH5α™ competent cells (Thermo Fisher Scientific) (hereafter DH5α) were used. DH5α bacterial cells were thawed on ice and aliquoted in 50 µL into 5 mL round-bottom tubes (Fisher Scientific, Falcon). 10 ng of plasmid was added to the bacteria and incubated for 30 min on ice. Heat shock was performed by incubating bacteria for exactly 45 s at 42 °C on a thermomixer (Eppendorf). Subsequently, cells were incubated for 5 min on ice. 450 µL pre-warmed SOC medium (Thermo Fisher Scientific, Invitrogen) was added to the mixture and incubated at 37°C for 1 h, shaking at 200 rpm. Then, 50 µL of bacteria-suspension were spread on lysogeny broth (LB) agar dishes, supplemented with the appropriate antibiotics, depending on the respective antibiotic resistance gene of the plasmid (**Table 22**). The agar dishes were kept for a few

minutes at RT to allow for the bacterial suspension to dry. Then the agar dishes were incubated upside down for 18-20 h at 37°C.

Table 22: Antibiotic resistance of cloning plasmids

PLASMID BACKBONE	ANTIBIOTIC RESISTANCE	ANTIBIOTIC CONCENTRATION IN LB MEDIUM
pEGFP	Kanamycin	50 µg/ mL
pDONR^{TM}221	Kanamycin	50 µg/ mL
pTRIPZ-GW	Ampicillin	100 µg/ mL

3.5.2. Inoculation and miniprep

After (re-)transformation, one to three single colonies were picked and inoculated into separate tubes containing 5 mL of LB medium, supplemented with the appropriate antibiotic (**Table 22**). Cultures were allowed to grow overnight at 37 °C on an orbital shaker, agitating at 200 rpm. The next day, 700 µL of bacteria were stored at 4 °C for potential cryopreservation (4.5.3) after sequence validation via Sanger sequencing (4.5.2). From the remaining volume of the culture, plasmids were isolated and purified using QIAprep Spin Miniprep Kit (Qiagen) according to the manufacturer's protocol. Plasmid DNA concentration was assessed by using a Nanodrop spectrophotometer.

3.5.3. Sequence validation via Sanger sequencing

To confirm successful cloning and (re-)transformation, i.e. plasmid identity and correct DNA sequence, Sanger sequencing was performed. Therefore, purified plasmids were sent with theappropriate primers (**Table 7**) to Microsyth SEQLAB (Göttingen). The obtained sequences were aligned by using either the Snapgene software (Insightful Science) or the NCBI reference sequence and the ApE software (M. Wayne Davis) (**Table 16**).

3.5.4. Cryopreservation of bacteria in glycerol stocks

To preserve plasmid DNA in desired bacteria for long-term storage and quick retransformation, glycerol stocks were established. Therefore, 700 µL from a total of 5 mL overnight grown liquid culture were added to 300 µL of 100% glycerol in cryogenic tubes and stored at -80°C.

3.5.5. GATEWAY cloning technology: table tet-inducible overexpression cell systems

The GATEWAY cloning (Katzen, 2007) was performed as described on the Thermo Fisher Scientific's web page (https://www.thermofisher.com/de/de/home/lifescience/cloning/gateway-cloning/protocols.html), summarized as follows.

3.5.5.1. AttB PCR and BP recombination reaction

For the BP-reaction, attB-flanked PCR products were produced by using attB- primers (**Table 6**) flanking full-length LATS1 or LATS2 coding sequence (CDS). The CDS were taken from pEGFP-LATS1 and pEGFP-LATS2 plasmids (kindly provided by Prof. Oren's lab; **Supplementary Figure 1** and **Supplementary Figure 2**). The PCR was set up as follow:

Table 23: attB PCR reaction mix

REAGENT	VOLUME/ REACTION	FINAL CONC.
5x Phusion HF Buffer	10 µL	1x (v/v)
10 mM dNTP	1 µL	200 µM
Forward Primer	2.5 µL	0.5 µM
Reverse Primer	2.5 µL	0.5 µM
Phusion HF Polymerase (NEB)	0.5 µL	1 unit
DMSO	1.5 µL	3% (v/v)
Template Plasmid	variable	<250 ng
Nuclease-free water	To 50 µL	

Table 24: attB PCR cycler settings

STEP	TEMP	TIME	CYCLE
Initial denaturation	98 °C	1 min	1x
Denaturation	98 °C	20 s	
Annealing	62 °C	30 s	20x
Elongation	72 °C	30 s/kb	
Final Extension	72 °C	105 s	1x
Hold	4 °C	∞	

The PCR amplicons were purified using the QIAquick PCR Purification Kit (Qiagen), according to the manufacturer's instructions. To extract and validate the PCR product, first it was stained with the loading dye (Thermo Scientific) and loaded on a 0.8% (w/v) agarose gel (0.8% (w/v) agarose (Merck, Sigma-Aldrich) in 1x (v/v) TAE buffer (40 mM Tris base (Merck, Sigma-Aldrich), 20 mM acetic acid (Biosolve) and 1 mM EDTA, supplemented with

1x (v/v) SYBR Safe DNA Gel Stain (Thermo Fisher Scientific, Invitrogen). Subsequently, the amplicons were cut out of the agarose gel with a razor blade and purified using QIAquick Gel Extraction Kit (Qiagen), according to the manufacturer's instructions. The flanking attB-sites of the PCR products and the attP-sites of the DONOR vector, pDONR^{TM}221, allows for the BP recombination reaction, integrating the gene sequence of interest into the vector. Here the enzymes of t he Gateway™ BP Clonase™ II Enzyme Mix (Thermo Fisher Scientific, Invitrogen) were used according to the manufacturer's instructions. The BP reaction mix (**Table 25**) was incubated for 2 h at 25 °C. The reaction was stopped by digesting BP Clonase II with 1 µL of proteinase K. The entry vector, pENTR, was amplified in a transformation reaction (Section 3.5.1) and cryopreserved in glycerol stocks (Section 3.5.4).

Table 25: BP reaction mix

REAGENT	(PER REACTION)
attB-PCR product (with attB-sites)	150 ng
pDONR^{TM}221 (with attR-sites)	150 ng
TE buffer	Fill up to 8 µL
BP Clonase^{TM} II	2 µL

3.5.5.2. Destination vector pTRIPZ-GW

The destination vector pTRIPZ-GW was kindly provided by Dr. Stefan Pusch (DKFZ). Briefly, Pusch's lab used the commercially available "TRIPZ Inducible Lentiviral shRNA vector" (https://horizondiscovery.com/en/gene-modulation/knockdown/shrna/products-/tripz-inducible-lentiviral-shrna-controls) and exchanged the shRNA-cassette by the GATEWAY-cloning cassette, creating the pTRIPZ-GW destination vector (**Supplementary Figure 8**), (not published).

3.5.5.3. LR recombination reaction

The flanking attL-sites of the gene sequences of LATS1 and LATS2 in the pENTR clones and the attR-sites of the GATEWAY vector pTRIPZ-GW allowed for the LR recombination reaction, integrating the gene sequence of interest into the final expression plasmid. Here the enzymes of the Gateway™ LR Clonase™ II Enzyme Mix (Thermo Fisher Scientific, Invitrogen) were used according to the manufacturer's instructions. The LR reaction mix

(**Table 26**) was incubated for 2 h at 25 °C. The reaction was stopped by digesting LR Clonase II with 1 µL of proteinase K. The expression plasmids pTRIPZ-GW LATS1, pTRIPZ-GW LATS1, and the control plasmid pTRIPZ-pGFP (the latter, provided by Dr. Stefan Pusch (DKFZ)) were amplified in a transformation reaction (Section 3.5.1) and cryopreserved in glycerol stocks (Section 3.5.4).

Table 26: LR reaction mix

REAGENT	(PER REACTION)
Entry vector (pENTR with attL-sites)	150 ng
Expression plasmid (pTRIPZ-GW with attR-sites)	150 ng
TE buffer	Fill up to 8 µL
LR Clonase™ II	2 µL

For amplifying expression plasmids, Stbl3™ chemically competent *E. coli* cells (Thermo Fisher Scientific), which are suitable for cloning lentiviral plasmids, were transformed with 1 µL of the LR reaction (Section 3.5.2). Single colonies were inoculated into separate tubes containing 30 mL of LB medium that was supplemented with the appropriate antibiotics (**Table 22**). Finally, plasmids were purified with NucleoBond Xtra midi kit for transfection-grade plasmid DNA (Macherey-Nagel), according to the manufacturer's instructions.

3.5.5.4. Lentivirus production

The efficiently transfected cell line HEK293T was used for lentiviral production. Briefly, 1 x10^6 cells were seeded in 10 cm dishes and 10 mL growth medium, composed of DMEM medium (Thermo Fisher Scientific, Gibco) complemented with 10% (w/v) FBS. The following day, for the preparation of the plasmid master mix (**Table 27**) the expression plasmid pTRIPZ-GW (**Supplementary Figure 8**), the packaging (**Supplementary Figure 6**) and the envelop plasmids (**Supplementary Figure 5**) were combined and incubated for 5 min at RT. TransIT-LT1 mix (**Table 28**) was prepared in parallel and added to the transfection mix The mix was incubated for another 30 min at RT. Growth media was reduced to 6 mL (without antibiotics) and the transfection mix was added dropwise and evenly distributed on top of the cells.

Table 27: Plasmin master mix

TRANSFECTION MIX (PER DISH)	AMOUNT
Packaging plasmid (pSPAX2)	1.8 µg
Envelop plasmid (pMD2.G)	0.3 µg
Expression plasmid (pTRIPZ -tGFP; -LATS1; -LATS2)	3 µg
Opti-MEM™ (without supplements)	Fill up to 22 µL

Table 28: Transfection mix

TransIT-LT1 MIX (PER DISH)	VOLUME
TransIT-LT1	18 µL
Opti-MEM™ (without supplements)	270 µL

3.5.5.5. Lentiviral transduction and stable cell line selection

To establish stable TET inducible cell systems for LATS1, LATS2 and turboGFP, replication deficient lentiviral particles were used. Hence, each cell line (MCF7, MCF10A, and ZR75.1) was transduced with each one of the three plasmids. Therefore, cells were seeded in 6-well plates (Thermo Fisher Scientific) in cell line-specific density (**Table 30**) aiming for ~30% confluency. The next day, the medium was removed and 500 µL of lentiviral particles (Section 3.5.5.4) were added or pippeted on the cells. An additional 1.5 mL of growth medium supplemented with 8 µg/mL of the cationic polymer polybrene (Merck, Sigma-Aldrich) was added to each well, in order to increase the lentiviral infection efficiency by neutralizing the charge impulsion of the virion and the cell surface. The next day, the medium was replaced by growth medium (i) (**Table 3-5**). Cell line selection started 20 h after infection by adding previously titrated cell line-specific antibiotics (Table 29).

Table 29: Cell-specific conditions for lentiviral transduction and cell selection

CELL LINE	SEEDING CELL DENSITY [6-WELL]	PUROMYCIN CONCENTRATION/DURATION
MCF7	2 x 10^5 cells/ 1 day before	1 µg/ mL for 5 days
MCF10A	1.5 x 10^5 cells/ 1 day before	3 µg/ mL for 3 days
ZR75.1	4 x 10^5 cells/ 2 days before	1 µg/ mL for 5 days

3.6. Pulsed SILAC and Click Chemistry

3.6.1. Cell culture for pulsed-SILAC

For pulsed-SILAC and click-chemistry (i.e. translatome- and secretome analysis) newly established TET-inducible overexpression cell systems in MCF7, MCF10A, and ZR75.1 cells (Section 3.5) were used. Experiments were conducted as described before (Eichelbaum *et al*, 2012; Eichelbaum & Krijgsveld, 2014), with a few adaptions, described here. MCF7, MCF10A, and ZR75.1 cell lines were grown in cell line-specific media (DMEM, DMEM F12, RPMI 1640, respectively) complemented with the additives required for the specific experimental steps (**Table 3**, **Table 4**, and **Table 5**). Each experiment was conducted in three biological replicates. Prior to the pulse experiment, cells were grown in medium labeled full-SILAC growth media (ii) (as described in Section 3.1.3) to ensure > 96% label incorporation. For the experiment, cells were seeded in 15 cm dishes containing 20 mL of pulse growth media (iii) supplemented with SILAC "medium" amino acids in cell line-specific cell numbers aiming for 70% confluency on the day of the pulse (**Table 30**). The next day and 16 h before the pulse experiment, cell media was switched to 15 mL starvation media (iv), with decreased serum and in the case of MCF10A cells, void of EGF. Before the pulse, the cells were washed with warm PBS and depleted of methionine, lysine, and arginine by incubation in 10 mL depletion media (v) for 30-40 min. Subsequently, cells were pulsed for 6 hours by adding cell line-specific titrated amount of doxycycline (dox) (Merck, Sigma-Aldrich) (**Table 31**) in 13 mL of pulse media (vi). The pulse media was supplemented with the methionine analog L-azidohomoalanine (AHA) and either SILAC "light" amino acids for control cells or SILAC "heavy" amino acids for LATS1- or LATS2-overexpressing cells, allowing to combine samples on the cell or protein level. For long-term DOX treatment, cells were pre-incubated with DOX and pulsed for the last 6 h hours of the total incubation time (**Table 31**).

Table 30: Cell seeding density and doxycycline concentration for pulse experiments

CELL LINE	SEEDING CELL DENSITY [15 cm dishes]	DOX CONCENTRATION	DURATION OF DOX-INDUCED OVEREXPRESSION
MCF7	3.5 x 10^6 and 2 x 10^6 cells / 1 day before	4 µM	6 h and 48 h

MCF10A	6 x 10^6 and 4 x 10^6 cells / 1 day before	2 µM	6 h and 24 h
ZR75.1	4 x 10^6 and 2.5 x 10^6 cells / 2 days before	4 µM	6 h and 72 h

After incubation, the supernatant was collected for secretome analysis. Therefore, 13 mL of supernatant was transferred into 15 mL tubes containing 130 µL of 1x (v/v) of cOmplete EDTA-free Protease Inhibitor Cocktail in PBS, inverted two times, centrifuged for 5 min at 500 x g. Cell-free supernatant was transferred into a new 15 mL tube in order to continue with the enrichment protocol or for flash-freezing in liquid nitrogen and subsequent storage in.

For translatome analysis, cells were washed two times with pre-warmed PBS, scraped from the dish with a cell lifter and transferred into a 1.5 mL tube. Subsequently, cells were centrifuged at 400 x g for 3 min at 4 °C. The supernatant wasdiscarded and cells were used either for enrichment (Section 3.6.2) or were stored at -80°C after flash freezing.

3.6.2. Enrichment of newly synthesized proteins by click chemistry

For enrichment of newly synthesized secreted proteins by click chemistry capture of azide-modified proteins, supernatant of the overexpression sample and the corresponding control were mixed in a 1:1 ratio (w/w) and half of the sample was concentrated down to a volume of ~ 250 µL, using a 15 mL 3 kDa cut-off filter system (Merck, Millipore) by centrifugation for 2 h with 5000 x g at 4 °C. The other half was flash-frozen and stored at -80 °C as a backup. The concentrated supernatant was transferred into a 2 mL tube containing 1450 µL of freshly prepared ureas lysis buffer (**Table 31**).

For enrichment of newly synthesized intracellular proteins by click chemistry cell pellets were lysed in 900 µL urea lysis buffer containing 1x (v/v) of cOmplete EDTA-free protease inhibitor cocktail. Complete cell lysis and shearing of the chromatin were performed in a Bioruptor Pico with 15-20 cycles of 30’’/30’’ (ON/OFF) at 4°C. Samples were centrifuged for 30 min at 4 °C and 15000 x g and protein concentration was determined by BCA assay following the manufacturer’s instructions. Sample overexpressing protein of interest and the corresponding control were mixed in a 1:1 protein ratio (w/w) and filled up to 1700 µL end volume with urea lysis buffer.

Table 31: Click reaction buffers and solutions

UREA LYSIS BUFFER	1-STEP REDUCATION/ ALKYLATION SOLUTION	DIGESTION BUFFER
200 mM HEPES (pH 8)	10 mM TCEP	100 mM Tris-HCl (pH 8)
0.5 M NaCl	40 mM CAA	2 mM $CaCl_2$
4% (w/v) CHAPS	in SDS-wash buffer (Click-iT™-Kit)	5% (v/v) ACN
8 M Urea		

The following reagents used from the Click-iT™ protein enrichment kit (Thermo Fisher Scientific, Invitrogen) are marked with the abbreviation Click-iT™-Kit.

For the click chemistry reaction 100 µL alkyne-agarose beads (Click-iT™-Kit) per sample were prepared by transferring the beads-slurry into a 2 mL tube and washing the beads with 1.9 mL of milli-Q water. Beads were centrifuged for 5 min at 1000 x g at RT and the supernatant was removed.

Next, the sample was alkylated by 42.5 µL of 600 mM iodoacetamide (IAA) (Bio-Rad) was added to each sample and incubated in a centrifuge, rotating at 15000 x g at 20 °C. Meanwhile, the reaction mix for the click reaction was prepared (**Table 32**).

Table 32: Reaction mix for [3+2] cyclo-addition click reaction

REAGENTS	VOL / REACTION
200 mM Cu(II) SO_4	10 µL
160 mM Cu(I) ligand THPTA (reaction additive I in Click-iT™-Kit)	62.5 µL
2 M aminoguanidine	10 µL
2 M sodium ascorbate (reaction additive II in Click-iT™-Kit)	10 µL

After alkylation, the sample was transferred to prior prepared alkyne agarose beads-containing tubes, and 93 µL of the reaction mix (**Table 32**) was added to each tube. The mixture was incubated for 2 h at 40 °C, shaking at 1600 rpm.

After the click reaction, the resin was pelleted by centrifugation for 1 min at 2000 x g at RT, and the supernatant was discarded. Agarose beads were washed with 1.9 mL Milli-Q water, the resin was pelleted by centrifugation for 1 min at 2000 x g at RT and the supernatant was discarded. Then, 2 mL of 1-Step reduction/alkylation solution (**Table 31**) was added and the sample was incubated for 15 min at 70°C, shaking at 1600 rpm.

Table 33: Washing buffers for click reaction

SDS-WASH BUFFER (Click-iT™-Kit)	GUANIDINE-WASH BUFFER	ACETONITRIL-WASH BUFFER
100 mM Tris-HCl (pH 8)	100 mM Tris-HCl (pH 8)	20% (v/v) ACN
1x SDS	6 M Guanidine-HCl	In LC/MS-grade water
250 mM NaCl	in LC/MS-grade water	
5 mM EDTA		

In parallel, chromatography/spin columns (Click-iT™-Kit) were prepared according to the manufacturer's protocol (Thermo Fisher Scientific, Invitrogen). After incubation, the sample was transferred with a cut P1000 tip to a chromatography/spin column. The sample was thoroughly washed with each of the 1 mL wash buffers (**Table 33**), in consecutive order as follows: 5 times with SDS-wash buffer, 2 times with LC/MS-grade water, 5 times with guanidine-wash buffer, 5 times with acetonitrile-wash buffer. After the last washing step, the cap of the chromatography/spin column was added and beads were carefully resuspended in digestion buffer (**Table 31**) and transferred with a cut P1000 tip into a 1.5 mL tube. Then beads were spun down by centrifugation for 1 min at 2000 x g and digestion buffer was removed, leaving over ~ 200 µL of buffer in the tube.

For overnight on-bead digestion 0.5 µg and 1 µg of sequencing grade modified trypsin was added to the secretome and translatome samples, respectively, and incubated overnight at 37 °C, shaking at 800 rpm. The next day, the agarose beads were pelleted by centrifugation for 5 min at 1000 x g. The peptide-containing supernatant was transferred to a new 1.5 mL tube. To dissolve the remaining peptides, 500 µL of LC/MS-grade water was added to the beads, briefly vortexed, spun down and the supernatant was transferred to a new tube. The reaction was stopped by adding 10% (v/v) of FA, ensuring a pH below 2.5. Samples were desalted using an Oasis PriME HLB µElution Plate (Section 3.3.4).

3.6.3. LC-MS data acquisition with 2 hour Top20 method

Sample fractionation prior to LC-MS analysis was performed as described in Section 3.3.3. Fractions were analyzed on an Orbitrap QE HF using the 2 hour Top20 method as described in Section 3.3.5.

3.6.4. Processing of SILAC raw MS-data

The raw mass spectra were analyzed with the same settings as described in Section 3.3.5, but with the following adjustments: The protein sequence database UniProtKB/Swiss-Prot *Homo sapiens* was updated on 06.11.2020. The type of quantification was set to standard – multiplicity 3 for SILAC quantification. For medium labels "Lys4" and "Arg6" and for heavy labels "Lys8" and "Arg10" were selected. Also, the MaxQuant software algorithm "Re-quantify" was enabled. The remaining settings of MaxQuant were set as default. Data interpretation of MaxQuant output files was performed as described in Section 3.8.

3.7. Enrichment of phosphopeptides using Fe^{3+}-IMAC column

3.7.1. Cell culture for phosphopeptide enrichment

For phosphoproteomic analysis, the newly established TET-inducible overexpression cell systems in MCF7, MCF10A, and ZR75.1 cells (Section 3.5) were fully SILAC labeled as described in Section 3.1.3. Each experiment was conducted in three biological replicates The LATS1-overexpressing cells were labeled in SILAC-light, the LATS2-overexpressing cells were labeled in SILAC-heav, and GFP-overexpressing control cells in SILAC-medium. Sample preparation and enrichment were performed according to Ruprech et. al (2015) (Ruprecht *et al*, 2015) with the adaptations of the protocol described in Clement et. al (2018) (Potel *et al*, 2018) and minor changes described herein. Therefore, a cell line-specific number (**Table 34**) of fully labelled SILAC cells were seeded in 10 cm dishes, adding 12 mL of full-SILAC growth media. For MCF10A cells, the media was changed to EGF-deprived growth media 16 hours before the experiment. The next day, cells were induced by adding cell line-specific titrated amounts of dox (**Table 34**) for either 2 hours or for cell-line-specific long-term treatment.

Table 34: Cell seeding density and doxycycline concentration for phosphopeptide enrichment experiments

CELL LINE	SEEDING CELL DENSITY [10 cm dishes]	DOX CONCENTRATION	DURATION OF DOX-INDUCED OVEREXPRESSION
MCF7	1.4 x 10^6 and 8 x 10^5 cells / 1 day before	4 µM	2 h and 48 h

MCF10A	2.5 x 10^6 and 2.5 x 10^6 cells / 1 day before	2 µM	2 h and 6 h
ZR75.1	2 x 10^6 and 1.5 x 10^6 cells / 2 days before	4 µM	2 h and 72 h

After cell line-specific incubation times, cell plates were put on ice, and media was aspirated. Subsequently, cells were washed two times with ice-cold PBS , lysed by adding 250 µL of lysis buffer (**Table 35**), distributed equally and incubated for 15 min on ice. The cell slurry was scraped from the dish with a cell lifter and transferred into a 1.5 mL tube. Complete cell lysis and shearing of chromatin were performed in a Bioruptor Pico with 15-20 cycles of 30''/30'' (ON/OFF) at 4°C. Samples were centrifuged for 30 min at 4 °C, 15000 x g and protein concentration was determined by BCA assay following the manufacturer's instructions. Corresponding SILAC-light, -medium, and -heavy samples were mixed in a 1:1:1 protein ratio (w/w/w). To remove residual nucleic acid and thereby avoid co-elution with phospho-peptides during phospho-enrichment steps, methanol/ chloroform protein precipitation was performed as described (Potel *et al*, 2018). The precipitate was resuspended in 200-300 µL of digestion buffer (**Table 35**) and digested with sequencing grade modified Trypsin/LysC in a 1:50 ratio (w/w), overnight at RT. The next day, the reaction was stopped and sodium-deoxycholate (SDC) (as part of the digestion buffer) was precipitated by acidifying with 10% (v/v) FA and thereby lowering the pH below 3.5. SDC was pelleted by centrifugation of the samples for 5 min at 14000 x g. The supernatant was desalted using C18 Sep-Pak resin columns (Waters) as described in the following section.

Table 35: Buffers for phosphopeptide enrichment

LYSIS BUFFER	DIGESTION BUFFER
8 M urea	100 mM Tris-HCl (pH 8.5)
40 mM Tris-HCl (pH 7.6)	1% (w/v) sodium-deoxycholate (SDC)
1x protease inhibitors	30 mM CAA
1x phosphatase inhibitors	5 mM TCEP
in water	in water

3.7.2. Desalting sample with C18 Sep-Pak resin columns

Prior to phosphopeptide enrichment (Section 3.7.3) and proteome fractionation (Section 3.7.4), samples were desalted using C18 Sep-Pak resin columns with 50 mg sorbent

(Waters) attached to an Extraction Manifold & Vacuum Pump (Waters). This allows for the liquid to pass through the column after every step, by applying vacuum. To prepare the column it was primed by adding 1 mL Buffer B (50% (v/v) ACN, 0.07% (v/v) TFA) and equilibrated by adding two times Buffer A (0.07% (v/v) TFA). Then the sample was loaded two consecutive times and washed 3 times with Buffer A. Finally, the sample was eluted by adding two times 150 µL Buffer B, incubating for 2 min, before applying the vacuum and collecting the eluate. The 300 µL sample was divided into 2 tubes containing 10 % for global proteome and 90% for phosphopeptide enrichment. Both samples were dried in a vacuum centrifuge.

3.7.3. Enrichment of phosphopeptides using Fe^{3+}-IMAC column

Phosphoenrichment was performed using a Fe^{3+}-IMAC column (Thermo Fisher Scientific) as described before ((Ruprecht *et al*, 2015, 2017; Potel *et al*, 2018)). The IMAC-column was charged with Fe^{3+} on an 1100 Series HPLC system (Agilent Technologie). The IMAC-column was flushed with LC/MS-grade water for 7 min at a flow rate of 3 mL/min. In case of column reuse the stripping was accomplished with EDTA stripping-solvent (50 mM EDTA (pH 8)) for 24 min at a flow rate of 1 mL/min in conjuction with an additional flushing step with LC/MS-grade water for 7 min at a flow rate of 3 mL/min. Then IMAC-column was charged with charging solvent (25 mM $FeCl_3$ (Merck, Sigma-Aldrich) in 100 mM acetic acid) for 30 min at a flow rate of 200 µL/min. Finally, the IMAC column was rinsed with 0.1 % (v/v) FA for 25 min at a flow rate of 2 mL/min.

For phosphopeptide enrichment charged column was connected to an UltiMate 3000 HPLC System (Thermo Fisher Scientific). Previously dried peptides (Section 3.7.2) were resuspended in 50 µL Loading Buffer (0.07% (v/v) TFA, 30% (v/v) ACN) and directly injected into the UltiMate 3000 HPLC using a syringe (Hamilton). For the mobile phase, Solvent A (0.07% (v/v) TFA and 30% (v/v) ACN) and Solvent B (0.3% ammonium hydroxide (NH_4OH)) were used in the following gradient: 0% B over 5 min at 200 µL/min flow, 0–16% B over 1 min and 45 sec at 3 mL/min flow, 16–26% B over 5 min at 550 µL/mL flow, 26-50% over 45 sec at 3 mL/min flow, and 50–0% B over 2 min at 3 mL/min flow and finally lowering the flow back to 200 µL/min. Both flowthrough and phosphopeptide fraction were collected according to the UV signal at 280 nm. Collected samples were dried by vacuum

centrifugation and resuspended in 1% (v/v) FA. Samples were desalted using Oasis PriME HLB µElution Plate as described in Section 3.3.4, prior to LC-MS analysis.

3.7.4. LC-MS data acquisition of phospho samples with single-shot 3 h method

The dried phospho sample was resuspended in 1% (v/v) FA in 50 mM citric acid (Biosolve) and analyzed using an Orbitrap QE HF mass spectrometer coupled to an Easy-nLC 1200 as described in Section 3.3.5, but with the following changes of the gradient: 0–2% B over 3 min, 2–25% B over 150 min, 25-40% over 30 min, 40–95% B over 1 min, and holding at 95% B for 5 min. The gradient returned to 2% B in 1 min and was held there for 20 min to prepare for the next injection. The QE HF mass spectrometer was operated in DDA mode using the 3-hour vendor-supplied default settings for phosphoproteomics. Briefly, full MS spectra were acquired in the orbitrap with a mass range of 375-1500 m/z and a resolution of 120000 FWHM. The AGC target was set to $1x10^6$ with a maximum injection time of 54 ms. Precursor ions were filtered according to charge state (required 2-7 z), and monoisotopic peak assignment. Previously interrogated precursors were excluded using a dynamic exclusion window of 45 s ± 10 ppm tolerance. For MS^2 scans AGC target was set to $2x10^5$, a maximum injection time of 90 ms and a resolution of 15000 FWHM. The isolation window was set to m/z 1.2, with a fixed first mass of m/z 110 and fixed HCD collision energy of 35%.

3.7.5. LC-MS data acquisition of proteome sample

Sample fractionation prior to LC-MS analysis was performed as described in Section 3.3.3. Fractionated proteome samples were acquired using the 2 hour Top20 method as described in Section 3.3.5.

3.7.6. Processing of phospho-proteome SILAC raw MS-data

The raw mass spectra were analyzed with the same settings as described in Section 3.6.4, in addition the variable modification “Phospho (STY)” was enabled. The remaining settings of MaxQuant were left at the default options. Data interpretation of MaxQuant output files was performed as described in Section 3.8.

3.8. Data interpretation

For data interpretation, the MaxQuant output files were further processed in R version 4.0.4 (https://www.R-project.org/ R Core Team (2021)) operated in Rstudio version 1.1.453 (http://www.rstudio.com/ - Rstudio Team 2020). For quantification, peptide intensities were log_2-transformed and median normalized. Proteins of the following categories were filtered out prior to differential expression analysis: only identified by site, potential contaminants, and reverse. Sample clustering was evaluated using t-SNE- and UMAP-plots (Section 3.8.1) and batch correction was applied if necessary. Differentially expressed proteins were assessed by applying "linear Models for Microarray Data" (limma)-moderated test statistics in R (Ritchie *et al*, 2015), with an adjustedp-value below 0.05 (p-values were adjusted according to Benjamini-Hochberg).

3.8.1. Evaluation of sample distribution using t-SNE and UMAP

Sample clustering was evaluated with t-distributed stochastic neighbor embedding (t-SNE) and uniform manifold approximation and projection (UMAP) analysis, applied via R packages (Maaten, 2008; McInnes *et al*, 2018). Perplexity (tSNE) or neighbors (UMAP) and iterations (both) were adjusted to the individual experimental setup.

3.8.2. Overrepresentation analysis (ORA) and Gene set enrichment analysis (GSEA)

For data interpretation, lists of significantly regulated proteins were subjected to ORA analysis (Liu & Ruan, 2013), either using the STRING functional protein associated network database (Szklarczyk *et al*, 2017) or the Molecular Signatures Database (MSigDB).(Subramanian *et al*, 2005; Liberzon *et al*, 2011) The MsigDB gene sets considered were: Hallmark gene sets (H), curated gene sets (C2), ontology gene sets (C5) and oncogenic gene set (C6).

Whole protein expression lists, ranked according to log_2 fold change (high to low) were subjected to gene set enrichment analysis (Subramanian *et al*, 2005) performed by using the R package fgsea (Korotkevich *et al*, 2021). Gene sets were taken from the REACTOME database (Wu & Haw, 2017) embedded in the R packages ReactomePA version (Yu & He, 2016) while the size of the gene sets was set to 15-500, and the number of permutations set to 10000.

3.8.3. Phosphoproteome data analysis

For phosphoproteome analysis, both normalized and un-normalized data was used. For normalization measured phosphopeptide abundance was adjusted to corresponding peptide abundance from non-enriched (global) MS analysis.

For phospho data interpretation the following R packages were used: (i) the Kinase-Substrate Enrichment Analysis (KSEA) (Lachmann & Ma'ayan, 2009; Casado *et al*, 2013; Wiredja *et al*, 2017) and (ii) PTM-SEA based on the first site-specific post-translational-modification (PTM) signatures database (PTMsigDB), (**Table 16**) (Krug *et al*, 2019). The KSEA tool for kinase activity inference from quantitative phosphoproteomics is taking advantage of the curated kinase-substrate network from the PhosphoSitePlus database (Hornbeck *et al*, 2015). It represents the activity of a kinase by calculating the mean phosphorylation of the corresponding substrates. The statistical significance is represented by the z-score (calculated by normalizing the log-fold change of substrates with the standard deviation (SD) of all phosphosites in the dataset).

PTMsigDB is providing a repository of site-specific PTM motif signatures, kinase activities, and curated signaling pathways compiled from different databases such as: (PhosphoSitePlus (PSP) (Hornbeck *et al*, 2015), Netpath (Kandasamy *et al*, 2010), and WikiPathways (Kutmon *et al*, 2016). It combines information about the sites that have been quantitatively characterized in perturbation studies, are known substrates of kinases or are known to be activated/deactivated in signaling pathways. PTM-SEA, adapted from the single sample Gene Set Enrichment Analysis approach (ssGSEA), carries out enrichment analysis based on the PTMsigDB (Krug *et al*, 2019). Similar to GSEA the enriched pathways are ranked according to a FDR-controlled enrichment score.

4. RESULTS AND DISCUSSION

4.1. Knockdown of LATS1, but not LATS2, perturbs proteins involved in cell cycle checkpoint control in luminal b breast cancer cells

As a starting point for gaining insight into LATS1 and LATS2 functionalities in breast cancer, each kinase was selectively downregulated. Subsequently, the effects on cell signaling networks were assessed by performing label-free global proteome analysis. In particular, the luminal breast cancer cell line ZR75.1 was subjected to siRNA-mediated silencing of LATS1, LATS2, or non-targeting control. Adequate knockdown efficacy after 24 h siRNA-mediated silencing of LATS1 and LATS2 was validated on the transcript level using quantitative polymerase chain reaction (qPCR), showing a significant reduction in the relative mRNA expression level of more than 71% for both kinases, compared to the control (**Figure 5A**). (Both siRNA-mediated knockdown and qPCR analaysis were performed by Noa Furth, WIZ, IL). Accordingly, immunoblot analysis showed a strong downregulation of LATS1 on the protein level (**Figure 5B**).

These samples were further processed to obtain a deep profile of LATS1- or LATS2-knockdown effects on the global proteome, obtained by MS-based label-free quantification (LFQ). To account for the broad dynamic range of peptides in a global proteome sample and to ensure deep proteome coverage, samples were fractionated prior to liquid chromatography-tandem mass spectrometry (LC-MS/MS). Hence, in three biological replicates for each kinase, over 8500 proteins were identified out of which more than 6500 were eligible for LFQ. In this analysis, LATS1 knockdown revealed 15 proteins that were significantly downregulated in their expression compared to the control (**Figure 5C**) (with a significance threshold set to at least 1.5-fold up-or downregulated protein expression levels and a false discovery rate (FDR) of 0.05).

Interestingly, these significantly downregulated proteins showed a highly interactive functional association network in STRING analysis (Szklarczyk *et al*, 2017) (**Figure 5E**). Moreover, proteins within this network revealed significant overrepresentation of genes categorized in ontology terms related to “cell cycle”, “spindle” and “amplification of signal from unattached kinetochores via a MAD2 inhibitory signal, and chromosome condensation”. This regulation of mitosis-related proteins induced by LATS1 knockdown

might be explained by the pivotal role of LATS1 in cell cycle regulation (Visser & Yang, 2010b; Hergovich, 2013; Furth & Aylon, 2017), such as the positive regulation of mitotic progression in which LATS1 has been described to localize at the mitotic spindle (Hirota T 2000; Iida S 2004), or the negative regulation of cyclin E/cyclin-dependent kinase (CDK) 2 in basal and genotoxic conditions in G_1/S transition (Matsuoka *et al*, 2007; Pefani *et al*, 2014). These findings were underlined by performing gene set enrichment analysis (GSEA) of the LATS1 knockdown dataset. Accordingly, gene sets related to "Cell Cycle Checkpoints", and more precisely "Mitotic Spindle Checkpoint", "Mitotic Anaphase", and "Resolution of Sister Chromatid Cohesion", were negatively enriched upon LATS1 knockdown (**Figure 5G**).

Furthermore, the gene set "RHO GTPases Activate Formins" was negatively enriched upon LATS1 knockdown. Interestingly, Rho GTPases and the actin cytoskeleton are known to function upstream of LATS1 and LATS2 kinases (Luo & Yu, 2019), suggesting that downregulation of LATS1 protein levels might influence upstream regulators through a feedback mechanism.

LATS2 knockdown, on the other hand, had no significant effect on the proteome level (**Figure 5D**). Of note, despite being detected in the control samples of qPCR and immunoblots (**Figure 5A** and **5B**), neither LATS1 nor LATS2 could be detected in the MS analysis, despite the deep proteome coverage. Furthermore, the overall expression levels of LATS1 and LATS2 are known to be very low in breast cancer (Furth & Aylon, 2017). Indeed, both kinases and especially LATS2 reveal low baseline expression levels in the ZR75.1 cell line used for this experiment, shown by the "Cancer Cell Line Encyclopedia"-dataset (Barretina *et al*, 2012) (**Figure 5F**). The lower levels of LATS2 and thereby the minor effects on the proteome upon its knockdown could be interpreted in two different ways. One potential explanation could be that the higher levels of LATS1 might reflect the overall higher relevance of the paralogue compared to LATS2 in this cell line, taking over important functions such as cell cycle regulation and control. Thereby knockdown of the already low expression levels of LATS2 might have a less profound effect, compared to LATS1. Alternatively, the low LATS2 levels in ZR75.1 could reflect the need of these cancer cells to keep LATS2 more strictly under control, i.e. low expression levels, in order for these cancer cells to survive. Either way, the differential effects of the knockdown indicate the potentially distinct roles of the paralogues.

Taken together, knockdown of LATS1, but not LATS2, caused perturbation of proteins involved in cell cycle regulating and checkpoints control in the luminal breast cancer cell line ZR75.1. Knocking down LATS1 and LATS2 individually enabled to draw specific conclusions for each kinase, suggesting LATS1 and LATS2 to have differential relevance in this cell system, i.e. cell cycle control and cell survival. Overall, due to the low basal expression levels of LATS1 and especially LATS2 in this cell line, the effects on the proteome were rather minor, limiting the conclusions we could draw from this dataset. Therefore, the experimental setup was reconsidered and we turned to a LATS1 and LATS2 overexpression system to further explore the impact of either LATS1- or LATS2-mediated changes on the protein level.

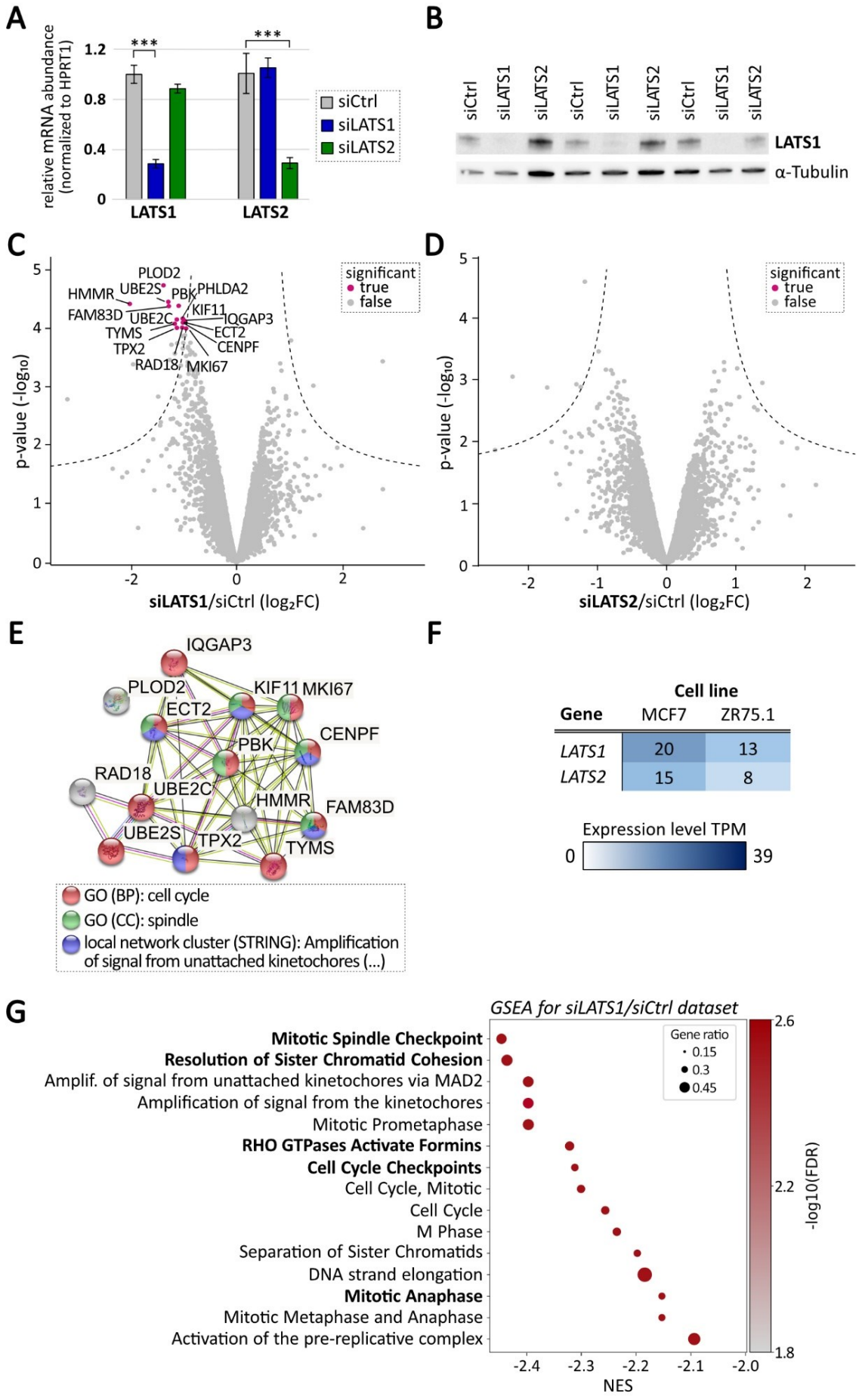
A
relative mRNA abundance (normalized to HPRT1)
1.2
0.8
0.4
0
***
***
LATS1
LATS2
siCtrl
siLATS1
siLATS2
B
siCtrl
siLATS1
siLATS2
siCtrl
siLATS1
siLATS2
siCtrl
siLATS1
siLATS2
LATS1
α-Tubulin
C
significant
true
false
PLOD2
HMMR
UBE2S
PBK
PHLDA2
FAM83D
UBE2C
KIF11
IQGAP3
TYMS
ECT2
TPX2
CENPF
RAD18
MKI67
p-value (-log10)
siLATS1/siCtrl (log2FC)
D
significant
true
false
p-value (-log10)
siLATS2/siCtrl (log2FC)
E
IQGAP3
PLOD2
KIF11
MKI67
ECT2
CENPF
PBK
RAD18
UBE2C
HMMR
FAM83D
UBE2S
TPX2
TYMS
GO (BP): cell cycle
GO (CC): spindle
local network cluster (STRING): Amplification of signal from unattached kinetochores (...)
F
Cell line
Gene
MCF7
ZR75.1
LATS1
20
13
LATS2
15
8
Expression level TPM
0
39
G
GSEA for siLATS1/siCtrl dataset
Mitotic Spindle Checkpoint
Resolution of Sister Chromatid Cohesion
Amplif. of signal from unattached kinetochores via MAD2
Amplification of signal from the kinetochores
Mitotic Prometaphase
RHO GTPases Activate Formins
Cell Cycle Checkpoints
Cell Cycle, Mitotic
Cell Cycle
M Phase
Separation of Sister Chromatids
DNA strand elongation
Mitotic Anaphase
Mitotic Metaphase and Anaphase
Activation of the pre-replicative complex
Gene ratio
0.15
0.3
0.45
-log10(FDR)
NES

Figure 5: siRNA-mediated knockdown of either LATS1 or LATS2 in ZR75.1 cells. (**A**) Validation of knockdown of either LATS1- or LATS2 in ZR75.1 cells by qPCR. Barplot shows relative mRNA abundance of LATS1 and LATS2, normalized to the HPRT-1 housekeeping gene, in either siLATS1 (blue), siLATS2 (green), or siControl (grey) samples. Error bars indicate standard deviation of three biological replicates, and asterisks significance ***p ≤ 0.001; according to unpaired t-test. (**B**) Validation of siRNA-mediated knockdown of LATS1 in ZR75.1 on the protein level via immunoblot, using anti-LATS1 and anti-α-Tubulin antibodies, used as a housekeeping gene. (**C**) and (**D**) Differential expression analysis using Limma moderated t-statistics for the comparison of either (C) siLATS1- or (D) siLATS2-mediated changes on the proteome. Grey color of dots indicates non-significantly, pink color indicates significantly changing proteins of three biological replicates each, with a p-value adjusted for multiple testing according to Benjamini-Hochberg, *adj. p ≤ 0.05 and a minimum log_2FC of +/- 0.58. (**E**) Cluster of significantly downregulated proteins upon LATS1 knockdown is illustrated by using the STRING functional protein associated network database (Szklarczyk *et al*, 2017). MsigDB gene sets: ontology gene sets (C5) biological process (red), cellular component (green) local network cluster (blue). Interaction score was kept at default (medium confidence of 0.4). (**F**) Baseline mRNA expression levels of LATS1 and LATS2 in ZR75.1 and MCF7 cell lines taken from "Cancer Cell Line Encyclopedia"-dataset (Barretina *et al*, 2012). RNA-seq Transcripts Per Kilobase Million (TPM) is represented in the background color of the cell. (**G**) Gene set enrichment analysis (GSEA) of changes on the proteome level upon LATS1 knockdown. Top 15 significantly enriched gene sets (left y-axis) are ranked according to the normalized enrichment score (NES) (x-axis) of each gene set. Color of dots represents -log_{10} FDR (right y-axis) and the size of dots represent the gene ratio (calculated by taking the enriched proteins divided by all proteins of the gene set within the dataset).

4.2. Transient LATS1- and LATS2- overexpression analysis by MS-based proteomics in luminal breast cancer cells

Besides reducing protein levels by knockdown, increasing protein levels by overexpression combined with deep proteome analysis offer an alternative for gaining insights into the functional impact of a given protein of interest on the proteome. Due to the low basal expression levels of LATS1 and LATS2 in breast cancer, represented by the cell lines MCF7 and ZR75.1 (**Figure 5F**), transient overexpression of each kinase was conducted. For this, MCF7, another luminal breast cancer cell, and ZR75.1 cells were transiently transfected with LATS1-GFP or LATS2-GFP overexpression plasmids for 24 h (**Figure 6**). Since the transfection efficiency was around 40 % in MCF7 cells and around 12 % in ZR75.1 cells, subsequent fluorescence-activated cell sorting (FACS) was applied to ensure two clean populations of GFP-positive and GFP-negative cells. For each cell line, four independent biological replicates were obtained. In order to be able to distinguish between different samples, the peptides were labeled beforehand with distinct stable isobaric mass-tags using the 10-plex tandem mass tag (TMT)-reagents (Thermo Fisher Scientific). TMT-labeling

allowed mixing and subsequent fractionation of the sample into 16 fractions each, using high-pH reversed-phase liquid chromatography (hpH-RPLC). All 16 fractions were analyzed by LC-MS using the synchronous precursor selection (SPS) MS^3 fragmentation method. Collectively, >7300 proteins were identified of which, after stringent filtering, around 6000 could be used for quantification, indicating great sampling depth.

In both cell lines, LATS1 and LATS2 were successfully overexpressed, with expression level ratios (LATS/control) of 3.8 [log_2] for LATS1, and 4.5 [log_2] for LATS2 in MCF7 cells (**Figure 7A** and **7B**, respectively), and 3.5 [log_2] for LATS1 and 4.7 [log_2] for LATS2 in ZR75.1 cells (**Figure 8A** and **8B**, respectively).

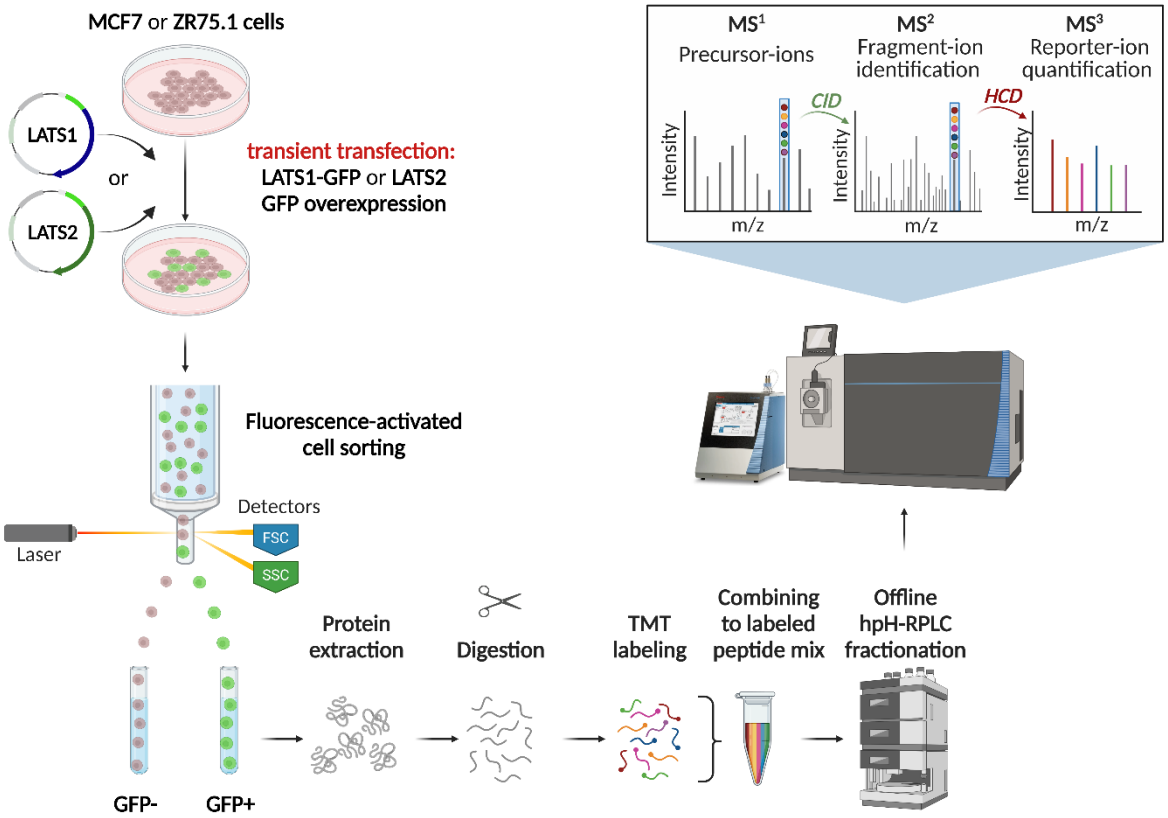

Figure 6: Workflow for global proteome analysis of differential protein expression after transient LATS1 or LATS2 overexpression detected by TMT-MS^3 analysis. MCF7 or ZR75.1 cells were transiently transfected for 24 h by lipofection using GFP-tagged LATS1- or LATS2-overexpression plasmids, in four biological replicates each. Subsequently, cells were sorted into GFP-positive (i.e. LATS1- or LATS2-overexpressing) and GFP-negative (control) cell populations by fluorescence-activated cell sorting (FACS). Following GFP-positive and GFP-negative cells were lysed, proteins extracted and digested into peptides using trypsin. The peptides were labeled by using isobaric 10-plex tandem mass tags (TMT), allowing for subsequent combining of the samples into one vial. Finally, peptides were off-line fractionated into 16 fractions using high pH reversed-phase liquid chromatography (hpH-RPLC) before being on-line injected by nano-UHPLC into a Fusion Tribrid mass spectrometer. LC-MS analyses were conducted in synchronous precursor selection (SPS) MS^3-mode.

4.2.1. Transient overexpression of LATS1 and LATS2 in MCF7 cells perturbs cell cycle and uncovers interplay of LATS2 with the planar cell polarity pathway and the SLIT/ROBO pathway

In MCF7 cells, transient overexpression of both kinases induced only minor changes in overall protein abundance, resulting in low statistical power of this dataset (**Figure 7A** and **7B**). Interestingly, however, GSEA of the LATS2 overexpression dataset revealed negative enrichment of gene sets involved in cell cycle regulation and control, such as "Mitotic Spindle Checkpoint", "Mitotic Prometaphase" and "Amplification of signal from the kinetochores". This suggests that also overexpression of LATS2 perturbs the cell cycle regulation, as observed in the transient knockdown experiments (Section 4.1).

Moreover, the gene set "PCP/PE pathway" was positively enriched in the LATS2-dataset (**Figure 7C**). This is in line with the Hippo pathway being described as the "sensor of physical cell shape", thus being highly sensitive to mechanical forces (Piccolo *et al*, 2014). Along these lines, it has been shown that many upstream regulators of the Hippo pathway are components of the apical-basal polarity complex such as tight junction, adherence junction, or apical-basal polarity protein complexes (Grusche *et al*, 2010; Meng *et al*, 2016; Totaro *et al*, 2018). Besides the well-studied effects of apical-basal polarity, however, there is emerging evidence for the planar cell polarity (PCP) complex/pathway to be a coordinator of Hippo pathway components (Yu & Guan, 2013). The PCP pathway controls the polarity along an axis perpendicular to the apical-basal axis ensuring coordination, alignment, and orientation of clustered cells within an epithelial plate (Simons & Mlodzik, 2008; Hergovich, 2013), mechanisms that are highly conserved from flies to mammals (Maung & Jenny, 2011). In *Drosophila*, PCP ensures the restriction of Yorkie (Yki, ortholog to mammalian YAP) activity in epithelial cells. Here, the key players of the PCP tissues organization are Fat (Ft, ortholog to mammalian FAT1-4) and Dachsous (Ds, ortholog to mammalian DCHS1, DCHS2), two large cell-cell adhesion molecules which are critical for activating the Hippo signaling cassette via phosphorylation of Hippo (Hpo, ortholog to mammalian MST1/ MST2) and Warts (Wts, ortholog to mammalian LATS1/LATS2) (Yu & Guan, 2013; Hergovich, 2013; Simons & Mlodzik, 2008). Yet, the Ft/Ds PCP system and its potential interaction with Hippo signaling in mammals remain poorly understood. In recent years, the mammalian FAT1, known to be a tumor suppressor, has been shown to interact with the Hippo core kinases

thereby facilitating the assembly of the Hippo complex. Further, it has been suggested that the activation of the Hippo kinases is mediated by thousand-and-one amino acids kinases (TAOK) (Martin *et al*, 2018), which are known to directly phosphorylate and thereby activate MST1 and MST2 (Boggiano *et al*, 2011; Poon *et al*, 2011). In line with this, *FAT1* knockout cells as well as in FAT1-low PDX mouse models showed loss of MST1 and LATS1 phosphorylation, ultimately resulting in Hippo pathway suppression and thereby YAP/TAZ activation (Li *et al*, 2018). The significant enrichment of the gene set "PCP/PE pathway" in the LATS2 dataset, allows the hypothesis, that PCP, next to the apical-basal polarity complex, might be an additional coordinator of Hippo signaling in mammals, suggesting a co-dependency between LATS2 and PCP. Moreover, given the high conservation of the Hippo signaling from *Drosophila* to mammals, it is likely, that a similar mechanism of key PCP effectors regulating Hippo signaling in *Drosophila*, might be true in the mammalian Hippo signaling, shedding light on its complex upstream regulation. However, to prove the hypothesis of positive interaction between LATS2 and the PCP pathway, further investigations are necessary.

Another positively enriched gene set was "Regulation of expression of SLITs and ROBOs" (**Figure 7C**). SLITs are secreted glycoproteins that bind to their corresponding Roundabout (ROBO) receptors. SLIT/ROBO signaling was initially discovered in the context of the nervous system in which it could be shown to be essential for axon guidance (Dickinson & Duncan, 2010). Besides, however, several SLITs and ROBOs have been reported to be aberrantly expressed during the development of various cancers and are involved in angiogenesis, inflammatory cell chemotaxis, tumor cell migration, and metastasis (Tong *et al*, 2019). The enrichment of genes involved in SLIT/ROBO signaling upon LATS2 overexpression opens the hypothesis that upon re-introduction of LATS2 by overexpression, LATS2 might react to the aberrant SLIT/ROBO signaling in cancer cells, ultimately influencing the expression of effector proteins. Additionally, given that SLIT are secreted proteins, it would be interesting to see, whether LATS2 overexpression might affect the secretion of SLIT proteins, which could be examined by secretome analysis upon LATS2 overexpression.

Hence, although the changes of protein abundance were not high enough to be significant in this dataset, LATS2 overexpression in MCF7 cells still had some effect on the cell signaling

machinery, allowing to uncover interesting observations such as the perturbation of cell cycle regulatory proteins or the potential interplay of LATS2 with signaling pathways, i.e. the PCP and SLIT/ROBO pathway. This underlines the notion that the highly sensitive signaling networks do not necessarily need extreme changes of protein abundance, but instead can also be responsive to even small changes in protein levels. Additionally, it is possible that the time point of 24 h overexpression was not ideal to detect protein changes upon LATS1 and LATS2 overexpression. Both shorter and longer overexpression might allow more insights into the effects of LATS1 and LATS2 on the proteome. Moreover, phenotype analysis, i.e proliferation, apoptosis, or cell cycle assays would help to interpret the changes seen on the proteome level, ultimately feeding into the overall understanding of LATS1 and LATS2 function in the context of breast cancer.

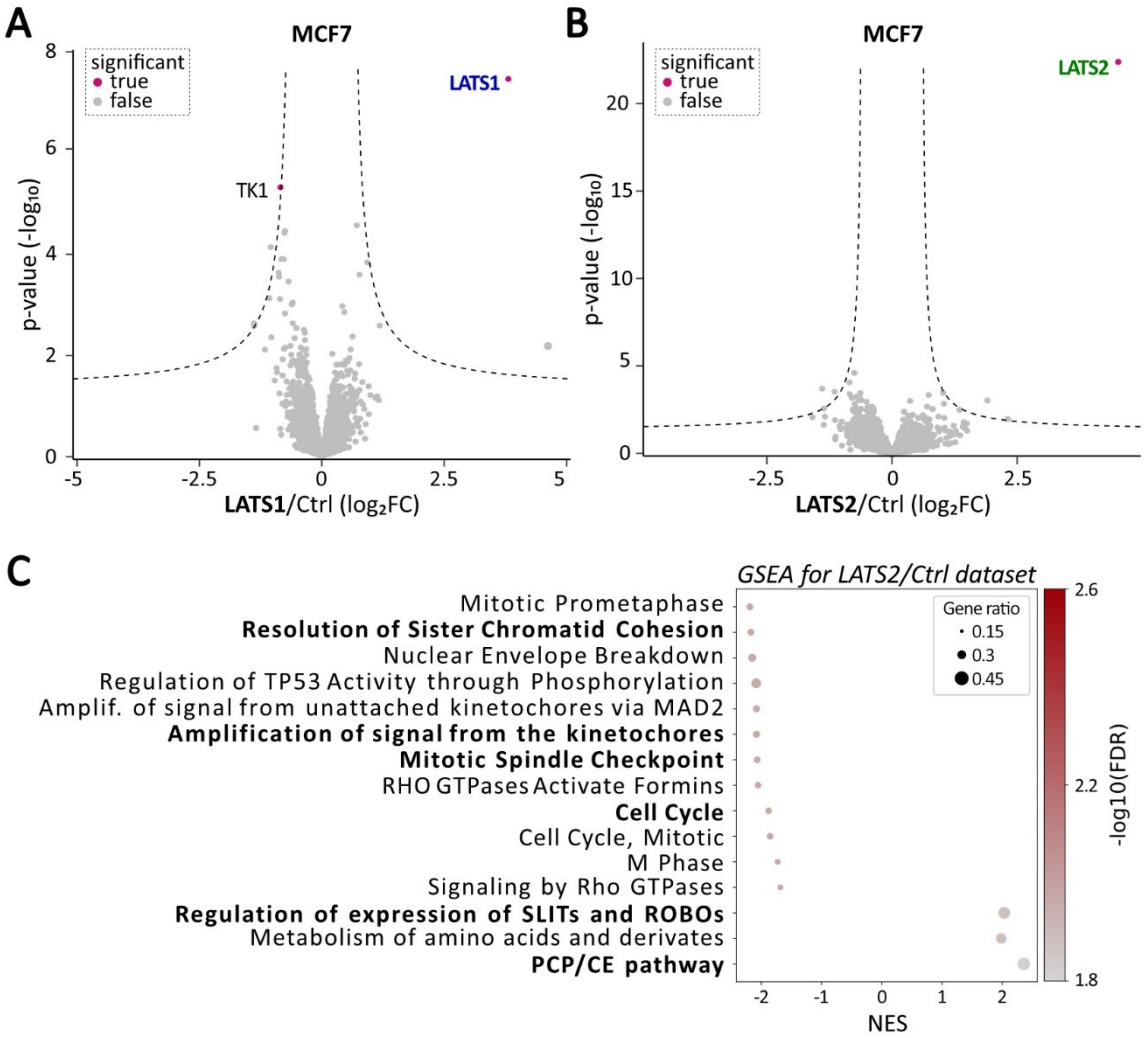

Figure 7: Effects on protein abundance upon transient overexpression of LATS1 or LATS2 in MCF7 cells. (**A**) and (**B**) Differential expression analysis using Limma moderated t-statistics for the comparison of changes on the proteome upon overexpression of either (A) LATS1 or (B) LATS2 in MCF7 cells, in three biological replicates each. Grey color of dots indicates non-significantly, pink

color indicates significantly changing proteins, with a p-value adjusted for multiple testing according to Benjamini-Hochberg, *adj. $p \leq 0.05$ and a minimum log_2FC of +/- 0.58. (**C**) Gene set enrichment analysis (GSEA) of changes on the proteome level upon LATS2 overexpression in MCF7. Top 15 significantly enriched gene sets (left y-axis) are ranked according to normalized enrichment score (NES) (x-axis) of each gene set. Color of dots represents $-log_{10}$ FDR (right y-axis) and the size of dots represent the gene ratio (calculated by taking the enriched proteins divided by all proteins of the gene set within the dataset).

4.2.2. Transient overexpression of LATS1 and LATS2 in ZR75.1 cells and the interplay with the tumor suppressors p53 and RUNX3

In ZR75.1 cells overexpression of LATS1 or LATS2 had a profound effect on protein expression of several proteins (**Figure 8A** and **8B**). GSEA for both datasets showed a number of significantly enriched gene set terms related to cell cycle and G_1/S DNA damage checkpoint (shown exemplarily for LATS1 in **Figure 8C**). Interestingly, this cell cycle checkpoint seems to be regulated via p53, reflected by enriched geneset such as “p53-Dependent G_1/S DNA damage checkpoint” and “Stabilization of p53”, possibly leading to the “Regulation of Apoptosis” via p53. In line with this, there is a close interplay of LATS1, and especially LATS2 with the tumor suppressor p53 on different regulatory levels. One is the positive feedback mechanism, in which LATS2 ensures the stabilization of p53 by inhibition of the p53-inhibitor MDM2. In response, p53 enhances *LATS2* gene transcription (Kostic & Shaw, 2000; Aylon *et al*, 2006, 2010). Moreover, p53 has been reported to boost the transcription of *LATS2* by binding to the *LATS2* promoter in response to oncogenic, metabolic, and developmental stress (Aylon *et al*, 2006, 2009, 2016). Although not as profound as the interaction with LATS2, also LATS1 can modulate p53-dependent apoptosis. This has been shown in the context of mutant KRAS (GTPase Kras) in which LATS1 sequesters MDM2 and thereby stabilizes p53 (Matallanas *et al*, 2011). Interestingly, for the experimental setup of this dataset, overexpression for 24 h was chosen over the 48 h due to induction of cell death that could be observed in the microscope (data not shown). This is especially interesting since, unlike many cancer cells, ZR75.1 harbors wild-type *TP53* (gene encoding p53) and *MDM2*. This suggests that overexpression of LATS1 and LATS2 might be sufficient to restore p53 tumor suppressor functions, likely via the inhibition of MDM2, thereby promoting the activation of p53 to exert G_1/S arrest and or apoptosis in these cancer cells. Therefore, the restoration of LATS1 and LATS2 expression might display a potential vulnerability of cancer cells harboring wild-type *TP53*, reflecting the tight

network between tumor suppressors, alerting each other in case of aberrant cell cycle progression in cancer cells.

Notably, as seen before in the LATS2 overexpression dataset of MCF7 a gene set related to the PCP pathway (“Asymmetric localization of PCP proteins”) was again positively enriched for both LATS1 and LATS2, strengthening the hypothesis of close interaction of both LATS kinases with the PCP pathway. In *Drosophila*, a hallmark of the PCP pathway is the asymmetric distribution of the proteins Strabismus (Stbm; also known as Van Gogh) and Prickle (Pk) on one side of the membrane and Frizzled (Fz), Dishevelled (Dsh), and Diego (Dgo) on the opposing side, antagonizing each other in the regulation of the downstream signaling (Seifert & Mlodzik, 2007). Similar localization patterns of the homologous of these proteins have been observed in vertebrates (Montcouquiol *et al*, 2003, 2006; Wang *et al*, 2006; Narimatsu *et al*, 2009), however, how these proteins ultimately affect downstream signaling and which processes are affected by this signaling still remains unclear. Since in both, MCF7 and ZR75.1 datasets, PCP signaling was positively enriched, however, this raises the hypothesis, that LATS1 and LATS2 might as well shape the signaling cascade of the PCP pathway.

Another gene set worth mentioning, which was positively enriched in the LATS1 dataset is “Regulation of RUNX3 expression and activity”. In *Drosophila* and HEK293T cells, it could be shown that phosphorylation of Yki/YAP by Wts/LATS1/2 facilitated the switch of YAP binding partners from Sd/TEAD4 to Lz/RUNX3 (Jang *et al*, 2017). The transcription factor RUNX3 (Runt-related transcription factor 3) is known to be a tumor suppressor regulating lineage determination, cell cycle arrest, and apoptosis (Ito *et al*, 2015), whereas binding of YAP to TEAD4 triggers gene expression related to oncogenic activity (Zhao *et al*, 2008). Thus, YAP-induced gene expression switches from growth-promoting to growth-suppressing mode. Therefore, it would be interesting to see whether this switch of YAP binding partners from “evil” to “good” by activating or overexpressing LATS1 might be conserved in breast cancer cells, opening a possible site of vulnerability.

Overall it seems that overexpression of the tumor suppressors LATS1 and LATS2 might alert and activate other tumor suppressors such as p53 or RUNX3 which are usually brought to quiescence in luminal breast cancer cells, reflecting the highly interactive network between the guardians of a cell.

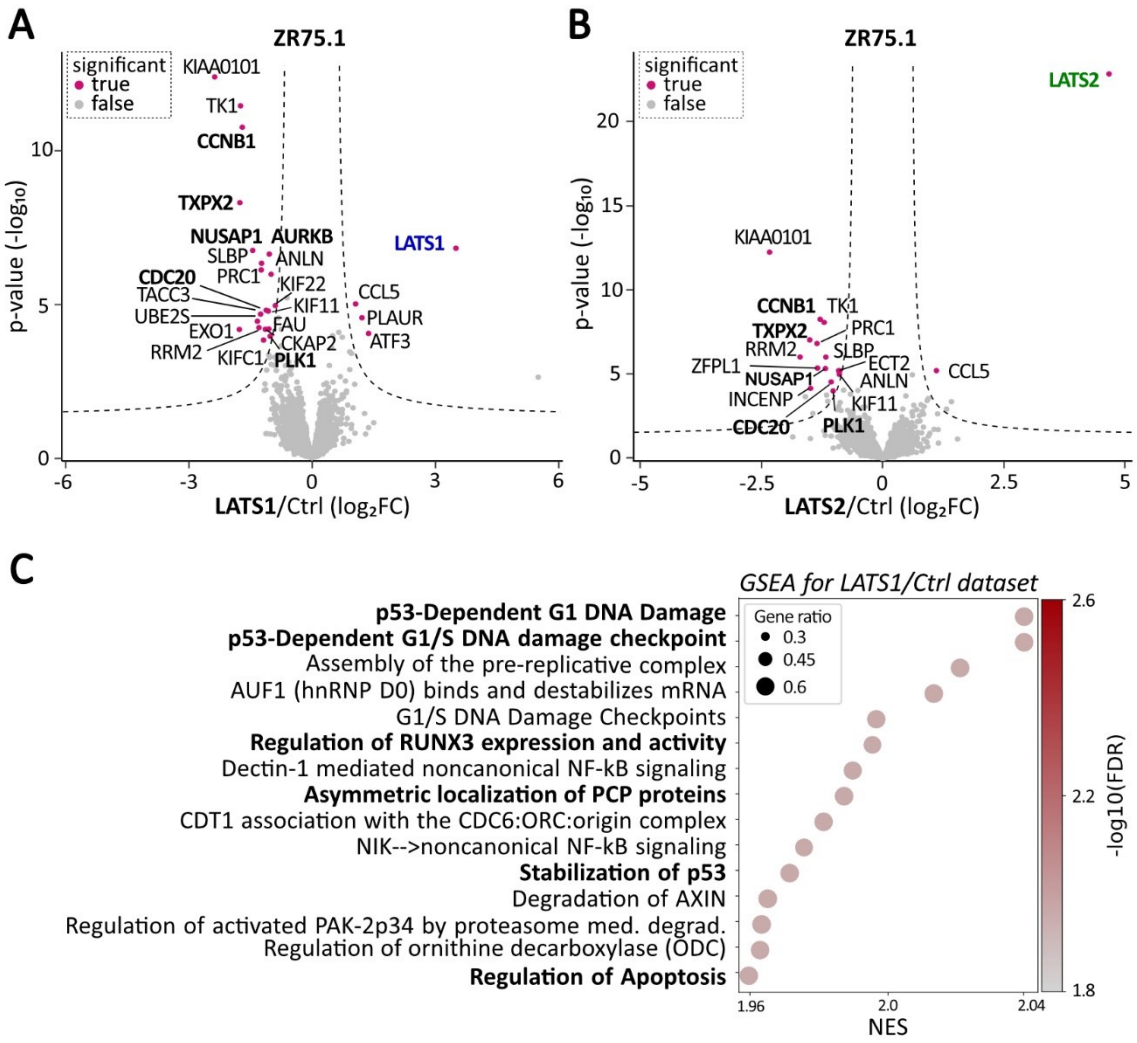

Figure 8: Effects on protein abundance upon transient overexpression of LATS1 or LATS2 in ZR75.1 cells. (**A**) and (**B**) Differential expression analysis using Limma moderated t-statistics for the comparison of changes on the proteome upon overexpression of either (A) LATS1 or (B) LATS2 in ZR75.1 cells, in three biological replicates each. Grey color of dots indicates non-significantly, pink color indicates significantly changing proteins, with a p-value adjusted for multiple testing according to Benjamini-Hochberg, *adj. $p \leq 0.05$ and a minimum log_2FC of +/- 0.58. (**C**) Gene set enrichment analysis of changes on the proteome level upon LATS1 overexpression in ZR75.1 cells. Top 15 significantly enriched gene sets (left y-axis) are ranked according to the normalized enrichment score (NES) (x-axis) of each gene set. Color of dots represents $-log_{10}$ FDR (right y-axis) and the size of dots represent the gene ratio (enriched proteins divided by all proteins of the gene set within the dataset).

4.2.3. LATS1 and LATS2 and the anaphase-promoting complex/cyclosome (APC/C) in ZR75.1 cells

Correlation of the LATS1 and LATS2 overexpression datasets in ZR75.1 cells showed that the majority of proteins have a similar trend of protein ratio in both datasets. Having a closer look at the common proteins that were at least 1.5-fold downregulated it becomes evident that a large subset is involved in the regulation of mitosis (**Figure 9A**). Indeed, these downregulated proteins revealed a high overrepresentation of gene ontology (GO) terms related to the regulation of mitosis, as shown by overrepresentation analysis (ORA) using the gene ontology sets (C5) (**Figure 9C**). Among those terms, "GO_ANAPHASE_PROMOTING _COMPLEX_DEPENDENT_CATABOLIC_PROCESS" was significantly overrepresented, narrowing down the rather broad term "mitotic cell cycle". Notably, the gene set "Mitotic Anaphase" was negatively enriched upon knockdown of LATS1 in ZR75.1 cells (Section 4.1), strengthening the notion of a pivotal role of LATS1 and LATS2 in cell cycle control, emphasizing mitotic anaphase and its key regulators.

An indicator of cell cycle phase or progression is the level of cyclins, which, like the name implies, show a distinctive cycling pattern throughout the individual cell cycle phases, thereby strictly regulating cell cycle progression (Fung & Poon, 2005). For instance, cyclin B1 (*CCNB1*) levels have their peak in metaphase and show a drastic drop in protein levels in anaphase (Brandeis & Hunt, 1996). Interestingly, upon LATS1 and LATS2 overexpression, cyclin B1 expression levels were significantly downregulated by -1.7 [$\log_2$] and -1.3 [$\log_2$] in the ZR75.1 LATS1- and LATS2-datasets, respectively (**Figure 8A** and **8B**, **Figure 9A**). Also in MCF7 cells, cyclin B1 was downregulated by -0.8 [$\log_2$] in LATS1 and -0.6 [$\log_2$] in LATS2 overexpression datasets. This might indicate that overexpression of LATS1 and LATS2 lead to progression from metaphase to anaphase.

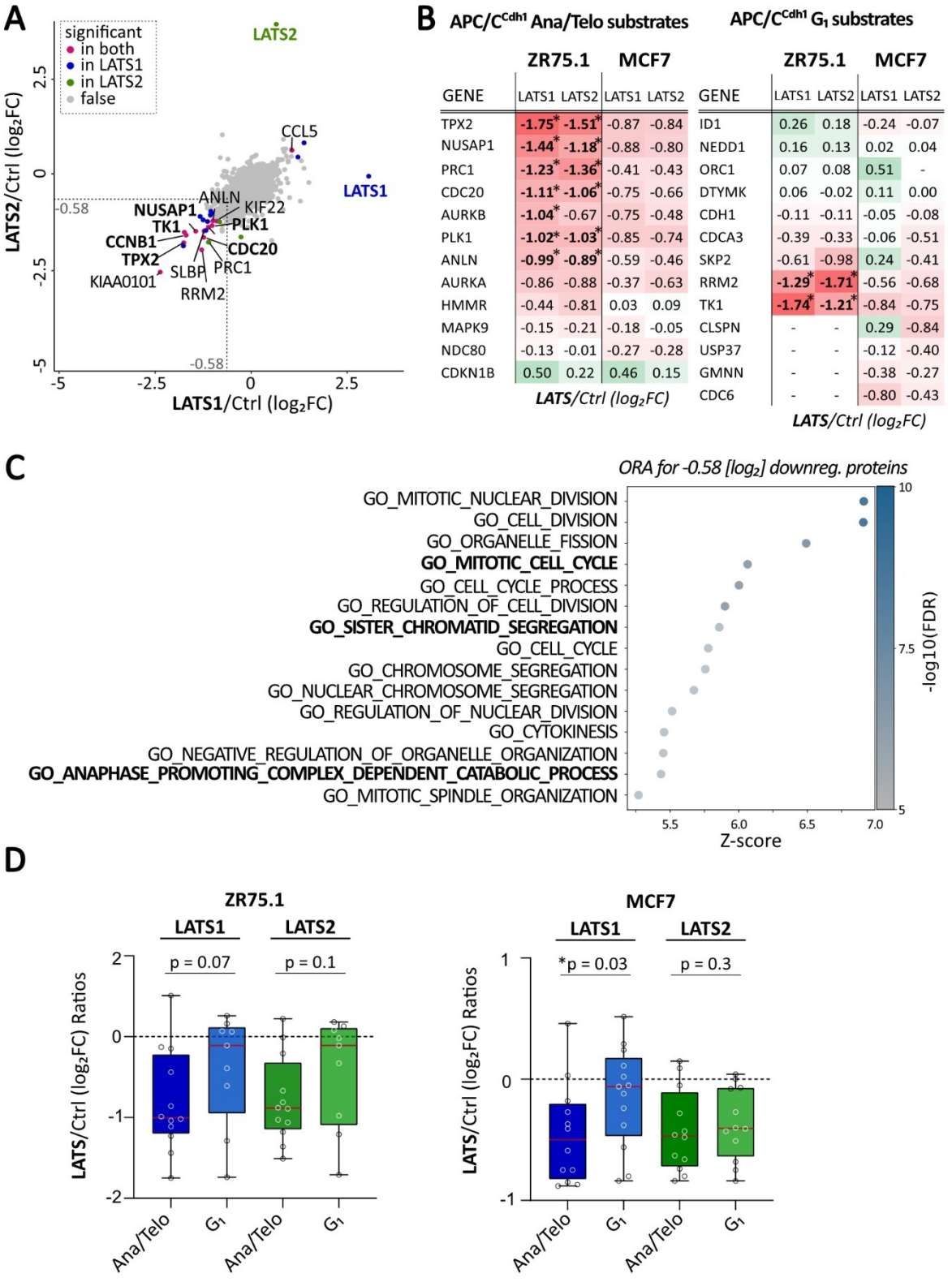

Figure 9: Correlation of effects on protein abundance upon transient overexpression of LATS1 or LATS2 in ZR75.1 cells and the APC/C complex. (**A**) Correlation of differential expression analysis of changes on the proteome upon overexpression of LATS1 (x-axis) versus LATS2 (y-axis) in ZR75.1 cells, of three biological replicates each (from the same dataset used in Figure 8A and 8B). Color of dots indicates the following: grey non-significantly, blue significantly changing only in LATS1, green significantly changing only in LATS2, and pink color significantly changing proteins in both LATS1 and LATS2-datasets, with a p-value adjusted for multiple testing according to Benjamini-Hochberg,

*adj. p ≤ 0.05 and a minimum log_2FC of +/- 0.58. (**B**) List of APC/C^{Cdh1} Ana/Telophase-substrates (left) or APC/C^{Cdh1} G_1-substrates (right) and corresponding protein ratios detected in the ZR75.1 and MCF7 dataset. Red color implies downregulation, green color implies upregulation, and numbers with an asterisk significantly changing proteins with an adj. p ≤ 0.05. (**C**) Overrepresentation analysis (ORA) of proteins depicted in the quarter of (A), which have a minimum log_2FC of - 0.58. Top 15 significantly enriched gene sets (left y-axis) are ranked according to the normalized Z-score (x-axis) of each gene set. Color of dots represents -log_{10} FDR (right y-axis) and the size of dots represent the gene ratio (calculated by taking the enriched proteins divided by all proteins of the gene set within the dataset). (**D**) Distribution of protein ratios of the depicted APC/C^{Cdh1} Ana/Telophase - substrates or G_1-substrates detected in the ZR75.1 dataset (left panel) and the MCF7 dataset (right panel), with p-value determined by one-tailed Mann-Whitney non-parametric t-test. White circles represent the ratio of each one protein.

The anaphase-promoting complex/cyclosome (APC/C) is a major key player in anaphase and overall cell cycle regulation. The activation of the ubiquitin E3 ligase APC/C, composed of 19 subunits, is governed by the two co-activator subunits Cdc20 and Cdh1, temporally coordinating cell cycle progression (Zhou *et al*, 2016). In particular, Cdc20 associates and thereby activates APC/C in early mitosis, ranging from prophase to anaphase onset, by targeting mitotic cyclins and securin (**Figure 10**). Subsequently, Cdh1 replaces Cdc20 in the middle of anaphase throughout telophase until reaching the G_1 phase, thereby covering the mitotic exit process, as well as entry into a new cell cycle. Thus, navigation through cell cycle progression is determined by the switch of APC/C-activators (Cdh1 and Cdc20) which in turn switches the repertoire of preferred substrates of the APC/C ligase (Garnett *et al*, 2009). As a consequence, expression levels, as well as modification status of the co-activators Cdc20 and Cdh1, is another indicator of what phase of the cell cycle a cell is currently in.

Interestingly, protein levels of Cdh1 remain stable (-0.1 [log_2]), whereas Cdc20 levels show significant downregulation by -1.1 [log_2], in both LATS1 and LATS2 overexpression datasets (**Figure 9B**). The same downward tendency for Cdc20 was observed in MCF7 cells (each -0.8 [log_2] and -0.7 [log_2] for LATS1 and LATS2, respectively). Thus, steady Cdh1 levels and downregulated Cdc20 levels might be indicative for the APC/C complex to be associated with Cdh1 rather than Cdc20, suggesting that cells have passed early anaphase.

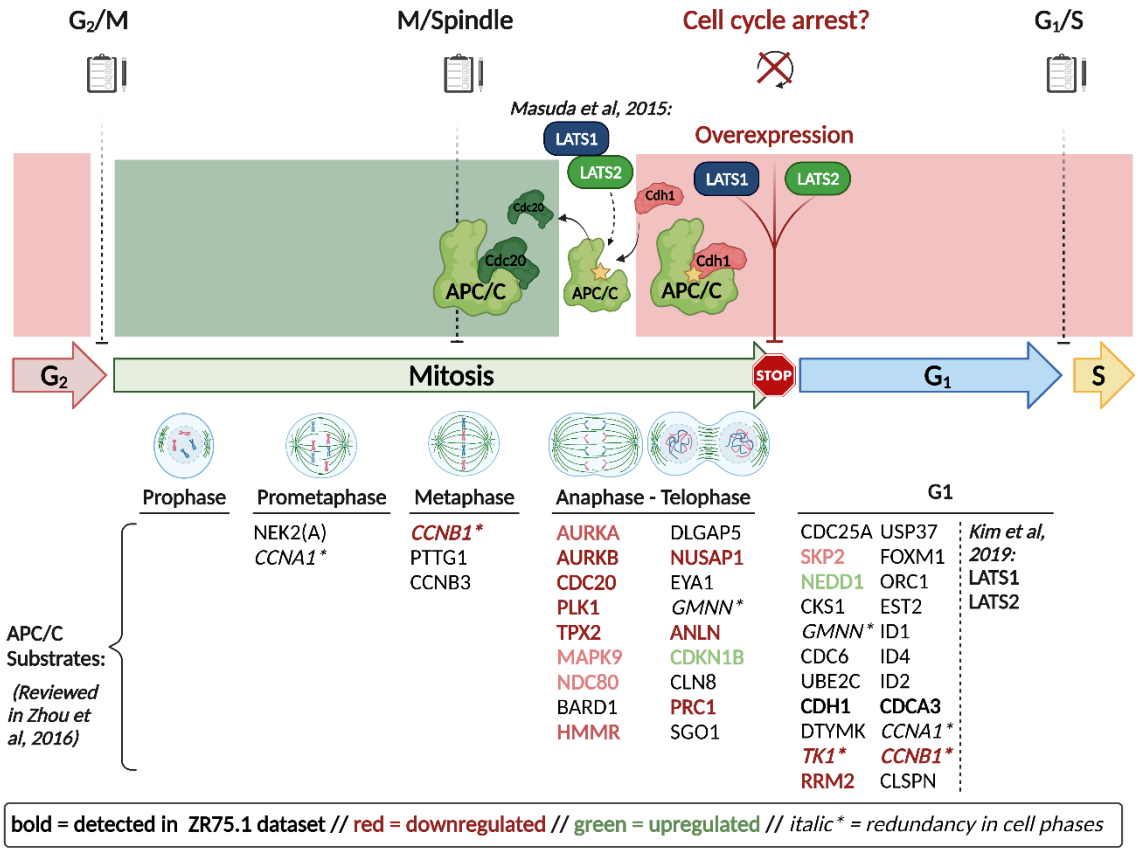

Figure 10: APC/C in cell cycle regulation. The activation of the ubiquitin E3 ligase APC/C is governed by the two co-activators Cdc20 and Cdh1 which are temporally coordinated through cell cycle progression. Cdc20 associates and thereby activates APC/C in early mitosis, ranging from prophase to anaphase onset (indicated by green background color), by targeting mitotic cyclins and securin. Cdh1 replaces Cdc20 in the middle of anaphase staying conjugated throughout telophase until reaching the G_1 phase, thereby covering the mitotic exit process, as well as entry into a new cell cycle (indicated by red background color). The switch of APC/C-activators leads in turn to a switch of the repertoire of preferred substrates of the APC/C ligase. Corresponding gene names of the substrates in the depicted cell cycle phases are depicted below (Gene names in bold indicate proteins that were detected in the ZR75.1 transient overexpression dataset and the color-coding of the gene names indicate whether they were found up- (green) or downregulated (red) in these datasets). LATS1 and LATS2 overexpression might push APC/C into anaphase by modifying APC/C subunit and thereby facilitating Cdh1 activation as described before (Masuda *et al*, 2015), and according to the present study, might induce mitotic cell cycle arrest, preventing mitotic exit. Schematic illustration adapted from Zhou *et al* (2016). Figure was created with BioRender.com.

Along these lines, LATS1 and LATS2 have been shown to regulate APC/C activity as well as being regulated themselves by the complex (outlined in more detail in the Introduction Section 1.1.2.3). Briefly, it has been shown that Dfb2 (yeast ortholog of LATS1) as part of the Mitotic Exit Network (MEN) complex, together with Cdc14 activates APC/C^{Cdh1} (Zachariae *et al*, 1998; Mohl *et al*, 2009; Zhou *et al*, 2016). Furthermore, in mammals LATS1 together with MOB1A, have been identified as components of the mammalian MEN (Bothos *et al*, 2005). Moreover, LATS1 and LATS2 have been found to positively modulate

the activity of APC/C^{Cdh1} by directly phosphorylating the APC/C subunit APC6, promoting the transition from metaphase to anaphase (Masuda *et al*, 2015). Thus, it is likely that in the present dataset LATS1 and LATS2 might as well positively modulate APC/C^{Cdh1} activity, facilitating the transition of cells into anaphase.

By comparing the ZR75.1 dataset with a dataset of APC/C^{Cdh1} specific substrates in anaphase/telophase (Zhou *et al*, 2016), 12 out of 18 "anaphase to telophase"-proteins could be detected (**Figure 9A, Figure 10**). Strikingly, out of those detected proteins, 7 for LATS1 and 6 for LATS2 were significantly downregulated, and ~3/4^{th} of those proteins were at least 1.5-fold downregulated (**Figure 9B**, left panel). Moreover, most of those proteins showed the same tendency in the MCF7 dataset. Overlapping the APC/C^{Cdh1} specific substrates of "G_1 phase" with the current dataset, however, only 3 out of 9 detected proteins in the ZR75.1 datasets and less than 1/4^{th} of the MCF7 datasets were downregulated, whereas the majority were centered around zero (**Figure 9B**, right panel). Ultimately, comparing the overall expression levels of the substrate proteins of both phases, a clear overrepresentation of downregulated proteins of the "anaphase to telophase"-substrates compared to "G_1 phase"-substrates becomes evident (**Figure 9D**). Hence, this suggests that LATS1 and LATS2 overexpression might lead to cells being arrested in anaphase to telophase, before being able to exit mitosis. This hypothesis is strengthened by the fact that in the present experiment cells were not synchronized prior to LATS1 and LATS2 overexpression, but still seem all to arrest in anaphase/telophase. Possibly, this hypothesis could be validated by flow cytometry or microscopy experiments using cell cycle phase-specific markers.

Intriguingly, if we follow the APC/C^{Cdh1} complex further along the cell cycle progression, a recent study could show that active APC/C^{Cdh1} targets LATS1 and LATS2 for degradation in G_1 phase, causing YAP/TAZ to peak in G_1 and thereby promote cell cycle progression (Kim *et al*, 2019). This would allow for another hypothesis saying that there might be a negative feedback loop between LATS1/2 and APC/C^{Cdh1}. In other words, LATS1 and LATS2 activate APC/C^{Cdh1} to proceed into anaphase and are then being degraded by APC/C^{Cdh1} in mid G_1 phase. However, since both, the LATS1/2-mediated activation of APC/C^{Cdh1} in mid mitosis (Masuda *et al*, 2015), and APC/C^{Cdh1}-mediated degradation in G_1 phase (Kim *et al*, 2019) have been shown in independet studies, the hypothesis of a negative-feedback loop needs further validation.

Taken together, this datasets suggest that LATS1 or LATS2 overexpression pushes cells over the M/Spindle checkpoint, thereby transitioning from metaphase to anaphase, reflected by the downregulation of Cdc20 and cyclin B1 as well as the downregulation of the APC/C^{Cdh1} substrates, possibly by enhancing APC/C^{Cdh1} activity, as it has been described before (Masuda *et al*, 2015). (**Figure 10**). At this point, recent studies could show that APC/C^{Cdh1} degrades LATS1 and LATS2 in G_1 phase, possibly as a necessary requirement to proceed with the cell cycle (Kim *et al*, 2019). However, artificially maintaining high LATS1 or LATS2 levels in the present study probably overrides APC/C^{Cdh1}- mediated degradation of LATS1/2 and induces cell cycle arrest, preventing transition into the mitotic exit.
Collectively, this suggests that besides LATS1 and LATS2 being involved in G_1/S and G_2/M checkpoint as described before (Hergovich, 2013; Furth & Aylon, 2017), overexpression of LATS1 and LATS2 in luminal breast cancer cells might help those cells progressing through the 3rd checkpoint, namely the M/Spindle checkpoint, presumably by activation of APC^{Cdh1}, but prevent the mitotic exit of these cells by arresting them in anaphase/telophase. Along these lines, it would be interesting to investigate, whether this arrest is reversible, or might lead to other consequences such as induction of apoptosis indicated by ORA analysis in the previous section (4.2.2). Thus, to prove this hypothesis, further studies are necessary, i.e. cell cycle analysis by flow cytometry or apoptose (and senescence) assays after prolonged LATS1/2 overexpression. Furthermore, phosphoproteomic analysis of APC/C subunits and interaction partners might help to better understand the interplay between LATS kinases and APC/C and ultimately their regulatory function in cell cycle control.

These findings encouraged us for a more in-depth analysis of LATS1- or LATS2-dependent changes on the proteome. However, we were reconsidering the experimental setup, since transient transfection and subsequent sorting using FACS, not only induces additional stress to the cells that might result in undesired signaling but also prevented the application of more advanced proteomic methods requiring high cell numbers. Furthermore, exact experimental control of the duration period of overexpression, as well as long-term overexpression, could not be easily implemented with the transient overexpression system. Thus, to overcome these limitations, a new Tet-inducible cell system was established, stably overexpressing either LATS1 or LATS2 in all cells upon induction which is described in the following sections.

4.3. Establishment of new stable Tet-inducible cell systems to further characterize LATS1 and LATS2

Transient overexpression systems are convenient and time-saving tools allowing for a first assessment of the effect of a protein of interest on a certain cell system, usually without the necessity the create and select for a new cell line. Albeit, these systems also come with some downsides, such as that the plasmid number inserted into one cell, and thereby the amplification of the protein product can not be controlled, due to the stochastic distribution of plasmids during transfection. To ensure a clean cell population of successfully transfected cells, selection markers, such as antibiotics or fluorescence tags combined with FACS are used. However, antibiotic selection or sorting of fluorescent-positive cells might cause stress, affecting cell signaling. Toxicity of transfection reagents and low transfection efficiency might result in overall low cell yield from an experiment, limiting the repertoire of subsequential analysis. Also, it is more difficult to control the starting point of gene expression and long-term experiments are limited by the doubling time of the individual cell type.

In the present study, these obstacles were taken into consideration. Along these lines, the rather minor effects observed upon transient overexpression of LATS1 or LATS2, e.g. in the LATS2 dataset of the MCF7 cell line (Section 4.2.1), the additional stress induced by FACS and potentially by the transfection reagent, and the low cell numbers prevented the utilization of more advanced MS-based methods. Thus we chose to generate stable Tet-inducible cell systems.

4.3.1. Creating Tet-inducible LATS1- and LATS2-overexpression systems in MCF10A, ZR75.1, and MCF7 cells

The challenge in generating the overexpression systems was the large coding sequences (CDS) of 3393 base pairs (bp) for LATS1 and 3276 bp for LATS2 (**Supplementary Table 1**), as well as the large Tet-inducible destination vector pTRIPZ < 12 kbp, carrying both, the TetO operator and tetracycline transactivator (tTA) sequence (**Supplementary Figure 8**). Hence, PCR-based attachment of the att-B flanking sites, necessary for the recombination reaction in the first step of the Gateway cloning (**Figure 11**, BP reaction) (Katzen, 2007), required optimization of the PCR protocol, i.e. by using a high-fidelity polymerase together with

adjusting the cosolvent DMSO in the reaction buffer. Additionally, the DNA sequence accuracy of the amplicon was strictly monitored by sanger sequencing. With the successful first Gateway cloning step, we were able to incorporate the CDS of LATS1 and LATS2 into the donor vector pDONR^{TM}221, thereafter called entry vector pENTR (**Figure 11**). This was followed by the next Gateway recombination reaction (LR reaction), ultimately incorporating the LATS1 and LATS2 CDS into pTRIPZ. Using lentiviral transduction allowed us to stably transduce MCF10A, MCF7, and ZR75.1 cells with the pTRIPZ plasmid, containing the Tet-ON system. The Tet-ON system, which is based on regulatory elements that control the activity of the tetracycline-resistance operon in *E.coli*, allows for stringently controlled gene expression upon administration of either tetracycline or its derivate doxycycline (dox) (Zhou *et al*, 2006b). The purity of the created cell line was ensured by taking advantage of antibiotic selection (here puromycin) and the concentration of dox was titrated for each cell line. Eventually, we were able to successfully establish stable Tet-inducible LATS1 and LATS2 expression system in the aforementioned breast (cancer) cell lines.

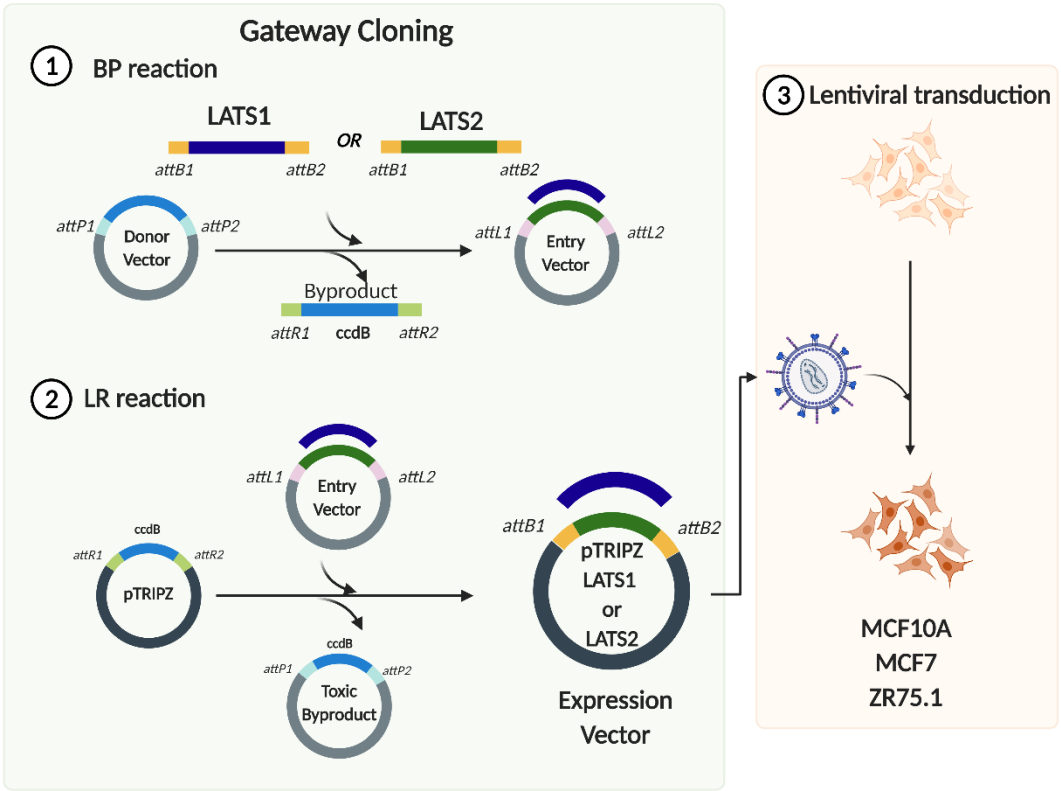

Figure 11: Cell line establishment by Gateway cloning and lentiviral induction. With the Gateway cloning technology (Katzen, 2007), a gene-sequence of interest (here LATS1-CDS (blue) or LATS2-CDS (green) into an expression vector (here pTRIPZ) via two recombination reactions, the (**1**) BP reaction, and the (**2**) LR reaction. In the (**1**) BP-reaction attB-flanked LATS1-CDS or LATS2-CDS are recombinantly exchanged with the attP-flanked toxic-ccdB byproduct of the donor vector to give rise to the pENTR vector, now carrying LATS1 and LATS2 CDS. The obtained pENTR serves as a carrier

for the gene of interest (here LATS1 and LATS2) allowing for easy subcloning into any destination vector of choice (here pTRIPZ containing Tet-inducible overexpression system). Thus, in the (**2**) LR-reaction the attL-flanked LATS1 or LATS2-CDS are recombinantly exchanged with the attR-flanked toxic-ccdB byproduct of pTRIPZ, giving rise to the pTRIPZ-LATS1 or pTRIPZ LATS2 expression vector. (**3**) Newly generated pTRIPZ plasmids were then transduced into MCF10A, ZR75.1, and MCF7 cells by lentiviral transduction. Figure was created with BioRender.com.

The cell lines chosen for these analyses share the origin of tissue, namely female breast tissue. Albeit, they have different properties: MCF7 and ZR75.1, as described before, serve as tumorigenic cell line models for luminal B subtype and luminal A breast cancer, respectively, harboring different oncogenic signatures. MCF10A serves as a model for the "physiologically healthy", i.e. non-tumorigenic genetic background. In theory, in MCF10A cells, there should be no oncogenic rewiring of signaling pathways, potentially counteracting LATS1/2 activity, which should facilitate a more natural readout of LATS1 or LATS2 induced changes on the proteome, thereby complementing the oncogenic cell lines. Therefore, this cell line was prioritized for analysis before ZR75.1 and MCF7. Generally, we believe that these three cell lines resemble a valuable source to gain insights into LATS1 and LATS2 functional activities in physiological as well as tumorigenic breast tissue backgrounds. The newly established inducible cell systems enabled us to overcome the aforementioned limitations by facilitating LATS1 and LATS2 overexpression in high cell numbers upon induction with dox. Ultimately, this allowed us to use more advanced, induction-time-sensitive as well as peptide enrichment-based MS-methodologies such as "Pulsed-SILAC and Click-Chemistry" to study the translatome (Eichelbaum *et al*, 2012; Eichelbaum & Krijgsveld, 2014), as well as Fe^{3+}-IMAC phosphopeptide enrichment to study the phosphoproteome (Ruprecht *et al*, 2015; Potel *et al*, 2018) (**Figure 12E**).

4.3.2. Validation of the newly established Tet-inducible LATS1- and LATS2-overexpression systems

To determine the optimal induction timepoint, Tet-inducible MCF10A cells were induced at consecutive time points over a period of 24 h with priorly titrated 2 µM concentration of dox. Quantification of relative mRNA expression levels showed a gradual increase of LATS1 and LATS2 mRNA upon dox-induction over time (**Figure 12A** and **12C**, respectively). Moreover, both LATS1 and LATS2 displayed a first plateau of expression levels between 2 h

- 6 h and a second plateau between 16 h - 24 h of overexpression. Prolonged induction of up to 48 h did not lead to higher expression levels than observed at the second plateau (data not shown). Notably, despite the use of the same vector system, the magnitude of LATS2 overexpression was 4- fold higher in the first plateau (**Figure 12A** and **12C**)**,** and 8-fold higher in the second plateau, compared to LATS1. Similar observations were made in the two breast cancer cell lines ZR75.1 and MCF7 transfected with the same lentiviral vector system (data not shown). Since the cell lines were created from a pooled population, insertion site-specific silencing can be excluded, given the randomness of insertion-site in different cells. Hence, a possible explanation might be that cells counteract actively LATS1 overexpression, possibly reflecting a control mechanism to ensure steady LATS1 levels. These steady levels might be more strictly controlled for LATS1 compared to LATS2, reflected by the high overexpression levels of LATS2.

The newly established Tet-inducible system was used for quantitative “nascent proteome” analysis as well as quantitative phosphoproteome analysis upon LATS1 or LATS2 overexpression. The nascent proteome was assessed by the in-house-developed “Pulsed-SILAC and Click-Chemistry” method enabling the selective enrichment (click-chemistry) and quantification (SILAC) of newly synthesized proteins (translatome) and secreted proteins (secretome) upon induced overexpression of either LATS1 or LATS2 (**Figure 12E** and **Figure 13A**) (Results of secretome analysis are not shown in this study). Here the time points 6 h and 20 h were chosen based on the time course experiments (**Figure 12A** and **12C**), facilitating insights into the cellular response to different LATS1 and LATS2 protein levels, as well as short- and long-term effects of LATS1 and LATS2 exposure on the proteome (**Figure 12E**). Specifically, in these experiments, cells were grown in SILAC “medium” growth media and switched for the pulse to either SILAC “light” in the case of GFP-control cells, or SILAC “heavy” in the case of LATS1- or LATS2-overexpressing cells, allowing for early combining of samples during sample preparation (**Figure 13A**). As depicted in the schematic overview, for each cell line (MCF10A, MCF7, and ZR75.1), LATS1 and LATS2 overexpression was induced for an “intermediated time point” of 6 h and a “long-term time point” of 20 h, 48 h, or 72 h for MCF10A, MCF7, and ZR75.1, respectively (**Figure 12E**). It should be noted, however, that the duration of the pulse itself was set to 6 h for all experiments, since long-term incubation with the methionine analog L-azidohomoalanine (AHA), allowing for the click-reaction of the peptide enrichment, is toxic for the cells.

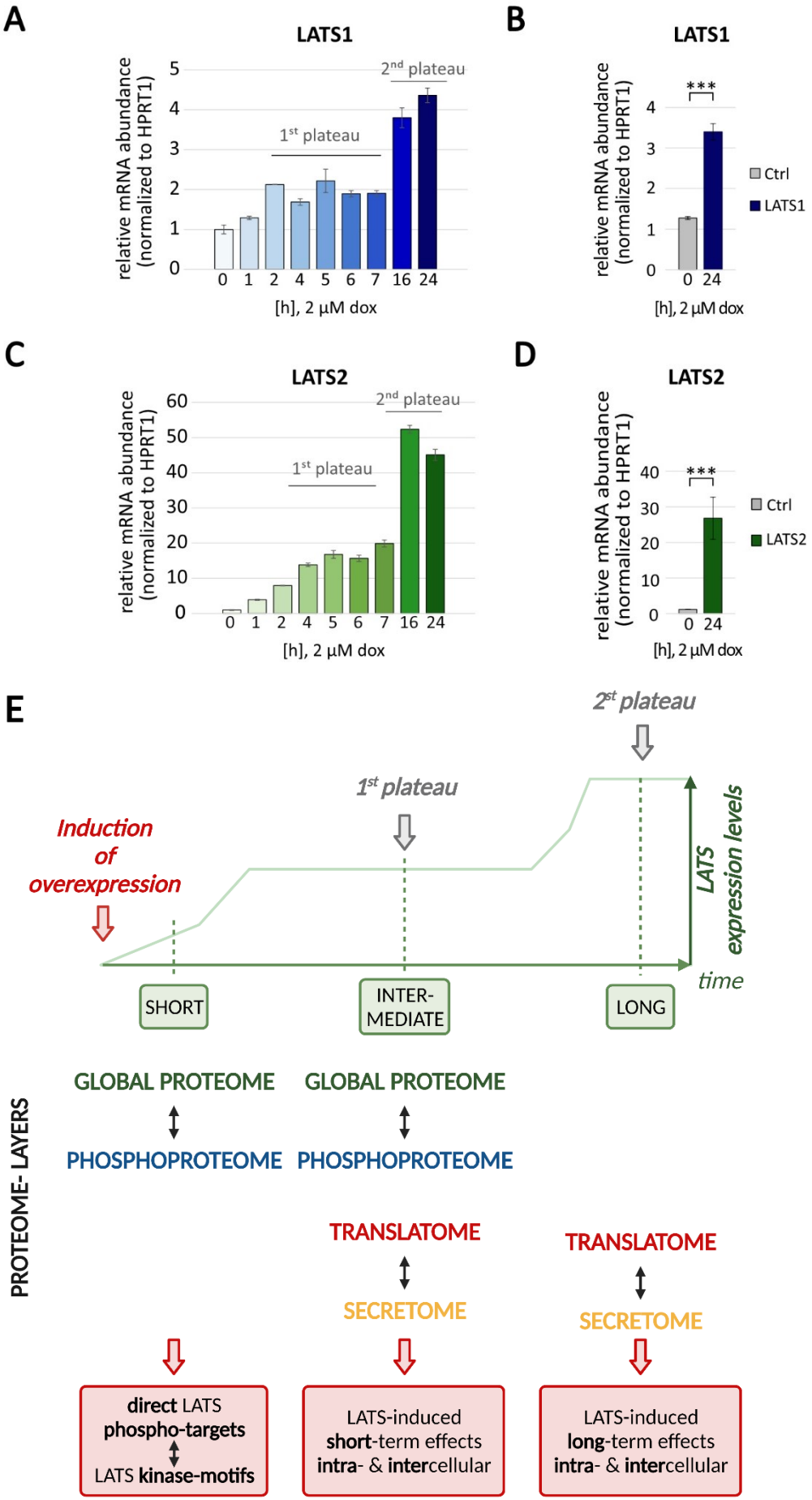
A
LATS1
relative mRNA abundance (normalized to HPRT1)
2nd plateau
1st plateau
0 1 2 4 5 6 7 16 24
[h], 2 µM dox
B
LATS1
***
Ctrl
LATS1
0 24
[h], 2 µM dox
C
LATS2
2nd plateau
1st plateau
0 1 2 4 5 6 7 16 24
[h], 2 µM dox
D
LATS2
***
Ctrl
LATS2
0 24
[h], 2 µM dox
E
2st plateau
1st plateau
Induction of overexpression
LATS expression levels
time
SHORT
INTER-MEDIATE
LONG
PROTEOME- LAYERS
GLOBAL PROTEOME
PHOSPHOPROTEOME
GLOBAL PROTEOME
PHOSPHOPROTEOME
TRANSLATOME
SECRETOME
TRANSLATOME
SECRETOME
direct LATS phospho-targets
LATS kinase-motifs
LATS-induced short-term effects intra- & intercellular
LATS-induced long-term effects intra- & intercellular

Figure 12: Utilization of newly established Tet-inducible overexpression system for LATS1 and LATS2 characterization by multilayered MS-based analysis. Relative mRNA expression levels of LATS1 (A and B) and LATS2 (C and D) in Tet-inducible MCF10A cells, normalized to the HPRT-1 housekeeping gene. (**A**) and (**C**) show mRNA expression levels after consecutive induction with 2 µM doxycycline (n=1). Error bars indicate the standard deviation of three technical replicates. (**B**) and (**D**) show average mRNA expression levels in GFP-control cells and LATS1- or LATS2-cells in each 3 biological replicates, after 24 h induction with 2 µM doxycycline. Error bars indicate standard deviation of biological replicates, and asterisks significance ***$p \leq 0.001$; according to unpaired t-test. (**E**) Schematic overview of the different proteome layers assessed at three different time points for LATS1 and LATS2 characterization, providing insights into direct targets and kinase-motifs of each kinase as well as short- and long-term effects of LATS1 and LATS2 overexpression on intra- and extracellular protein abundance. Figure (E) was created with BioRender.com.

Translatome analysis provides an in-depth view of the newly translated proteome, by specifically enriching and quantifying proteins that change their rate of synthesis upon LATS1/2 overexpression. At the same time, proteins whose translation is not affected by LATS1/2 overexpression will not be included in the measurement. This enables to uncover even small changes in the abundance of newly synthesized proteins which might be hard to detect in global proteome analysis.

Complementary to the detection of intracellular signaling events assessed by translatome analysis, the supernatant was collected, allowing for secretome analysis (not included in this study) which can give insights into LATS1/2-induced intercellular communication.

Moreover, to fully characterize the kinase activity of LATS1 and LATS2, phosphoproteome analysis was performed using Fe^{3+}-IMAC phosphopeptide enrichment. Therefore, a third time point of 2 h induction was chosen, in order to be able to capture direct LATS1 and LATS2 targets, potentially giving insight into LATS1- and LATS2-specific target motifs (**Figure 12E**). The second time point of 6 h for phosphoproteome analysis, on the other hand, allowed for insights into LATS1- and LATS2-induced, or potentially secondary (indirect) phosphorylation events. Since the latter time-point overlaps with the translatome analysis, it serves as an additional source of information about potentially regulatory phosphorylation sites on a protein of interest.

Collectively, this multilayered proteomics-based analysis, combining powerful cell systems with advanced MS-methodologies serves as a profound source of information helping to elucidate distinct and shared functionalities and characteristics of LATS1 and LATS2 kinases in the context of breast (cancer) tissue.

4.4. Differences of LATS1 and LATS2 on translatome dynamics

The strength of combining the newly established Tet-inducible LATS1- and LATS2-overexpression systems with the pulsed-SILAC and click-chemistry method was illustrated by the number of detected proteins that significantly change in their abundance upon LATS1 or LATS2 overexpression (**Figure 13**). In the MCF10A translatome datasets, 8600 proteins could be identified out of which more than 7700 were quantified. Notably, upon 6 h overexpression, 75 proteins and 120 proteins changed significantly in their abundance in the LATS1 and LATS2 dataset (**Figure 13B** and **13D**), respectively. Whereas, after 20 h overexpression, 170 proteins, and 386 proteins could be detected as significantly changing in the LATS1 and LATS2 datasets (**Figure 13C** and **13E**), respectively.

The overall aim of this study is to gain insights into new LATS1 and LATS2 functions. Accordingly, to draw a full picture, LATS1 and LATS2 have been individually studied by overexpressing each one of them separately. This allows for the comparison of LATS1 and LATS2 and the identification of shared or unique functions. In this chapter, the focus will be on their unique functions.

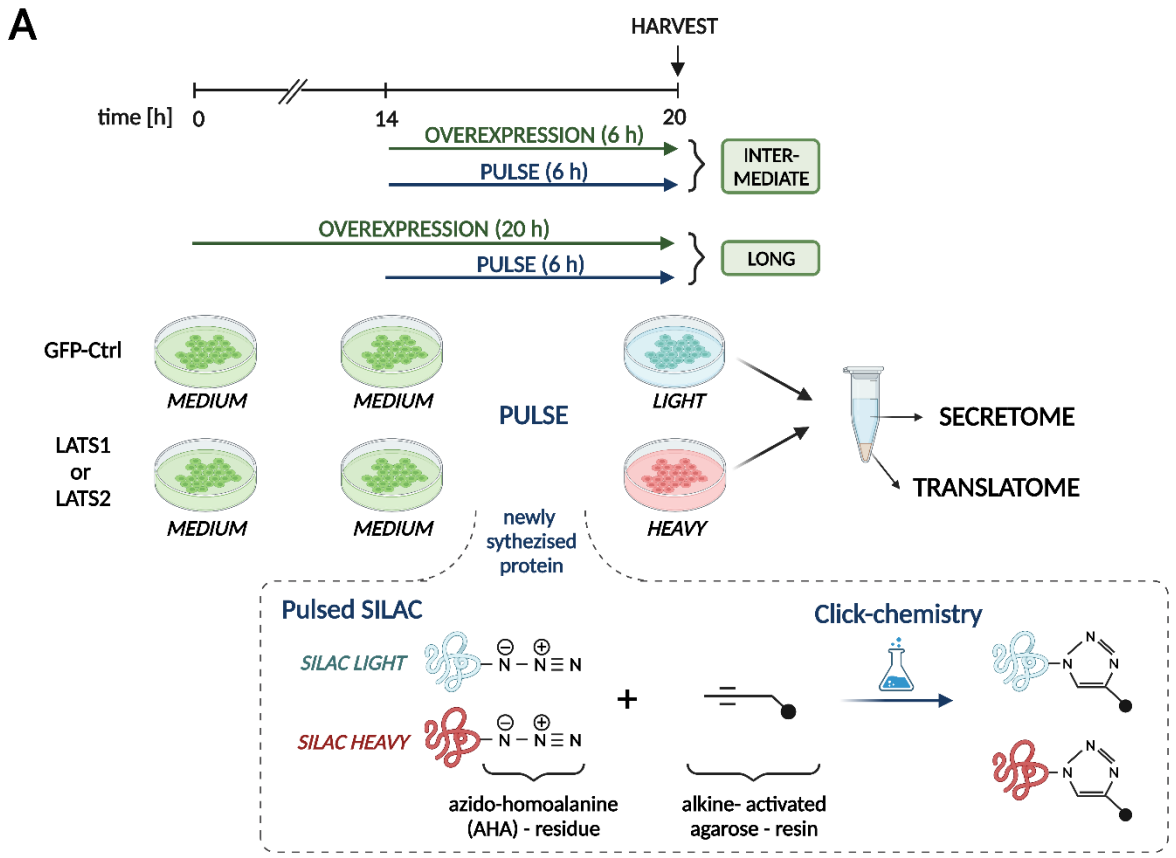

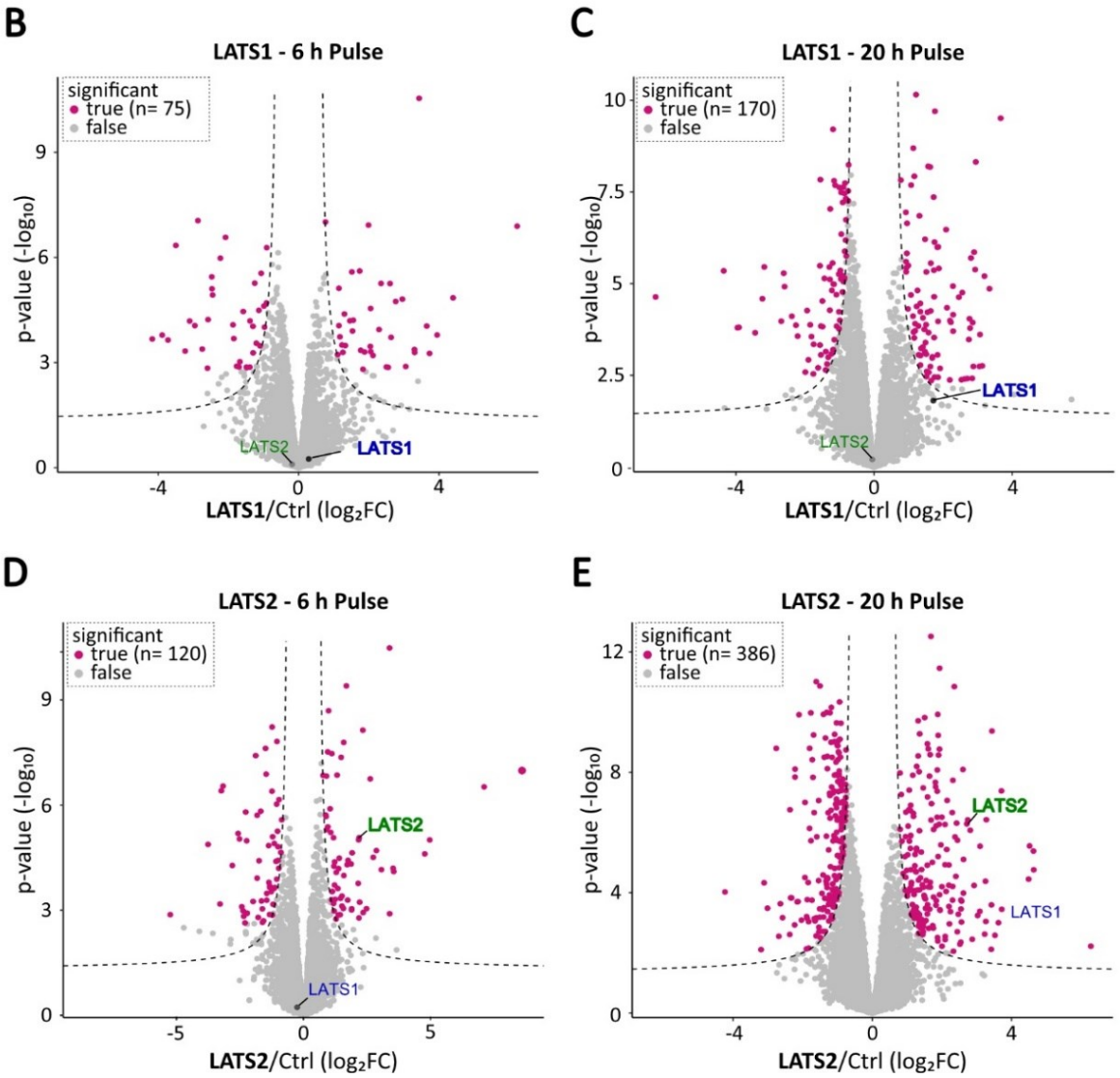

Figure 13: Translatome analysis reflecting the effects on the translatome upon induced overexpression of LATS1 or LATS2 in MCF10A cells. (**A**) Experimental setup of pulsed-SILAC and click-chemistry for translatome and secretome analysis. Upper panel: Tet-inducible overexpression of LATS1 or LATS2 and GFP-control for 20 h (long) or 6 h (intermediate). Pulse starts in the last 6 h of the experiment. Bottom panel: during pulse methionine is replaced by its analog L-azido-homoalanine (AHA) together with a switch of SILAC amino acids from "medium" to "light" (control) and "heavy" (LATS1 or LATS2). For subsequent enrichment, samples are mixed 1:1. Pulsed-SILAC allows for the enrichment and metabolic labeling (SILAC) of newly synthesized proteins by click-chemistry (AHA) covalently coupling the azide-containing proteins to an alkyne-activated resin. Figure (A) was created with BioRender.com. (**B**-**E**) Differential expression analysis using Limma moderated t-statistics for the comparison of changes on the translatome upon (**B** and **D**) 6 h or (**C** and **E**) 20 h overexpression of either (**B** and **C**) LATS1 or (**D** and **E**) LATS2 in MCF10A cells; three biological replicates each. Grey color of dots indicates non-significantly, pink color indicates significantly changing proteins, with a p-value adjusted for multiple testing according to Benjamini-Hochberg, *adj. $p \leq 0.05$ and a minimum log_2FC of +/- 0.58.

4.4.1. Proteins regulated differentially by LATS1 and LATS2 overexpression

To gain insights into newly synthesized proteins upon overexpression of either LATS1 or LATS2, translatome analyses were performed. Therefore, the Tet-inducible MCF10A cells were induced for 20 h by administration of 2 µM dox in LATS1- and LATS2-, as well as GFP-overexpression cell systems (the latter serving as a control). The pulse was started in the last 6 h of the total 20 h overexpression time (**Figure 13A**), allowing for enrichment of newly synthesized proteins at high expression levels of LATS1 with a protein ratio of 1.7 [log_2] and LATS2 with a protein ratio of 2.7 [log_2] (**Figure 13C, 13E** and **Figure 14C**).

Correlation of the LATS1 and LATS2 datasets allowed us to examine proteins which are differentially regulated by LATS1 and LATS2. The 20 h translatome datasets of MCF10A cells revealed 15 proteins for LATS1 and 37 proteins for LATS2 significantly changing their protein abundance upon overexpression in one dataset and at the same time showing an inverse expression level in the other dataset (**Figure 14A** and **14B**). These proteins indicate that the paralogues are functioning in different pathways. However, the datasets also revealed a high correlation between the LATS1 and LATS2 translatomes.

Notably, upon 20 h overexpression of LATS2 (protein ratio of 2.7 [log_2]), also LATS1 protein levels increased significantly (protein ratio of 2.6 [log_2]) in MCF10A cells (**Figure 14A** and **14C**), suggesting a co-regulation of LATS1 by LATS2. Interestingly, a similar effect was observed upon 48 h of LATS2 overexpression in MCF7 cells (**Figure 14E**), reflected by protein ratios of 3.2 [log_2] for LATS2 and 2.9 [log_2] for LATS1. In contrast, this co-regulation of LATS1 could not be observed in the ZR75.1 dataset (**Figure 14F**), suggesting a context-specific mechanism. Furthermore, in MCF10A cells this co-regulation could not be observed upon 6 h overexpression, suggesting a delayed response of LATS1 protein levels to the overexpression of LATS2 (**Figure 14C**).

Along these lines, we next asked on which regulatory level this co-regulation is taking place. For this, we analyzed how the relative mRNA expression levels of one kinase are affected by the induced overexpression of the other kinase. In line with protein ratios at 6 h overexpression (**Figure 14C**), analysis of mRNA ratios at 6 h LATS overexpression (**Figure 14D**) revealed no mutual regulation. Interestingly, however, although mRNA ratios of 16 h and 24 h overexpression showed a slight mutual regulation for both LATS1 and LATS2 mRNA levels (ratios between 0.8 – 1.1 [log_2]) (**Figure 14D**), only LATS1 protein levels increase in

the LATS2 overexpression dataset (**Figure 14C**). In other words, even though LATS2 mRNA levels were increased in the LATS1 dataset, this was not reflected in the protein level. Moreover, comparing the magnitude of mRNA expression levels relative to the expression levels of newly translated proteins, it becomes evident that the increase of LATS1 protein levels in the LATS2 dataset is not fully reflected by the increase of mRNA levels. This could indicate that the increase in LATS1 protein levels might be due to LATS2 stabilizing mRNA levels of LATS1 rather than upregulating its transcript levels. Yet, further experiments, such as mRNA stability assays would be necessary to prove this hypothesis.

Taken together, these observations suggest that LATS2 is upstream of LATS1, thereby increasing LATS1 protein levels possibly by stabilization of LATS1 mRNA levels. This co-regulation is exclusively one-directional and not mutual. Moreover, given the high LATS1 protein levels in the LATS2 dataset, LATS2 functions can not be fully separated from LATS1 which has to be kept in mind for the following data interpretation.

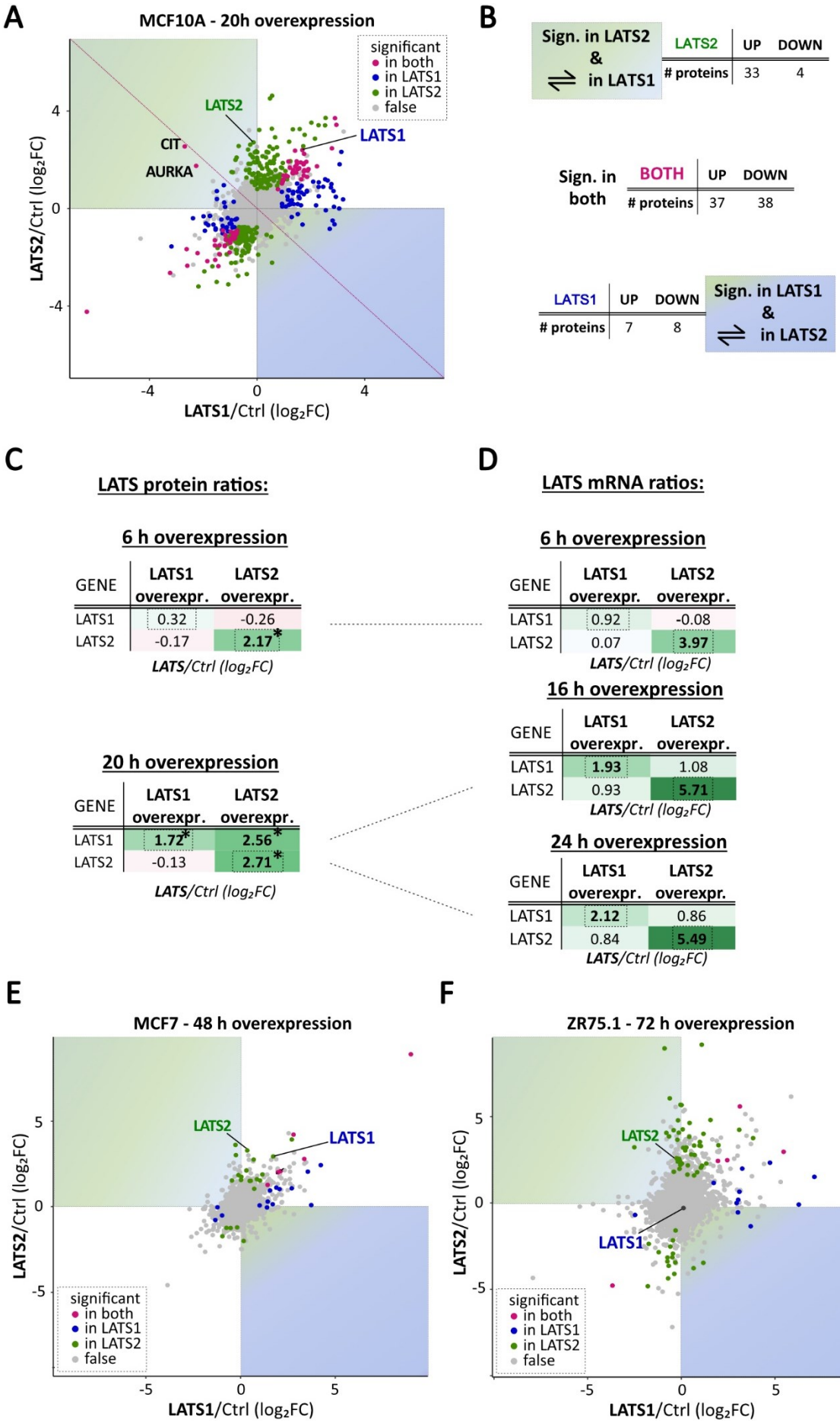
A
MCF10A - 20h overexpression
significant
in both
in LATS1
in LATS2
false
LATS2
LATS1
CIT
AURKA
LATS2/Ctrl (log2FC)
LATS1/Ctrl (log2FC)
B
Sign. in LATS2 & in LATS1
LATS2 UP DOWN
proteins 33 4
Sign. in both
BOTH UP DOWN
proteins 37 38
LATS1 UP DOWN
proteins 7 8
Sign. in LATS1 & in LATS2
C
LATS protein ratios:
6 h overexpression
GENE LATS1 overexpr. LATS2 overexpr.
LATS1 0.32 -0.26
LATS2 -0.17 2.17*
LATS/Ctrl (log2FC)
20 h overexpression
GENE LATS1 overexpr. LATS2 overexpr.
LATS1 1.72* 2.56*
LATS2 -0.13 2.71*
LATS/Ctrl (log2FC)
D
LATS mRNA ratios:
6 h overexpression
GENE LATS1 overexpr. LATS2 overexpr.
LATS1 0.92 -0.08
LATS2 0.07 3.97
LATS/Ctrl (log2FC)
16 h overexpression
GENE LATS1 overexpr. LATS2 overexpr.
LATS1 1.93 1.08
LATS2 0.93 5.71
LATS/Ctrl (log2FC)
24 h overexpression
GENE LATS1 overexpr. LATS2 overexpr.
LATS1 2.12 0.86
LATS2 0.84 5.49
LATS/Ctrl (log2FC)
E
MCF7 - 48 h overexpression
LATS2
LATS1
significant
in both
in LATS1
in LATS2
false
LATS2/Ctrl (log2FC)
LATS1/Ctrl (log2FC)
F
ZR75.1 - 72 h overexpression
LATS2
LATS1
significant
in both
in LATS1
in LATS2
false
LATS2/Ctrl (log2FC)
LATS1/Ctrl (log2FC)

Figure 14: Correlation of LATS1 and LATS2 translatome datasets reveals distinct and common regulation of newly synthesized proteins. (**A**), (**E**) and (**F**) Correlation of differential expression analysis of changes on the translatome upon overexpression of LATS1 (x-axis) versus LATS2 (y-axis) in (A) MCF10A (= correlation of the datasets in Figure 13C and 13E), (E) MCF7, and (F) ZR75.1 cells; in three biological replicates each. Color of dots indicates the following: grey non-significantly, blue significantly changing only in LATS1, green significantly changing only in LATS2, and pink color significantly changing proteins in both LATS1- and LATS2-datasets, with a p-value adjusted for multiple testing according to Benjamini-Hochberg, *adj. $p \leq 0.05$ and a minimum log_2FC of +/- 0.58. The proteins in the upper quarter show proteins that are upregulated in the LATS2 (log_2FC of > 0.58) and show a downwards tendency in the LATS1 (log_2FC of < 0) dataset. The proteins in the bottom quarter show proteins that are upregulated in the LATS1 (log_2FC of > 0.58) and show a downwards tendency in the LATS2 (log_2FC of < 0) dataset. (**B**) Numbers of proteins that are significantly regulated in LATS1 (upper panel) of LATS2 (bottom panel), but show inverse expression levels in the corresponding other datasets. The middle panel shows the number of proteins significantly up- or downregulated by both LATS1 and LATS2. (**C**) Protein ratio levels and (**D**) mRNA ratio levels of LATS1 and LATS2 in translatome datasets of MCF10A cells. Red color implies downregulation, green color implies upregulation, and numbers with an asterisk depict significantly changing proteins with an adj. $p \leq 0.05$.

4.4.2. Differential regulation of Aurora kinases and other proteins important for chromosomal segregation and cytokinesis by LATS1 and LATS2

By correlating the LATS1 and LATS2 20 h translatome datasets of MCF10A cells, the two proteins Citron Rho-interacting kinase (CIT) and Aurora A (AurA) were especially interesting candidates since they both show significant upregulation in the LATS2 dataset and at the same time significant downregulation in the LATS1 dataset (**Figure 14A**).

In particular, the kinase CIT showed an inverse expression in the MCF10A translatome datasets, being 2.6 [log_2]-fold upregulated upon LATS2 overexpression, but -2.7 [log_2]-fold downregulated upon LATS1 overexpression. CIT, as an effector of cytokinesis, has been described to form a complex with the Kinesin-like protein 14 (KIF14) at the central spindle and midbody, required for efficient cytokinesis (Gruneberg *et al*, 2006). Interestingly, in the present study, KIF14 showed a slight increase of protein levels upon LATS2 overexpression (0.8 [log_2]), and a slight downregulation upon LATS1 overexpression (-0.6 [log_2]), similar to CIT. This suggests that LATS2, but not LATS1 alone, contributes to CIT upregulation and activity, thereby possibly ensuring efficient cytokinesis.

The second protein which showed opposing expression levels upon 20 h LATS1 or LATS2 overexpression is the kinase AurA. Specifically, AurA showed significant upregulation in the LATS2 dataset (1.8 [log_2]), whereas, significant downregulation in the LATS1 dataset (-2.3 [log_2]) (**Figure 14A** and **Figure 15A**). Interestingly, however, in MCF10A global

proteome analysis, 6 h overexpression of either LATS1 or LATS2, caused a significant decrease in AurA and Aurora B (AurB) protein expression levels (**Figure 15A**). At first sight, this might reflect a discrepancy between the 6 h translatome and 6 h global proteome analysis, given that the downregulation of AurA and AurB can only be detected in the global proteome analysis. Yet, it should be noted that by performing a translatome experiment, only newly synthesized proteins can be detected, whereas protein degradation of proteins with a rather low turnover rate can not. In other words, the turnover rate of a protein, the magnitude of expression, together with the duration time of the pulse, determines whether protein degradation can be detected or not. Hence, in the case of AurA and AurB, the degradation rate might not lie within the 6 h of the pulse.

Collectively, this suggests that LATS1 and LATS2 overexpression for 6 h leads to downregulation of AurA and AurB, as does overexpression of LATS1 for 20 h (**Figure 15A** and **15C**, box (I-III)). Conversely, prolonged overexpression of LATS2 for 20 h, and with this a timely delayed co-expression of LATS1, seem to switch the mode of action, resulting in overexpression of AurA and AurB instead (**Figure 15A** and **15C**, box (IV)).

As outlined before (Introduction Section 1.1.2.3) the homologs AurA, AurB, and AuroraC (AurC) are cruical players in mitosis ensuring proper spindle assembly, and cytokinesis. Hereby they act in a special and temperal coordinated manner (Nigg, 2001; Salaun *et al*, 2008; Willems *et al*, 2018). In particular, in early mitosis AurA ensures G_2/M-transition by promoting centrosome maturation and mitotic spindle assembly, followed by middle to late mitosis, where AurB and AurC, as members of the so-called “chromosome passenger complex” (CPC) take care of proper chromosome binding to kinetochores and chromosome segregation (Willems *et al*, 2018).

Intriguingly, along these lines, LATS1 and LATS2 have been described to be in crosstalk with AurA and AurB, proposed as the AurA-LATS1/2-AurB (ALB)-axis (Yabuta *et al*, 2011). The ALB-axis starts with AurA phosphorylating LATS2 at serine (Ser)-380 (**Figure 15D**). This phosphorylation causes LATS2 to localize to the central spindle together with AurB. The last player of the “ALB-quartet”, LATS1, is also recruited to the spindle pole and is known to phosphorylate AurB and other members of the CPC. Ultimately, the interplay and re-localization of the ALB-quartet ensure correct chromosome segregation before allowing mitotic progression (Yabuta *et al*, 2011).

In this study, we observed that LATS2 overexpression for 20 h, induces co-expression of LATS1 and significant upregulation of AurA and AurB (**Figure 15A** and **15C**, box (IV)). Additionally, complementary phosphoproteomic analysis in MCF10A cells revealed significant upregulation of the LATS2^{S380} phosphorylation site (3.4 [log_2] unnormalized or 0.65 [log_2] normalized to the global proteome) upon LATS2 overexpression (**Figure 15B**) indicating AurA activity. Additionally, however, a second phosphorylation site, on serine Ser-576 was found to be significantly upregulated upon LATS2 overexpression (3.75 [log_2] unnormalized or 1.0 [log_2] normalized to the global proteome) (**Figure 15B**). Possibly, this phosphorylation of LATS2 might promote the observed LATS1 co-expression which could, in turn, explain the time delay of the co-expression.

Along these lines, three out of four members of the CPC were found to be significantly upregulated upon 20 h LATS2 overexpression, suggesting the CPC complex to be activated potentially driving the progression of chromosome segregation.

Together, LATS2-induced and potentially LATS1-assisted overexpression of AurA and AurB, and the new LATS2^{S576} phosphorylation might reflect novel regulatory switches in the ALB axis. Thus, this might allow for the hypothesis that for the ALB-quartet to promote progression of mitosis by upregulation of AurA and AurB, it requires both, LATS1 and LATS2 (**Figure 15A** and **15C**, box (IV)), whereas if only one paralogue solely is upregulated it leads to downregulation of AurA and AurB and thereby mitotic arrest (**Figure 15A** and **15C**, box (I-III)).

It should be kept in mind that high protein levels of AurA have been shown to promote tumorigenesis. Moreover, AurA and AurB have been described to be upregulated in aneuploidy cells (Willems *et al*, 2018). Thus, downregulation of AurA and AurB would be in line with LATS1 and LATS2 being described as tumor suppressors. However, further investigations are required to fully understand the functional roles of the four kinases in physiological as well as tumorigenic contexts.

Collectively, these datasets show that there is a strong co-dependency between all four effectors of the ALB-pathway, adding a few more cues to the pre-existing model. **Figure 15D** summarizes the pre-existing model (indicated in grey), and observations made in this study (indicated color). Moreover, these results underline the different functions of LATS1 or LATS2 alone or their joint activity after LATS2 overexpression. The former being reflected

by AurA and AurB downregulation which might result in inhibition of cell cycle progression, whereas the latter, being reflected by AurA and AurB upregulation which might promote cell cycle progression. Thus, these findings highlight the important roles of LATS1 and LATS2 in chromosome segregation and cytokinesis, reflected by the changes in protein abundance of major regulators of these processes, upon LATS1 and LATS2 overexpression.

A

Aurora kinase protein ratios:

GENE	LATS1 OVEREXPR.	LATS2 OVEREXPR.	EXPERIMENT	TIME POINT
AURKA	-1.20*	-1.10*	GLOBAL	6h
	0.20	-0.10	TRANS	6h
	-2.30*	1.80*	TRANS	20h

LATS/Ctrl (log_2FC)

GENE	LATS1 OVEREXPR.	LATS2 OVEREXPR.	EXPERIMENT	TIME POINT
AURKB	-1.60*	-1.50*	GLOBAL	6h
	0.30	0.10	TRANS	6h
	-0.30	2.40*	TRANS	20h

LATS/Ctrl (log_2FC)

B

P-sites on LATS2

GENE	AMINO ACID +POSITION	AMINO ACID SEQUENCE	LATS1 OVEREXPR.	LATS2 OVEREXPR.	TIME POINT
LATS2	S380	RDSLQKPGLEAPPR	0.24	1.32*	2 h
	S380	RDSLQKPGLEAPPR	0.27	3.39*	6 h
LATS2	S576	QIQTSPVPVRK	0.66	3.75*	6 h

LATS/Ctrl (log_2FC)

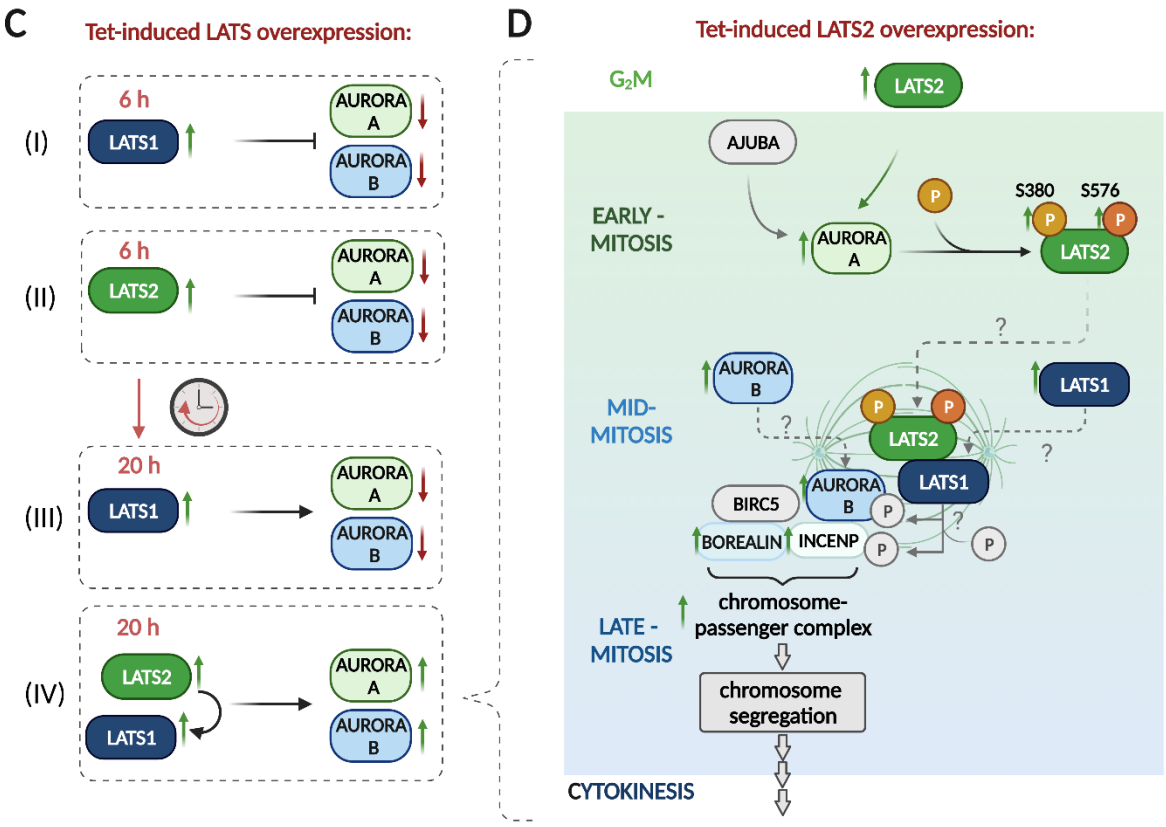

Figure 15: Distinct regulation of Aurora kinases by LATS1 and LATS2. (**A**) Protein ratio levels of Auroro A (left panel) and Aurora B (right panel) in the LATS1 and LATS2 translatome datasets of MCF10A cells. Red color implies downregulation, green color implies upregulation, and numbers with an asterisk depict significantly changing proteins with an adj. $p \leq 0.05$. (**B**) Ratios of phosphorylation site on LATS2 at different localizations upon LATS1 or LATS2 overexpression for 2 h or 6 h, acquired in phosphoproteome analysis. Green color implies upregulation, and numbers with an asterisk depict significantly changing phosphorylation sites with an adj. $p \leq 0.05$. (**C**) Schematic summary of results in (A): LATS1 6 h (I), LATS2 6 h (II), or LATS1 20 h (III) overexpression (solely) leads to AurA and AurB downregulation. 20 h LATS2 overexpression (IV) induces timely delayed LATS1 co-expression and leads to AurA and AurB upregulation. (**D**) Scheme of the AurA-LATS-AurB- axis. In color effects demonstrated in this study upon Tet-induced overexpression of LATS2 for 20 h. In grey are proteins involved in the depicted pathway described in the literature, but not detected in this dataset. Dashed-arrows show potential re-localization of proteins to the spindle-apparatus, as described in the literature. For more details see text in this section. Figures (C) and (D) were created with BioRender.com.

4.4.3. Reciprocal roles of LATS1 and LATS2 in cell cycle regulation

We next asked whether reciprocal regulation of cell cycle effectors (such as AurA, AurB and, CIT), by LATS1 and LATS2 overexpression, might imply reciprocal effects on cell cycle regulation. Therefore, we performed GSEA analysis for LATS1 and LATS2 translatome datasets. Intriguingly, differentially expressed proteins upon 20 h LATS2 overexpression were significantly enriched for "G_2/M checkpoint" and "E2F targets" (known to regulate G_1/S transition) genesets within the hallmarks MsigDB (Liberzon *et al*, 2011, 2015), whereas contrarily, the 20 h LATS1 dataset showed downregulation of proteins in these gene sets (**Figure 16A** and **16B**, respectively). Also, after only 6 h overexpression of both, LATS1 and LATS2, genes involved in both genesets were downregulated (**Figure 16D** and **16C**, respectively). Of note, CDK1, which is included in both, "G_2/M checkpoint" and "E2F targets" genesets, has been described to be sufficient to drive cell cycle in mammalian cells (Santamaría *et al*, 2007). In line with the GSEA, expression levels of CDK1 showed significant upregulation of 1.5 [$\log_2$] upon 20 h LATS2 overexpression, and again contrarily, downregulation of -0.9 [$\log_2$] upon 20 h LATS1 overexpression. Collectively, this suggests that 20 h LATS2 overexpression is activating cell cycle progression, whereas, in the remaining three datasets, the cell cycle seems to be repressed. Thus, this is in line with the hypothesis deduced from regulation of the ALB-quartet, i.e. to promote cell cycle progression, it requires both, LATS1 and LATS2, reflected by the 20 h LATS2 overexpression showing a co-induction of LATS1 after a time delay (Section 4.4.2). And in contrast, if only

one paralogue solely is upregulated, which can be seen after only 6 h overexpression of both paralogues or after 20 h LATS1 overexpression, it leads to repression of the cell cycle. LATS1 has been described to be involved in both, the negative regulation of G_1/S and G_2/M checkpoint (Nishiyama *et al*, 1999; Yang *et al*, 2001; Chiyoda *et al*, 2012; Matsuoka *et al*, 2007; Pefani *et al*, 2014), as well as to positively regulate mitotic progression (Hirota *et al*, 2000; Iida *et al*, 2004). In the present study, LATS1 overexpression negatively regulated proteins involved the G_2/M checkpoint and E2F targets, suggesting G_2/M and possibly G_1/S arrest. It will be interesting to investigate whether these arrests can be observed phenotypically by cell cycle analysis, e.g. using flow cytometry.

Also, LATS2 has been described in both, promotion of cell cycle progression by ensuring proper cytokinesis (Ganem *et al*, 2014) and negative regulation of G_1/S transition by downregulation of cyclin E/CDK2 kinase activity (Li *et al*, 2003). Interestingly, LATS2 has also been described to be an activator of the DREAM (dimerization partner (DP), RB-like, E2F and MuvB) complex, a large transcription complex repressing genes required for cell cycle progression, resulting in cell quiescence (Litovchick *et al*, 2011). Dependent on the binding of either E2F- or CHR- promotor elements, the DREAM complex represses proteins of G_1/S or G_2/M phase, respectively (Sadasivam & DeCaprio, 2013; Fischer & Müller, 2017). Thus, in this scenario, LATS2 promotes cell cycle repression, which is in contrast to what was observed upon 20 h LATS2 overexpression in the present study. Interestingly, along these lines, ORA analysis of significantly upregulated proteins in the 20 h LATS2 dataset, showed a significant overlapped with the “FISCHER_G2_M_CELL_CYCLE” and “FISCHER_DREAM_ TARGETS” dataset (**Supplementary Table 2**). Thus, this indicates deactivation of the transcription repressor complex and thereby it is contradictive to the role of LATS2 described by Tschöp and co-workers (Tschöp *et al*, 2011). Briefly, they show that partial knockdown of LATS2 leads to, as they refer to “unexpected effects of LATS2”, namely defects in the assembly of the DREAM repressor complex and thus suppression of RB-induced senescence markers. Moreover, they show that with “physiological” LATS2 expression levels, LATS2 phosphorylates and thereby activates DYRK1A, which in turn phosphorylates LIN52, a component of MuvB. This phosphorylation event ultimately triggers DREAM complex assembly and the entering of quiescence (Litovchick *et al*, 2011). The authors conclude that low levels of LATS2, as observed in many tumor cells, may prevent cells from entering cell cycle arrest via DREAM or RB1. Together with the observed

effects of the present study, these findings underpin the notion that protein expression levels of LATS2 might act as a regulative for the decision between either cell cycle progression or cell cycle arrest.

Collectively, the present study showed significant enrichment of proteins involved in G_2/M as well as E2F-targets, together with the enrichment of DREAM-targets upon 20 h LATS2 overexpression, suggesting that LATS2 promotes cell cycle progression. Furthermore, this might be explained by deactivating the DREAM complex, a core regulator of quiescence. Moreover, LATS1 overexpression alone was not sufficient to cause the same effects as seen by LATS2 overexpression. This, together with the regulation of AurA and AurB described in the chapter before (4.4.2), strengthens the notion of different individual functions of LATS1 and LATS2 in cell cycle regulation.

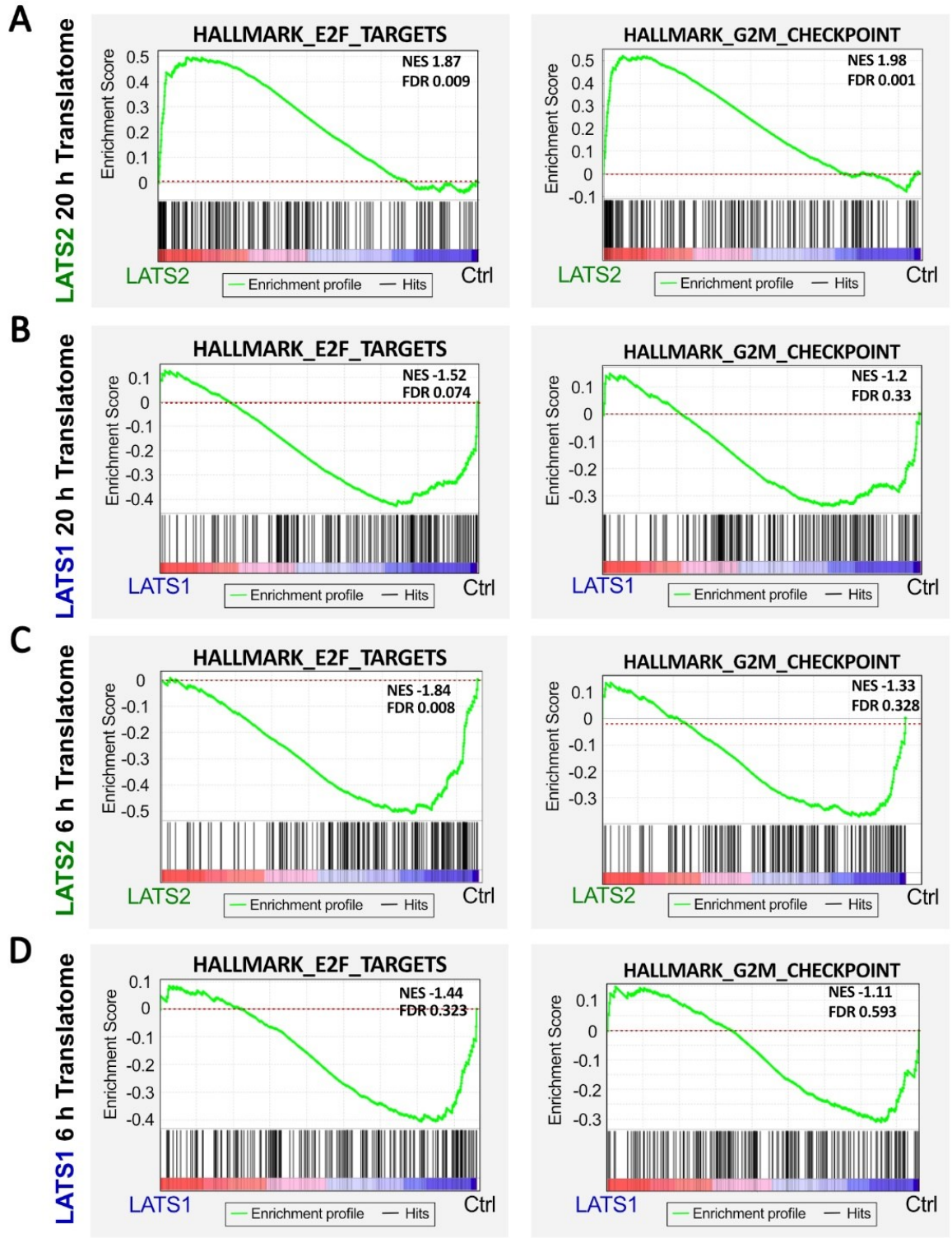

Figure 16: GSEA of MCF10A translatome datasets reveals opposing enrichment of cell cycle related gene sets. GSEA was performed with differential protein expression values of (**A**) the LATS2 20 h translatome dataset, (**B**) the LATS1 20 h translatome dataset, (**C**) the LATS2 6 h translatome dataset, and (**D**) the LATS1 6 h translatome dataset, against the hallmarks gene sets from MsigDB. The green curve indicates the enrichment profile, calculated as the running sum of the weighted enrichment score obtained from the GSEA software. Normalized enrichment score (NES) and adjusted p-value/FDR are reported within each graph.

4.5. Insights into novel phosphorylation targets of the protein kinases LATS1 and LATS2

As LATS1 and LATS2 are serine-threonine kinases, it is tempting to learn more about their regulatory functions by having a closer look at their impact on the phosphoproteome. However, so far only a few studies defined direct LATS1 or LATS2 targets with the corresponding phosphorylation site (Table 36). The post translational modification (PTM) signatures database (PTMsigDB), provides a repository of site-specific PTM motif signatures, kinase activities, and signaling pathways curated from literature (Krug *et al*, 2019). Albeit advanced MS-based phosphoproteomics identified almost 300,000 phosphophorylation sites, only approximately ~15,780 of all identified phosphosites can be assigned as substrates of a certain kinase. Yet, by searching for LATS1 and LATS2 substrates, out of these 15,780 substrates, only 26 entries can be found for LATS2 and none for LATS1. This reflects an insufficient coverage compared to well-defined kinases such as CDK1 or AURKB with 494 or 180 specifically assigned phosphophorylation sites, respectively. Moreover, manual validation by tracing back the original study describing this phosphorylation site revealed that some of these LATS2-assigned phosphorylation sites can actually be phosphorylated by both, LATS1 and LATS2. Thus, there is a need for in-depth studies focusing on LATS1- and LATS2-specific substrates and the prediction of specific kinase motifs that will facilitate a better understanding of their role in regulatory processes.

Table 36: LATS1 and LATS2 motif sequences reported in the literature.

KINASE	GENE	UNIPROT ID	POSITION	AMINO ACID	(7-**PHOS**-7)	SOURCE
LATS1	PPP1R12A	O14974	696	T	ARQSRRS**T**QGVTLTD	(Chiyoda *et al*, 2012)
	PPP1R12A	O14974	445	S	LGLRKTG**S**YGALAEI	(Chiyoda *et al*, 2012)
	PPP1R12A	O14974	695	S	QARQSRR**S**TQGVTLT	(Chiyoda *et al*, 2012)
	PPP6R3	Q5H9R7	579	S	QDDIGNV**S**FDRVSDI	(Chiyoda *et al*, 2012)
	YAP1	P46937	397	S	TYHSRDE**S**TDSGLSM	(Chiyoda *et al*, 2012)
LATS2	AMOT	Q4VCS5	175	S	QGHVRSL**S**ERLMQMS	(Chan *et al*, 2011)
	AMOTL2	Q9Y2J4	159	S	HGHVRSL**S**ERLLQLS	(Chan *et al*, 2011)
	CDKN1A	P38936	146	S	GRKRRQT**S**MTDFYHS	(Suzuki *et al*, 2013)
	SNAI1	O95863	203	T	QGHVRTH**T**GEKPFSC	(Zhang *et al*, 2012)
	WWTR1 (TAZ)	Q9GZV5	89	S	AQHVRSH**S**SPASLQL	(Lei *et al*, 2008; Liu *et al*, 2010)
	WWTR1 (TAZ)	Q9GZV5	311	S	PYHSREQ**S**TDSGLGL	(Lei *et al*, 2008; Liu *et al*, 2010)
	YWHAG (14-3-3γ)	P61981	59	S	VVGARRS**S**WRVISSI	(Okada *et al*, 2011)

LATS1 & LATS2	CDC26	Q8NHZ8	7	T	_MLRRKP**T**RLELKLD	(Masuda *et al*, 2015)
	INCENP	Q9NQS7	894	S	RYHKRTS**S**AVWNSPP	(Yabuta *et al*, 2016)
	KIF23	Q02241	814	S	LRHRRSR**S**AGDRWVD	(Fesquet *et al*, 2015)
	KIF23	Q02241	716	S	QLHRRSN**S**CSSISVA	(Fesquet *et al*, 2015)
	YAP1	P46937	61	S	IVHVRGD**S**ETDLEAL	(Zhao *et al*, 2007; Hao *et al*, 2008)
	YAP1	P46937	109	S	KSHSRQA**S**TDAGTAG	Zhao et al. 2007a; Hao et al. 2008)
	YAP1	P46937	127	S	PQHVRAH**S**SPASLQL	Zhao et al. 2007a; Hao et al. 2008)
	YAP1	P46937	164	S	AQHLRQS**S**FEIPDDV	Zhao et al. 2007a; Hao et al. 2008)
	YAP1	P46937	381	S	TYHSRDE**S**TDSGLSM	Zhao et al. 2007a; Hao et al. 2008)

In this study, the Tet-inducible cell systems, established in MCF10A, ZR75.1, and MCF7 were used (i) to screen for novel phosphorylation substrates of LATS1 and LATS2, and (ii) to assess the effects of LATS1 or LATS2 overexpression on global phosphorylation dynamics. Together this will provide a valuable layer of information for defining the functions of these two kinases.

Hence, to gain insights into LATS1- or LATS2-induced phosphorylation events, quantitative phosphoproteome analyses were performed by combining Fe^{3+}-immobilized metal affinity chromatography (IMAC) phosphopeptide enrichment (Ruprecht *et al*, 2015, 2017; Potel *et al*, 2018) combined with in-depth global proteome quantification using SILAC. Two time points were chosen, one ("short") after 2 h of dox-induced LATS1 or LATS2 overexpression to catch direct LATS1/2-kinase substrates, and a second ("intermediate") after 6 h of dox-induced overexpression, covering LATS substrates at higher LATS1/2 protein levels, as well as potentially secondary downstream effects of LATS overexpression (**Figure 12E**). For each time point, LATS1-, GFP-control, and LATS2-overexpressing cells, metabolically labeled with SILAC-light, -medium, and -heavy, respectively, were combined in one sample, whereof 90% was used for phosphopeptide enrichment and 10% for global proteome analysis. In a 3 h gradient, single-shot measurement between ~7500 and 8700 phosphopeptides could be quantified in all three cell lines. Corresponding global proteome samples were fractionated prior to LC-MS^2 analysis thereby achieving a protein depth of ~6700 to 7800 quantified proteins.

Working with phosphoproteome data always comes with the decision of whether to normalize the phosphorylation sites to the global proteome or not. Both options come with advantages and disadvantages, which will be briefly discussed in the following. The

rationale behind working with proteome-normalized phospho-data is that the detected changes in phosphorylation site abundance can either be due to a decrease or increase of the phosphorylation site itself or to a change of the protein level of the modified protein, rather than the site. Thus, in theory, subtracting the log fold-change of the protein level itself from the log fold-change of the phosphorylation site should enable to see only the relative changes in phosphorylation levels. Therefore, in many studies, the changes in phospho-site abundance are normalized by the changes of the overall changes in protein abundance, hereafter referred to as normalized phospho-data. However, this approach comes with some drawbacks: First, many phosphosites might not be successfully matched to the global proteome (dependent on the depth of MS-analysis), resulting in a potentially significant loss of quantified phosphorylation sites due to a low overlap between proteome and phosphoproteome. This low overlap can be explained by many factors, such as (i) the stochasticity of the MS algorithm for choosing the peptides that will be quantified and identified, prioritizing those of high abundance, and, along these lines (ii) the distinct dynamic range and complexity of a global proteome compared to a phosphoproteome, or (iii) low sampling depth. Second, if both the protein level and a phosphosite on this protein are upregulated, it implies that the responsible kinase had to increase its phosphorylation rates in order to keep pace with the increased protein levels. Thus, the kinase exhibits an elevated activity, but normalization would eliminate this information.
Therefore, we decided to analyze both unnormalized and normalized phosphoproteome data to faciliate full insights while avoiding the elimination of information.

For both time points, significant changes in the abundance of phosphorylation sites, as well as changes in the global proteome could be observed upon LATS1 and LATS2 overexpression in MCF10A cells (**Figure 17A** and **17B, Supplementary Figure 11**). It should be noted, however, that by using global proteome analysis, significant overexpression could only be detected for LATS2 after 6 h of induction (**Figure 17A**) resulting in 2.75 [log_2]-fold upregulation, whereas fot 6 h of LATS1 induction, and for 2 h induction of LATS1 or LATS2, protein ratios of LATS1 and LATS2 could either not be detected or were not changing (**Supplementary Figure 11A**). By comparing global proteome to translatome datasets, a similar relative expression level has been observed in the 6 h translatome dataset, showing only a slight increase of protein ratio (0.32 [log_2]) after 6 h overexpression of LATS1,

however, reaching higher ratio levels (1.72 [log_2]) after 20 h of induction (**Supplementary Figure 11A**). Thus, this suggests that this system requires longer induction times for LATS1 to reach steady protein levels, compared to LATS2. As a consequence, we can not say for sure whether the effects seen in this dataset are caused by LATS1 overexpression. Therefore, this will be taken into consideration for data interpretation of the phosphoproteome.

4.5.1. LATS1- and LATS2-induced phosphoproteome dynamics

In the scope of the Hippo pathway discovery one of the first described direct targets of LATS1 and LATS2 was YAP, being inactivated by LATS1/2-mediated phosphorylation (Zhao et al. 2007, Genes& Dev, Hao et al. 2008; Oka et al. 2008; Zhang et al.2008). YAP comprises five LATS1/2 phosphorylation consensus motifs (Ser-61, Ser-109, Ser-127, Ser-164, and Ser-397), of which the phosphorylation site YAP^{S127} has been described to result in cytoplasmatic retention of YAP by the adaptor protein 14-3-3 (Zhao *et al*, 2007). As a consequence, this prevents the transcription of YAP target genes, involved in cell proliferation, migration, and survival (Pan, 2010; Piccolo *et al*, 2014; Yu *et al*, 2015).

Interestingly, upon 6 h LATS2 overexpression, nine phosphorylation sites on YAP could be detected, out of which all but one showed a positive tendency (**Figure 17B** and **Table 37**). Moreover, all five previously described phosphorylation sites, harboring the LATS1/2-motif sequence HxRxx(**S**/T) (see section 4.5.2) could be detected, of which four were upregulated upon LATS2 overexpression. Indeed, YAP^{S127} was upregulated by 0.76 [log_2] and, consistently, YAP targets, such as TK1, PLK1, CYR61, and ECT2 were significantly downregulated, whereas YAP protein levels did not change upon LATS2 overexpression (**Figure 17A**). This suggests that LATS2 is sufficient to phosphorylate these phosphophorylation sites, resulting in the inactivation of YAP by nuclear exclusion, reflected by the downregulation of YAP target genes in the global proteome. Moreover, none of the remaining upregulated phosphorylation sites on YAP (Ser-128, Ser-138, Thr-141, and Thr-143), out of which three were signficantly upregulated showed an overlap with the LATS1/2-motif sequence HxRxx(**S**/T). Therefore it can be assumed, that other kinases might target these phosphosites. To date, only one out of these four phosphorylation sites, YAP^{S138}, has been functionally described to be phosphorylated by

JNK to regulate apoptosis (Tomlinson *et al*, 2010). However, the regulatory effect or corresponding kinases for the other three phosphorylation sites remain unknown. Thus, this suggests that in these cases LATS2 might not phosphorylate YAP itself, but activate other kinases to phosphorylate and thereby modulate YAP function.

Another interesting phosphorylation site strongly regulated in this dataset is TAZ^{S89} (or WWRT1^{S89}). This particular phosphorylation site is known to be targeted by LATS1/2 phosphorylation (like YAP^{S127}), leading to TAZ nuclear exclusion by the adaptor protein 14-3-3 (Lei *et al*, 2008). Surprisingly, in the LATS2 6 h dataset, TAZ^{S89} was found to be significantly downregulated (-1.1 [log_2]), which might seem paradoxical at first. However, it should be noted that TAZ could not be detected on the global proteome level. This could be explained by a drop in TAZ protein levels due to proteasomal degradation. Thus, given that the phosphorylation on TAZ^{S89} assigns TAZ for cytoplasmatic retention and/or proteasomal degradation (Lei *et al*, 2008), it is possible that TAZ could not be detected on the global proteome, due to the low protein levels. Yet, due to phosphopeptide enrichment, the phosphorylation on TAZ^{S89} could still be detected. For both YAP and TAZ, the LATS1/2-mediated phosphorylation and subsequent cytoplasmatic retention can be seen as a transient state, with two optional ways of progression. One option is an eventual release from cytoplasmatic retention by dephosphorylation, thereby enabling YAP/TAZ to move back into the nucleus and initiate target gene transcription. The other option is to mark them for proteasomal degradation. The latter mechanism is also mediated by LATS1/2-mediated phosphorylation on YAP^{S381} and TAZ^{S311}, priming both for subsequent phosphorylation by casein kinase 1δ/ε (YAP^{S397} and TAZ ^{S314}), ultimately resulting in SCFβ-TrCP E3 ligase-induced degradation (Hao *et al*, 2008; Zhao *et al*, 2010; Liu *et al*, 2010). Thus, retention (and potential release) or proteasomal degradation of YAP/TAZ are dependent on an equilibrium of multiple signals. This dataset indicates that YAP is sequestered in the cytoplasm upon 6h LATS2 overexpression, but not (yet) degraded, whereas TAZ seems to be subjected for degradation. This leads to the hypothesis that LATS2 is sufficient to induce TAZ degradation, whereas it only leads to YAP sequestering. As a result, both mechanisms deactivate the oncogenes by preventing target gene transcription. Yet, contrarily, to reverse this deactivation would require protein synthesis for TAZ, whereas for YAP, dephosphorylation would be sufficient, ultimately determining the speed of this reaction. However, further experiments will be required to validate these hypotheses in order to

understand the dynamic interplay and regulatory mechanisms between the two pairs of paralogues, LATS1/LATS2 and YAP/TAZ.

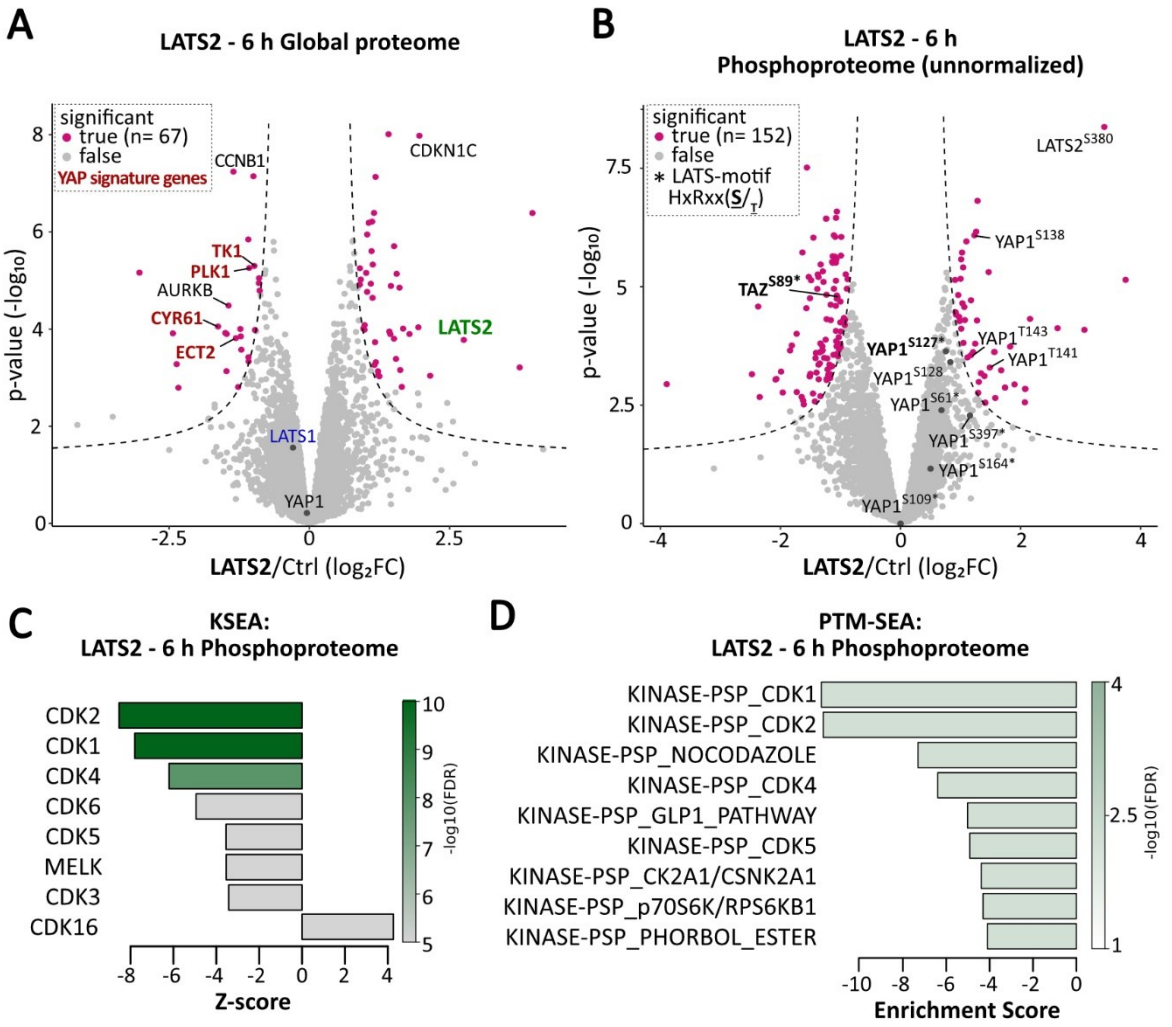

Figure 17: Effects of 6 h LATS2 overexpression on the phosphoproteome in MCF10A cells. (**A**) and (**B**) Differential expression analysis using limma moderated t-statistics for the comparison of changes on the (A) global proteome and (B) phosphoproteome upon 6 h overexpression of LATS2 in MCF10A cells, each in three biological repliactes. Grey color of dots indicates non-significantly, pink color indicates significantly changing proteins or phosphosites, with a p-value adjusted for multiple testing according to Benjamini-Hochberg, *adj. p ≤ 0.05 and a minimum log_2FC of +/- 0.58. Protein names in red indicate YAP target genes. Phosphorylation sites with an asterisk indicate overlap with the LATS1/2-specific motif sequence HxRxx(S/T). (**C**) Kinase-Substrate Enrichment Analysis (KSEA) and (**D**) Post Translational Modification-signature enrichment analysis (PTM-SEA) of the LATS2 6 h phosphoproteome dataset in MCF10A. Top significantly enriched kinases or gene sets (left y-axis) are ranked according to Z-Score or enrichment score (x-axis). Color of bars represents -log_{10} FDR (right y-axis).

To interpret the changes in the phosphoproteome induced by LATS1 or LATS2 overexpression, two bioinformatic tools, Kinase-Substrate Enrichment Analysis (KSEA) and Post Translational Modification-Signature Enrichment Analysis (PTM-SEA), were used. KSEA

is a substrate-centered approach that allows to determine the kinase activity within a phosphoproteome dataset, based on sequence motif alignment of kinases with the detected phosphorylation sites (Lachmann & Ma'ayan, 2009; Casado *et al*, 2013; Wiredja *et al*, 2017). PTM-SEA, adapted the single sample Gene Set Enrichment Analysis (ssGSEA) approach, carrying out enrichment analysis of PTM-site signature sets and is based on PTMSigDB (Krug *et al*, 2019).

Interestingly, both enrichment analyses showed reduced kinase activity of several cyclin-dependent kinases (CDK1, CDK2, CDK4, CDK5), but increased activity of CDK16 upon 6 h LATS2 overexpression (**Figure 17C** and **17D**). (It should be noted that both analysis tools are based on the PSP database which might explain a certain overlay of the results). Accordingly, LATS2 (as well as LATS1) has been described to downregulate cyclin E/CDK2 activity, thereby negatively regulating G_1/S transition (Li *et al*, 2003; Pefani *et al*, 2014). Along these lines, both have been described to negatively regulate cyclin A/B-Cdc2 (also referred to as CDK1) kinase activity in the scope of G_2/M checkpoint (Nishiyama *et al*, 1999; Yang *et al*, 2001), although in mechanistically distinct ways (Introduction Section 1.1.2.3). Moreover, it has been shown that FAT1-mediated activation of LATS1/2, leads to a decrease in CDK6 expression (Li *et al*, 2018). Yet, the present study adds CDK1, CDK4, CDK5 to the list of LATS2-regulated CDKs.

Collectively, this indicates that LATS2 mediates cell cycle regulation by modulating the activity of CDKs. However, given the high similarity of the kinase-motif sequence between CDKs, further experiments will be required to validate whether all of those CDKs are truly regulated by LATS2 overexpression.

4.5.2. Discovery of novel phosphorylation targets of the protein kinases LATS1 and LATS2

As mentioned before, only a few direct substrates are known for the kinases LATS1 and LATS2. Most of them are shared between the paralogues or not defined exclusively for either of the two kinases. Yet, manual compilation of these unique and shared phosphorylation targets (**Table 36**) allowed us to predict three different kinase-phosphorylation motifs (**Figure 18**) by using the motif and logo analysis tool provided by the PhosphoSite Plus webpage (https://www.phosphosite.org/sequenceLogoAction). For

LATS1 only five specific phosphorylation sites were described in the literature. Also, the corresponding motif (**S**/T)xxxV was less pronounced, suggesting valine on position +4 based on 3/5 sequences. Thus, the small number of input sequences could not define a clear motif (**Figure 18A**). With seven LATS2-specific phosphorylation sites, the motif for LATS2 (HVRxx(**S**/T)xR) was stronger, predicting histidine on position -5 (6 out of 7 sequences), valine on position -4 (4 out of 7 sequences), and arginine on position -3 (7 out of 7 sequences) (**Figure 18C** and **18D**). A combined motif, compiled by nine shared substrates of LATS1 and LATS2, resulted in the motif HxRxx(**S**/T) (**Figure 18E**), which is in accordance with what was previously described in the literature (Zhao *et al*, 2010; Chiyoda *et al*, 2012; Hergovich, 2013).

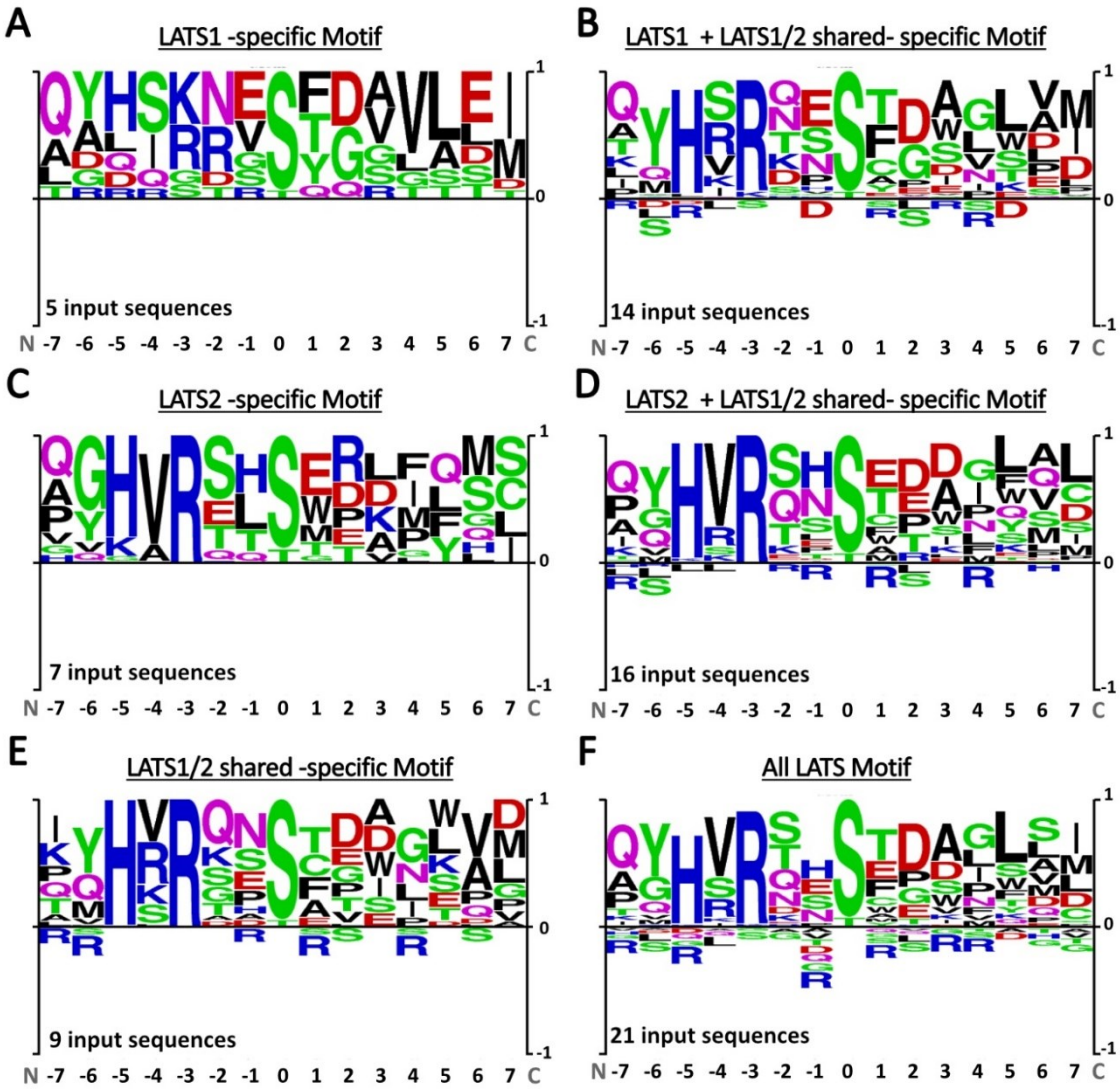

Figure 18: Motif analysis for LATS1 and LATS2 based on literature. The sequence logos are based on multiple alignment analysis of LATS1 and LATS2 substrates (Table 36), using the motif and logo analyses tool provided by the PhosphoSite Plus webpage (https://www.phosphosite.org/sequenceLogoAction). All motifs were defined to have seven amino acids before and after the

phosphorylation residues (0). Amino acids are depicted in one letter code and size correlates with their abundance in the respective position. (**A**) LATS1-specific predicted motif based on five input sequences from LATS1-only substrates. (**B**) LATS1-specific predicted motif based on five input sequences from LATS1-only substrates together with nine LATS1/2-shared substrates. (**C**) LATS2-specific predicted motif based on seven input sequences from LATS2-only substrates. (**D**) LATS2-specific predicted motif based on seven input sequences from LATS2-only substrates together with the nine LATS1/2-shared substrates. (**E**) LATS1/2-shared predicted motif based on nine LATS1/2-shared substrates. (**F**) LATS1/2-shared predicted motif based on all 21 substrates of LATS1-only, LATS2-only, and LAST1/2-shared.

These motifs compiled from the literature were utilized for the discovery of potential new substrates of LATS1 and LATS2. Therefore, the motif HxRxx(**S**/T) was used for filtering both LATS1 and LATS2 datasets, since out of the small number of input sequences, no LATS1 or LATS2-specific motif could be assigned. The potential substrates were filtered with this motif and put into 3 classes, based on the confidence to be a true substrate, as explained in the following.

Given the strong overexpression of LATS2, detected after 6 h induction, potential substrates found in this dataset are assigned to class I, representing the highest confidence. Here both unnormalized and proteome-normalized phosphophorylation sites were included if they showed at least 25% increased expression levels compared to the control (**Table 37,** upper block).

Substrates showing at least 25% upregulation (unnormalized and proteome-normalized) from the remaining datasets (LATS1 6 h, LATS1 2 h, and LATS2 2h) form class II substrates (**Table 37,** bottom block). (It should be noted, that although in the LATS1 6 h dataset protein levels are not as high as in the LATS2 6 h dataset, LATS1 is likely active since YAP targets are downregulated (**Supplementary Figure 11F**)).

Finally we included a third class, class III, of potential substrates, showing a change in the abundance of the phosphorylation site, but lacking the corresponding information on the protein level. Thus, these substrates are filtered to have an overlap with the motif sequence, regardless of the fold change of the phosphorylation site (**Supplementary Table 3**). Although the likelihood of false positives is high for substrates in the class III, the example of TAZ^{S89}, described in chapter 4.5.1 encouraged us to still consider them as valuable.

With these criteria, eight class I, 21 class II and 182 class III phosphorylation sites of potential new LATS1 and/or LATS2 targets could be identified. Given that one of the

filtering criteria was the motif sequence (HxRxx(**S**/T)) there was a high redundancy in the phosphorylation sites detected in the four datasets. Ultimately, 17 (or 53) non-redundant potential phosphorylation sites in class I and II (or class III) could be detected. Among those, at least one LATS1/2-mediated phosphorylation site described in the literature, such as YAP^{S127} and YAP^{S61}, was found to be upregulated in each of the four datasets (LATS1 2h, LATS1 6h, LATS2 2h, LATS2 6h), serving as a positive control.

Table 37: Potential LATS1 and LATS2 kinase substrates. Depicted are phosphosites quantified in the MCF10A phosphoproteome dataset. Phosphosite ratios are in log_2, unnormalized, and normalized to the protein abundance measured on the global proteome. MS-detected amino acid sequences (black) are supplemented with corresponding amino acids (grey) to depict motif sequence (underlined). The phosphorylated amino acid is depicted in bold and underlined.

	GENE	POS	AMINO ACID	UN-NORM.	NORM.	ADJ. P. VAL	LOCAL. PROB.	UNIPROT ID	SEQUENCE	OVEREXPR.
				LATS/Ctrl (log_2FC)						
CLASS I	YAP1	397	S	1.16*	**1.21***	0.06	96%	P46937	HSRDE**S**TDSGLSMSSYSVPR	6 h LATS2
	YAP1	127	S	0.76*	**0.81***	0.01	92%	P46937	HVRAH**S**SPASLQLGAVSPGTLTPT GVVSGPAATPTAQHLR	6 h LATS2
	YAP1	61	S	0.68*	**0.73***	0.05	100%	P46937	HVRGD**S**ETDLEALFNAVMNPK	6 h LATS2
	YAP1	164	S	0.50	0.55	0.24	82%	P46937	HLRQS**S**FEIPDDVPLPAGWEMAK	6 h LATS2
	TGFB1I1	403	S	0.46	0.32	0.29	100%	O43294	HARRG**S**LCATCGLPVTGR	6 h LATS2
	MNAT1	279	S	0.45	0.63	0.68	100%	P51948	HVRAASPQDLAGGYTSSLACHR	6 h LATS2
	NUMB	438	S	0.34	0.14	0.18	100%	P49757	HRRTP**S**EADRWLEEVSK	6 h LATS2
	PI4K2A	462	S	-0.14	0.49	0.21	97%	Q9BTU6	HQRSS**S**ESYTQSFQSR	6 h LATS2
CLASS II	YAP1	397	S	0.72	0.76	0.19	96%	P46937	HSRDE**S**TDSGLSMSSYSVPR	6 h LATS1
	MNAT1	279	S	0.65	0.79	0.54	100%	P51948	HVRAASPQDLAGGYTSSLACHR	6 h LATS1
	SUFU	342	S	0.52	0.32	0.22	100%	Q9UMX1	HDRAP**S**RKDSLESDSSTAIIPHELIR	6 h LATS1
	TGFB1I1	403	S	0.37	0.65	0.39	100%	O43294	HARRG**S**LCATCGLPVTGR	6 h LATS1
	ZBTB7B	369	T	0.37	-0.10	0.60	97%	O15156	HMR**T**HTGEKPFACEVCGVR	6 h LATS1
	ALKBH5	361	S	0.20	**0.58***	0.00	100%	Q6P6C2	HRRRG**S**FSSENYWR	6 h LATS1
	PI4K2A	462	S	0.26	0.49	0.21	97%	Q9BTU6	HQRSS**S**ESYTQSFQSR	6 h LATS1
	YAP1	61	S	0.28	0.33	0.29	100%	P46937	HVRGD**S**ETDLEALFNAVMNPK	6 h LATS1
	HNRNPUL2	228	S	0.39	0.12	0.04	99%	Q1KMD3	HSRSK**S**PLPPEEEAK	2 h LATS2
	YAP1	397	S	0.37	0.54	0.32	96%	P46937	HSRDE**S**TDSGLSMSSYSVPR	2 h LATS2
	RBSN	548	S	0.09	0.41	0.19	96%	Q9H1K0	HTRTR**S**LDFR	2 h LATS2
	YAP1	127	S	0.16	0.33	0.19	92%	P46937	HVRAH**S**SPASLQLGAVSPGTLTPT GVVSGPAATPTAQHLR	2 h LATS2
	YAP1	61	S	0.17	0.34	0.20	100%	P46937	HVRGD**S**ETDLEALFNAVMNPK	2 h LATS2
	PI4KB	277	S	0.27	0.36	0.33	98%	Q9BTU6	HQRSK**S**DATASISLSSNLK	2 h LATS2
	SUFU	342	S	0.55	1.23	0.16	100%	Q9UMX1	HDRAP**S**RKDSLESDSSTAIIPHELIR	2 h LATS1
	TJP2	296	S	0.53	0.40	0.18	100%	Q9UDY2	EHPH**S**RSP**S**PEPR	2 h LATS1
	TGFB1I1	403	S	0.49	0.66	0.31	100%	O43294	HARRG**S**LCATCGLPVTGR	2 h LATS1
	SRRM2	1878	S	0.46	0.37	0.02	100%	Q9UQ35	HRRS**S**RTPLISR	2 h LATS1
	SGTB	295	S	0.37	0.56	0.57	99%	Q96EQ0	HIRSR**S**FSSSAEEHS	2 h LATS1
	YAP1	61	S	0.34	0.30	0.16	100%	P46937	HVRGD**S**ETDLEALFNAVMNPK	2 h LATS1
	HNRNPUL2	228	S	0.32	0.10	0.06	99%	Q1KMD3	HSRSK**S**PLPPEEEAK	2 h LATS1

Upon 6 h overexpression of both LATS1 and LATS2, the Ser-279 phosphorylation on CDK-activating kinase assembly factor MAT1 (MNTA^{S279}) was upregulated. Interestingly, MNTA has been implicated in cell cycle control by stabilizing the CDK-activating kinase (CAK) enzymatic complex (consisting of cyclin H/CDK7), which in turn activates cyclin-activated kinases CDK1, CDK2, CDK4, and CDK6 (Tirode *et al*, 1999). This is in line with the observation in the previous section (4.5.1), showing a downregulated activity for all four CDKs in PTM-SEA and KSEA analysis (**Figure 17C** and **17D**). Hence, LATS1 and LATS2- mediated MNTA^{S279} phosphorylation might inhibit CAK activation, and therefore inhibit subsequent CDK1, CDK2, CDK4, and CDK6 activation. Thus, adding potential new insights in LATS1/2-mediated cell cycle regulation.

Another interesting phosphosite that was upregulated upon both LATS1 and LATS2 overexpression is Ser-403 on TGFB1I1^{S403} (transforming growth factor beta-1-induced transcript 1 protein, also known as *Hic-5*). In particular, TGFB1I1 is a molecular adaptor that has been described to link several intracellular signaling modules to the plasma membrane receptors, thereby regulating (among others) Wnt, TGFβ, and SLIT-ROBO signaling (Sha *et al*, 2020; Shibanuma *et al*, 1994; Jones *et al*, 2009). Interestingly, in the present study, transient LATS2 overexpression in MCF7 revealed potential co-dependency of LATS2 with the SLIT/ROBO pathway. Therefore, the TGFB1I1^{S403} upregulation might possibly promote the activation of the ROBO/SLIT pathway by LATS2-mediated phosphorylation. Moreover, LATS1/2 phosphorylation of TGFB1I1^{S403} might add another connecting point to the intertwining between Hippo-, Wnt-, and TGFβ-signaling pathway which has been described previously. Briefly, the three pathways have been described to be part of a higher-order network regulating and coordinating cell signaling in development and homeostasis (Attisano & Wrana, 2013).

It should be noted that the majority of potentially LATS1- and LATS2-mediated phosphorylation sites were found in both LATS1 and LATS2 datasets, suggesting a significant overlap of target proteins between the paralogues. Partially, this might be explained also by the fact that we used the shared motif sequence (HxRxx(**S**/T)) for filtering. Also considering 85% amino acid sequence identity in the kinase domain of the two paralogues might explain the preference for the same targets. Furthermore, given the rather small changes in phosphorylation site abundance upon induction of LATS1 and LATS2 overexpression, for future experiments, it might be beneficial to prolong the induction time

to ensure high LATS1 and LATS2 protein levels. Ultimately, increasing the number of validated LATS1- or LATS2-specific substrates will allow for more specific kinase-substrate motifs and therefore help to answer whether the substrate preferences of LATS1 and LATS2 are distinct or shared.

Collectively, this phosphoproteome dataset provides insights into LATS1/2-mediated effects on cell signaling as well as potential new LATS1/2 targets. In particular, it might add cues to LATS1/2-mediated regulation of CDK-activity via MNTA^{S279} phosphorylation. Moreover, LATS1/2 phosphorylation of TGFB1I1^{S403}, might again connect LATS1/2 with ROBO/SLIT signaling as well as with Hippo/Wnt/TGFbeta signaling. Furthermore, the considerable overlap of LATS1- and LATS2-kinase substrates described in the literature and observed in this study, suggests LATS1 and LATS2 share the majority of their targets.

4.6. Concluding remarks and Outlook

The aim of this study was to uncover novel distinct and shared functions of LATS1 and LATS2 allowing for in-depth characterization of the two kinases. Therefore, different knockdown and overexpression cell systems were combined with multi-layered MS-based proteomics analysis.

Hereby global proteome analysis upon LATS1 and LATS2 overexpression pointed towards an interplay of LATS1 and LATS2 with the transcription factors and tumor suppressors RUNX3 and p53 in luminal B breast cancer cells (Section 4.2.2). Thus, this might suggest a tight network between tumor suppressors, alerting each other in case of aberrant cell signaling in cancer cells. Hence it would be interesting to see whether overexpression of LATS1 and/or LATS2 indeed leads to gene expression induced by p53 or RUNX3, which could be validated by qPCR of their target genes. Furthermore, the combination with proliferation assays and apoptosis assays upon prolonged overexpression will reveal whether LATS1 or LATS2 re-introduction is sufficient to activate tumor suppressor functions in these cells.

Furthermore, the present study strengthens the notion of cross-talk between both kinases with the cell polarity pathway PCP (Section 4.2.1 and 4.2.2). In *Drosophila*, the cross-talk of the PCP pathway and Hippo has been well established, and a similar mechanism might act in mammals. For follow-up experiments, it will be particularly informative to consider 3D cell culture or soft agar assays to better recapitulate the mechanical forces in the extracellular matrix that the PCP pathway responds to.

Another potential connection revealed in this study links LATS2 with the poorly understood ROBO/SLIT signaling pathway (Section 4.2.1 and 4.5.2). A first intuitive follow-up experiment would be a secretome analysis which might allow to detect secreted SLIT in the extracellular space and determine whether its abundance is influenced by LATS2 protein levels. In addition, the identification of the SLIT-ligand might even help to identify the corresponding ROBO receptor and thereby the downstream signaling.

Of note, the strongest effect induced by manipulation of LATS1 and LATS2 protein levels was observed for proteins involved in cell cycle regulation. In particular, the data in this study suggests that overexpression of LATS1 or LATS2 in luminal B breast cancer cells (i) facilitates metaphase to anaphase transition, but leads to (ii) a novel cell cycle arrest in late anaphase (Section 4.2.3). These two hypotheses are strengthened by the proteomic

data which showed (i) the downregulation of Cdc20 protein levels together with constant Cdh1 levels, indicating that APC/C is associated with Cdh1, and accordingly, (ii) the downregulation of APC/C^{Cdh1} substrates, which are specific for anaphase/telophase, indicating a cell cycle arrest. Cell cycle analyses using flow cytometry or microscopy together with cell cycle markers for metaphase, anaphase, and G_1-phase will be key experiments to validate these hypotheses. Moreover, it will be interesting to see whether this potential cell cycle arrest is only temporary or whether prolonged LATS1/2 overexpression leads to senescence, apoptosis, or continuation of the cell cycle. Accordingly, apoptosis assays (e.g. TUNEL assay) and senescence assays (β-Galactosidase assay), together with proteome analysis will help to gain insights into these mechanisms.

Translatome analysis of LATS1 and LATS2 overexpression in another cell system (Tet-inducible overexpression) and a non-tumorigenic cell line (MCF10A) also pointed towards the involvement of LATS1/2 in cell cycle control (Section 4.4), in this case to the G_1/S and G_2/M checkpoints. In these experiments, 6 h overexpression of LATS1 or LATS2, and 20 h overexpression of LATS1 revealed negative enrichment of E2F target proteins (known to regulate G_1/S transition) and proteins involved in the G_2/M checkpoint (Section 4.4.3), as well as downregulation of AurA and AurB (Section 4.4.2). This supports data in the literature according to which LATS1 or LATS2 overexpression induces the cell cycle checkpoint/arrest. Interestingly, however, prolonged LATS2 overexpression (20 h), revealed positive enrichment of proteins in the gene sets “E2F targets” and “G_2/M checkpoint”, as wells as upregulation of AurA and AurB levels. Moreover, 20 h LATS2 overexpression induces a delayed co-expression of LATS1. Thus, although LATS1 and LATS2 had been identified as tumor suppressor genes, this study indicates that this might only be true as long as either LATS1 or LATS2 is expressed without the other. Simultaneous upregulation of both LATS1 and LATS2 seems to maintain cell cycle progression instead, which challenges the view in the literature that LATS1 and LATS2 exclusively promote G_1/S or G_2/M arrest. Thus, to validate these hypotheses it would be interesting to use cell cycle analyses by flow cytometry (e.g. by using propidium iodide together with BrdU). Furthermore, proliferation assays would potentially confirm whether long-term LATS2 overexpression promotes cell cycle progression.

Another layer of information was added by conducting complementary phosphoproteome analysis (Section 4.5). Here phosphopeptide enrichment analysis using PTM-SEA and

kinase-activity analysis using KSEA indicated that LATS2 upregulation decreases the activity of CDK1, CDK2, CDK4, and CDK5 (Section 4.5.1). Therefore it would be interesting to see whether this might be causal for potential cell cycle arrests as suggested by the translatome analysis. Furthermore, phosphoproteome analysis provided a source for regulatory phosphorylation sites on potentially novel LATS1- and LATS2-substrates (Section 4.5.2) but, considering that the relative expression of phosphorylation sites of known LATS1/2 substrates (e.g. YAP^{127S}) was increased only slightly, additional time points for phosphoproteome analysis should be considered for future experiments. Thus finding the "sweet spot" of LATS1 or LATS2 activity upon overexpression, will allow us to corroborate the list of potential LATS1/2 substrates and therefore to better understand their involvement in cell signaling.

Collectively, this study provides a profound source of information to elucidate distinct and shared functions of the tumor suppressors LATS1 and LATS2 in cell signaling. Ultimately, these findings allow for a better understanding of the tumor suppressors and their involvement in cell cycle regulation which may enable valuable new directions for cancer therapy.

5. REFERENCES

Aebersold R & Mann M (2003) Mass spectrometry-based proteomics. *Nature* 422: 198–207

Agami R, Blandino G, Oren M & Shaul Y (1999) Interaction of c-Abl and p73α and their collaboration to induce apoptosis. *Nature* 399: 809–812

Andersson L & Porath J (1986) Isolation of phosphoproteins by immobilized metal (Fe3+) affinity chromatography. *Anal Biochem* 154: 250–254

Attisano L & Wrana JL (2013) Signal integration in TGF-β,WNT, and Hippo pathways. *F1000Prime Rep* 5

Aylon Y, Gershoni A, Rotkopf R, Biton IE, Porat Z, Koh AP, Sun X, Lee Y, Fiel M-I, Hoshida Y, *et al* (2016) The LATS2 tumor suppressor inhibits SREBP and suppresses hepatic cholesterol accumulation. *Genes Dev* 30: 786–797

Aylon Y, Michael D, Shmueli A, Yabuta N, Nojima H & Oren M (2006) A positive feedback loop between the p53 and Lats2 tumor suppressors prevents tetraploidization. *Genes Dev* 20: 2687–2700

Aylon Y, Ofir-Rosenfeld Y, Yabuta N, Lapi E, Nojima H, Lu X & Oren M (2010) The Lats2 tumor suppressor augments p53-mediated apoptosis by promoting the nuclear proapoptotic function of ASPP1. *Genes Dev* 24: 2420–2429

Aylon Y, Yabuta N, Besserglick H, Buganim Y, Rotter V, Nojima H & Oren M (2009) Silencing of the Lats2 tumor suppressor overrides a p53-dependent oncogenic stress checkpoint and enables mutant H-Ras-driven cell transformation. *Oncogene* 28: 4469–79

Bae SJ & Luo X (2018) Activation mechanisms of the Hippo kinase signaling cascade. *Biosci Rep* 38: 1–14

Baghdady YZ & Schug KA (2019) Qualitative evaluation of high pH mass spectrometry-compatible reversed phase liquid chromatography for altered selectivity in separations of intact proteins. *J Chromatogr A* 1599: 108–114

Bantscheff M, Schirle M, Sweetman G, Rick J & Kuster B (2007) Quantitative mass spectrometry in proteomics: A critical review. *Anal Bioanal Chem* 389: 1017–1031

Barnum KJ & O'Connell MJ (2014) Cell cycle regulation by checkpoints. *Methods Mol Biol* 1170: 29–40

Barretina J, Caponigro G, Stransky N, Venkatesan K, Margolin AA, Kim S, Wilson CJ, Lehár J, Kryukov G V, Sonkin D, *et al* (2012) The Cancer Cell Line Encyclopedia enables predictive modelling of anticancer drug sensitivity. *Nature* 483: 603–607

Barron DA & Kagey JD (2014) The role of the Hippo pathway in human disease and tumorigenesis. *Clin Transl Med* 3: 25

Boggiano JC, Vanderzalm PJ & Fehon RG (2011) Tao-1 phosphorylates Hippo/MST kinases to regulate the Hippo-Salvador-Warts tumor suppressor pathway. *Dev Cell* 21: 888–895

Bothos J, Tuttle RL, Ottey M, Luca FC & Halazonetis TD (2005) Human LATS1 is a mitotic exit network kinase. *Cancer Res* 65: 6568–6575

Brandeis M & Hunt T (1996) The proteolysis of mitotic cyclins in mammalian cells persists from the end of mitosis until the onset of S phase. *EMBO J* 15: 5280–5289

Britschgi A, Duss S, Kim S, Couto JP, Brinkhaus H, Koren S, De Silva D, Mertz KD, Kaup D, Varga Z, *et al* (2017) The Hippo kinases LATS1 and 2 control human breast cell fate via crosstalk with ERα. *Nature* 541: 541–545

Brönstrup M (2004) Absolute quantification strategies in proteomics based on mass spectrometry. *Expert Rev Proteomics* 1: 503–512

Burkhart JM, Schumbrutzki C, Wortelkamp S, Sickmann A & Zahedi RP (2012) Systematic and quantitative comparison of digest efficiency and specificity reveals the impact of trypsin quality on MS-based proteomics. *J Proteomics* 75: 1454–1462

Casado P, Rodriguez-Prados JC, Cosulich SC, Guichard S, Vanhaesebroeck B, Joel S & Cutillas PR (2013) Kinase-substrate enrichment analysis provides insights into the heterogeneity of signaling pathway activation in leukemia cells. *Sci Signal* 6

Chan SW, Lim CJ, Chong YF, Pobbati A V, Huang C & Hong W (2011) Hippo pathway-independent restriction of TAZ and YAP by angiomotin. *J Biol Chem* 286: 7018–7026

Chen Y, Han H, Seo G, Vargas RE, Yang B, Chuc K, Zhao H & Wang W (2020) Systematic analysis of the Hippo pathway organization and oncogenic alteration in evolution. *Sci Reports 2020 101* 10: 1–12

Chiyoda T, Sugiyama N, Shimizu T, Naoe H, Kobayashi Y, Ishizawa J, Arima Y, Tsuda H, Ito M, Kaibuchi K, *et al* (2012) LATS1/WARTS phosphorylates MYPT1 to counteract PLK1 and regulate mammalian mitotic progression. *J Cell Biol* 197: 625–41

Choudhary C & Mann M (2010) Decoding signalling networks by mass spectrometry-based proteomics. *Nat Rev Mol Cell Biol* 11: 427–439

Couzens AL, Knight JDR, Kean MJ, Teo G, Weiss A, Dunham WH, Lin Z-Y, Bagshaw RD, Sicheri F, Pawson T, *et al* (2013) Protein Interaction Network of the Mammalian Hippo Pathway Reveals Mechanisms of Kinase-Phosphatase Interactions. *Sci Signal* 6: rs15–rs15

Cox J & Mann M (2008) MaxQuant enables high peptide identification rates, individualized p.p.b.-range mass accuracies and proteome-wide protein quantification. *Nat Biotechnol* 26: 1367–1372

Cox J & Mann M (2009) Computational Principles of Determining and Improving Mass Precision and Accuracy for Proteome Measurements in an Orbitrap. *J Am Soc Mass Spectrom* 20: 1477–1485

Cox J, Neuhauser N, Michalski A, Scheltema RA, Olsen J V & Mann M (2011) Andromeda: a peptide search engine integrated into the MaxQuant environment. *J Proteome Res* 10: 1794–805

Craig Venter J, Adams MD, Myers EW, Li PW, Mural RJ, Sutton GG, Smith HO, Yandell M, Evans CA, Holt RA, *et al* (2001) The sequence of the human genome. *Science (80-)* 291: 1304–1351

Crick FH (1958) On protein synthesis. *Symp Soc Exp Biol* 12: 138–163

Cristea IM, Gaskell SJ & Whetton AD (2004) Proteomics techniques and their application to hematology. *Blood* 103: 3624–3634

Dickinson RE & Duncan WC (2010) The SLIT-ROBO pathway: A regulator of cell function with implications for the reproductive system. *Reproduction* 139: 697–704

Dieterich DC, Link AJ, Graumann J, Tirrell DA & Schuman EM (2006) Selective identification of newly synthesized proteins in mammalian cells using bioorthogonal noncanonical amino acid tagging (BONCAT). *Proc Natl Acad Sci U S A* 103: 9482–9487

Doerr A (2015) In pursuit of PTMs. *Nat Methods*: 20

Dong J, Feldmann G, Huang J, Wu S, Zhang N, Comerford SA, Gayyed MFF, Anders RA, Maitra A & Pan D (2007) Elucidation of a Universal Size-Control Mechanism in Drosophila and Mammals. *Cell* 130: 1120–1133

Duarte TT & Spencer CT (2016) Personalized proteomics: The future of precision medicine. *Proteomes* 4

Dunphy K, Dowling P, Bazou D & O'Gorman P (2021) Current methods of post-translational modification analysis and their applications in blood cancers. *Cancers (Basel)* 13

Eichelbaum K & Krijgsveld J (2014) Combining pulsed SILAC labeling and click-chemistry for quantitative secretome analysis. *Methods Mol Biol* 1174: 101–114

Eichelbaum K, Winter M, Diaz MB, Herzig S & Krijgsveld J (2012) Selective enrichment of newly synthesized proteins for quantitative secretome analysis. *Nat Biotechnol* 30: 984–990

Eng JK, McCormack AL & Yates JR (1994) An approach to correlate tandem mass spectral data of peptides with amino acid sequences in a protein database. *J Am Soc Mass Spectrom* 5: 976–989

Feng Y, Hu S, Li L, Peng X & Chen F (2020) Long noncoding RNA HOXA-AS2 functions as an oncogene by binding to EZH2 and suppressing LATS2 in acute myeloid leukemia (AML). *Cell Death Dis* 11: 1–12

Fesquet D, De Bettignies G, Bellis M, Espeut J & Devault A (2015) Binding of Kif23-iso1/CHO1 to 14-3-3 is regulated by sequential phosphorylations at two lats kinase consensus sites. *PLoS One* 10

Ficarro SB, McCleland ML, Stukenberg PT, Burke DJ, Ross MM, Shabanowitz J, Hunt DF & White FM (2002) Phosphoproteome analysis by mass spectrometry and its application to Saccharomyces cerevisiae. *Nat Biotechnol* 20: 301–305

Fischer M & Müller GA (2017) Cell cycle transcription control: DREAM/MuvB and RB-E2F complexes. *Crit Rev Biochem Mol Biol* 52: 638–662

Forbes SA, Bindal N, Bamford S, Cole C, Kok CY, Beare D, Jia M, Shepherd R, Leung K, Menzies A, *et al* (2011) COSMIC: Mining complete cancer genomes in the catalogue of somatic mutations in cancer. *Nucleic Acids Res* 39

Fredens J, Engholm-Keller K, Giessing A, Pultz D, Larsen MR, Højrup P, Møller-Jensen J & Førgeman NJ (2011) Quantitative proteomics by amino acid labeling in C. elegans. *Nat Methods* 8: 845–847

Fujii H, Zhou W & Gabrielson E (1996) Detection of frequent allelic loss of 6q23-q25.2 in microdissected human breast cancer tissues. *Genes Chromosom Cancer* 16: 35–39

Fung TK & Poon RYC (2005) A roller coaster ride with the mitotic cyclins. *Semin Cell Dev Biol* 16: 335–342

Furth N & Aylon Y (2017) The LATS1 and LATS2 tumor suppressors: Beyond the hippo pathway. *Cell Death Differ* 24: 1488–1501

Furth N, Pateras IS, Rotkopf R, Vlachou V, Rivkin I, Schmitt I, Bakaev D, Gershoni A, Ainbinder E, Leshkowitz D, *et al* (2018) LATS1 and LATS2 suppress breast cancer progression by maintaining cell identity and metabolic state. *Life Sci alliance* 1: e201800171

Ganem NJ, Cornils H, Chiu SY, O'Rourke KP, Arnaud J, Yimlamai D, Théry M, Camargo FD & Pellman D (2014) Cytokinesis failure triggers hippo tumor suppressor pathway activation. *Cell* 158: 833–848

Garnett MJ, Mansfeld J, Godwin C, Matsusaka T, Wu J, Russell P, Pines J & Venkitaraman AR (2009) UBE2S elongates ubiquitin chains on APC/C substrates to promote mitotic exit. *Nat Cell Biol* 11: 1363–1369

Geiger T, Cox J, Ostasiewicz P, Wisniewski JR & Mann M (2010) Super-SILAC mix for quantitative proteomics of human tumor tissue. *Nat Methods* 7: 383–385

Gholami M, Mirfakhraie R, Movafagh A, Jalaeekhoo H, Kalahroodi R, Zare-Abdollahi D & Zare-Karizi S (2014) The expression analysis of LATS2 gene in de novo AML patients. *Med Oncol* 31: 1–4

Goldhirsch A, Wood WC, Coates AS, Gelber RD, Thürlimann B & Senn HJ (2011) Strategies for subtypes-dealing with the diversity of breast cancer: Highlights of the St Gallen international expert consensus on the primary therapy of early breast cancer 2011. *Ann Oncol* 22: 1736–1747

Gorbsky GJ (2001) The mitotic spindle checkpoint. *Curr Biol* 11

Goulev Y, Fauny J, Gonzalez-Marti B, Flagiello D, Silber J & Zider A (2008) SCALLOPED interacts with YORKIE, the nuclear effector of the hippo tumor-suppressor pathway in Drosophila. *Curr Biol* 18: 435–441

Grawenda AM & O'Neill E (2015) Clinical utility of RASSF1A methylation in human malignancies. *Br J Cancer* 113: 372–381

Gruhler A, Schulze WX, Matthiesen R, Mann M & Jensen ON (2005) Stable isotope labeling of Arabidopsis thaliana cells and quantitative proteomics by mass spectrometry. *Mol Cell Proteomics* 4: 1697–1709

Gruneberg U, Neef R, Li X, Chan EHY, Chalamalasetty RB, Nigg EA & Barr FA (2006) KIF14 and citron kinase act together to promote efficient cytokinesis. *J Cell Biol* 172: 363–372

Grusche FA, Richardson HE & Harvey KF (2010) Upstream Regulation of the Hippo Size Control Pathway. *Curr Biol* 20: R574–R582

Gygi SP, Rist B, Gerber SA, Turecek F, Gelb MH & Aebersold R (1999) Quantitative analysis of complex protein mixtures

using isotope-coded affinity tags. *Nat Biotechnol* 17: 994–999
Halder G, Johnson RL & Liu J (2011) Hippo signaling: growth control and beyond. *Development* 138: 9–22
Hanahan D & Weinberg RA (2000) The hallmarks of cancer. *Cell* 100: 57–70
Hao Y, Chun A, Cheung K, Rashidi B & Yang X (2008) Tumor Suppressor LATS1 Is a Negative Regulator of Oncogene YAP. *J Biol Chem* 283: 5496–5509
Hartley H (1951) Origin of the word 'protein'. *Nature* 168: 244
Hartwell LH & Weinert TA (1989) Checkpoints: Controls that ensure the order of cell cycle events. *Science (80-)* 246: 629–634
Harvey KF, Pfleger CM & Hariharan IK (2003) The Drosophila Mst ortholog, hippo, restricts growth and cell proliferation and promotes apoptosis. *Cell* 114: 457–467
Harvey KF, Zhang X & Thomas DM (2013) The Hippo pathway and human cancer. *Nat Rev Cancer* 13: 246–57
He Z, Li R & Jiang H (2021) Mutations and Copy Number Abnormalities of Hippo Pathway Components in Human Cancers. *Front Cell Dev Biol* 9: 1123
Hergovich A (2013) Regulation and functions of mammalian LATS/NDR kinases: looking beyond canonical Hippo signalling. *Cell Biosci* 3: 32
Hirate Y, Hirahara S, Inoue KI, Suzuki A, Alarcon VB, Akimoto K, Hirai T, Hara T, Adachi M, Chida K, *et al* (2013) Polarity-dependent distribution of angiomotin localizes hippo signaling in preimplantation embryos. *Curr Biol* 23: 1181–1194
Hirota T, Morisaki T, Nishiyama Y, Marumoto T, Tada K, Hara T, Masuko N, Inagaki M, Hatakeyama K & Saya H (2000) Zyxin, a regulator of actin filament assembly, targets the mitotic apparatus by interacting with h-warts/LATS1 tumor suppressor. *J Cell Biol* 149: 1073–1086
Hori T, Takaori-Kondo A, Kamikubo Y & Uchiyama T (2000) Molecular cloning of a novel human protein kinase, kpm, that is homologous to warts/lats, a Drosophila tumor suppressor. *Oncogene* 19: 3101–3109
Hornbeck P V, Zhang B, Murray B, Kornhauser JM, Latham V & Psp PR (2015) PhosphoSitePlus , 2014 : mutations , PTMs and recalibrations. *Nucleic Acids Res* 43: 512–520
Hsu JL, Huang SY, Chow NH & Chen SH (2003) Stable-Isotope Dimethyl Labeling for Quantitative Proteomics. *Anal Chem* 75: 6843–6852
Hua K, Jin J, Zhao J, Song J, Song H, Li D, Maskey N, Zhao B, Wu C, Xu H, *et al* (2016) MiR-135b, upregulated in breast cancer, promotes cell growth and disrupts the cell cycle by regulating LATS2. *Int J Oncol* 48: 1997–2006
Huang H, Zhang W, Pan Y, Gao Y, Deng L, Li F, Li F, Ma X, Hou S, Xu J, *et al* (2017a) YAP suppresses lung squamous cell carcinoma progression via deregulation of the DNP63-GPX2 axis and ros accumulation. *Cancer Res* 77: 5769–5781
Huang J, Wu S, Barrera J, Matthews K & Pan D (2005) The Hippo signaling pathway coordinately regulates cell proliferation and apoptosis by inactivating Yorkie, the Drosophila homolog of YAP. *Cell* 122: 421–434
Huang M, Hou J, Wang Y, Xie M, Wei C, Nie F, Wang Z & Sun M (2017b) Long Noncoding RNA LINC00673 Is Activated by SP1 and Exerts Oncogenic Properties by Interacting with LSD1 and EZH2 in Gastric Cancer. *Mol Ther* 25: 1014–1026
Hunter T (1998) The Croonian Lecture 1997. The phosphorylation of proteins on tyrosine: Its role in cell growth and disease. *Philos Trans R Soc B Biol Sci* 353: 583–605
Iida S, Hirota T, Morisaki T, Marumoto T, Hara T, Kuninaka S, Honda S, Kosai K, Kawasuji M, Pallas DC, *et al* (2004) Tumor suppressor WARTS ensures genomic integrity by regulating both mitotic progression and G1 tetraploidy checkpoint function. *Oncogene* 23: 5266–5274
Ito Y, Bae SC & Chuang LSH (2015) The RUNX family: Developmental regulators in cancer. *Nat Rev Cancer* 15: 81–95
Jang JW, Kim MK, Lee YS, Lee JW, Kim DM, Song SH, Lee JY, Choi BY, Min B, Chi XZ, *et al* (2017) RAC-LATS1/2 signaling regulates YAP activity by switching between the YAP-binding partners TEAD4 and RUNX3. *Oncogene* 36: 999–1011
Janssen A, Colmenares SU & Karpen GH (2018) Heterochromatin: Guardian of the Genome. *Annu Rev Cell Dev Biol* 34: 265–288
Jia J, Zhang W, Wang B, Trinko R & Jiang J (2003) The Drosophila Ste20 family kinase dMST functions as a tumor suppressor by restricting cell proliferation and promoting apoptosis. *Genes Dev* 17: 2514–2519
Jones CA, Nishiya N, London NR, Zhu W, Sorensen LK, Chan AC, Lim CJ, Chen H, Zhang Q, Schultz PG, *et al* (2009) Slit2-Robo4 signalling promotes vascular stability by blocking Arf6 activity. *Nat Cell Biol* 11: 1325–1331
Justice RW, Zilian O, Woods DF, Noll M & Bryant PJ (1995) The Drosophila tumor suppressor gene warts encodes a homolog of human myotonic dystrophy kinase and is required for the control of cell shape and proliferation. *Genes Dev* 9: 534–546
Kamikubo Y, Takaori-Kondo A, Uchiyama T & Hori T (2003) Inhibition of Cell Growth by Conditional Expression of kpm, a Human Homologue of Drosophila warts/lats Tumor Suppressor. *J Biol Chem* 278: 17609–17614
Kandasamy K, Sujatha Mohan S, Raju R, Keerthikumar S, Sameer Kumar GS, Venugopal AK, Telikicherla D, Navarro DJ, Mathivanan S, Pecquet C, *et al* (2010) NetPath: A public resource of curated signal transduction pathways. *Genome Biol* 11
Kastan MB & Bartek J (2004) Cell-cycle checkpoints and cancer. *Nature* 432: 316–323
Katzen F (2007) Gateway(®) recombinational cloning: a biological operating system. *Expert Opin Drug Discov* 2: 571–589
Ke H, Pei J, Ni Z, Xia H, Qi H, Woods T, Kelekar A & Tao W (2004) Putative tumor suppressor Lats2 induces apoptosis through downregulation of Bcl-2 and Bcl-xL. *Exp Cell Res* 298: 329–338
Khoury GA, Baliban RC & Floudas CA (2011) Proteome-wide post-translational modification statistics: Frequency analysis and curation of the swiss-prot database. *Sci Rep* 1

Kim W, Cho YS, Wang X, Park O, Ma X, Kim H, Gan W, Jho E hoon, Cha B, Jeung Y ji, *et al* (2019) Hippo signaling is intrinsically regulated during cell cycle progression by APC/CCdh1. *Proc Natl Acad Sci U S A* 116: 9423–9432

Kingdon KH (1923) A Method for the Neutralization of Electron Space Charge by Positive Ionization at Very Low Gas Pressures. *Phys Rev* 21: 408

Korotkevich G, Sukhov V, Budin N, Shpak B, Artyomov MN & Sergushichev A (2021) Fast gene set enrichment analysis. *bioRxiv*: 60012

Kostic C & Shaw PH (2000) Isolation and characterization of sixteen novel p53 response genes. *Oncogene* 19: 3978–3987

Krug K, Mertins P, Zhang B, Hornbeck P, Raju R, Ahmad R, Szucs M, Mundt F, Forestier D, Jane-Valbuena J, *et al* (2019) A Curated Resource for Phosphosite-specific Signature Analysis. *Mol Cell Proteomics* 18: 576–593

Krüger M, Moser M, Ussar S, Thievessen I, Luber CA, Forner F, Schmidt S, Zanivan S, Fässler R & Mann M (2008) SILAC Mouse for Quantitative Proteomics Uncovers Kindlin-3 as an Essential Factor for Red Blood Cell Function. *Cell* 134: 353–364

Kutmon M, Riutta A, Nunes N, Hanspers K, Willighagen EL, Bohler A, Mélius J, Waagmeester A, Sinha SR, Miller R, *et al* (2016) WikiPathways: Capturing the full diversity of pathway knowledge. *Nucleic Acids Res* 44: D488–D494

Lachmann A & Ma'ayan A (2009) KEA: Kinase enrichment analysis. *Bioinformatics* 25: 684–686

Lai ACY, Tsai CF, Hsu CC, Sun YN & Chen YJ (2012) Complementary Fe3+- and Ti4+-immobilized metal ion affinity chromatography for purification of acidic and basic phosphopeptides. *Rapid Commun Mass Spectrom* 26: 2186–2194

Lai Z-C, Wei X, Shimizu T, Ramos E, Rohrbaugh M, Nikolaidis N, Ho L-L & Li Y (2005) Control of cell proliferation and apoptosis by mob as tumor suppressor, mats. *Cell* 120: 675–685

Lander ES, Linton LM, Birren B, Nusbaum C, Zody MC, Baldwin J, Devon K, Dewar K, Doyle M, Fitzhugh W, *et al* (2001) Initial sequencing and analysis of the human genome. *Nat 2001 4096822* 409: 860–921

Larsen MR, Thingholm TE, Jensen ON, Roepstorff P & Jørgensen TJD (2005) Highly selective enrichment of phosphorylated peptides from peptide mixtures using titanium dioxide microcolumns. *Mol Cell Proteomics* 4: 873–886

Lee EYHP, To H, Shew JY, Bookstein R, Scully P & Lee WH (1988) Inactivation of the retinoblastoma susceptibility gene in human breast cancers. *Science (80-)* 241: 218–221

Lei Q-Y, Zhang H, Zhao B, Zha Z, Bai F, Pei X, Zhao S, Xiong Y & Guan K (2008) TAZ Promotes Cell Proliferation and Epithelial-Mesenchymal Transition and Is Inhibited by the Hippo Pathway □. 28: 2426–2436

Levy D, Adamovich Y, Reuven N & Shaul Y (2008) Yap1 Phosphorylation by c-Abl Is a Critical Step in Selective Activation of Proapoptotic Genes in Response to DNA Damage. *Mol Cell* 29: 350–361

Li J, Chen X, Ding X, Cheng Y, Zhao B, Lai ZC, AlHezaimi K, Hakem R, Guan KL & Wang CY (2013) LATS2 suppresses oncogenic Wnt signaling by disrupting β-Catenin/BCL9 interaction. *Cell Rep* 5: 1650–1663

Li W, Sun M, Zang C, Ma P, He J, Zhang M, Huang Z, Ding Y & Shu Y (2016) Upregulated long non-coding RNA AGAP2-AS1 represses LATS2 and KLF2 expression through interacting with EZH2 and LSD1 in non-small-cell lung cancer cells. *Cell Death Dis* 7

Li Y, Pei J, Xia H, Ke H, Wang H & Tao W (2003) Lats2, a putative tumor suppressor, inhibits G1/S transition. *Oncogene* 22: 4398–4405

Li Z, Razavi P, Li Q, Toy W, Liu B, Ping C, Hsieh W, Sanchez-Vega F, Brown DN, Da Cruz Paula AF, *et al* (2018) Loss of the FAT1 Tumor Suppressor Promotes Resistance to CDK4/6 Inhibitors via the Hippo Pathway. *Cancer Cell* 34: 893-905.e8

Liberzon A, Birger C, Thorvaldsdóttir H, Ghandi M, Mesirov JP & Tamayo P (2015) The Molecular Signatures Database Hallmark Gene Set Collection. *Cell Syst* 1: 417–425

Liberzon A, Subramanian A, Pinchback R, Thorvaldsdóttir H, Tamayo P & Mesirov JP (2011) Molecular signatures database (MSigDB) 3.0. *Bioinformatics* 27: 1739–1740

Lindemann C, Thomanek N, Hundt F, Lerari T, Meyer HE, Wolters D & Marcus K (2017) Strategies in relative and absolute quantitative mass spectrometry based proteomics. *Biol Chem* 398: 687–699

Litovchick L, Florens LA, Swanson SK, Washburn MP & Decaprio JA (2011) DYRK1A protein kinase promotes quiescence and senescence through DREAM complex assembly. *Genes Dev* 25: 801–813

Liu CY, Zha ZY, Zhou X, Zhang H, Huang W, Zhao D, Li T, Chan SW, Lim CJ, Hong W, *et al* (2010) The hippo tumor pathway promotes TAZ degradation by phosphorylating a phosphodegron and recruiting the SCFβ-TrCP E3 ligase. *J Biol Chem* 285: 37159–37169

Liu L & Ruan J (2013) Network-based pathway enrichment analysis. *Proc - 2013 IEEE Int Conf Bioinforma Biomed IEEE BIBM 2013*: 218–221

Liu Y, Beyer A & Aebersold R (2016) On the Dependency of Cellular Protein Levels on mRNA Abundance. *Cell* 165: 535–550

Livak KJ & Schmittgen TD (2001) Analysis of relative gene expression data using real-time quantitative PCR and the 2-ΔΔCT method. *Methods* 25: 402–408

Luo J & Yu F-X (2019) GPCR-Hippo Signaling in Cancer. *Cells* 8: 426

Maaten L van der (2008) Visualizing Data using t-SNE. *J Mach Learn Res* 164: 2579–2605

Makarov A (2000) Electrostatic axially harmonic orbital trapping: A high-performance technique of mass analysis. *Anal Chem* 72: 1156–1162

Manning G, Whyte DB, Martinez R, Hunter T & Sudarsanam S (2002) The protein kinase complement of the human genome. *Science (80-)* 298: 1912–1934

Margolis RL, Lohez OD & Andreassen PR (2003) G1 tetraploidy checkpoint and the suppression of tumorigenesis. *J Cell Biochem* 88: 673–683

Marshall AG, Blakney GT, Chen T, Kaiser NK, McKenna AM, Rodgers RP, Ruddy BM & Xian F (2013) Mass Resolution and Mass Accuracy: How Much Is Enough? *Mass Spectrom* 2: S0009–S0009

Martin D, Degese MS, Vitale-Cross L, Iglesias-Bartolome R, Valera JLC, Wang Z, Feng X, Yeerna H, Vadmal V, Moroishi T, *et al* (2018) Assembly and activation of the Hippo signalome by FAT1 tumor suppressor. *Nat Commun* 9: 2372

Masuda K, Chiyoda T, Sugiyama N, Segura-Cabrera A, Kabe Y, Ueki A, Banno K, Suematsu M, Aoki D, Ishihama Y, *et al* (2015) LATS1 and LATS2 phosphorylate CDC26 to modulate assembly of the tetratricopeptide repeat subcomplex of APC/C. *PLoS One* 10

Matallanas D, Romano D, Al-Mulla F, O'Neill E, Al-Ali W, Crespo P, Doyle B, Nixon C, Sansom O, Drosten M, *et al* (2011) Mutant K-Ras Activation of the Proapoptotic MST2 Pathway Is Antagonized by Wild-Type K-Ras. *Mol Cell* 44: 893–906

Matsuoka S, Ballif BA, Smogorzewska A, McDonald ER, Hurov KE, Luo J, Bakalarski CE, Zhao Z, Solimini N, Lerenthal Y, *et al* (2007) ATM and ATR substrate analysis reveals extensive protein networks responsive to DNA damage. *Science (80-)* 316: 1160–1166

Maung SMTW & Jenny A (2011) Planar cell polarity in drosophila. *Organogenesis* 7: 165–179

McAlister GC, Nusinow DP, Jedrychowski MP, Wühr M, Huttlin EL, Erickson BK, Rad R, Haas W & Gygi SP (2014) MultiNotch MS3 enables accurate, sensitive, and multiplexed detection of differential expression across cancer cell line proteomes. *Anal Chem* 86: 7150–8

McInnes L, Healy J & Melville J (2018) UMAP: Uniform Manifold Approximation and Projection for Dimension Reduction.

McPherson JP, Tamblyn L, Elia A, Migon E, Shehabeldin A, Matysiak-Zablocki E, Lemmers B, Salmena L, Hakem A, Fish J, *et al* (2004) Lats2/Kpm is required for embryonic development, proliferation control and genomic integrity. *EMBO J* 23: 3677–3688

Meng Z, Moroishi T & Guan KL (2016) Mechanisms of Hippo pathway regulation. *Genes Dev* 30: 1–17

Michalski A, Damoc E, Hauschild JP, Lange O, Wieghaus A, Makarov A, Nagaraj N, Cox J, Mann M & Horning S (2011) Mass spectrometry-based proteomics using Q exactive, a high-performance benchtop quadrupole orbitrap mass spectrometer. *Mol Cell Proteomics* 10: M111.011015

Mohl DA, Huddleston MJ, Collingwood TS, Annan RS & Deshaies RJ (2009) Dbf2-Mob1 drives relocalization of protein phosphatase Cdc14 to the cytoplasm during exit from mitosis. *J Cell Biol* 184: 527–539

Montcouquiol M, Rachel RA, Lanford PJ, Copeland NG, Jenkins NA & Kelley MW (2003) Identification of Vangl2 and Scrb1 as planar polarity genes in mammals. *Nature* 423: 173–177

Montcouquiol M, Sans N, Huss D, Kach J, David Dickman J, Forge A, Rachel RA, Copeland NG, Jenkins NA, Bogani D, *et al* (2006) Asymmetric localization of Vangl2 and Fz3 indicate novel mechanisms for planar cell polarity in mammals. *J Neurosci* 26: 5265–5275

Moradian A, Kalli A, Sweredoski MJ & Hess S (2014) The top-down, middle-down, and bottom-up mass spectrometry approaches for characterization of histone variants and their post-translational modifications. *Proteomics* 14: 489–497

Moroishi T, Hayashi T, Pan WW, Fujita Y, Holt M V., Qin J, Carson DA & Guan KL (2016) The Hippo Pathway Kinases LATS1/2 Suppress Cancer Immunity. *Cell* 167: 1525-1539.e17

Moulder R, Goo YA & Goodlett DR (2016) Label-free quantitation for clinical proteomics. In *Methods in Molecular Biology* pp 65–76. Methods Mol Biol

Narimatsu M, Bose R, Pye M, Zhang L, Miller B, Ching P, Sakuma R, Luga V, Roncari L, Attisano L, *et al* (2009) Regulation of Planar Cell Polarity by Smurf Ubiquitin Ligases. *Cell* 137: 295–307

Nigg EA (2001) Mitotic kinases as regulators of cell division and its checkpoints. *Nat Rev Mol Cell Biol* 2: 21–32

Niida H & Nakanishi M (2006) DNA damage checkpoints in mammals. *Mutagenesis* 21: 3–9

Nishiyama Y, Hirota T, Morisaki T, Hara T, Marumoto T, Iida S, Makino K, Yamamoto H, Hiraoka T, Kitamura N, *et al* (1999) A human homolog of Drosophila warts tumor suppressor, h-warts, localized to mitotic apparatus and specifically phosphorylated during mitosis. *FEBS Lett* 459: 159–65

Noviello C, Courjal F & Theillet C (1996) Loss of Heterozygosity on the Long Arm of Chromosome 6 in Breast Cancer: Possibly Four Regions of Deletion. *Clin Cancer Res* 2: 1601–1606

Oeljeklaus S, Schummer A, Suppanz I & Warscheid B (2014) SILAC labeling of yeast for the study of membrane protein complexes. *Methods Mol Biol* 1188: 23–46

Oh H & Irvine KD (2008) In vivo regulation of Yorkie phosphorylation and localization. *Development* 135: 1081–1088

Okada N, Yabuta N, Suzuki H, Aylon Y, Oren M & Nojima H (2011) A novel Chk1/2-Lats2-14-3-3 signaling pathway regulates P-body formation in response to UV damage. *J Cell Sci* 124: 57–67

Olsen J V., Ong S-E & Mann M (2004) Trypsin Cleaves Exclusively C-terminal to Arginine and Lysine Residues *. *Mol Cell Proteomics* 3: 608–614

Olsen J V, de Godoy LMF, Li G, Macek B, Mortensen P, Pesch R, Makarov A, Lange O, Horning S & Mann M (2005) Parts per million mass accuracy on an Orbitrap mass spectrometer via lock mass injection into a C-trap. *Mol Cell Proteomics* 4: 2010–21

Ong SE, Blagoev B, Kratchmarova I, Kristensen DB, Steen H, Pandey A & Mann M (2002) Stable isotope labeling by amino acids in cell culture, SILAC, as a simple and accurate approach to expression proteomics. *Mol Cell Proteomics* 1: 376–386

Pan D (2010) The hippo signaling pathway in development and cancer. *Dev Cell* 19: 491–505

Pan W-W, Moroishi T, Koo JH & Guan K-L (2019) Cell type-dependent function of LATS1/2 in cancer cell growth. *Oncogene* 38: 2595–2610

Pantalacci S, Tapon N & Léopold P (2003) The salvador partner Hippo promotes apoptosis and cell-cycle exit in Drosophila. *Nat Cell Biol* 5: 921–927

Paulo JA & Schweppe DK (2021) Advances in quantitative high-throughput phosphoproteomics with sample multiplexing. *Proteomics* 21: 2000140

Pefani DE, Latusek R, Pires I, Grawenda AM, Yee KS, Hamilton G, Van Der Weyden L, Esashi F, Hammond EM & O'Neill E (2014) RASSF1A-LATS1 signalling stabilizes replication forks by restricting CDK2-mediated phosphorylation of BRCA2. *Nat Cell Biol* 16: 962–971

Perkins DN, Pappin DJC, Creasy DM & Cottrell JS (1999) Probability-based protein identification by searching sequence databases using mass spectrometry data. In *Electrophoresis* pp 3551–3567. Wiley-VCH Verlag

Piccolo S, Dupont S & Cordenonsi M (2014) The Biology of YAP/TAZ: Hippo Signaling and Beyond. *Physiol Rev* 94: 1287–1312

Poon CLC, Lin JI, Zhang X & Harvey KF (2011) The sterile 20-like kinase Tao-1 controls tissue growth by regulating the Salvador-Warts-Hippo pathway. *Dev Cell* 21: 896–906

Posewitz MC & Tempst P (1999) Immobilized gallium(III) affinity chromatography of phosphopeptides. *Anal Chem* 71: 2883–2892

Potel CM, Lin MH, Heck AJR & Lemeer S (2018) Defeating major contaminants in Fe3- immobilized metal ion affinity chromatography (IMAC) phosphopeptide enrichment. *Mol Cell Proteomics* 17: 1028–1034

Rauniyar N & Yates JR (2014) Isobaric labeling-based relative quantification in shotgun proteomics. *J Proteome Res* 13: 5293–309

Ren F, Zhang L & Jiang J (2010) Hippo signaling regulates Yorkie nuclear localization and activity through 14-3-3 dependent and independent mechanisms. *Dev Biol* 337: 303

Reuven N, Adler J, Meltser V & Shaul Y (2013) The Hippo pathway kinase Lats2 prevents DNA damage-induced apoptosis through inhibition of the tyrosine kinase c-Abl. *Cell Death Differ* 20: 1330–1340

Ritchie ME, Phipson B, Wu D, Hu Y, Law CW, Shi W & Smyth GK (2015) limma powers differential expression analyses for RNA-sequencing and microarray studies. *Nucleic Acids Res* 43: e47

Ross PL, Huang YN, Marchese JN, Williamson B, Parker K, Hattan S, Khainovski N, Pillai S, Dey S, Daniels S, *et al* (2004) Multiplexed protein quantitation in Saccharomyces cerevisiae using amine-reactive isobaric tagging reagents. *Mol Cell Proteomics* 3: 1154–1169

Rozanova S, Barkovits K, Nikolov M, Schmidt C, Urlaub H & Marcus K (2021) Quantitative Mass Spectrometry-Based Proteomics: An Overview. In *Methods in Molecular Biology* pp 85–116. Methods Mol Biol

RStudio Team (2020). RStudio: Integrated Development for R. RStudio, PBC, Boston, MA URL http://www.rstudio.com/.

Ruprecht B, Koch H, Domasinska P, Frejno M, Kuster B & Lemeer S (2017) Optimized Enrichment of Phosphoproteomes by Fe-IMAC Column Chromatography. In *Methods in molecular biology (Clifton, N.J.)* pp 47–60.

Ruprecht B, Koch H, Medard G, Mundt M, Kuster B & Lemeer S (2015) Comprehensive and Reproducible Phosphopeptide Enrichment Using Iron Immobilized Metal Ion Affinity Chromatography (Fe-IMAC) Columns. *Mol Cell Proteomics* 14: 205–215

Sadasivam S & DeCaprio JA (2013) The DREAM complex: Master coordinator of cell cycle-dependent gene expression. *Nat Rev Cancer* 13: 585–595

Salaun P, Rannou Y & Claude P (2008) Cdk1, plks, auroras, and neks: The mitotic bodyguards. In *Advances in Experimental Medicine and Biology* pp 41–56. Adv Exp Med Biol

Santamaría D, Barrière C, Cerqueira A, Hunt S, Tardy C, Newton K, Cáceres JF, Dubus P, Malumbres M & Barbacid M (2007) Cdk1 is sufficient to drive the mammalian cell cycle. *Nature* 448: 811–815

Scigelova M & Makarov A (2006) Orbitrap mass analyzer - Overview and applications in proteomics. In *Proteomics* pp 16–21. Proteomics

Seifert JRK & Mlodzik M (2007) Frizzled/PCP signalling: A conserved mechanism regulating cell polarity and directed motility. *Nat Rev Genet* 8: 126–138

Senko MW, Remes PM, Canterbury JD, Mathur R, Song Q, Eliuk SM, Mullen C, Earley L, Hardman M, Blethrow JD, *et al* (2013) Novel parallelized quadrupole/linear ion trap/orbitrap tribrid mass spectrometer improving proteome coverage and peptide identification rates. *Anal Chem* 85: 11710–11714

Sha L, Ma D & Chen C (2020) Exosome-mediated Hic-5 regulates proliferation and apoptosis of osteosarcoma via Wnt /β-catenin signal pathway. *Aging (Albany NY)* 12: 23598–23608

Sharif AAD & Hergovich A (2018) The NDR/LATS protein kinases in immunology and cancer biology. *Semin Cancer Biol* 48: 104–114

Shenoy A & Geiger T (2014) Super-SILAC: Current trends and future perspectives. *Expert Rev Proteomics* 12: 13–19

Shi X, Liu Z, Liu Z, Feng X, Hua F, Hu X, Wang B, Lu K & Nie F (2018) Long noncoding RNA PCAT6 functions as an oncogene by binding to EZH2 and suppressing LATS2 in non-small-cell lung cancer. *EBioMedicine* 37: 177–187

Shibanuma M, Mashimo J, Kuroki T & Nose K (1994) Characterization of the TGF beta 1-inducible hic-5 gene that encodes a putative novel zinc finger protein and its possible involvement in cellular senescence. *J Biol Chem* 269: 26767–26774

Simons M & Mlodzik M (2008) Planar cell polarity signaling: from fly development to human disease. *Annu Rev Genet* 42:

517–540
Sinha A & Mann M (2020) A beginner's guide to mass spectrometry—based proteomics. *Biochem (Lond)* 42: 64–69
Song W, Zhang J, Zhang J, Sun M & Xia Q (2019) Overexpression of lncRNA PIK3CD-AS1 promotes expression of LATS1 by competitive binding with microRNA-566 to inhibit the growth, invasion and metastasis of hepatocellular carcinoma cells. *Cancer Cell Int* 19
Soufi B, Kumar C, Gnad F, Mann M, Mijakovic I & MacEk B (2010) Stable isotope labeling by amino acids in cell culture (SILAC) applied to quantitative proteomics of bacillus subtilis. *J Proteome Res* 9: 3638–3646
St John MA, Tao W, Fei X, Fukumoto R, Luisa Carcangiu M, Brownstein DG, Parlow AF, McGrath J & Xu T (1999) Mice deficient of Lats1 develop soft-tissue sarcomas, ovarian tumours and pituitary dysfunction
Steen H & Mann M (2004) The ABC's (and XYZ's) of peptide sequencing. *Nat Rev Mol Cell Biol* 5: 699–711
Su T, Ludwig MZ, Xu J & Fehon RG (2017) Kibra and Merlin Activate the Hippo Pathway Spatially Distinct from and Independent of Expanded. *Dev Cell* 40: 478-490.e3
Subramanian A, Tamayo P, Mootha VK, Mukherjee S, Ebert BL, Gillette MA, Paulovich A, Pomeroy SL, Golub TR, Lander ES, *et al* (2005) Gene set enrichment analysis: a knowledge-based approach for interpreting genome-wide expression profiles. *Proc Natl Acad Sci U S A* 102: 15545–50
Sun D, Wang Y, Wang H & Xin Y (2020) The novel long non-coding RNA LATS2-AS1-001 inhibits gastric cancer progression by regulating the LATS2/YAP1 signaling pathway via binding to EZH2. *Cancer Cell Int* 20: 1–15
Sury MD, Chen JX & Selbach M (2010) The SILAC fly allows for accurate protein quantification in vivo. *Mol Cell Proteomics* 9: 2173–2183
Suzuki H, Yabuta N, Okada N, Torigata K, Aylon Y, Oren M & Nojima H (2013) Lats2 phosphorylates p21/CDKN1A after UV irradiation and regulates apoptosis. *J Cell Sci* 126: 4358–4368
Szklarczyk D, Morris JH, Cook H, Kuhn M, Wyder S, Simonovic M, Santos A, Doncheva NT, Roth A, Bork P, *et al* (2017) The STRING database in 2017: quality-controlled protein–protein association networks, made broadly accessible. *Nucleic Acids Res* 45: D362–D368
Takahashi Y, Miyoshi Y, Takahata C, Irahara N, Taguchi T, Tamaki Y & Noguchi S (2005) Down-Regulation of LATS1 and LATS2 mRNA Expression by Promoter Hypermethylation and Its Association with Biologically Aggressive Phenotype in Human Breast Cancers. *Clin Cancer Res* 11: 1380–1385
Tao W, Zhang S, Turenchalk GS, Stewart RA, St John MAR, Chen W & Xu T (1999) Human homologue of the Drosophila melanogaster lats tumour suppressor modulates CDC2 activity. *Nat Genet 1999 212* 21: 177–181
Tapon N, Harvey K, Bell D, Wahrer D, Schiripo T, Haber D & Hariharan IK (2002) salvador Promotes both cell cycle exit and apoptosis in Drosophila and is mutated in human cancer cell lines. *Cell* 110: 467–478
Theile M, Seitz S, Arnold W, Jandrig B, Frege R, Schlag PM, Haensch W, Guski H, Winzer KJ, Barrett JC, *et al* (1996) A defined chromosome 6q fragment (at D6S310) harbors a putative tumor suppressor gene for breast cancer. *Oncogene* 13: 677–685
Thingholm TE, Jensen ON, Robinson PJ & Larsen MR (2008) SIMAC (Sequential Elution from IMAC), a phosphoproteomics strategy for the rapid separation of monophosphorylated from multiply phosphorylated peptides. In *Molecular and Cellular Proteomics* pp 661–671. Mol Cell Proteomics
Thompson A, Schäfer J, Kuhn K, Kienle S, Schwarz J, Schmidt G, Neumann T & Hamon C (2003) Tandem mass tags: A novel quantification strategy for comparative analysis of complex protein mixtures by MS/MS. *Anal Chem* 75: 1895–1904
Ting L, Rad R, Gygi SP & Haas W (2011) MS3 eliminates ratio distortion in isobaric multiplexed quantitative proteomics. *Nat Methods* 8: 937–940
Tirode F, Busso D, Coin F & Egly JM (1999) Reconstitution of the transcription factor TFIIH: Assignment of functions for the three enzymatic subunits, XPB, XPD, and cdk7. *Mol Cell* 3: 87–95
Tomlinson V, Gudmundsdottir K, Luong P, Leung K-Y, Knebel A & Basu S (2010) JNK phosphorylates Yes-associated protein (YAP) to regulate apoptosis. *Cell Death Dis* 1: 29
Tong M, Jun T, Nie Y, Hao J & Fan D (2019) The role of the SLIT/Robo signaling pathway. *J Cancer* 10: 2694–2705
Totaro A, Panciera T & Piccolo S (2018) YAP/TAZ upstream signals and downstream responses. *Nat Cell Biol* 20: 888–899
Tschöp K, Conery AR, Litovchick L, DeCaprio JA, Settleman J, Harlow E & Dyson N (2011) A kinase shRNA screen links LATS2 and the pRB tumor suppressor. *Genes Dev* 25: 814–830
Tsiamis V, Ienasescu HI, Gabrielaitis D, Palmblad M, Schwämmle V & Ison J (2019) One Thousand and One Software for Proteomics: Tales of the Toolmakers of Science. *J Proteome Res* 18: 3580–3585
Udan RS, Kango-Singh M, Nolo R, Tao C & Halder G (2003) Hippo promotes proliferation arrest and apoptosis in the Salvador/Warts pathway. *Nat Cell Biol* 5: 914–920
Visser S & Yang X (2010a) Identification of LATS transcriptional targets in HeLa cells using whole human genome oligonucleotide microarray. *Gene* 449: 22–29
Visser S & Yang X (2010b) LATS tumor suppressor: A new governor of cellular homeostasis. *Cell Cycle* 9: 3892–3903
Walther TC & Mann M (2010) Mass spectrometry-based proteomics in cell biology. *J Cell Biol* 190: 491–500
Wan L, Sun M, Liu GJ, Wei CC, Zhang EB, Kong R, Xu TP, Huang M De & Wang ZX (2016) Long noncoding RNA PVT1 promotes non-small cell lung cancer cell proliferation through epigenetically regulating LATS2 expression. *Mol Cancer Ther* 15: 1082–1094
Wang J, Hamblet NS, Mark S, Dickinson ME, Brinkman B, Segil N, Fraser SE, Chen P, Wallingford JB & Wnyshaw-Boris A (2006) Dishevelled genes mediate a conserved mammalian PCP pathway to regulate convergent extension during neurulation. *Development* 133: 1767–1778

Wang W, Li X, Huang J, Feng L, Dolinta KG & Chen J (2014) Defining the Protein–Protein Interaction Network of the Human Hippo Pathway. *Mol Cell Proteomics* 13: 119–131

Wei X, Shimizu T & Lai Z-C (2007) Mob as tumor suppressor is activated by Hippo kinase for growth inhibition in Drosophila. *EMBO J* 26: 1772–1781

Wilkins MR, Sanchez JC, Gooley AA, Appel RD, Humphery-Smith I, Hochstrasser DF & Williams KL (1996) Progress with proteome projects: Why all proteins expressed by a genome should be identified and how to do it. *Biotechnol Genet Eng Rev* 13: 19–50

Wilkinson ME, Charenton C & Nagai K (2020) RNA Splicing by the Spliceosome. *Annu Rev Biochem* 89: 359–388

Willems E, Dedobbeleer M, Digregorio M, Lombard A, Lumapat PN & Rogister B (2018) The functional diversity of Aurora kinases: a comprehensive review. *Cell Div* 13: 7

Wiredja DD, Koyutürk M & Chance MR (2017) The KSEA App: a web-based tool for kinase activity inference from quantitative phosphoproteomics. *Bioinformatics* 33: 3489–3491

Wu G & Haw R (2017) Functional Interaction Network Construction and Analysis for Disease Discovery. *Methods Mol Biol* 1558: 235–253

Wu S, Huang J, Dong J & Pan D (2003) hippo encodes a Ste-20 family protein kinase that restricts cell proliferation and promotes apoptosis in conjunction with salvador and warts. *Cell* 114: 445–456

Wu S, Liu Y, Zheng Y, Dong J & Pan D (2008) The TEAD/TEF family protein Scalloped mediates transcriptional output of the Hippo growth-regulatory pathway. *Dev Cell* 14: 388–398

Xia H, Qi H, Li Y, Pei J, Barton J, Blackstad M, Xu T & Tao W (2002) LATS1 tumor suppressor regulates G2/M transition and apoptosis. *Oncogene* 21: 1233–1241

Xu T, Wang W, Zhang S, Stewart RA & Yu W (1995) Identifying tumor suppressors in genetic mosaics: the Drosophila lats gene encodes a putative protein kinase. *Development* 121: 1053–63

Xu Y, Ji K, Wu M, Hao B, Yao K tai & Xu Y (2019) A miRNA-HERC4 pathway promotes breast tumorigenesis by inactivating tumor suppressor LATS1. *Protein Cell* 10: 595–605

Yabuta N, Fujii T, Copeland NG, Gilbert DJ, Jenkins NA, Nishiguchi H, Endo Y, Toji S, Tanaka H, Nishimune Y, *et al* (2000) Structure, Expression, and Chromosome Mapping of LATS2, a Mammalian Homologue of the Drosophila Tumor Suppressor Gene lats/warts. *Genomics* 63: 263–270

Yabuta N, Mukai S, Okada N, Aylon Y & Nojima H (2011) The tumor suppressor Lats2 is pivotal in Aurora A and Aurora B signaling during mitosis. *Cell Cycle* 10: 2724–2736

Yabuta N, Okada N, Ito A, Hosomi T, Nishihara S, Sasayama Y, Fujimori A, Okuzaki D, Zhao H, Ikawa M, *et al* (2007) Lats2 is an essential mitotic regulator required for the coordination of cell division. *J Biol Chem* 282: 19259–71

Yabuta N, Yoshida K, Mukai S, Kato Y, Torigata K & Nojima H (2016) Large tumor suppressors 1 and 2 regulate Aurora-B through phosphorylation of INCENP to ensure completion of cytokinesis. *Heliyon* 2

Yamashita M & Fenn JB (1984) Electrospray ion source. Another variation on the free-jet theme. *J Phys Chem* 88: 4451–4459

Yang J, Wagner SA & Beli P (2015) Illuminating spatial and temporal organization of protein interaction networks by mass spectrometry-based proteomics. *Front Genet* 6: 344

Yang X, Li D ming, Chen W & Xu T (2001) Human homologue of Drosophila lats, LATS1, negatively regulate growth by inducing G2/M arrest or apoptosis. *Oncogene* 20: 6516–6523

Yang X, Yu K, Hao Y, Li DM, Stewart R, Insogna KL & Xu T (2004) LATS1 tumour suppressor affects cytokinesis by inhibiting LIMK1. *Nat Cell Biol* 6: 609–617

Yin F, Yu J, Zheng Y, Chen Q, Zhang N & Pan D (2013) Spatial organization of hippo signaling at the plasma membrane mediated by the tumor suppressor merlin/NF2. *Cell* 154: 1342

Yu F-X & Guan K-L (2013) The Hippo pathway: regulators and regulations. *Genes Dev* 27: 355–71

Yu F-X, Zhao B & Guan K-L (2015) Hippo Pathway in Organ Size Control, Tissue Homeostasis, and Cancer. *Cell* 163: 811–828

Yu G & He Q-Y (2016) ReactomePA: an R/Bioconductor package for reactome pathway analysis and visualization. *Mol BioSyst* 12: 477–479

Zachariae W, Schwab M, Nasmyth K & Seufert W (1998) Control of cyclin ubiquitination by CDK-regulated binding of Hct1 to the anaphase promoting complex. *Science (80-)* 282: 1721–1724

Zanconato F, Cordenonsi M & Piccolo S (2016) YAP/TAZ at the Roots of Cancer. *Cancer Cell* 29: 783–803

Zhang K, Rodriguez-Aznar E, Yabuta N, Owen RJ, Mingot JM, Nojima H, Nieto MA & Longmore GD (2012) Lats2 kinase potentiates Snail1 activity by promoting nuclear retention upon phosphorylation. *EMBO J* 31: 29–43

Zhang Y, Hu CF, Chen J, Yan LX, Zeng YX & Shao JY (2010) LATS2 is De-methylated and overexpressed in nasopharyngeal carcinoma and predicts poor prognosis. *BMC Cancer* 10

Zhao B, Li L, Tumaneng K, Wang C-Y & Guan K-L (2010) A coordinated phosphorylation by Lats and CK1 regulates YAP stability through SCF -TRCP. *Genes Dev* 24: 72–85

Zhao B, Wei X, Li W, Udan RS, Yang Q, Kim J, Xie J, Ikenoue T, Yu J, Li L, *et al* (2007) Inactivation of YAP oncoprotein by the Hippo pathway is involved in cell contact inhibition and tissue growth control. *Genes Dev* 21: 2747–61

Zhao B, Ye X, Yu J, Li L, Li W, Li S, Yu J, Lin JD, Wang CY, Chinnaiyan AM, *et al* (2008) TEAD mediates YAP-dependent gene induction and growth control. *Genes Dev* 22: 1962–1971

Zhao BS, Roundtree IA & He C (2016) Post-transcriptional gene regulation by mRNA modifications. *Nat Rev Mol Cell Biol* 18: 31–42

Zhou H, Xu S, Ye M, Feng S, Pan C, Jiang X, Li X, Han G, Fu Y & Zou H (2006a) Zirconium phosphonate-modified porous silicon for highly specific capture of phosphopeptides and MALDI-TOF MS analysis. *J Proteome Res* 5: 2431–2437

Zhou X, Vink M, Klaver B, Berkhout B & Das AT (2006b) Optimization of the Tet-On system for regulated gene expression through viral evolution. *Gene Ther* 13: 1382–1390

Zhou Z, He M, Shah AA & Wan Y (2016) Insights into APC/C: From cellular function to diseases and therapeutics. *Cell Div* 11: 9

Zimmerman M & Snow B (2012) An Introduction to Nutrition. *Independent*

6. APPENDIX

6.1. Supplementary Figures

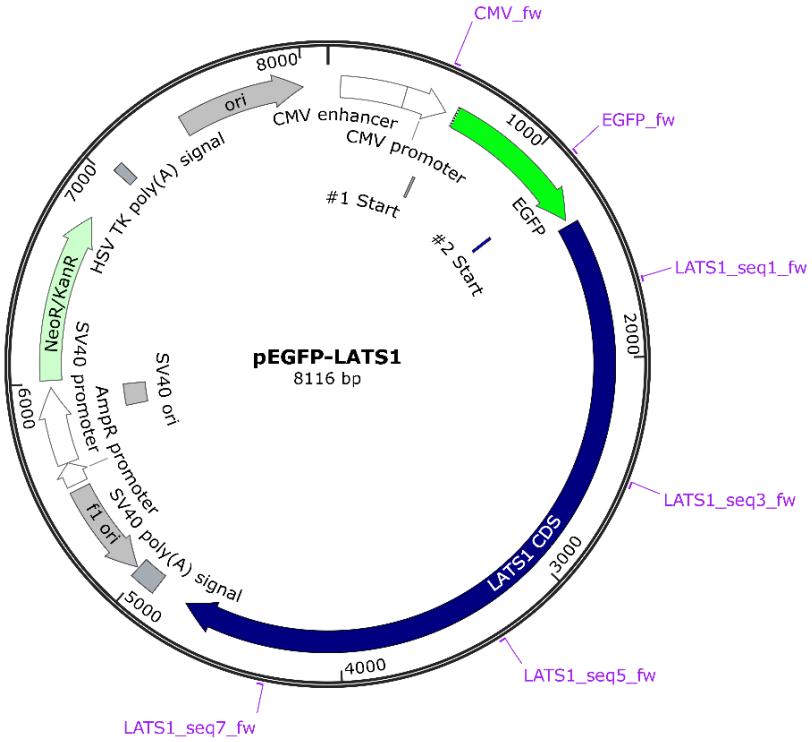

Supplementary Figure 1: pEGFP-LATS1 vector map.

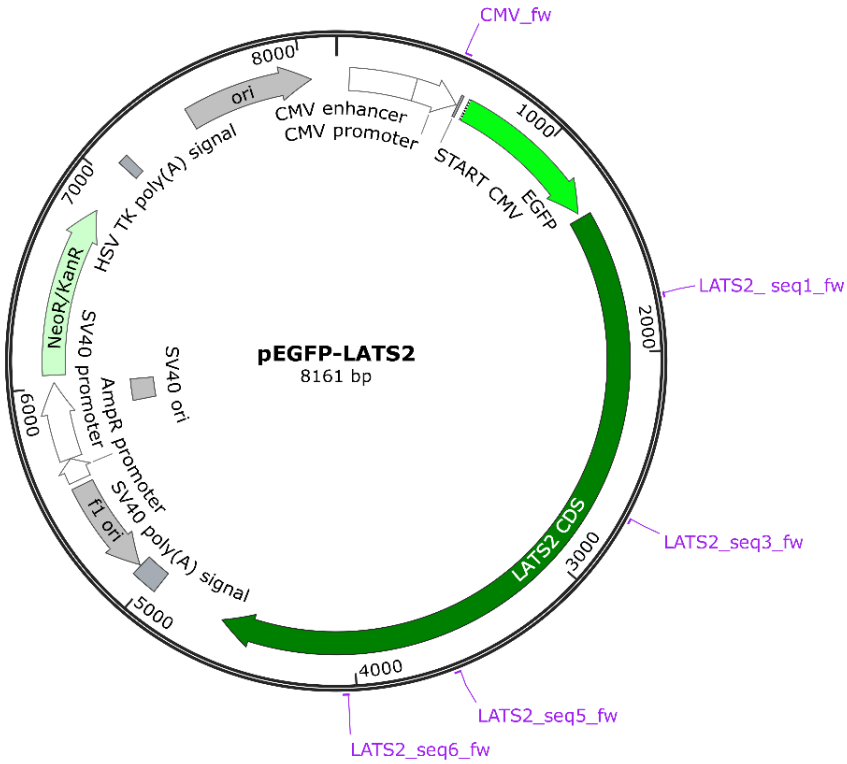

Supplementary Figure 2: pEGFP-LATS2 vector map.

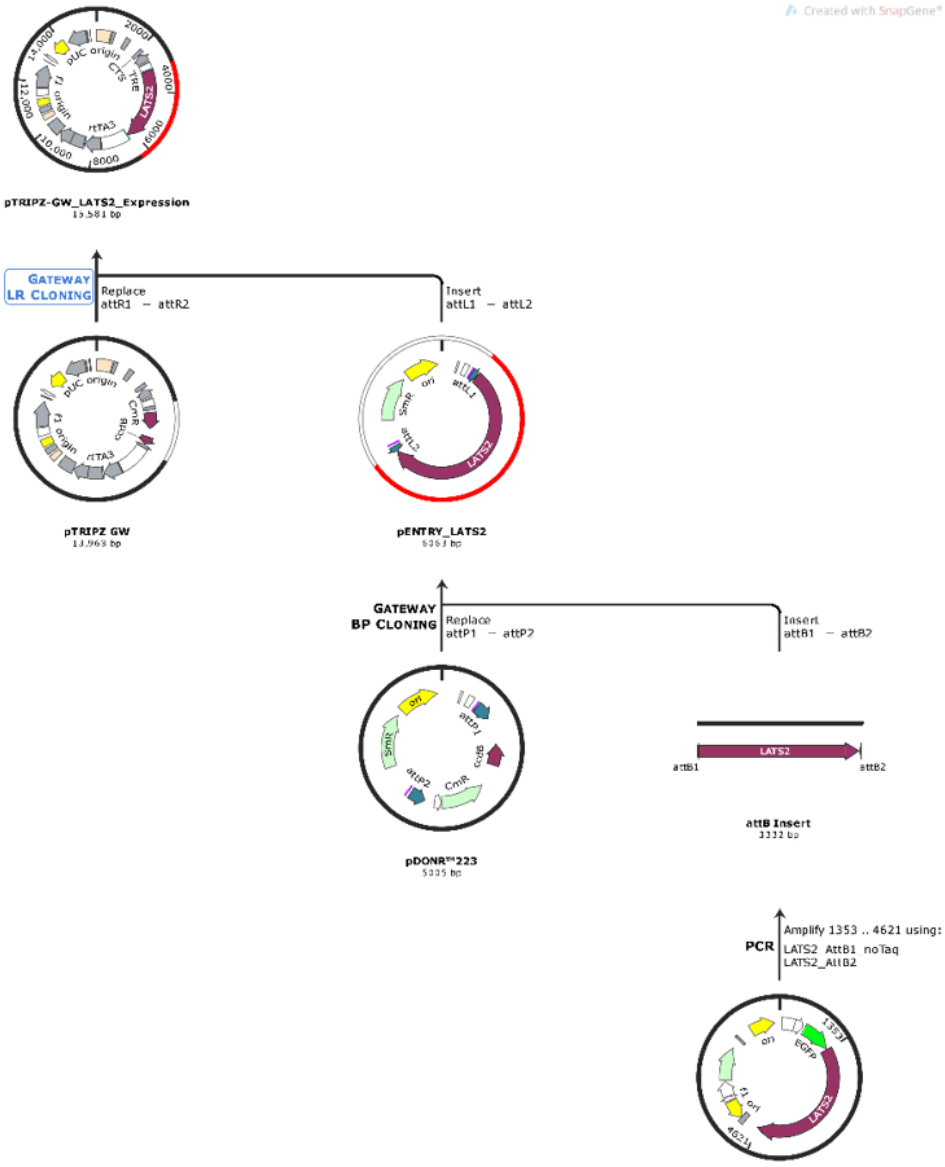

Supplementary Figure 3: Cloning scheme of Gateway cloning.

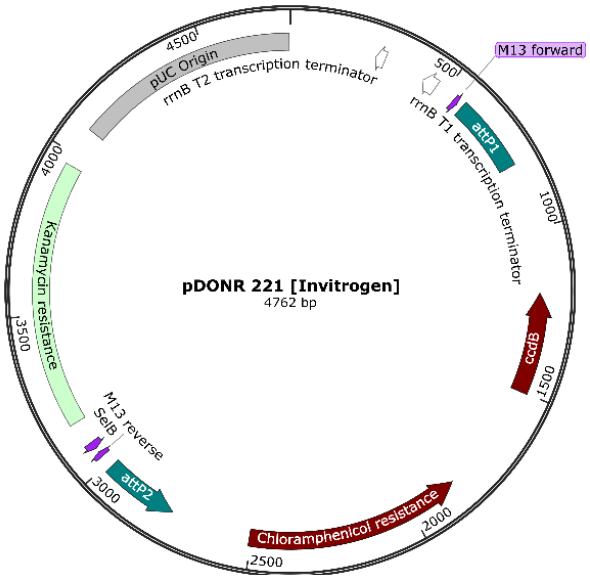

Supplementary Figure 4: pDONR 221 vector map.

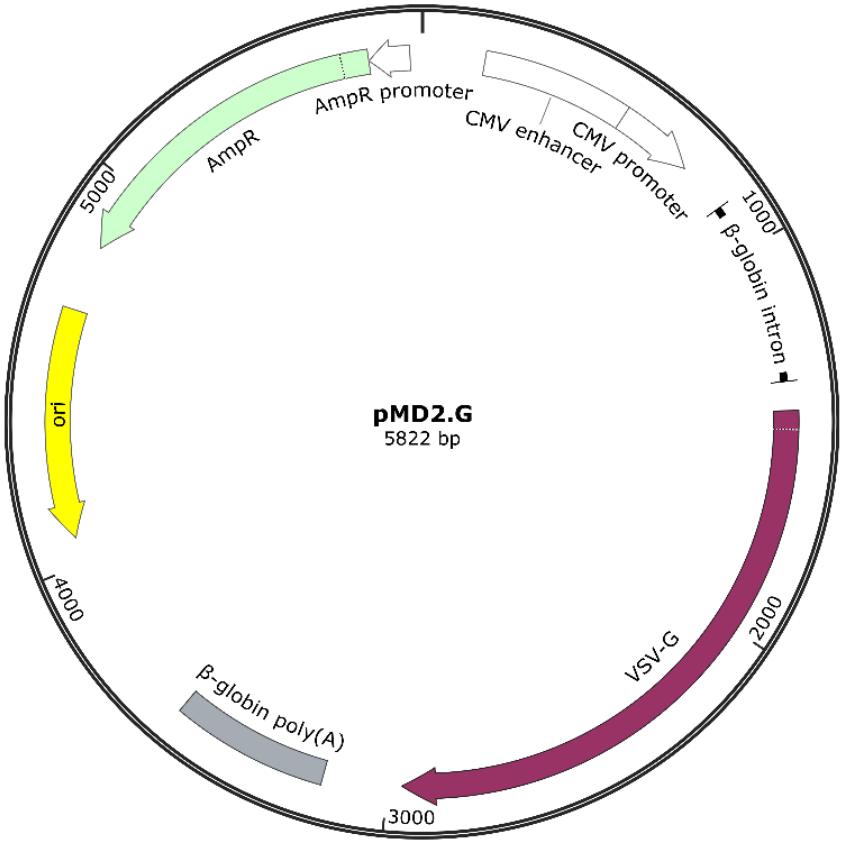

Supplementary Figure 5: pMD2.G vector map.

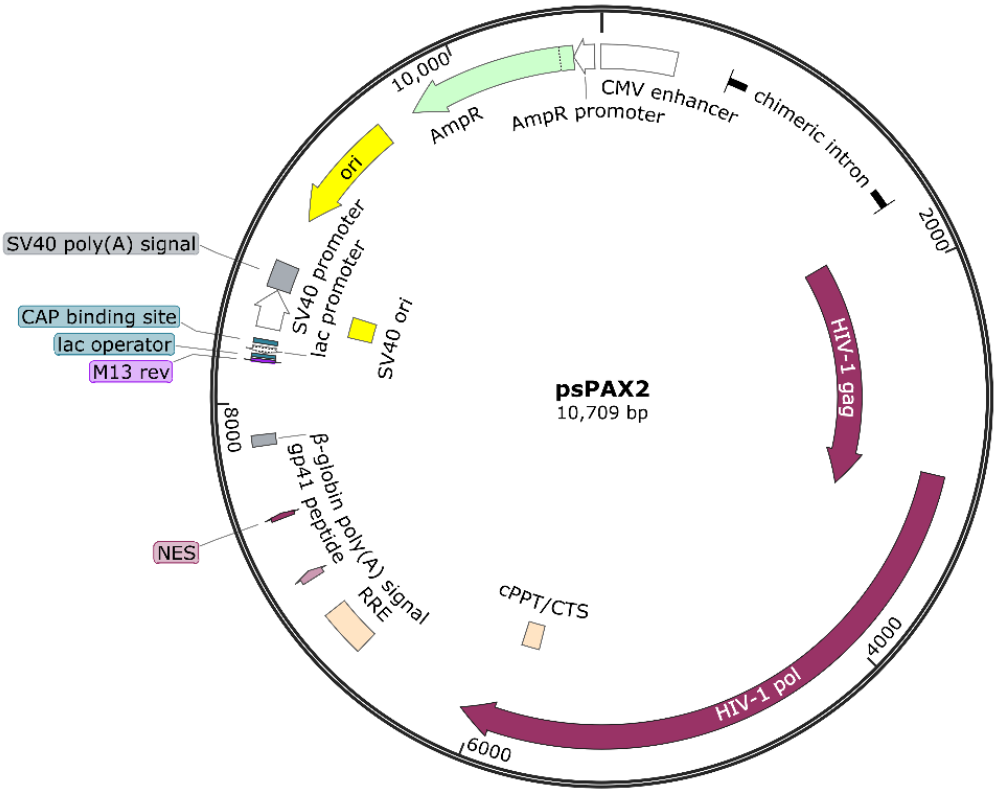

Supplementary Figure 6: psPAX2 vector map.

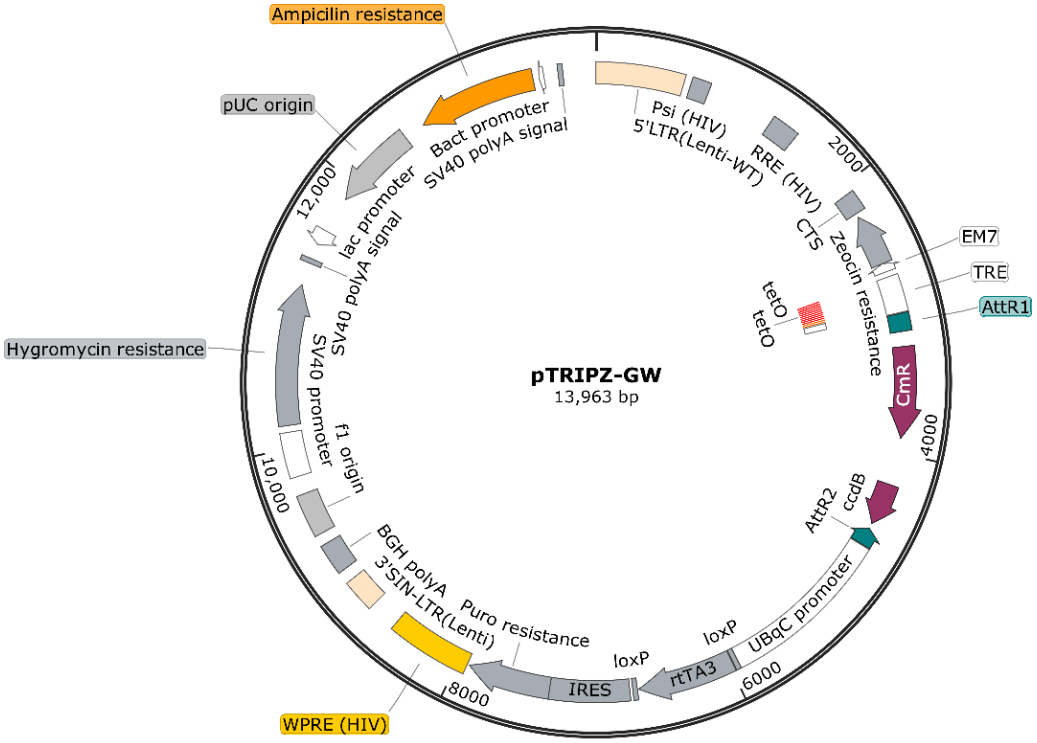

Supplementary Figure 7: pTRIPZ-GW tGFP vector map.

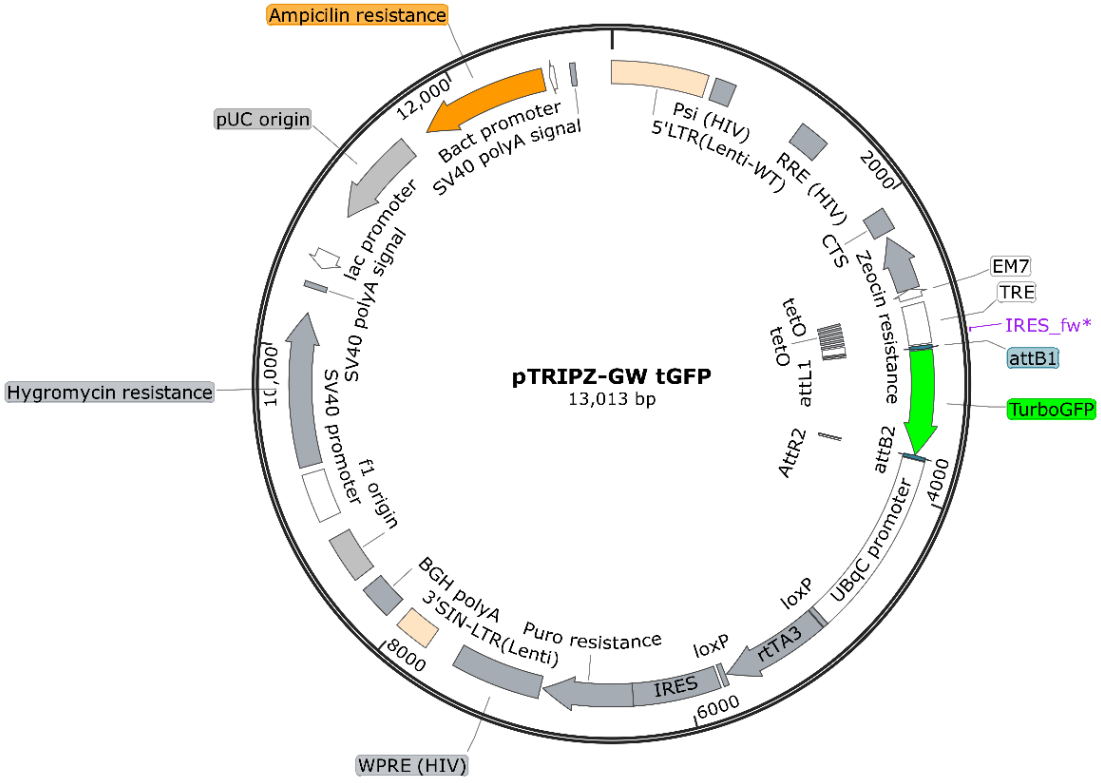

Supplementary Figure 8: pTRIPZ-GW vector map.

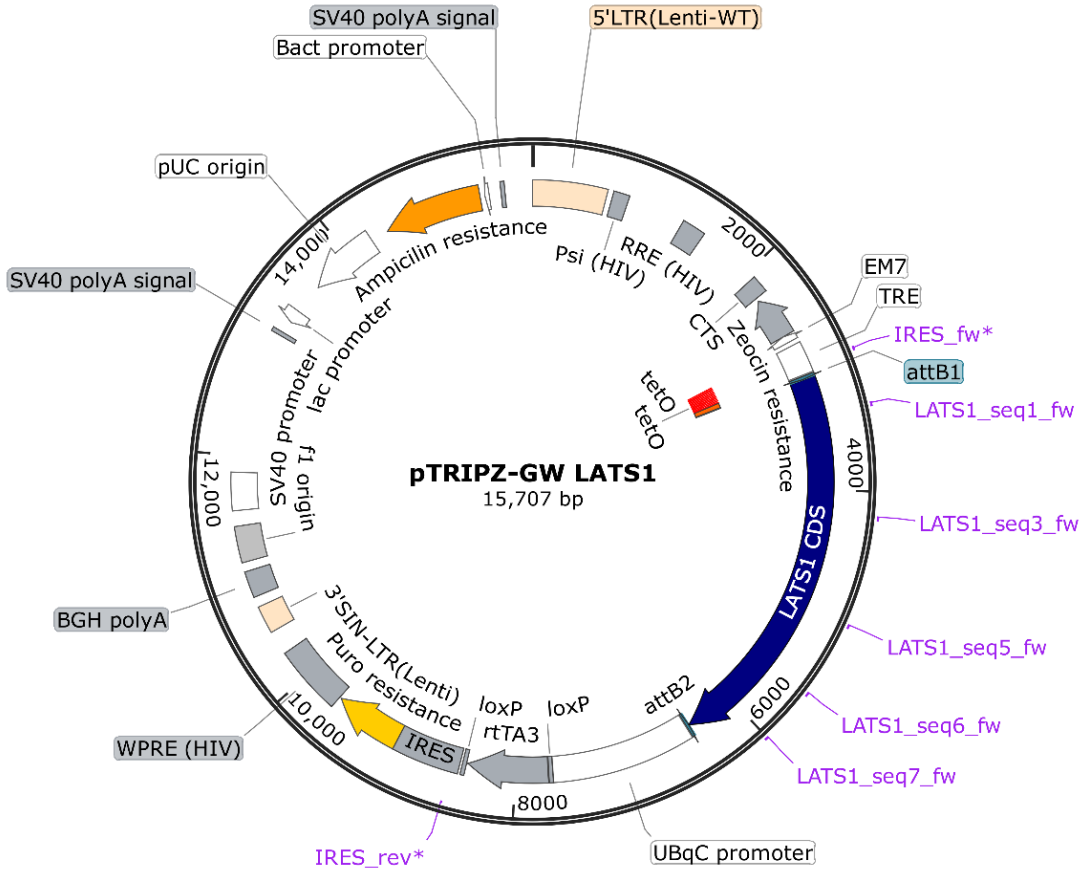

Supplementary Figure 9: pTRIPZ-GW LATS1 vector map

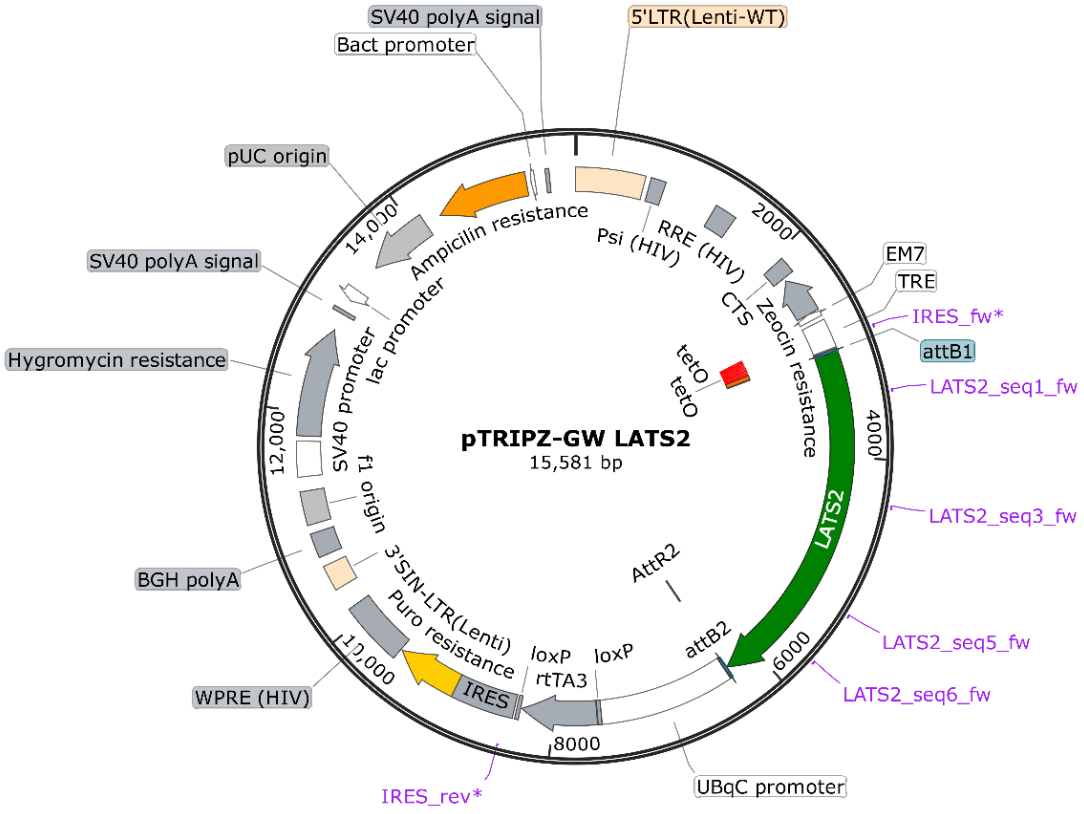

Supplementary Figure 10: pTRIPZ-GW LATS2 vector map

A

CELL LINE	GENE	GLOBAL PROTEOME 2 h: LATS1 OVEREXPR.	GLOBAL PROTEOME 2 h: LATS2 OVEREXPR.	GLOBAL PROTEOME 6 h: LATS1 OVEREXPR.	GLOBAL PROTEOME 6 h: LATS2 OVEREXPR.	TRANSLATOME 6 h: LATS1 OVEREXPR.	TRANSLATOME 6 h: LATS2 OVEREXPR.	TRANSLATOME 20 h: LATS1 OVEREXPR.	TRANSLATOME 20 h: LATS2 OVEREXPR.
MCF10A	**LATS1**	-0.23	-0.01	-0.20	-0.29	0.32	-0.26	**1.72***	**2.56***
	LATS2	n.d.	n.d.	-0.43	**2.75***	-0.17	**2.17***	-0.13	**2.71***
		***LATS*/Ctrl (log_2FC)**		***LATS*/Ctrl (log_2FC)**		***LATS*/Ctrl (log_2FC)**		***LATS*/Ctrl (log_2FC)**	

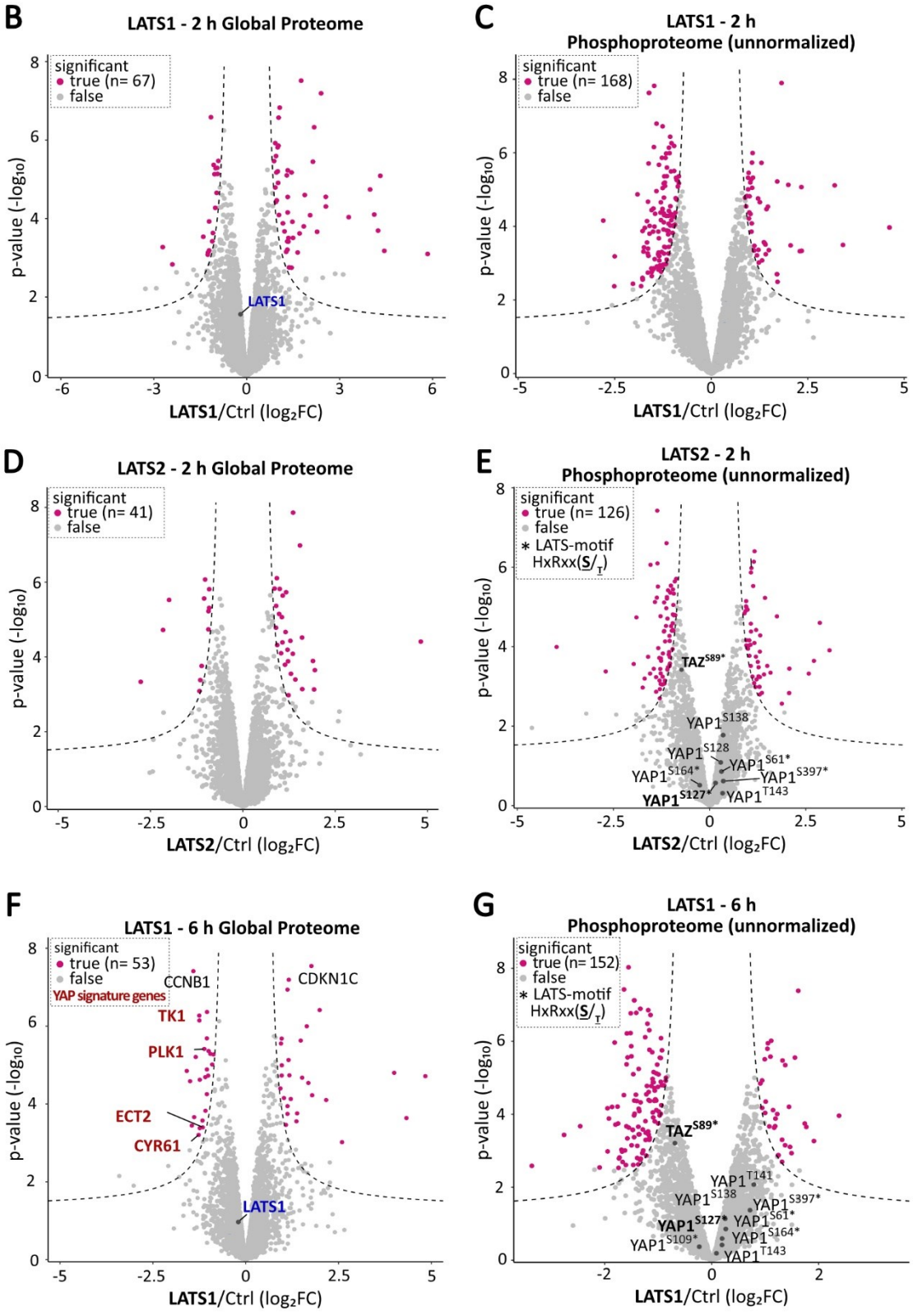

Supplementary Figure 11: Effects of LATS1 or LATS2 overexpression on the phosphoproteome in MCF10A cells. (A) Protein ratio levels of LATS1 and LATS2 in global proteome analysis that corresponds to phosphoproteome analysis, and translatome analysis in MCF10A cells upon LATS overexpression. Red color implies downregulation, green color implies upregulation, and numbers with an asterisk depict significantly changing proteins with an adj. p ≤ 0.05. (**B-G**) Differential expression analysis using limma moderated t-statistics for the comparison of changes on the (**B, D, F**) global proteome and (**C, E, F**) phosphoproteome upon overexpression of LATS1 or LATS2 in MCF10A cells. Grey color of dots indicates non-significant, pink color indicates significantly changing proteins or phosphosites, with a p-value adjusted for multiple testing according to Benjamini-Hochberg, *adj. p ≤ 0.05 and a minimum $\log_2$FC of +/- 0.58. Protein names in red indicate YAP target genes. Phosphosites with an asterisk indicate overlap with the LATS1/2-specific motif sequence HxRxx(S/T).

6.2. Gene sequences

Supplementary Table 1: Coding nucleotide sequence of selected genes.

GENE NAME **[SPECIES]** **(NCBI_CCDS)**	**SEQUENCE**
EGFP [*Mycobacterium tuberculosis H37Rv*]	ATGGTGAGCAAGGGCGAGGAGCTGTTCACCGGGGTGGTGCCCATCCTGGTCGAGCTGGACGGCGACGTAAACGGCCAC AAGTTCAGCGTGTCCGGCGAGGGCGAGGGCGATGCCACCTACGGCAAGCTGACCCTGAAGTTCATCTGCACCACCGGCA AGCTGCCCGTGCCCTGGCCCACCCTCGTGACCACCCTGACCTACGGCGTGCAGTGCTTCAGCCGCTACCCCGACCACATGA AGCAGCACGACTTCTTCAAGTCCGCCATGCCCGAAGGCTACGTCCAGGAGCGCACCATCTTCTTCAAGGACGACGGCAACT ACAAGACCCGCGCCGAGGTGAAGTTCGAGGGCGACACCCTGGTGAACCGCATCGAGCTGAAGGGCATCGACTTCAAGGA GGACGGCAACATCCTGGGGCACAAGCTGGAGTACAACTACAACAGCCACAACGTCTATATCATGGCCGACAAGCAGAAG AACGGCATCAAGGTGAACTTCAAGATCCGCCACAACATCGAGGACGGCAGCGTGCAGCTCGCCGACCACTACCAGCAGA ACACCCCCATCGGCGACGGCCCCGTGCTGCTGCCCGACAACCACTACCTGAGCACCCAGTCCGCCCTGAGCAAAGACCCCA ACGAGAAGCGCGATCACATGGTCCTGCTGGAGTTCGTGACCGCCGCCGGGATCACTCTCGGCATGGACGAGCTGTACAAG
LATS1 [*Homo sapiens*] (NCBI- CCDS #34551.1)	ATGAAGAGGAGTGAAAAGCCAGAAGGATATAGACAAATGAGGCCTAAGACCTTTCCTGCCAGTAACTATACTGTCAGTAG CCGGCAAATGTTACAAGAAATTCGGGAATCCCTTAGGAATTTATCTAAACCATCTGATGCTGCTAAGGCTGAGCATAACAT GAGTAAAATGTCAACCGAAGATCCTCGACAAGTCAGAAATCCACCCAAATTTGGGACGCATCATAAAGCCTTGCAGGAAA TTCGAAACTCTCTGCTTCCATTTGCAAATGAAACAAATTCTTCTCGGAGTACTTCAGAAGTTAATCCACAAATGCTTCAAGA CTTGCAAGCTGCTGGATTTGATGAGGATATGGTTATACAAGCTCTTCAGAAAACTAACAACAGAAGTATAGAAGCAGCAA TTGAATTCATTAGTAAAATGAGTTACCAAGATCCTCGACGAGAGCAGATGGCTGCAGCAGCTGCCAGACCTATTAATGCCA GCATGAAACCAGGGAATGTGCAGCAATCAGTTAACCGCAAACAGAGCTGGAAAGGTTCTAAAGAATCCTTAGTTCCTCAG AGGCATGGCCCGCCACTAGGAGAAAGTGTGGCCTATCATTCTGAGAGTCCCAACTCACAGACAGATGTAGGAAGACCTTT GTCTGGATCTGGTATATCAGCATTTGTTCAAGCTCACCCTAGCAACGGACAGAGAGTGAACCCCCCACCACCACCTCAAGT AAGGAGTGTTACTCCTCCACCACCTCCAAGAGGCCAGACTCCCCCTCCAAGAGGTACAACTCCACCTCCCCCTTCATGGGA ACCAAACTCTCAAACAAAGCGCTATTCTGGAAACATGGAATACGTAATCTCCCGAATCTCTCCTGTCCCACCTGGGGCATG GCAAGAGGGCTATCCTCCACCACCTCTCAACACTTCCCCCATGAATCCTCCTAATCAAGGACAGAGAGGCATTAGTTCTGTT CCTGTTGGCAGACAACCAATCATCATGCAGAGTTCTAGCAAATTTAACTTTCCATCAGGGAGACCTGGAATGCAGAATGGT ACTGGACAAACTGATTTCATGATACACCAAAATGTTGTCCCTGCTGGCACTGTGAATCGGCAGCCACCACCTCCATATCCTC TGACAGCAGCTAATGGACAAAGCCCTTCTGCTTTACAAACAGGGGGATCTGCTGCTCCTTCGTCATATACAAATGGAAGTA TTCCTCAGTCTATGATGGTGCCAAACAGAAATAGTCATAACATGGAACTATATAACATTAGTGTACCTGGACTGCAAACAA ATTGGCCTCAGTCATCTTCTGCTCCAGCCCAGTCATCCCCGAGCAGTGGGCATGAAATCCCTACATGGCAACCTAACATACC AGTGAGGTCAAATTCCTTTAATAACCCATTAGGAAATAGAGCAAGTCACTCTGCTAATTCTCAGCCTTCTGCTACAACAGTC ACTGCAATTACACCAGCTCCTATTCAACAGCCTGTGAAAAGTATGCGTGTATTAAAACCAGAGCTACAGACTGCTTTAGCA CCTACACACCCTTCTTGGATACCACAGCCAATTCAAACTGTTCAACCCAGTCCTTTTCCTGAGGGAACCGCTTCAAATGTGA CTGTGATGCCACCTGTTGCTGAAGCTCCAAACTATCAAGGACCACCACCACCCTACCCAAAACATCTGCTGCACCAAAACCC ATCTGTTCCTCCATACGAGTCAATCAGTAAGCCTAGCAAAGAGGATCAGCCAAGCTTGCCCAAGGAAGATGAGAGTGAAA AGAGTTATGAAAATGTTGATAGTGGGGATAAAGAAAAGAAACAGATTACAACTTCACCTATTACTGTTAGGAAAAACAAG AAAGATGAAGAGCGAAGGGAATCTCGTATTCAAAGTTATTCTCCTCAAGCATTTAAATTCTTTATGGAGCAACATGTAGAA AATGTACTCAAATCTCATCAGCAGCGTCTACATCGTAAAAAACAATTAGAGAATGAAATGATGCGGGTTGGATTATCTCAA GATGCCCAGGATCAAATGAGAAAGATGCTTTGCCAAAAAGAATCTAATTACATCCGTCTTAAAAGGGCTAAAATGGACAA GTCTATGTTTGTGAAGATAAAGACACTAGGAATAGGAGCATTTGGTGAAGTCTGTCTAGCAAGAAAAGTAGATACTAAGG CTTTGTATGCAACAAAAACTCTTCGAAAGAAAGATGTTCTTCTTCGAAATCAAGTCGCTCATGTTAAGGCTGAGAGAGATA TCCTGGCTGAAGCTGACAATGAATGGGTAGTTCGTCTATATTATTCATTCCAAGATAAGGACAATTTATACTTTGTAATGGA CTACATTCCTGGGGGTGATATGATGAGCCTATTAATTAGAATGGGCATCTTTCCAGAAAGTCTGGCACGATTCTACATAGC AGAACTTACCTGTGCAGTTGAAAGTGTTCATAAAATGGGTTTTATTCATAGAGATATTAAACCTGATAATATTTTGATTGAT CGTGATGGTCATATTAAATTGACTGACTTTGGCCTCTGCACTGGCTTCAGATGGACACACGATTCTAAGTACTATCAGAGT

GGTGACCATCCACGGCAAGATAGCATGGATTTCAGTAATGAATGGGGGGATCCCTCAAGCTGTCGATGTGGAGACAGACT
GAAGCCATTAGAGCGGAGAGCTGCACGCCAGCACCAGCGATGTCTAGCACATTCTTTGGTTGGGACTCCCAATTATATTGC
ACCTGAAGTGTTGCTACGAACAGGATACACACAGTTGTGTGATTGGTGGAGTGTTGGTGTTATTCTTTTTGAAATGTTGGT
GGGACAACCTCCTTTCTTGGCACAAACACCATTAGAAACACAAATGAAGGTTATCAACTGGCAAACATCTCTTCACATTCCA
CCACAAGCTAAACTCAGTCCTGAAGCTTCTGATCTTATTATTAAACTTTGCCGAGGACCCGAAGATCGCTTAGGCAAGAAT
GGTGCTGATGAAATAAAAGCTCATCCATTTTTTAAAACAATTGACTTCTCCAGTGACCTGAGACAGCAGTCTGCTTCATACA
TTCCTAAAATCACACACCCAACAGATACATCAAATTTTGATCCTGTTGATCCTGATAAATTATGGAGTGATGATAACGAGGA
AGAAAATGTAAATGACACTCTCAATGGATGGTATAAAAATGGAAAGCATCCTGAACATGCATTCTATGAATTTACCTTCCG
AAGGTTTTTTGATGACAATGGCTACCCATATAATTATCCGAAGCCTATTGAATATGAATACATTAATTCACAAGGCTCAGAG
CAGCAGTCGGATGAAGATGATCAAAACACAGGCTCAGAGATTAAAAATCGCGATCTAGTATATGTTTAA

LATS2

[*Homo sapiens*]

(NCBI-CCDS #9294.1)

ATGAGGCCAAAGACTTTTCCTGCCACGACTTATTCTGGAAATAGCCGGCAGCGACTGCAAGAGATTCGTGAGGGGTTAAA
GCAGCCATCCAAGTCTTCGGTTCAGGGGCTACCCGCAGGACCAAACAGTGACACTTCCCTGGATGCCAAAGTCCTGGGGA
GCAAAGATGCCACCAGGCAGCAGCAGCAGATGAGAGCCACCCCAAAGTTCGGACCTTATCAGAAAGCCTTGAGGGAAAT
CAGATATTCCTTGTTGCCTTTTGCTAATGAATCGGGCACCTCTGCAGCTGCAGAAGTGAACCGGCAAATGCTGCAGGAACT
GGTGAACGCAGGATGCGACCAGGAGATGGCTGGCCGAGCTCTCAAGCAGACTGGCAGCAGGAGCATCGAGGCCGCCCT
GGAGTACATCAGCAAGATGGGCTACCTGGACCCGAGGAATGAGCAGATTGTGCGGGTCATTAAGCAGACCTCCCCAGGA
AAGGGGCTCATGCCAACCCCAGTGACGCGGAGGCCCAGCTTCGAAGGAACCGGCGATTCGTTTGCGTCCTACCACCAGCT
GAGCGGTACCCCCTACGAGGGCCCAAGCTTCGGCGCTGACGGCCCCACGGCGCTGGAGGAGATGCCGCGGCCGTACGTG
GACTACCTTTTCCCCGGAGTCGGCCCCCACGGGCCCGGCCACCAGCACCAGCACCCACCCAAGGGCTACGGTGCCAGCGT
AGAGGCAGCAGGGGCACACTTCCCGCTGCAGGGCGCGCACTACGGGCGGCCGCACCTGCTGGTGCCTGGGGAACCCCTG
GGCTACGGAGTGCAGCGCAGCCCCTCCTTCCAGAGCAAGACGCCGCCGGAGACCGGGGGTTACGCCAGCCTGCCCACGA
AGGGCCAGGGAGGACCGCCAGGCGCCGGCCTCGCTTTCCCACCCCCTGCCGCCGGGCTCTACGTGCCGCACCCACACCAC
AAGCAGGCCGGTCCCGTGGCCCACCAGCTGCATGTGCTGGGCTCCCGCAGCCAGGTGTTCGCCAGCGACAGCCCCCCGCA
GAGCCTGCTCACTCCCTCGCGGAACAGCCTCAACGTGGACCTGTATGAATTGAGCAGCACCTCCGTCCAGCAGTGGCCGG
CTGCCACCCTGGCCCGCCGGGACTCCCTGCAGAAGCCGGGCCTGGAGGCGCCGCCGCGCGCGCACGTGGCCTTCCGGCCT
GACTGCCCAGTGCCCAGCAGGACCAACTCCTTCAACAGCCACCAGCCGCGGCCCGGTCCGCCTGGCAAGGCCGAGCCCTC
CCTGCCCGCCCCCAACACCGTGACGGCTGTCACGGCCGCGCACATCTTGCACCCGGTGAAGAGCGTGCGTGTGCTGAGGC
CGGAGCCGCAGACGGCTGTGGGGCCCTCGCACCCCGCCTGGGTGCCCGCGCCTGCCCCGGCCCCCGCCCCCGCCCCCGCC
CCGGCTGCGGAGGGCTTGGACGCCAAGGAGGAGCATGCCCTGGCGCTGGGCGGCGCAGGCGCCTTCCCGCTGGACGTG
GAGTACGGAGGCCCAGACCGGAGGTGCCCGCCTCCGCCCTACCCGAAGCACCTGCTGCTGCGCAGCAAGTCGGAGCAGT
ACGACCTGGACAGCCTGTGCGCAGGCATGGAGCAGAGCCTCCGTGCGGGCCCCAACGAGCCCGAGGGCGGCGACAAGA
GCCGCAAAAGCGCCAAGGGGGACAAAGGCGGAAAGGATAAAAAGCAGATTCAGACCTCTCCCGTTCCCGTCCGCAAAAA
CAGCAGAGACGAAGAGAAGAGAGAGTCACGCATCAAGAGCTACTCGCCATACGCCTTTAAGTTCTTCATGGAGCAGCACG
TGGAGAATGTCATCAAAACCTACCAGCAGAAGGTTAACCGGAGGCTGCAGCTGGAGCAAGAAATGGCCAAAGCTGGACT
CTGTGAAGCTGAGCAGGAGCAGATGCGGAAGATCCTCTACCAGAAAGAGTCTAATTACAACAGGTTAAAGAGGGCCAAG
ATGGACAAGTCTATGTTTGTCAAGATCAAAACCCTGGGGATCGGTGCCTTTGGAGAAGTGTGCCTTGCTTGTAAGGTGGA
CACTCACGCCCTGTACGCCATGAAGACCCTAAGGAAAAAGGATGTCCTGAACCGGAATCAGGTGGCCCACGTCAAGGCCG
AGAGGGACATCCTGGCCGAGGCAGACAATGAGTGGGTGGTCAAACTCTACTACTCCTTCCAAGACAAAGACAGCCTGTAC
TTTGTGATGGACTACATCCCTGGTGGGGACATGATGAGCCTGCTGATCCGGATGGAGGTCTTCCCTGAGCACCTGGCCCG
GTTCTACATCGCAGAGCTGACTTTGGCCATTGAGAGTGTCCACAAGATGGGCTTCATCCACCGAGACATCAAGCCTGATAA
CATTTTGATAGATCTGGATGGTCACATTAAACTCACAGATTTCGGCCTCTGCACTGGGTTCAGGTGGACTCACAATTCCAAA
TATTACCAGAAAGGGAGCCATGTCAGACAGGACAGCATGGAGCCCAGCGACCTCTGGGATGATGTGTCTAACTGTCGGTG
TGGGGACAGGCTGAAGACCCTAGAGCAGAGGGCGCGGAAGCAGCACCAGAGGTGCCTGGCACATTCACTGGTGGGGAC
TCCAAACTACATCGCACCCGAGGTGCTCCTCCGCAAAGGGTACACTCAACTCTGTGACTGGTGGAGTGTTGGAGTGATTCT
CTTCGAGATGCTGGTGGGGCAGCCGCCCTTTTTGGCACCTACTCCCACAGAAACCCAGCTGAAGGTGATCAACTGGGAGA
ACACGCTCCACATTCCAGCCCAGGTGAAGCTGAGCCCTGAGGCCAGGGACCTCATCACCAAGCTGTGCTGCTCCGCAGAC
CACCGCCTGGGGCGGAATGGGGCCGATGACCTGAAGGCCCACCCCTTCTTCAGCGCCATTGACTTCTCCAGTGACATCCG
GAAGCAGCCAGCCCCCTACGTTCCCACCATCAGCCACCCCATGGACACCTCGAATTTCGACCCCGTAGATGAAGAAAGCCC
TTGGAACGATGCCAGCGAAGGTAGCACCAAGGCCTGGGACACACTCACCTCGCCCAATAACAAGCATCCTGAGCACGCAT
TTTACGAATTCACCTTCCGAAGGTTCTTTGATGACAATGGCTACCCCTTTCGATGCCCAAAGCCTTCAGGAGCAGAAGCTTC
ACAGGCTGAGAGCTCAGATTTAGAAAGCTCTGATCTGGTGGATCAGACTGAAGGCTGCCAGCCTGTGTACGTGTAG

turboGFP

[*Pontellina plumata*]

atggagagcgacgagagcggcctgcccgccatggagatcgagtgccgcatcaccggcaccctgaacggcgtggagttcgagctggtgggcggcggagagggc
acccccgagcagggccgcatgaccaacaagatgaagagcaccaaaggcgccctgaccttcagcccctacctgctgagccacgtgatgggctacggcttctacc
acttcggcacctaccccagcggctacgagaaccccttcctgcacgccatcaacaacggcggctacaccaacacccgcatcgagaagtacgaggacggcggcgt
gctgcacgtgagcttcagctaccgctacgaggccggccgcgtgatcggcgacttcaaggtgatgggcaccggcttccccgaggacagcgtgatcttcaccgaca
agatcatccgcagcaacgccaccgtggagcacctgcaccccatgggcgataacgatctggatggcagcttcacccgcaccttcagcctgcgcgacggcggctac
tacagctccgtggtggacagccacatgcacttcaagagcgccatccaccccagcatcctgcagaacgggggcccatgttcgccttccgccgcgtggaggagga
tcacagcaacaccgagctgggcatcgtggagtaccagcacgccttcaagaccccggatgcagatgccggtgaagaatga

Supplementary Table 2: ORA analysis results of upregulated proteins in 20 h LATS2 translatome dataset. Proteins with at least >0.58 log_2-fold change in the 20 h LATS2 translatome dataset were used as an input and the entire dataset as the background for ORA analysis. Here the gene ontology sets C2: curated gene sets, CGP: chemical and genetic perturbations were used as a database.

GENE SET	-LOG$_{10}$(FDR)	Zscore
FLORIO_NEOCORTEX_BASAL_RADIAL_GLIA_DN	20.8	10.3
DUTERTRE_ESTRADIOL_RESPONSE_24HR_UP	20.0	10.0
ROSTY_CERVICAL_CANCER_PROLIFERATION_CLUSTER	19.9	10.0
FISCHER_G2_M_CELL_CYCLE	**16.6**	**9.1**
CHIANG_LIVER_CANCER_SUBCLASS_PROLIFERATION_UP	16.1	9.0
SOTIRIOU_BREAST_CANCER_GRADE_1_VS_3_UP	14.2	8.5
CHANG_CYCLING_GENES	13.9	8.4
WHITEFORD_PEDIATRIC_CANCER_MARKERS	13.9	8.4
TANG_SENESCENCE_TP53_TARGETS_DN	13.8	8.3
CROONQUIST_IL6_DEPRIVATION_DN	13.5	8.2
GOBERT_OLIGODENDROCYTE_DIFFERENTIATION_UP	13.5	8.2
HORIUCHI_WTAP_TARGETS_DN	13.5	8.2
KONG_E2F3_TARGETS	13.5	8.2
LEE_EARLY_T_LYMPHOCYTE_UP	13.3	8.1
KANG_DOXORUBICIN_RESISTANCE_UP	12.9	8.0
KOBAYASHI_EGFR_SIGNALING_24HR_DN	12.6	7.9
POOLA_INVASIVE_BREAST_CANCER_UP	12.2	7.8
HOFFMANN_LARGE_TO_SMALL_PRE_BII_LYMPHOCYTE_UP	11.6	7.6
ZHOU_CELL_CYCLE_GENES_IN_IR_RESPONSE_24HR	11.4	7.5
GRAHAM_CML_DIVIDING_VS_NORMAL_QUIESCENT_UP	11.2	7.5
GOLDRATH_ANTIGEN_RESPONSE	11.0	7.4
GAVIN_FOXP3_TARGETS_CLUSTER_P6	11.0	7.4
AMUNDSON_GAMMA_RADIATION_RESPONSE	11.0	7.4
BURTON_ADIPOGENESIS_PEAK_AT_24HR	10.8	7.3
CROONQUIST_NRAS_SIGNALING_DN	10.7	7.3
WU_APOPTOSIS_BY_CDKN1A_VIA_TP53	10.7	7.3
ZHENG_GLIOBLASTOMA_PLASTICITY_UP	10.0	7.1
LE_EGR2_TARGETS_UP	9.9	7.0
FISCHER_DREAM_TARGETS	**9.9**	**7.0**

Supplementary Table 3: Potential LATS1 and LATS2 kinase substrates class III. Depicted are phosphosites quantified in the MCF10A phosphoproteome datasets. Phosphosite ratios are in log_2, and unnormalized.

GENE	POS	AMINO ACID	UN - NORM.	ADJ. P. VAL	LOCAL. PROB.	UNIPROT ID	SEQUENCE	OVEREXPR.
SUFU	342	S	0.55	0.16	100%	Q1KMD3	APSRKDSLESDSSTAIIPHELIR	2 h LATS1
TJP2	296	S	0.53	0.18	100%	P46937	EHPHSRSPSPEPR	2 h LATS1
TGFB1I1	403	S	0.49	0.31	100%	Q9UBF8	RGSLCATCGLPVTGR	2 h LATS1
SRRM2	1878	S	0.46	0.02	100%	P50402	SRTPLISR	2 h LATS1
SGTB	295	S	0.37	0.57	99%	O75592	SRSFSSSAEEHS	2 h LATS1
YAP1	61	S	0.34	0.16	100%	Q9UMX1	GDSETDLEALFNAVMNPK	2 h LATS1
HNRNPUL2	228	S	0.32	0.06	99%	P46937	SKSPLPPEEEAK	2 h LATS1
SRRM2	510	S	0.29	0.15	100%	P46937	SRSPQWR	2 h LATS1
BUD13	123	T	0.24	0.28	100%	P34932	HFRHDTPDSSPRR	2 h LATS1
PRPF38B	527	S	0.24	0.24	100%	Q7Z5L9	RRSQSIEQESQEK	2 h LATS1
RBBP6	772	S	0.22	0.35	100%	Q96TC7	YHSRSRSPQAFR	2 h LATS1
YAP1	109	S	0.16	0.76	100%	Q9H1K0	QASTDAGTAGALTPQHVR	2 h LATS1
TRA2B	83	S	0.15	0.41	100%	P46937	SRSYSRDYR	2 h LATS1
YAP1	127	S	0.15	0.50	92%	Q9UHB7	AHSSPASLQLGAVSPGTLTPTG VVSGPAATPTAQHLR	2 h LATS1
IRF2BP2	240	S	0.14	0.43	100%	Q96EQ0	RPASVSSSAAVEHEQR	2 h LATS1
RAB11FIP5	307	S	0.12	0.56	100%	Q6P6C2	TYSDEANQMR	2 h LATS1
YAP1	397	S	0.09	0.86	96%	Q9UQ35	DESTDSGLSMSSYSVPR	2 h LATS1
NUMB	438	S	0.08	0.74	100%	O43294	TPSEADRWLEEVSK	2 h LATS1
SYNRG	1075	S	0.07	0.70	100%	Q9BRD0	SLSLGDKEISR	2 h LATS1
PHLDB1	324	S	0.04	0.85	100%	Q9UDY2	KGGHERPPSPGLR	2 h LATS1
MATR3	188	S	0.03	0.91	100%	Q8TDB6	RDSFDDRGPSLNPVLDYDHGSR	2 h LATS1
ZFYVE20	548	S	0.03	0.93	96%	Q9UMZ2	TRSLDFR	2 h LATS1
AFF4	212	S	0.02	0.93	98%	Q7Z6E9	SKSPRDPDANWDSPSR	2 h LATS1
ALKBH5	361	S	0.02	0.95	100%	P43243	RGSFSSENYWR	2 h LATS1
HSPA4	76	S	0.00	1.00	100%	P49757	AFSDPFVEAEK	2 h LATS1
DTX3L	9	S	-0.12	0.61	100%	P49023	ASHLRPPSPLLVR	2 h LATS1
AAK1	637	S	-0.15	0.39	100%	Q9UQ35	ILSDVTHSAVFGVPASK	2 h LATS1
ASAP1	839	S	-0.16	0.53	100%	Q5VTL8	TLSDPPSPLPHGPPNK	2 h LATS1
LMO7	246	S	-0.17	0.82	100%	Q9BXF6	REDSFESLDSLGSR	2 h LATS1
YAP1	164	S	-0.17	0.65	82%	Q2M2I8	QSSFEIPDDVPLPAGWEMAK	2 h LATS1
RMDN3	46	S	-0.18	0.58	99%	Q9ULH1	SQSLPNSLDYTQTSDPGR	2 h LATS1
PXN	533	S	-0.21	0.55	100%	P46937	RGSLCSGCQKPITGR	2 h LATS1
RBM23	149	S	-0.23	0.20	100%	Q86UU1	EKSPVREPVDNLSPEER	2 h LATS1
FAM53C	122	S	-0.25	0.32	100%	O94885	SLSVPVDLSR	2 h LATS1
PI4KB	277	S	-0.27	0.40	98%	P62995	SKSDATASISLSSNLK	2 h LATS1
ZNF787	89	T	-0.35	0.24	97%	Q86U06	THTGERPNACADCGK	2 h LATS1
MYCBP2	2789	S	-0.36	0.19	100%	Q9NYF3	SLSPNHNTLQTLK	2 h LATS1
SASH1	407	S	-0.48	0.32	96%	Q6DD87	TCSFGGFDLTNR	2 h LATS1
EMD	171	S	-0.57	0.34	100%	Q9GZV5	DSAYQSITHYRPVSASR	2 h LATS1
WWTR1	89	S	-0.65	0.02	99%	Q09161	SHSSPASLQLGTGAGAAGSPAQQHAHLR	2 h LATS1
NCBP1	21	T	-0.94	0.03	73%	Q6DD87	RKTSDANETEDHLESLICK	2 h LATS1
SH3KBP1	436	S	-1.23	0.01	100%	Q8WWI1	GDSPKIDLAGSSLSGILDKDLSDR	2 h LATS1
ZNF787	145	T	-1.65	0.03	100%	Q96B97	IHTGEKPYTCPDCGR	2 h LATS1
YAP1	397	S	0.72	0.19	96%	P46937	DESTDSGLSMSSYSVPR	6 h LATS1
MNAT1	279	S	0.65	0.54	100%	P46937	AASPQDLAGGYTSSLACHR	6 h LATS1
SUFU	342	S	0.52	0.22	100%	P46937	APSRKDSLESDSSTAIIPHELIR	6 h LATS1
TGFB1I1	403	S	0.37	0.39	100%	P46937	RGSLCATCGLPVTGR	6 h LATS1
ZBTB7B	369	T	0.37	0.60	97%	O43294	THTGEKPFACEVCGVR	6 h LATS1
SGTB	295	S	0.31	0.69	99%	P51948	SRSFSSSAEEHS	6 h LATS1
HNRNPUL2	228	S	0.30	0.09	99%	P49757	SKSPLPPEEEAK	6 h LATS1

PHLDB1	324	S	0.29	0.18	100%	Q1KMD3	KGGHERPPSPGLR	6 h LATS1
YAP1	61	S	0.28	0.36	100%	Q7Z5L9	GDSETDLEALFNAVMNPK	6 h LATS1
PI4K2A	462	S	0.26	0.48	97%	Q6P6C2	SSSESYTQSFQSR	6 h LATS1
SRRM2	1878	S	0.23	0.21	100%	Q9BRD0	SRTPLISR	6 h LATS1
PARD3	144	S	0.21	0.51	78%	P43243	RSSDPALIGLSTSVSDSNFSSEEPSR	6 h LATS1
MYCBP2	2789	S	0.21	0.49	100%	Q86UU1	SLSPNHNTLQTLK	6 h LATS1
YAP1	164	S	0.20	0.64	82%	Q8TEW0	QSSFEIPDDVPLPAGWEMAK	6 h LATS1
ALKBH5	361	S	0.20	0.41	100%	O75592	RGSFSSENYWR	6 h LATS1
EMD	171	S	0.19	0.80	100%	O15156	DSAYQSITHYRPVSASR	6 h LATS1
TJP2	296	S	0.18	0.75	100%	Q9ULH1	EHPHSRSPSPEPR	6 h LATS1
TRA2B	83	S	0.18	0.36	100%	Q9UDY2	SRSYSRDYR	6 h LATS1
FAM83B	542	S	0.14	0.70	61%	Q9UQ35	LRSSLVFKPTLPEQK	6 h LATS1
BUD13	123	T	0.12	0.64	100%	Q5VTL8	HFRHDTPDSSPRR	6 h LATS1
SRRM2	510	S	0.11	0.60	100%	P62995	SRSPQWR	6 h LATS1
PRPF38B	527	S	0.11	0.63	100%	P46937	RRSQSIEQESQEK	6 h LATS1
RBBP6	772	S	0.10	0.73	100%	Q5T0W9	YHSRSRSPQAFR	6 h LATS1
SYNRG	1075	S	0.09	0.67	100%	Q9UMZ2	SLSLGDKEISR	6 h LATS1
NUMB	438	S	0.09	0.76	100%	Q9BXF6	TPSEADRWLEEVSK	6 h LATS1
IRF2BP2	240	S	0.08	0.73	100%	Q9UQ35	RPASVSSSAAVEHEQR	6 h LATS1
RMDN3	46	S	0.07	0.88	99%	Q9NYF3	SQSLPNSLDYTQTSDPGR	6 h LATS1
YAP1	127	S	0.04	0.89	92%	Q7Z6E9	AHSSPASLQLGAVSPGTLTPTG VVSGPAATPTAQHLR	6 h LATS1
ASAP1	839	S	0.04	0.92	100%	P34932	TLSDPPSPLPHGPPNK	6 h LATS1
PI4KB	277	S	-0.01	0.99	98%	P49023	SKSDATASISLSSNLK	6 h LATS1
AAK1	637	S	-0.01	0.96	100%	Q96EQ0	ILSDVTHSAVFGVPASK	6 h LATS1
HSPA4	76	S	-0.08	0.76	100%	Q9UMX1	AFSDPFVEAEK	6 h LATS1
ZNF787	89	T	-0.10	0.83	97%	Q9BTU6	THTGERPNACADCGK	6 h LATS1
MATR3	188	S	-0.10	0.66	100%	Q86U06	RDSFDDRGPSLNPVLDYDHGSR	6 h LATS1
FAM53C	122	S	-0.20	0.57	100%	Q2M2I8	SLSVPVDLSR	6 h LATS1
YAP1	109	S	-0.20	0.68	100%	P50402	QASTDAGTAGALTPQHVR	6 h LATS1
DTX3L	9	S	-0.21	0.39	100%	Q9UBF8	ASHLRPPSPLLVR	6 h LATS1
PXN	533	S	-0.22	0.48	100%	Q96TC7	RGSLCSGCQKPITGR	6 h LATS1
RBM23	149	S	-0.25	0.20	100%	Q9UHB7	EKSPVREPVDNLSPEER	6 h LATS1
RAB11FIP5	307	S	-0.26	0.24	100%	Q96B97	TYSDEANQMR	6 h LATS1
AFF4	212	S	-0.27	0.25	98%	Q8TDB6	SKSPRDPDANWDSPSR	6 h LATS1
C1orf172	11	S	-0.28	0.58	100%	P22059	PRPGHPRPASGPPR	6 h LATS1
OSBP	379	S	-0.56	0.49	55%	Q8NAX2	TGSNISGASSDISLDEQYKHQLEETKK	6 h LATS1
WWTR1	89	S	-0.69	0.02	99%	Q6DD87	SHSSPASLQLGTGAGAAGSPAQQHAHLR	6 h LATS1
SH3KBP1	436	S	-0.69	0.10	100%	Q5SW79	GDSPKIDLAGSSLSGILDKDLSDR	6 h LATS1
CEP170	1259	T	-0.84	0.13	65%	Q9GZV5	LRTSPALK	6 h LATS1
NCBP1	21	T	-1.18	0.01	73%	Q09161	RKTSDANETEDHLESLICK	6 h LATS1
TDP1	61	S	-1.48	0.01	99%	Q9NUW8	KISPVKFSNTDSVLPPKR	6 h LATS1
HNRNPUL2	228	S	0.39	0.04	99%	Q1KMD3	SKSPLPPEEEAK	2 h LATS2
YAP1	397	S	0.37	0.50	96%	P46937	DESTDSGLSMSSYSVPR	2 h LATS2
PI4KB	277	S	0.27	0.46	98%	Q9UBF8	SKSDATASISLSSNLK	2 h LATS2
EMD	171	S	0.25	0.75	100%	P50402	DSAYQSITHYRPVSASR	2 h LATS2
MYCBP2	2789	S	0.24	0.43	100%	O75592	SLSPNHNTLQTLK	2 h LATS2
SUFU	342	S	0.17	0.73	100%	Q9UMX1	APSRKDSLESDSSTAIIPHELIR	2 h LATS2
YAP1	61	S	0.17	0.53	100%	P46937	GDSETDLEALFNAVMNPK	2 h LATS2
YAP1	127	S	0.16	0.54	92%	P46937	AHSSPASLQLGAVSPGTLTPTG VVSGPAATPTAQHLR	2 h LATS2
HSPA4	76	S	0.15	0.57	100%	P34932	AFSDPFVEAEK	2 h LATS2
IRF2BP2	240	S	0.11	0.64	100%	Q7Z5L9	RPASVSSSAAVEHEQR	2 h LATS2
RMDN3	46	S	0.10	0.84	99%	Q96TC7	SQSLPNSLDYTQTSDPGR	2 h LATS2
ZFYVE20	548	S	0.09	0.80	96%	Q9H1K0	TRSLDFR	2 h LATS2
YAP1	109	S	0.08	0.93	100%	P46937	QASTDAGTAGALTPQHVR	2 h LATS2
AFF4	212	S	0.07	0.77	98%	Q9UHB7	SKSPRDPDANWDSPSR	2 h LATS2

SGTB	295	S	-0.01	1.00	99%	Q96EQ0	SRSFSSSAEEHS	2 h LATS2
ALKBH5	361	S	-0.03	0.94	100%	Q6P6C2	RGSFSSENYWR	2 h LATS2
SRRM2	1878	S	-0.05	0.81	100%	Q9UQ35	SRTPLISR	2 h LATS2
TGFB1I1	403	S	-0.06	0.94	100%	O43294	RGSLCATCGLPVTGR	2 h LATS2
BUD13	123	T	-0.06	0.84	100%	Q9BRD0	HFRHDTPDSSPRR	2 h LATS2
TJP2	296	S	-0.07	0.91	100%	Q9UDY2	EHPHSRSPSPEPR	2 h LATS2
DTX3L	9	S	-0.07	0.82	100%	Q8TDB6	ASHLRPPSPLLVR	2 h LATS2
SYNRG	1075	S	-0.08	0.75	100%	Q9UMZ2	SLSLGDKEISR	2 h LATS2
RBBP6	772	S	-0.08	0.81	100%	Q7Z6E9	YHSRSRSPQAFR	2 h LATS2
MATR3	188	S	-0.09	0.71	100%	P43243	RDSFDDRGPSLNPVLDYDHGSR	2 h LATS2
NUMB	438	S	-0.12	0.68	100%	P49757	TPSEADRWLEEVSK	2 h LATS2
PXN	533	S	-0.14	0.76	100%	P49023	RGSLCSGCQKPITGR	2 h LATS2
SRRM2	510	S	-0.14	0.52	100%	Q9UQ35	SRSPQWR	2 h LATS2
PRPF38B	527	S	-0.15	0.54	100%	Q5VTL8	RRSQSIEQESQEK	2 h LATS2
RAB11FIP5	307	S	-0.16	0.51	100%	Q9BXF6	TYSDEANQMR	2 h LATS2
AAK1	637	S	-0.19	0.34	100%	Q2M2I8	ILSDVTHSAVFGVPASK	2 h LATS2
ASAP1	839	S	-0.19	0.52	100%	Q9ULH1	TLSDPPSPLPHGPPNK	2 h LATS2
YAP1	164	S	-0.26	0.55	82%	P46937	QSSFEIPDDVPLPAGWEMAK	2 h LATS2
PHLDB1	324	S	-0.28	0.20	100%	Q86UU1	KGGHERPPSPGLR	2 h LATS2
SASH1	407	S	-0.29	0.62	96%	O94885	TCSFGGFDLTNR	2 h LATS2
TRA2B	83	S	-0.37	0.08	100%	P62995	SRSYSRDYR	2 h LATS2
RBM23	149	S	-0.42	0.06	100%	Q86U06	EKSPVREPVDNLSPEER	2 h LATS2
FAM53C	122	S	-0.43	0.14	100%	Q9NYF3	SLSVPVDLSR	2 h LATS2
ZNF787	89	T	-0.44	0.20	97%	Q6DD87	THTGERPNACADCGK	2 h LATS2
WWTR1	89	S	-0.73	0.01	99%	Q9GZV5	SHSSPASLQLGTGAGAAGSPAQQHAHLR	2 h LATS2
NCBP1	21	T	-0.80	0.07	73%	Q09161	RKTSDANETEDHLESLICK	2 h LATS2
ZNF787	145	T	-0.83	0.16	100%	Q6DD87	IHTGEKPYTCPDCGR	2 h LATS2
LMO7	246	S	-0.91	0.29	100%	Q8WWI1	REDSFESLDSLGSR	2 h LATS2
SH3KBP1	436	S	-1.22	0.02	100%	Q96B97	GDSPKIDLAGSSLSGILDKDLSDR	2 h LATS2
YAP1	397	S	1.16	0.06	96%	P46937	DESTDSGLSMSSYSVPR	6 h LATS2
YAP1	127	S	0.76	0.01	92%	P46937	AHSSPASLQLGAVSPGTLTPTG VVSGPAATPTAQHLR	6 h LATS2
YAP1	61	S	0.68	0.05	100%	P46937	GDSETDLEALFNAVMNPK	6 h LATS2
YAP1	164	S	0.50	0.24	82%	P46937	QSSFEIPDDVPLPAGWEMAK	6 h LATS2
TGFB1I1	403	S	0.46	0.29	100%	O43294	RGSLCATCGLPVTGR	6 h LATS2
MNAT1	279	S	0.45	0.68	100%	P51948	AASPQDLAGGYTSSLACHR	6 h LATS2
NUMB	438	S	0.34	0.18	100%	P49757	TPSEADRWLEEVSK	6 h LATS2
HNRNPUL2	228	S	0.29	0.10	99%	Q1KMD3	SKSPLPPEEEAK	6 h LATS2
IRF2BP2	240	S	0.26	0.20	100%	Q7Z5L9	RPASVSSSAAVEHEQR	6 h LATS2
ALKBH5	361	S	0.21	0.39	100%	Q6P6C2	RGSFSSENYWR	6 h LATS2
BUD13	123	T	0.18	0.45	100%	Q9BRD0	HFRHDTPDSSPRR	6 h LATS2
MATR3	188	S	0.17	0.43	100%	P43243	RDSFDDRGPSLNPVLDYDHGSR	6 h LATS2
PHLDB1	324	S	0.16	0.46	100%	Q86UU1	KGGHERPPSPGLR	6 h LATS2
PARD3	144	S	0.16	0.63	78%	Q8TEW0	RSSDPALIGLSTSVSDSNFSSEEPSR	6 h LATS2
MYCBP2	2789	S	0.12	0.70	100%	O75592	SLSPNHNTLQTLK	6 h LATS2
ZBTB7B	369	T	0.10	0.90	97%	O15156	THTGEKPFACEVCGVR	6 h LATS2
ASAP1	839	S	0.06	0.86	100%	Q9ULH1	TLSDPPSPLPHGPPNK	6 h LATS2
TJP2	296	S	0.05	0.93	100%	Q9UDY2	EHPHSRSPSPEPR	6 h LATS2
SRRM2	1878	S	0.04	0.83	100%	Q9UQ35	SRTPLISR	6 h LATS2
PRPF38B	527	S	0.02	0.93	100%	Q5VTL8	RRSQSIEQESQEK	6 h LATS2
TRA2B	83	S	0.02	0.92	100%	P62995	SRSYSRDYR	6 h LATS2
YAP1	109	S	0.00	1.00	100%	P46937	QASTDAGTAGALTPQHVR	6 h LATS2
FAM83B	542	S	0.00	1.00	61%	Q5T0W9	LRSSLVFKPTLPEQK	6 h LATS2
SYNRG	1075	S	0.00	0.99	100%	Q9UMZ2	SLSLGDKEISR	6 h LATS2
RAB11FIP5	307	S	-0.01	0.96	100%	Q9BXF6	TYSDEANQMR	6 h LATS2
SRRM2	510	S	-0.03	0.89	100%	Q9UQ35	SRSPQWR	6 h LATS2
FAM53C	122	S	-0.04	0.91	100%	Q9NYF3	SLSVPVDLSR	6 h LATS2

RBBP6	772	S	-0.10	0.73	100%	Q7Z6E9	YHSRSRSPQAFR	6 h LATS2
HSPA4	76	S	-0.10	0.69	100%	P34932	AFSDPFVEAEK	6 h LATS2
PXN	533	S	-0.10	0.76	100%	P49023	RGSLCSGCQKPITGR	6 h LATS2
SGTB	295	S	-0.11	0.89	99%	Q96EQ0	SRSFSSSAEEHS	6 h LATS2
SUFU	342	S	-0.12	0.79	100%	Q9UMX1	APSRKDSLESDSSTAIIPHELIR	6 h LATS2
PI4K2A	462	S	-0.14	0.70	97%	Q9BTU6	SSSESYTQSFQSR	6 h LATS2
RBM23	149	S	-0.22	0.26	100%	Q86U06	EKSPVREPVDNLSPEER	6 h LATS2
AAK1	637	S	-0.24	0.23	100%	Q2M2I8	ILSDVTHSAVFGVPASK	6 h LATS2
EMD	171	S	-0.25	0.72	100%	P50402	DSAYQSITHYRPVSASR	6 h LATS2
PI4KB	277	S	-0.26	0.37	98%	Q9UBF8	SKSDATASISLSSNLK	6 h LATS2
RMDN3	46	S	-0.29	0.41	99%	Q96TC7	SQSLPNSLDYTQTSDPGR	6 h LATS2
AFF4	212	S	-0.32	0.18	98%	Q9UHB7	SKSPRDPDANWDSPSR	6 h LATS2
SH3KBP1	436	S	-0.33	0.37	100%	Q96B97	GDSPKIDLAGSSLSGILDKDLSDR	6 h LATS2
DTX3L	9	S	-0.37	0.14	100%	Q8TDB6	ASHLRPPSPLLVR	6 h LATS2
OSBP	379	S	-0.41	0.61	55%	P22059	TGSNISGASSDISLDEQYKHQLEETKK	6 h LATS2
C1orf172	11	S	-0.46	0.36	100%	Q8NAX2	PRPGHPRPASGPPR	6 h LATS2
ZNF787	89	T	-0.64	0.13	97%	Q6DD87	THTGERPNACADCGK	6 h LATS2
CEP170	1259	T	-1.01	0.09	65%	Q5SW79	LRTSPALK	6 h LATS2
WWTR1	89	S	-1.05	0.00	99%	Q9GZV5	SHSSPASLQLGTGAGAAGSPAQQHAHLR	6 h LATS2
NCBP1	21	T	-1.14	0.02	73%	Q09161	RKTSDANETEDHLESLICK	6 h LATS2
TDP1	61	S	-1.35	0.01	99%	Q9NUW8	KISPVKFSNTDSVLPPKR	6 h LATS2

6.3. List of Figures

6.4. List of Tables

7. ACKNOWLEDGMENTS

"The PhD is a journey, not a destination"

- (adapted from Ralph Waldo Emerson's original quote "Life is a journey, not a destination")

I would like to take the opportunity to thank all the people who have accompanied me throughout that journey. The presented work would not have been possible without your support – thank you very much.

First, I would like to express gratitude to my supervisor Jeroen Krijgsveld. You gave me the chance to change tracks, to set the right course, and to realize my journey as a PhD in a second attempt. Your trust in me as a young scientist gave me the necessary freedom to unfold, yet your helpful counsel gave me guidance when needed. You encouraged my curiosity and fascination for science, allowing me to shape my own scientific path. For this, I am deeply grateful.
Furthermore, I would like to thank my thesis advisory and defense committee members Prof. Matthias Mayer, Prof. Claudia Scholl, Prof. Moshe Oren, Prof. Ursula Klingmüller, and Prof. Stefan Wiemann for your interest in my work and the valuable support and feedback in the past years. I would like to give special thanks to Prof. Moshe Oren, together with Dr. Yael Aylon, who warmly welcomed me in their lab at the Weizmann Institute in Israel, generously shared cell pellets, cell lines and plasmids with me, as well as their seemingly infinite knowledge in the field of biology. The passionate discussions about biology were contagious and inspiring. Also, I would like to especially thank Prof. Claudia Scholl for allowing me to establish the Tet-inducible cell lines in her S2-lab, and particularly her lab members Stefanie Reinhart and Claudia Kraut for their hands-on support in this regard.
Additionally, I would like to thank Stefan Pusch for not only generously sharing cell lines and plasmids with me, but especially for the fruitful discussions and scientific advice.

Next, I would like to thank all the present and former B230's, also known as my cherished colleagues and members of the Krijgsveld lab:

In this regard, I wish to especially mention Mathias Kalxdorf – what would I have done without you? I am eternally grateful for the countless times you have gifted me your time, despite your packed work days, to help me navigate around roadblocks represented by the never ending R!-challenges I've come up against. You are one of the most brilliant scientists I have encountered thus far – as we say: "ein echter Fuchs". Most importantly though, thank you for your friendship.
Another special thank you goes to my favorite Greek, Dimitris Papageorgiou. You have been an invaluable source of knowledge in mass spec, biochemistry, and R-programming. And not to forget your unceasing wealth of (semi-)philosophical Greek sayings and advice – teaching me that the PhD is not a sprint, but a marathon. Above all, you became a true friend, my male bestie, helping me in

so many ways to tackle that marathon, be it with fun moments as office mates and bench-neighbors or unforgettable Bent bar visits.
Torsten Müller, for the always welcomed coffee breaks, your unassuming way of helping me with MS questions, for a lot of fun as bench neighbors, and not to forget for the many times you have reminded me to believe in myself.
Karim Aljakouch, for being on this journey with me from beginning to end, be it as the dream team Batman and Robin in our fight against chromatin-bound proteins or during recharging walks around the block sharing thoughts and laughter.
Marco Jochem, for always being my favorite master student and being part of the reasons I enjoyed coming to the lab on a daily basis and not to forget sharing unforgetable times at the Bent Bar.
Georg Kliewer, for being you. With your heart in the right place and rhythm in your blood, seasoned with a dash of craziness, your presence and person enriched the lab for me.
Gertjan Kramer and Gianluca Sigismondo – former and current lab wise men, respectively – for sharing your expertise in all things mass spec and your molecular biological methods with me, as well as for always having a helpful tip at hand concerning the experiments I've conducted.
Roman Ladig, for the great times as office mates, for providing me with (hard!) Haribo, tea, and your always open ear.
And, of course, all my other colleagues at B230, for creating such a pleasurable and productive atmosphere during my time at the lab.

My sincere gratitude also goes out to all my dearest friends outside the lab.

A special thank you goes to Philipp Spahn, not only for your never-ending support by proof reading this thesis, the one before that (Master thesis), and the one before that (Bachelor thesis), but especially for being a constant support throughout my journey, helping me grow from a little chick to a … scientist. You've always helped me find my balance in chaotic times and shared the passion for biology with me. Without you, this work would not have been possible – thank you very much.
I am also especially grateful to Mona Zink, Luisa Henkel and Sophia Föhr. Be it with barbeques in the foothills of the Alps, walks through the Odenwald, or even just plenty of coffees, a glass of wine here and there, or "Bianca's Special", you gave me the necessary opportunities to recharge. "And whenever we laugh, a problem dies somewhere" – with you, there was and is never a lack of laughter and levity. Thank you that I can always count on you.

Last and most importantly, my biggest thank you – from the bottom of my heart – goes to my Mom, Dad, René and Laura, for your boundless support in all that I do. Mom and Dad, thank you for always supporting me in the pursuit of my dreams – from the biology studies in Tübingen to the PhD in Heidelberg. You have gone with me through highs and lows without the slightest doubt that I wouldn't succeed and simultaneously giving me the unwavering certainty that in your eyes I could never fail. You gave me strength and the tools to navigate this journey. I couldn't imagine a more caring and loving family – I am eternally grateful for you.